JSCSEN 80(7)839–969(2015)

ISSN 1820-7421(Online)

Journal of the Serbian Chemical Society

Electronic version

Volume 80 : : 2015 : : 85 Years of the Journal

1930 Glasnik Hemijskog Društva Kraljevine Jugoslavije
Journal of the Chemical Society of the Kingdom of Yugoslavia

1947 Glasnik hemijskog društva Beograd
Journal of the Chemical Society of Belgrade

1985 Journal of the Serbian Chemical Society

VOLUME 80

No 7

BELGRADE 2015

Available on line at

www.shd.org.rs/JSCS/

The full search of JSCS
is available through

DOAJ DIRECTORY OF OPEN ACCESS JOURNALS
www.doaj.org

Journal of the Serbian Chemical Society
JSCS-info@shd.org.rs • www.shd.org.rs/JSCS

J. Serb. Chem. Soc. Vol. 80, No. 7 (2015)

CONTENTS

Published by the Serbian Chemical Society
Karnegijeva 4/III, P.O. Box 36, 11120 Belgrade, Serbia
Printed by the Faculty of Technology and Metallurgy
Karnegijeva 4, P.O. Box 35-03, 11120 Belgrade, Serbia

Journal of the Serbian Chemical Society
JSCS-info@shd.org.rs • www.shd.org.rs/JSCS
J. Serb. Chem. Soc. 80 (7) 839–852 (2015)
JSCS–4763
UDC 547.71.8+547.639.5+546.98+
542.913:615.281/.282
Original scientific paper

Synthesis and antimicrobial activity of azepine and thiepine derivatives

NINA BOŽINOVIĆ[1#], IRENA NOVAKOVIĆ[2#], SLAĐANA KOSTIĆ RAJAČIĆ[2#], IGOR M. OPSENICA[1*#] and BOGDAN A. ŠOLAJA[1**#]

[1]*Faculty of Chemistry, University of Belgrade, Studentski trg 16, P. O. Box 51, 11158, Belgrade, Serbia and* [2]*Institute of Chemistry, Technology, and Metallurgy, University of Belgrade, Njegoševa 12, 11000 Belgrade, Serbia*

(Received 16 January, revised 2 February, accepted 6 February 2015)

Abstract: A series of new pyridobenzazepine and pyridobenzothiepine derivatives was synthesized by Pd-catalyzed formation of C–N and C–S bonds. All synthesized compounds were tested for their *in vitro* antimicrobial activity. The pyridobenzazepine derivatives showed better antibacterial and antifungal activity than the corresponding dipyridoazepine analogue. Among the synthesized azepines, derivative **8** displayed potent activity against the tested bacteria (*MIC* ranged 39–78 μg mL^{-1}), while azepine **12** showed promising antifungal activity (*MIC* ranged 156–313 μg mL^{-1}). The synthesized thiepine derivatives exhibited weak antibacterial activity, but showed pronounced antifungal activity.

Keywords: azepines; thiepines; heterocycles; palladium; antibacterials; antifungal.

INTRODUCTION

The tricyclic moieties of 5*H*-dibenz[*b*,*f*]azepine (**1**)[1] and dibenzo[*b*,*f*]thiepine (**2**)[2] are important heterocyclic pharmacophores in a number of drugs. Carbamazepine (**3**) and opipramol (**4**) belong to the dibenzazepine group of heterocyclic compounds. Carbamazepine (**3**) is an anticonvulsant used to treat seizures, nerve pain and bipolar disorder,[1a] while opipramol (**4**) is a tricyclic antidepressant (TCA) and is used to treat generalized anxiety disorders.[1b] The dibenzothiepine zotepine (**5**) is an atypical antipsychotic, and it is used to treat schizophrenia (Fig. 1).[3]

Over the past few decades, several different strategies were developed for the synthesis of 5*H*-dibenz[*b*,*f*]azepines[4] and dibenzo[*b*,*f*]thiepines.[2,4e,5] The use of palladium-catalyzed reactions is an efficient procedure for the synthesis of 5*H*-

*,** Corresponding authors. E-mails: (*)igorop@chem.bg.ac.rs; (**)bsolaja@chem.bg.ac.rs
Serbian Chemical Society member.
doi: 10.2298/JSC150116013B

-dibenz[*b*,*f*]azepines,[6] and methods based on the double *N*-arylation reaction are of particular relevance.[7] Hitherto, only one method employing a Pd-catalyzed reaction for the construction of the dibenzothiepine core has been reported.[8] The Mizoroki–Heck cyclisation of the corresponding diaryl thioether was used for the synthesis of dibenzothiepine **2**.

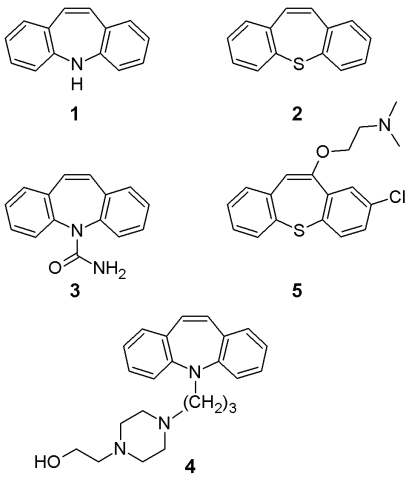

Fig. 1. Tricyclic 5*H*-dibenz[*b*,*f*]azepines and dibenzo[*b*,*f*]thiepines.

Recently, a simple and efficient Pd-catalyzed method was developed for the synthesis of 5*H*-pyrido[4,3-b:3',4'-f]benzazepine and 5*H*-dipyrido[4,3-b][1]azepine compounds (Scheme 1).[9]

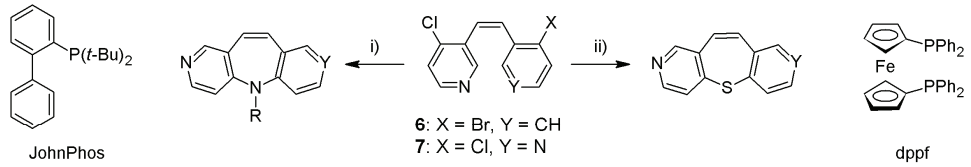

Reagents and conditions: i) $Pd(OAc)_2$ (5 mol%), JohnPhos (10 mol%), RNH_2, NaO*t*-Bu, PhMe, 100 °C; ii) $Pd(OAc)_2$ (5 mol%), dppf (10 mol%), KSAc, NaO*t*-Bu, PhMe, 175 °C, μW.

Scheme 1. Pd-catalyzed synthesis of 5*H*-pyrido[4,3-b][1]benzazepine and 5*H*-dipyrido[4,3-b:3',4'-f]azepine compounds.

The protocol is based on a Pd-catalyzed double amination reaction of the corresponding stilbenes. Additionally, as an expansion of the methodology, for the first time Pd-catalyzed formation of C–S bonds was applied to the ring closure of a thiepine derivatives from the corresponding stilbene precursors and an *S*-nucleophile (Scheme 1). Formerly, the synthesized azepines and thiepines are shown in Fig. 2.

Herein, the synthesis of some new pyridobenzazepine and pyridobenzothiepine derivatives using the previously described methodology is presented. All synthesized compounds were evaluated for their *in vitro* antimicrobial activity against eight bacterial and three fungal pathogenic strains.

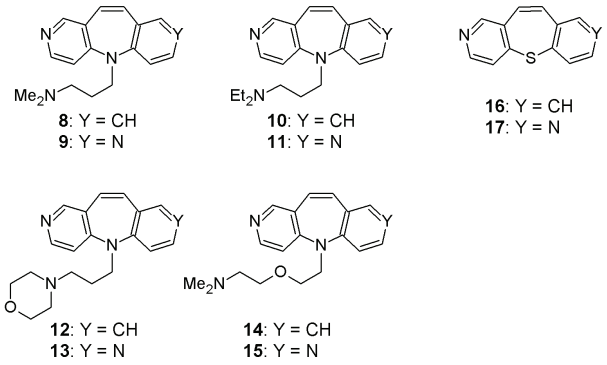

Fig. 2. Structures of the synthesized azepine and thiepine derivatives.

RESULTS AND DISCUSSION

Chemistry

The Wittig reaction between phosphonium salt **22**[9] and aldehydes **19**[10] and **21**[11] provided the corresponding *Z*-stilbenes **24** and **25**, respectively, in high yield. For the preparation of ethylene derivative **26**, commercially available 2-bromo-5-fluorobenzaldehyde **23** was used (Scheme 2).

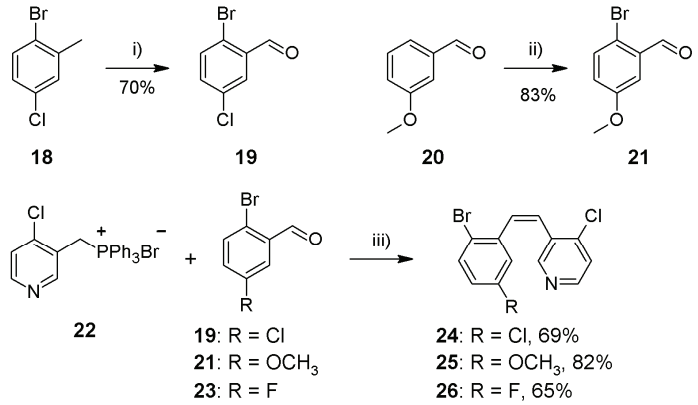

Reagents and conditions: i) a) CrO_3, Ac_2O, AcOH, H_2SO_4; b) MeOH, H_2O, H_2SO_4, Δ; ii) a) Br_2, AcOH, r.t.; b) $Na_2S_2O_3$, H_2O; iii) KO*t*-Bu, THF, r.t.

Scheme 2. The synthesis of *Z*-stilbenes **24**–**26**.

The syntheses of new iminostilbene compounds **27**–**30** were achieved using the previously described reaction conditions for Pd-catalyzed double amination reactions (Scheme 3).[9]

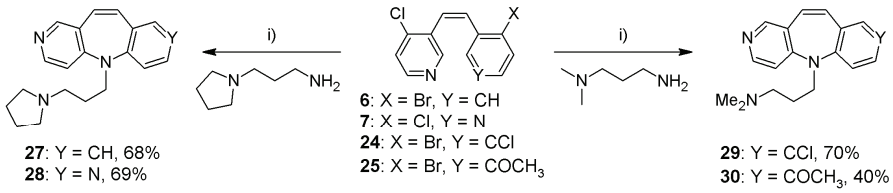

Reagents and conditions: i) $Pd(OAc)_2$ (5 mol%), JohnPhos (10 mol%), amine (3 equiv), NaO*t*-Bu (2.8 equiv), PhMe, 100 °C

Scheme 3. The synthesis of new pyridobenzazepine and dipyridoazepine compounds.

The reactions of *Z*-stilbenes **6**, **7** and **24**–**26** with potassium thioacetate (1.2 equiv.) in the presence of a catalyst composed from $Pd_2(dba)_3$ (5 mol %) and dppf (10 mol %) under microwave-mediated heating afforded the thiepine derivatives **16**, **17** and **31**–**33** in moderate yields (Scheme 4). It should be noted that higher proportions of KSAc (2.4 eqiuv.) resulted in significantly better yields of **31** and **32**, whereas the yield of thiepines **16** and **33** did not improve. In the case of stilbene **7**, the higher load of KSAc resulted in a complex reaction mixture.

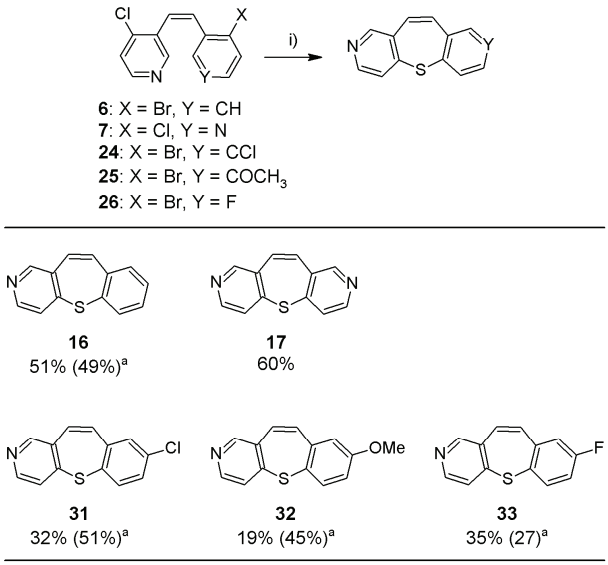

Reagents and conditions: i) Pd_2dba_3 (5 mol%), dppf (10 mol%), KSAc (1.2 equiv), NaO*t*-Bu (1.2 equiv), PhMe, 170 °C, μW

[a]2.4 equiv KSAc

Scheme 4. The synthesis of thiepine derivatives.

In the next synthetic step, the thiepine compound **31** was chemically transformed into its tetrahydro and biphenyl derivatives **34** and **35**, respectively. After N-methylation, and $NaBH_4$ reduction, the tetrahydro derivative **34** was obtained in 66% yield. The Suzuki–Miyaura reaction on thiepine **31** with phenylboronic acid gave derivative **35** in moderate yield (Scheme 5). The coupling reaction was performed with the catalytic system $Pd(OAc)_2$/SPhos–K_3PO_4 in toluene. These transformations of thiepine **31** opened up new possibilities for the preparation of structurally diverse substituted thiepines.

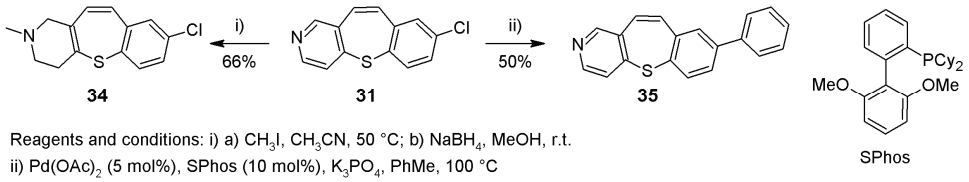

Scheme 5. The transformations of thiepine compound **31**.

Antimicrobial activity

The synthesized azepine derivatives were screened for their antibacterial and antifungal activities against five Gram-negative bacteria (*Escherichia coli*, *Proteus hauseri*, *Pseudomonas aeruginosa*, *Salmonella enterica* subsp. *enterica* serovar Enteritidis and *Klebsiella pneumoniae*), three Gram-positive bacteria (*Staphylococcus aureus*, *Micrococcus luteus* ATCC 10240 and *M. luteus* ATCC 4698) and three fungal strains (*Candida albicans*, *Saccharomyces cerevisiae* and *Aspergillus brasiliensis*). Amikacin (AMK) and chloramphenicol (CHL) were used as standard antibacterials, and nystatin (NYT) and fluconazole (FLC) were used as antifungal reference compounds. The minimum inhibitory concentration (*MIC*) was determined as the lowest concentration of the compound that resulted in inhibition of bacterial, respectively fungal growth, using a broth microdilution method.

The results of antibacterial activities of azepine derivatives are given in Table I. The azepines **8**–**15** and **27**–**30** exhibited lower antibacterial activity with respect to amikacin (Table I). Compound **8** was more potent than chloramphenicol against three Gram-negative bacteria (*E. coli*, *P. hauseri* and *P. aeruginosa*) and one Gram–positive bacteria (*M. luteus* ATCC 4698).

All pyridobenzazepine derivatives (**8**, **10**, **12**, **14** and **27**) showed higher inhibitory activity than the corresponding dipyridoazepine analogues (**9**, **11**, **13**, **15** and **28**) against all bacteria. Azepine **8** with an *N*,*N*-dimethyl substituent was 4 times more potent than the corresponding *N*,*N*-diethyl substituted analogue **10**. Additionally, **27**, which incorporates the side chain nitrogen in pyrrolidine ring was more potent than **10**, but less active than **8**. The results of the antibacterial screening for compounds **8** and **14** revealed that the introduction of an oxygen

atom in the side chain significantly decreased the antibacterial activity. The substituted azepines **29** and **30** showed lower antibacterial potency than **8** against all the screened bacteria.

TABLE I. Antibacterial minimal inhibitory concentrations (*MIC* / μg mL^{-1}) of the azepine derivatives

Cmpd.	Gram-negative bacteria					Gram-positive bacteria		
	E. coli	*P. hauseri*	*P. aerugi-nosa*	*S. enterica*	*K. pneu-moniae*	*S. aureus*	*M. luteus* ATCC 10240	*M. luteus* ATCC 4698
8	39	78	78	78	78	39	78	39
9	1250	1250	1250	1250	625	1250	1250	2500
10	156	313	313	625	625	156	313	313
11	1250	1250	1250	1250	1250	1250	1250	1250
12	39	313	313	313	313	39	156	78
13	1250	2500	1250	1250	1250	2500	1250	2500
14	313	625	625	625	625	313	625	313
15	1250	1250	1250	1250	1250	1250	1250	1250
27	78	156	313	313	313	156	156	156
28	625	625	625	625	625	625	625	625
29	78	156	313	313	313	156	313	156
30	156	313	313	313	625	313	313	313
AMK	5	7	50	8	8	11	2	2
CHL	62	125	250	43	62	15	31	125

Finally, among the synthesized azepines, derivative **8** was the most active one and showed a broad spectrum of antibacterial activity (MIC ranged 39–78 μg mL^{-1}).

The minimum inhibitory concentrations (*MIC*) of the synthesized azepines against three fungal strains are presented in Table II. Compounds **12** and **27** showed excellent activity (*MIC* = 156 μg mL^{-1}) against *C. albicans* and *S. cerevisiae*; they were more potent than nystatin and fluconazole. Compounds **12** and **27** are 16 times more active than nystatin against *C. albicans*, and 8 times more potent against *S. cerevisiae* than nystatin. In addition, compound **8** was more potent than nystatin and fluconazole against *S. cerevisiae*, while derivative **29** was more active than the reference compounds against the *C. albicans* strain.

Compounds **12** and **30** showed a four-fold greater potency (*MIC* = 313 μg mL^{-1}) than nystatin in inhibiting the growth of the *A. brasiliensis* strain, but were less active when compared to fluconazole. Again, as with the antibacterial activity, it was observed that the pyridobenzazepine derivatives (**8**, **10**, **12**, **14** and **27**) showed better antifungal activity than the corresponding dipyridoazepine analogues (**9**, **11**, **13**, **15** and **28**).

The synthesized thiepines were screened for their antibacterial and antifungal activities against four Gram-negative bacteria (*E. coli*, *P. hauseri*, *P. aeruginosa* and *Salmonella enterica* subsp. *enterica* serovar Enteritidis), four Gram-

-positive bacteria (*Clostridium sporogenes*, *S. aureus*, *M. luteus* ATCC 10240 and *Kocuria rhizophila*) and three fungal strains (*C. albicans*, *S. cerevisiae* and *A. brasiliensis*), using a disk diffusion method. Amikacin (AMK) was used as the standard antibacterial drug, and nystatin (NYT) was used as the antifungal reference compound. The antimicrobial activity was evaluated based on the diameter of the zone of inhibition.

TABLE II. Antifungal minimal inhibitory concentrations (*MIC* / μg mL^{-1}) of the azepine derivatives

Cmpd.	*C. albicans*	*S. cerevisiae*	*A. brasiliensis*
8	2500	156	1250
9	2500	1250	1250
10	625	625	625
11	1250	1250	1250
12	156	156	313
13	2500	1250	1250
14	625	313	625
15	1250	1250	1250
27	156	156	625
28	625	625	1250
29	156	313	625
30	313	313	313
NYT	2500	1250	1250
FLC	313	313	156

The results of antimicrobial activities of thiepine derivatives (Table III) revealed that all the tested thiepines displayed weak antibacterial activity with inhibition zones of 10–20 mm.

TABLE III. Antibacterial activity expressed as inhibition diameter zones in millimetres (mm) of thiepine derivatives

Cmpd.[a]	Gram–negative bacteria				Gram–positive bacteria			
	E. coli	*P. hauseri*	*P. aeruginosa*	*S. enterica*	*C. sporogenes*	*S. aureus*	*M. luteus* ATCC 10240	*K. rhizophila*
16	N.A.[b]	N.A.	N.A.	N.A.	N.A.	N.A.	N.A.	N.A.
17	14	10	N.A.	10	16	N.A.	N.A.	N.A.
31	14	N.A.	N.A.	N.A.	20	N.A.	N.A.	10
32	14	10	N.A.	10	14	N.A.	N.A.	N.A.
33	N.A.	N.A.	N.A.	N.A.	N.A.	N.A.	N.A.	N.A.
34	10	14	N.A.	N.A.	10	N.A.	N.A.	N.A.
35	N.A.	N.A.	N.A.	N.A.	N.A.	N.A.	N.A.	N.A.
AMK[c]	26	26	25	25	24	24	27	23

[a] Compounds concentration 1 mg disk^{-1}; [b] N.A.: no activity (inhibition zone <10 mm); [c] AMK concentration 30 μg disk^{-1}

On the other hand, with the exception of **31**, all compounds exhibited pronounced antifungal activity against the three fungal strains (Table IV). The investigation of antifungal screening revealed that at a concentration of 1000 μg disk^{-1}, compounds **16**, **17**, **32**, **33**, **34** and **35** were very potent, and showed complete growth inhibition against the *C. albicans* and *S. cerevisiae* strains. Among synthesized thiepines, compound **32** showed excellent antifungal activity particularly on the *C. albicans* strain with an inhibition zone of 50 mm at 250 μg disk^{-1}, 28 mm at 125 μg disk^{-1} and 14 mm at 62.5 μg disk^{-1} concentrations. In addition, compound **32** at a concentration 125 μg disk^{-1} displayed moderate activity against the *A. brasiliensis* and *S. cerevisiae* strains (growth inhibition zones 12–18 mm). All the tested thiepine derivatives were completely inactive against the fungal strains at a concentration 31.3 μg disk^{-1}.

TABLE IV. Antifungal activity of the thiepine derivatives expressed as diameter of the inhibition zones in millimetres (mm)

Cmpd.	*C. albicans*[a]				*S. cerevisiae*[b]				*A. brasiliensis*[a]			
	Concentration, μg disk^{-1}											
	1000	500	250	125	1000	500	250	125	1000	500	250	125
16	C.I.[c]	12	10	N.A.[d]	C.I.	18	15	11	18	14	12	10
17	C.I.	C.I.	30	N.A.	C.I.	20	16	12	C.I.	16	12	10
31	N.A.	N.A.	N.A.	N.A.	N.A.	N.A.	N.A.	N.A.	N.A.	N.A.	N.A.	N.A.
32	C.I.	C.I.	50	28	C.I.	30	22	18	C.I.	30	20	12
33	C.I.	14	N.A.	N.A.	C.I.	22	16	12	12	10	N.A.	N.A.
34	C.I.	C.I.	10	N.A.	C.I.	26	18	N.A.	C.I.	10	N.A.	N.A.
35	C.I.	14	N.A.	N.A.	C.I.	16	10	N.A.	12	N.A.	N.A.	N.A.

[a]Nystatin concentration 30 μg disk^{-1}, 30 mm including disk; [b]nystatin concentration 30 μg disk^{-1}, 54 mm including disk; [c]complete inhibition; [d]no activity (inhibition zone <10 mm)

EXPERIMENTAL

Instrumentation

Microwave reactions were performed in a Biotage Initiator 2.5 microwave reactor. Melting points were determined using a Boetius PMHK apparatus (Carl Zeiss, Germany) and are not corrected. The IR spectra were recorded on a Perkin-Elmer spectrophotometer FTIR 1725X. The NMR spectra were recorded on a Bruker Ultrashield Advance III spectrometer (500 MHz) using TMS as the internal standard. The chemical shifts are expressed in ppm (δ) values and coupling constants (J) in Hz. The ESI–MS (HRMS) spectra were acquired on an Agilent Technologies 1200 Series instrument equipped with a Zorbax Eclipse Plus C18 column and a DAD detector in combination with a 6210 Time-of-Flight LC/MS instrument in the positive ion mode. The samples were dissolved in MeOH. GC/MS spectra were acquired on an Agilent Technologies 7890A instrument equipped with a DB-5 MS column and 5975C MSD and FID detector. Lobar LichroPrep Si 60 or LichroPrep RP-18 columns (Merck, Germany), coupled to a Waters RI 401 detector, were used for preparative column chromatography. Thin-layer chromatography was performed on pre-coated Merck silica gel 60 F254 and Merck RP-18 F254 plates. The solution MeOH (NH_3) stands for a combination MeOH/ /NH_3 aq. = 9:1. The compounds were analyzed for purity using an Agilent 1200 HPLC system

equipped with Quat pump (G1311B) and DAD detector 1260 VL (other details are presented in the Supplementary material to this paper). All compounds were >95 % pure.

Chemistry

(2-Bromo-5-chlorophenyl)methanediyl diacetate. A mixture of 1-bromo-4-chloro-2--methylbenzene (1.0 g, 4.9 mmol), acetic anhydride (6.4 mL), acetic acid (5.0 mL) and concentrated sulphuric acid (1.5 mL) was cooled to 0 °C in an ice bath. Then an acetic acid (5.0 mL) solution of CrO_3 (1.8 g, 18.0 mmol) was dropwisely added into the stirred mixture over 1.5 h. The mixture was stirred for the next 2 h at 0 °C. The product was filtered, washed with water (50 mL) and dried under reduced pressure.

*2-Bromo-5-chlorobenzaldehyde (**19**).* (2-Bromo-5-chlorophenyl)methanediyl diacetate (1.5 g, 4.7 mmol) was refluxed in MeOH–H_2O (15 mL, 1/1 *V*/*V*) containing H_2SO_4 (1.6 mL) for 30 min. The reaction mixture was then diluted with H_2O (15 mL) and extracted with EtOAc (3×20 mL). The combined organic layers were washed with H_2O (20 mL) and brine (20 mL), dried over Na_2SO_4 and concentrated under reduced pressure. The residue and 1 M hydrochloric acid (4.0 mL) were heated for 3 h in THF (15 mL) under reflux. The solvent was removed under reduced pressure. The residue was purified by column chromatography (SiO_2, hexane/EtOAc = 95/5). Yield: 0.84 g, 83 %.

*2-Bromo-5-methoxybenzaldehyde (**21**).* To the solution of *meta*-anisaldehyde (3.03 g, 22.3 mmol) in AcOH (5.0 mL), Br_2 (1.4 mL, 26.8 mmol, 1.2 eq.) was drop wisely added, and the reaction mixture was stirred for 36 h at room temperature. Upon completion, the reaction was quenched with a saturated solution of Na_2SO_3 (25 mL), then poured into water (10 mL), and extracted with EtOAc (3×25 mL). The combined organic layers were washed with water (3×20 mL) and brine (15 mL), dried (Na_2SO_4), and concentrated to give the desired 2-bromo--5-methoxybenzaldehyde (**21**, 3.99 g, 83 %).

*3-[(Z)-2-(2-Bromo-5-chlorophenyl)ethenyl]-4-chloropyridine (**24**).* To a suspension of phosphonium salt **22** (0.55 g, 1.2 mmol) in THF (12 mL) KO*t*-Bu (0.16 g, 1.4 mmol) was added. After 30 min, a solution of 2-bromo-5-chlorobenzaldehyde (0.26 g, 1.2 mmol) in THF (3 mL) was added over 5 min. The reaction mixture was stirred at room temperature for 16 h, when it was quenched with sat. aqueous soln. of $NaHCO_3$. The aqueous phase was separated and extracted with EtOAc (3×25 mL). The organic extracts were combined, dried over Na_2SO_4, concentrated under vacuum and purified by column chromatography (SiO_2, hexane/EtOAc = 95/5) to yield the *Z*-isomer (270 mg, 69 %).

*3-[(Z)-2-(2-Bromo-5-methoxyphenyl)ethenyl]-4-chloropyridine (**25**).* To a suspension of phosphonium salt **22** (0.14 g, 0.30 mmol) in THF (1.6 mL) was added KO*t*-Bu (40 mg, 0.36 mmol). After 30 min, a solution of 2-bromo-5-methoxybenzaldehyde (65 mg, 0.30 mmol) in THF (2 mL) was added over 5 min. The reaction mixture was stirred at room temperature and after 18 h, it was quenched with $NaHCO_3$. The aqueous phase was separated and extracted with EtOAc (3×10 mL). The organic extracts were combined, dried over Na_2SO_4, concentrated under vacuum and purified by preparative column chromatography (RP, MeOH/H_2O = = 8:2) to yield the *Z*-isomer (60 mg, 82 %).

*3-[(Z)-2-(2-Bromo-5-fluorophenyl)ethenyl]-4-chloropyridine (**26**).* To a suspension of phosphonium salt **22** (0.45 g, 0.96 mmol) in THF (12 mL) was added KO*t*-Bu (0.13 g, 1.2 mmol). After 30 min, a solution of 2-bromo-5-fluorobenzaldehyde (0.19 g, 0.96 mmol) in THF (2 mL) was added over 5 min. The reaction mixture was stirred at room temperature and after 18 h, it was quenched with saturated aqueous solution of $NaHCO_3$ (15 mL). The aqueous phase was separated and extracted with EtOAc (3×20 mL). The organic extracts were com-

bined, dried over Na_2SO_4, concentrated under vacuum and purified by preparative column chromatography (RP, MeOH/H_2O = 8:2) to yield compound **26** (196 mg, 65 %).

General procedure for Pd-catalyzed amination

A reaction tube containing a stirring bar was evacuated and backfilled with argon. The tube was then charged with $Pd(OAc)_2$ (5 mol %), JohnPhos (10 mol %) and NaO*t*-Bu (2.8 eq.) and filled with argon. Toluene was added. After stirring at room temperature for 5 min, an aryl halide (1 eq.) and amine (3 eq.) were added, the tube was filled with argon and capped. Reaction mixture was heated to 100 °C and stirred at the same temperature. Products were purified by preparative column chromatography: SiO_2, CH_2Cl_2/MeOH(NH_3) = 9/1.

*5-[3-(Pyrrolidin-1-yl)propyl]-5*H-*pyrido[4,3-b][1]benzazepine (**27**).* Following the general procedure, a mixture of 3-[(*Z*)-2-(2-bromophenyl)ethenyl]-4-chloropyridine (24 mg, 0.080 mmol), 3-(pyrrolidin-1-yl)propan-1-amine (31 μL, 0.24 mmol), sodium *tert*-butoxide (22 mg, 0.23 mmol), $Pd(OAc)_2$ (0.9 mg, 5 mol %), JohnPhos (2.4 mg, 10 mol %) and toluene (1.5 mL) was stirred at 100 °C for 48 h. Yield: 17 mg, 68 %.

*5-[3-(Pyrrolidin-1-yl)propyl]-5*H-*dipyrido[4,3-*b*:3',4'-f]azepine (**28**).* Following the general procedure, a mixture of 3,3′-(*Z*)-ethene-1,2-diylbis(4-chloropyridine) (20 mg, 0.080 mmol), 3-(pyrrolidin-1-yl)propan-1-amine (31 μL, 0.24 mmol), sodium *tert*-butoxide (22 mg, 0.23 mmol), $Pd(OAc)_2$ (0.9 mg, 5 mol %), JohnPhos (2.4 mg, 10 mol %) and toluene (1.5 mL) was stirred at 100 °C for 24 h. Yield: 17 mg, 69 %.

*3-(8-Chloro-5*H-*pyrido[4,3-*b*][1]benzazepin-5-yl)-*N,N-*dimethylpropan-1-amine (**29**).* Following the general procedure, a mixture of 3-[(*Z*)-2-(2-bromo-5-chlorophenyl)ethenyl]-4--chloropyridine (26 mg, 0.080 mmol), 3-(dimethylamino)-1-propylamine (30 μL, 0.24 mmol), sodium *tert*-butoxide (22 mg, 0.23 mmol), $Pd(OAc)_2$ (0.9 mg, 5 mol %), JohnPhos (2.4 mg, 10 mol %) and toluene (1.5 mL) was stirred at 100 °C for 48 h. Yield: 18 mg, 70 %.

*3-(8-Methoxy-5*H-*pyrido[4,3-*b*][1]benzazepin-5-yl)-*N,N-*dimethylpropan-1-amine (**30**).* Following the general procedure, a mixture of 3-[(*Z*)-2-(2-bromo-5-methoxyphenyl)ethenyl]--4-chloropyridine (26 mg, 0.080 mmol), 3-(dimethylamino)-1-propylamine (30 μL, 0.24 mmol), sodium *tert*-butoxide (22 mg, 0.23 mmol), $Pd(OAc)_2$ (0.9 mg, 5 mol %), JohnPhos (2.4 mg, 10 mol %) and toluene (1.5 mL) was stirred at 100 °C for 48 h. Yield: 10 mg, 40 %.

General procedure for the synthesis of the thiepine derivatives

A reaction tube containing a stirring bar was evacuated and backfilled with argon. The tube was charged with tris(dibenzylideneacetone)dipalladium (Pd_2dba_3, 5 mol %), dppf (10 mol %), NaO*t*-Bu (1.2 eq.), aryl halide (1 eq.) and $KSCOCH_3$ (1.2 eq.) and evacuated and backfilled with argon. The flask was capped with a rubber septum, and toluene was added. The reaction mixture was heated in a Biotage initiator 2.5 microwave at 170 °C for 60 min. After completion of the reaction, the mixture was cooled to room temperature. The products were purified by column chromatography: SiO_2, hexane/EtOAc = 8/2.

*[1]Benzothiepino[3,2-*c*]pyridine (**16**).* Following the general procedure, a mixture of 3-[(*Z*)-2-(2-bromophenyl)ethenyl]-4-chloropyridine (35 mg, 0.12 mmol), $KSCOCH_3$ (16 mg, 0.14 mmol), sodium *tert*-butoxide (14 mg, 0.14 mmol), Pd_2dba_3 (5.4 mg, 5 mol %), dppf (6.6 mg, 10 mol %) and toluene (1.5 mL) was heated in a Biotage Initiator 2.5 microwave at 170 °C for 60 min. Yield: 13 mg, 51 %.

*Pyrido[3',4':6,7]thiepino[3,2-*c*]pyridine (**17**).* Following the general procedure, a mixture of 3,3′-(*Z*)-ethene-1,2-diylbis(4-chloropyridine) (30 mg, 0.12 mmol), $KSCOCH_3$ (16 mg, 0.14 mmol), sodium *tert*-butoxide (14 mg, 0.14 mmol), Pd_2dba_3 (5.4 mg, 5 mol %), dppf (6.6

mg, 10 mol %) and toluene (1.5 mL) was heated in a Biotage initiator 2.5 microwave at 170 °C for 60 min. Yield: 15 mg, 60 %.

*8-Chloro[1]benzothiepino[3,2-*c*]pyridine (**31**).* Following the general procedure, a mixture of 3-[(*Z*)-2-(2-bromo-5-chlorophenyl)ethenyl]-4-chloropyridine (29 mg, 0.088 mmol), $KSCOCH_3$ (12 mg, 0.11 mmol), sodium *tert*-butoxide (10 mg, 0.11 mmol), Pd_2dba_3 (4.0 mg, 5 mol %), dppf (4.9 mg, 10 mol %) and toluene (1.1 mL) was heated in a Biotage initiator 2.5 microwave at 170 °C for 60 min. Yield: 6.8 mg, 32 %.

*8-Methoxy[1]benzothiepino[3,2-*c*]pyridine (**32**).* Following the general procedure, a mixture of 3-[(*Z*)-2-(2-bromo-5-methoxyphenyl)ethenyl]-4-chloropyridine (60 mg, 0.18 mmol), $KSCOCH_3$ (25 mg, 0.22 mmol), sodium *tert*-butoxide (21 mg, 0.22 mmol), Pd_2dba_3 (8.5 mg, 5 mol %), dppf (10 mg, 10 mol %) and toluene (2.3 mL) was heated in a Biotage initiator 2.5 microwave at 170 °C for 60 min. Yield: 8.4 mg, 19 %.

*8-Fluoro[1]benzothiepino[3,2-*c*]pyridine (**33**).* Following the general procedure, a mixture of 3-[(*Z*)-2-(2-bromo-5-fluorophenyl)ethenyl]-4-chloropyridine (30 mg, 0.096 mmol), $KSCOCH_3$ (13 mg, 0.12 mmol), sodium *tert*-butoxide (11 mg, 0.12 mmol), Pd_2dba_3 (4.4 mg, 5 mol %), dppf (5.3 mg, 10 mol %) and toluene (1.2 mL) was heated in a Biotage Initiator 2.5 microwave at 170 °C for 60 min. Yield: 7.6 mg, 35 %.

*8-Chloro-2-methyl-1,2,3,4-tetrahydro[1]benzothiepino[3,2-*c*]pyridine (**34**).* A solution of 8-chloro[1]benzothiepino[3,2-*c*]pyridine (17 mg, 0.068 mmol) in MeCN (3 mL) was refluxed with an excess of methyl iodide (25 μL, 0.27 mmol, 4 eq.). After 2 h, the solvent was removed under reduced pressure. The resulting yellow solid was dissolved in dry methanol (3 mL) and $NaBH_4$ (6.0 mg, 0.13 mmol) was added under an inert atmosphere at room temperature. After 15 min, the MeOH was removed under reduced pressure. The crude residue was dissolved in EtOAc and washed with H_2O. The organic layer was dried over anhydrous Na_2SO_4, concentrated under vacuum and purified by column chromatography (SiO_2, EtOAc/MeOH = 1:1) to yield the product (11.8 mg, 66 %).

*8-Phenyl[1]benzothiepino[3,2-*c*]pyridine (**35**).* A reaction tube containing a stirring bar was evacuated and backfilled with Ar. The tube was then charged with $Pd(OAc)_2$ (0.9 mg, 5 mol %), SPhos (3.2 mg, 10 mol %), phenylboronic acid (12 mg, 0.095 mmol, 1.2 eq.) and anhydrous K_3PO_4 (34 mg, 0.16 mmol, 2.0 eq.). The tube was capped with a rubber septum and filled with argon. Dry toluene (1.0 mL) was added through the septum and the resulting mixture was stirred at room temperature for 2 min. 8-Chloro[1]benzothiepino[3,2-*c*]pyridine (20 mg, 0.079 mmol) was added and the tube was sealed. The reaction mixture was heated at 100 °C for 18 h. The reaction mixture was allowed to cool to room temperature. The product was purified by column chromatography (SiO_2, hexane/EtOAc = 8/2). Yield: 11.5 mg, 50 %.

Antimicrobial evaluation

Microbroth dilution method. The antimicrobial activity was evaluated using a broth microdilution method according to NCCLS (National Committee for Clinical Laboratory Standards (2000) Approval standard document M7-A5, Villanova, PA, USA). The following Gram-negative bacterial strains used were: *Escherichia coli* (ATCC 25922), *Proteus hauseri* (ATCC 13315), *Pseudomonas aeruginosa* (ATCC 9027), *Salmonella enterica* subsp. *enterica* serovar Enteritidis (ATCC 13076) and *Klebsiella pneumoniae* (ATCC 10031). The Gram-positive bacterial strains used were: *Staphylococcus aureus* (ATCC 6538), *Micrococcus luteus* (ATCC 10240) and *M. luteus* (ATCC 4698). The employed fungal species were: *Candida albicans* (ATCC 10231), *Saccharomyces cerevisiae* (ATCC 9763) and *Aspergillus brasiliensis* (ATCC 16404). *MIC* determination was performed by a serial dilution method in sterile 96-well microtitre plates. Fresh Mueller–Hinton broth (for bacteria) and Sabouraud dextrose

broth (for fungi) were used. Stock solutions of the compounds were prepared in dimethyl sulphoxide (DMSO), and then serial dilutions of the compounds were made in the concentration range from 10,000 to 4.9 μg mL^{-1}. Amikacin (AMK) and chloramphenicol (CHL) were used as positive controls for the bacteria, while nystatin (NYT) and fluconazole (FLC) were used as positive controls for the fungi. The solvent (DMSO) served as negative control. In each well of the plate, ten microlitres of bacterial cultures (10^6 cells mL^{-1}) for antibacterial activity and 10 mL of fungal cultures (10^5 spores mL^{-1}) were inoculated. The microtiter plates were incubated at 37 °C for 24 h for the bacteria or at 28 °C for 48 h for the fungi. The *MIC* was determined as the lowest concentration that resulted in inhibition of bacterial or fungal growth.

Disk diffusion method. Antimicrobial activity was evaluated using a disk diffusion method according to NCCLS (National Committee for Clinical Laboratory Standards (1997) Approval standard document M2-A6 Performance standards for antibacterial disk susceptibility test, Wayne, PA, USA).

Antibacterial activity. The antibacterial activity was evaluated using four different strains of Gram-negative bacteria: *E. coli* (ATCC 25922), *P. hauseri* (ATCC 13315), *P. aeruginosa* (ATCC 9027) and *S. enterica* subsp. *enterica* serovar Enteritidis (ATCC 13076), and four different strains of the Gram-positive bacteria: *Clostridium sporogenes* (ATCC 19404), *S. aureus* (ATCC 6538), *M. luteus* (ATCC 10240) and *Kocuria rhizophila* (ATCC 9341). The determination of antibacterial activity was performed using the disk diffusion method. In each Petri dish (90 mm diameter), 22 mL of nutrient agar and 100 μL of bacterial suspension were added. The test substances were dissolved in CH_2Cl_2 (1 mg 100 μL^{-1}) and then 100 μL of solution was applied to a filter paper disk (8 mm in diameter) and the solvent was evaporated. The loaded disks were placed on the surface of the medium and left for 30 min at room temperature for compound diffusion. Amikacin 30 μg per filter paper disk (8 mm in diameter) was used as the positive control, while the disks of the same diameter impregnated with 100 μL of CH_2Cl_2 were used as the negative control. The plates were incubated for 24 h at 37 °C. The zones of inhibition were recorded in millimetres.

Antifungal activity. The antifungal activity was tested against three different strains: *C. albicans* (ATCC 10231), *S. cerevisiae* (ATCC 9763) and *A. brasiliensis* (ATCC 16404). Sabouraud dextrose agar was prepared according to the manufacture's instruction. Into each sterile Petri dish (90 mm diameter), 22 mL of previously prepared agar suspension was poured and 100 μL of fungi was added. The test compounds were dissolved in CH_2Cl_2 and applied on filter paper disk (8 mm in diameter) at final concentrations 1000, 500, 250, 125, 62.5 and 31.3 μg/disk. Nystatin (30 μg $disk^{-1}$) was used as a positive control while a disk impregnated with CH_2Cl_2 was used as the negative control. Petri dishes were incubated for 48 h at 28 °C. The zone of inhibition was measured in millimetres, including the disk.

CONCLUSIONS

New pyridobenzazepine and pyridobenzothiepine derivatives were synthesized using a methodology for Pd-catalyzed formation of C–N and C–S bonds.[9] Additionally, the successful transformations of thiepine **31** to tetrahydro and biphenyl derivatives opened up new possibilities for the preparation of structurally diverse substituted derivatives. All newly and previously synthesized compounds were evaluated for their *in vitro* antimicrobial activity against eight bacterial and three fungal pathogenic strains. All pyridobenzazepine derivatives

showed better antibacterial and antifungal activity than the corresponding dipyridoazepine analogues. Among the synthesized azepines, derivative **8** was the most active and showed a broad spectrum of antibacterial activity (*MIC* ranged 39–78 μg mL^{-1}). The synthesized thiepine derivatives exhibited weak antibacterial activity but, on the other hand, with the exception of **31**, all thiepines showed pronounced antifungal activity.

SUPPLEMENTARY MATERIAL

Analytical and spectral data of the compounds, as well as copies of the corresponding ^{1}H-NMR and ^{13}C-NMR spectra of the products and HPLC purity chromatograms are available electronically from http://www.shd.org.rs/JSCS/, or from the corresponding author on request.

Acknowledgments. This research was financially supported by the Ministry of Education, Science and Technological Development of the Republic of Serbia (Grant No. 172008) and the Serbian Academy of Sciences and Arts.

ИЗВОД

СИНТЕЗА И АНТИМИКРОБНА АКТИВНОСТ АЗЕПИНСКИХ И ТИЕПИНСКИХ ДЕРИВАТА

НИНА БОЖИНОВИЋ[1], ИРЕНА НОВАКОВИЋ[2], СЛАЂАНА КОСТИЋ РАЈАЧИЋ[2], ИГОР М. ОПСЕНИЦА[1] и БОГДАН А. ШОЛАЈА[1]

[1]*Хемијски факултет, Универзитет у Београду, Студентски трг 16, п. пр 51, 11158, Београд и* [2]*Институт за хемију, технологију и металургију, Универзитет у Београду, Његошева 12, 11000 Београд*

Синтетисана је серија пиридобензазепинских и пиридобензотиепинских деривата формирањем C–N и C–S веза помоћу катализатора на бази Pd и испитана је њихова *in vitro* антимикробна активност. Синтетисани пиридобензазепински деривати показују већу антибактеријску и антифунгалну активност у поређењу са одговарајућим дипиридоазепинским дериватима. Азепин **8** показао је највећу антибактеријску активност (*MIC* у опсегу 39–78 μg mL^{-1}), а азепин **12** показао се као најактивнији дериват према испитаним сојевима гљива (*MIC* у опсегу 156–313 μg mL^{-1}). Синтетисани тиепински деривати имају слабу антибактеријску активност, али са друге стране имају добру антифунгалну активност.

(Примљено 16. јануара, ревидирано 2. фебруара, прихваћено 6. фебруара 2015)

REFERENCES

1. a) B. LeDuc, in *Foye's Principles of Medicinal Chemistry*, 6th ed.; T. L. Lemke, D. A. Williams, Eds., Lippincott Williams & Wilkins, Philadelphia, PA, 2007, p. 521; b) K. C. Miles, *Emergency medicine: a comprehensive study guide*, 6th ed., J. E. Tintinalli, G. D. Kelen, J. S. Stapczynski, Eds., McGraw–Hill, New York, NY, 2004, p. 1025
2. M. Protiva, *J. Heterocycl. Chem.* **33** (1996) 497, and references cited therein
3. I. Ueda, Y. Sato, S. Maeno, S. Umio, *Chem. Pharm. Bull.* **26** (1978) 3058
4. a) L. J. Kricka, A. Ledwith, *Chem. Rev.* **74** (1974) 101, and references cited therein; b) A. Knell, D. Monti, M Maciejewski, A. Baiker, *Appl. Catal., A* **121** (1995) 139; c) G. P. Tokmakov, I. I. Grandberg, *Tetrahedron* **51** (1995) 2091; d) E.-C. Elliott, E. R. Bowkett, J. L. Maggs, J. Bacsa, B. K. Park, S. L. Regan, P. M. O'Neill, A. V. Stachulski *Org. Lett.*

13 (2011) 5592; e) T. Matsuda, S. Sato, *J. Org. Chem.* **78** (2013) 3329; f) E.-C. Elliott, J. L. Maggs, B. K. Park, P. M. O'Neill, A. V. Stachulski, *Org. Biomol. Chem.* **11** (2013) 8426
5. a) H. Shirani, T. Janosik, *J. Org. Chem.* **72** (2007) 8984; b) H. Shirani, J. Bergman, T. Janosik *Tetrahedron* **65** (2009) 8350; c) M. Saito, T. Yamamoto, I. Osaka, E. Miyazaki, K. Takimiya, H. Kuwabara, M. Ikeda, *Tetrahedron Lett.* **51** (2010) 5277
6. a) L. A. Arnold, W. Luo, R. K. Guy, *Org. Lett.* **6** (2004) 3005; b) D. Tsvelikhovsky, S. L. Buchwald, *J. Am. Chem. Soc.* **132** (2010) 14048; c) N. Della Ca', G. Maestri, M. Malacria, E. Derat, M. Catellani, *Angew. Chem. Int. Ed.* **50** (2011) 12257; d) M. Tian, A. Abdelrahman, S. Weinhausen, S. Hinz, S. Weyer, S. Dosa, A. El-Tayeb, C. E. Müller, *Bioorg. Med. Chem.* **22** (2014) 1077
7. a) C. Song, D. B. Walker, T. M. Swager, *Macromolecules* **43** (2010) 5233; b) S. Sinning, M. Musgaard, M. Jensen, K. Severinsen, L. Celik, H. Koldsø, T. Meyer, M. Bols, H. H. Jensen, B. Schiøtt, O. Wiborg, *J. Biol. Chem.* **285** (2010) 8363; c) H. Christensen, C. Schjøth-Eskesen, M. Jensen, S. Sinning, H. H. Jensen, *Chem. Eur. J.* **17** (2011) 10618; d) X. Zhang, Y. Yang, Y. Liang, *Tetrahedron Lett.* **53** (2012) 6406; e) J. Tsoung, J. Panteleev, M. Tesch, M. Lautens, *Org. Lett.* **16** (2014) 110
8. T. H. Jepsen, M. Larsen, M. Jørgensen, M. B. Nielsen, *Synlett* **23** (2012) 418
9. N. Božinović, I. Opsenica, B. A. Šolaja, *Synlett* **24** (2013) 49
10. S. Tu, L.-H. Xu, L.-Y. Ye, X. Wang, Y. Sha, Z.-Y. Xiao, *J. Agric. Food Chem.* **56** (2008) 5247
11. S. A. Snyder, T. C. Sherwood, A. G. Ross, *Angew. Chem. Int. Ed.* **49** (2010) 5146.

Journal of the Serbian Chemical Society
JSCS@tmf.bg.ac.rs • www.shd.org.rs/JSCS
J. Serb. Chem. Soc. 80 (7) S221–S245 (2015) *Supplementary material*

SUPPLEMENTARY MATERIAL TO

Synthesis and antimicrobial activity of azepine and thiepine derivatives

NINA BOŽINOVIĆ[1#], IRENA NOVAKOVIĆ[2#], SLAĐANA KOSTIĆ RAJAČIĆ[2#], IGOR M. OPSENICA[1*#] and BOGDAN A. ŠOLAJA[1**#]

[1]Faculty of Chemistry, University of Belgrade, Studentski trg 16, P. O. Box 51, 11158, Belgrade, Serbia and [2]Institute of Chemistry, Technology, and Metallurgy, University of Belgrade, Njegoseva 12, 11000 Belgrade, Serbia

J. Serb. Chem. Soc. 80 (7) (2015) 839–852

ANALYTICAL AND SPECTRAL DATA OF THE COMPOUNDS

(2-Bromo-5-chlorophenyl)methanediyl diacetate. Yield: 1.31 g, 84 %; colourless powder; m.p.: 65–67 °C; IR (ATR, cm^{-1}): 3077, 2995, 1759, 1466, 1435, 1374, 1234, 1202, 1140, 1096, 1068, 1032, 1006, 880; ^{1}H-NMR (500 MHz, $CDCl_3$, δ / ppm): 7.85 (1H, *s*), 7.54–7.50 (2H, *m*), 7.27–7.22 (1H, *m*), 2.16 (6H, *s*); ^{13}C-NMR (125 MHz, $CDCl_3$, δ / ppm): 168.23, 136.59, 134.30, 133.87, 131.12, 128.15, 120.33, 88.40, 20.66.

*2-Bromo-5-chlorobenzaldehyde (**19**).* White solid; m.p.; 72–74 °C; IR (ATR, cm^{-1}): 3351, 3060, 2884, 1689, 1578, 1455, 1390, 1283, 1248, 1188, 1125, 1091, 1031, 899, 820; ^{1}H-NMR (500 MHz, $CDCl_3$, δ / ppm): 10.30 (1H, *s*), 7.88 (1H, *d*, J = 2.5 Hz), 7.60 (1H, *d*, J = 8.5 Hz), 7.43 (1H, *dd*, J = 2.5 Hz, J = 8.0 Hz); ^{13}C-NMR (125 MHz, $CDCl_3$, δ / ppm): 190.49, 135.12, 135.03, 134.61, 134.44, 129.66, 124.61; GC-MS, *RT* 23 min (*m/z* (%)): 218.9 ([M^+] (100)), 190.9 (24), 138.0 (14), 110.0 (29), 84.0 (5), 75.0 (47), 50.0 (15).

*2-Bromo-5-methoxybenzaldehyde (**21**).* Colourless solid; m.p.: 76–78 °C; IR (ATR, cm^{-1}): 3339, 3095, 3074, 3008, 2981, 2944, 2876, 2845, 2746, 1890, 1677, 1689, 1600, 1570, 1471, 1419, 1384, 1301, 1281, 1243, 1200, 1169, 1136, 1061, 1014, 932, 866, 820; ^{1}H-NMR (500 MHz, $CDCl_3$, δ / ppm): 10.31 (1H, *s*), 7.52 (1H, *d*, J = 8.5 Hz), 7.42 (1H, *d*, J = 3.0 Hz), 7.03 (1H, *dd*, J = 3.0 Hz, J = 9.0 Hz), 3.84 (3H, *s*); ^{13}C-NMR (125 MHz, $CDCl_3$, δ / ppm): 191.77, 159.25, 134.54, 133.95, 123.11, 117.95, 112.66, 55.71; GC-MS, *RT* 14.92 min (*m/z* (%)): 213.9 ([M^+] (100)), 184.9 (15), 171.9 (14), 156.9 (8), 144.9 (16), 134.0 (10), 106.0 (20), 92.0 (16), 75.0 (18), 63.0 (55), 50.0 (9).

*,** Corresponding authors. E-mails: (*)igorop@chem.bg.ac.rs; (**)bsolaja@chem.bg.ac.rs

3-[(Z)-2-(2-Bromo-5-chlorophenyl)ethenyl]-4-chloropyridine (***24***). Colourless powder; m.p.: 65–67 °C; IR (ATR, cm^{-1}): 3107, 3081, 3054, 2967, 2928, 1754, 1732, 1639, 1572, 1546, 1471, 1449, 1404, 1386, 1309, 1267, 1224, 1204, 1166, 1109, 1087, 1023, 973, 936, 903, 882, 826; ^{1}H-NMR (500 MHz, $CDCl_3$, δ / ppm): 8.34 (1H, *d*, *J* = 5.5 Hz), 8.15 (1H, *s*), 7.51 (1H, *d*, *J* = 8.5 Hz), 7.34 (1H, *d*, *J* = 5.5 Hz), 7.07 (1H, *dd*, *J* = 2.0 Hz, *J* = 9.0 Hz), 6.92–6.89 (1H, *m*), 6.84 (1H, *d*, *J* = 11.5 Hz), 6.79 (1H, *d*, *J* = 12.0 Hz); ^{13}C-NMR (125 MHz, $CDCl_3$, δ / ppm) 150.92, 149.18, 143.29, 138.12, 133.99, 133.27, 132.17, 130.97, 130.12, 129.37, 126.03, 124.41, 121.77; (+)ESI-HRMS *m/z*: calcd. for [M+H$^+$]: 327.92899. Found: 327.92792.

3-[(Z)-2-(2-Bromo-5-methoxyphenyl)ethenyl]-4-chloropyridine (***25***). Colourless oil; IR (ATR, cm^{-1}): 3397, 3007, 2935, 2835, 2356, 1618, 1591, 1567, 1464, 1411, 1346, 1295, 1237, 1174, 1129, 1082, 1052, 1016, 934, 872, 821; ^{1}H-NMR (500 MHz, $CDCl_3$, δ / ppm): 8.32 (1H, *d*, *J* = 5.5 Hz), 8.21 (1H, *s*), 7.46 (1H, *d*, *J* = 8.5 Hz), 7.34 (1H, *d*, *J* = 5.5 Hz), 6.91 (1H, *d*, *J* = 12.0 Hz), 6.74 (1H, *d*, *J* = 12.0 Hz), 6.69–6.64 (1H, *m*), 6.46 (1H, *d*, *J* = 3.0 Hz), 3.53 (3H, *s*); ^{13}C-NMR (125 MHz, $CDCl_3$, δ / ppm): 158.59, 150.82, 148.40, 143.60, 136.99, 133.63, 133.58, 131.75, 124.84, 124.42, 115.70, 115.56, 114.33, 55.24; (+)ESI-HRMS *m/z*: calcd. for [M + H$^+$]: 323.97853. Found: 323.97699.

3-[(Z)-2-(2-Bromo-5-fluorophenyl)ethenyl]-4-chloropyridine (***26***). Colourless powder; m.p.: 109–110 °C; IR (ATR, cm^{-1}): 3403, 3041, 2924, 2850, 1632, 1599, 1574, 1550, 1460, 1413, 1344, 1275, 1221, 1177, 1143, 1102, 1082, 1032, 962, 882, 819; ^{1}H-NMR (500 MHz, $CDCl_3$, δ / ppm): 8.33 (1H, *d*, *J* = 5.5 Hz), 8.16 (1H, *s*), 7.54 (1H, *dd*, *J* = 5.5 Hz, *J* = 8.5 Hz), 7.34 (1H, *d*, *J* = 5.5 Hz), 6.90–6.75 (3H, *m*), 6.64 (1H, *dd*, *J* = 3.0 Hz, *J* = 9.0 Hz); ^{13}C-NMR (125 MHz, $CDCl_3$, δ / ppm): 161.53 (*d*, *J* = 245.5 Hz), 150.98, 149.17, 143.29, 138.22 (*d*, *J* = 8.1 Hz), 134.18 (*d*, *J* = 8.1Hz), 132.46, 131.04, 125.93, 124.41, 118.20, 117.26 (*d*, *J* = 23.5), 116.67 (*d*, *J* = 22.6 Hz); (+)ESI-HRMS *m/z*: calcd. for [M+H$^+$]: 311.95854. Found: 311.95788.

*5-[3-(Pyrrolidin-1-yl)propyl]-5*H*-pyrido[4,3-*b*][1]benzazepine* (***27***). Yellow oil; IR (ATR, cm^{-1}): 3340, 3023, 2960, 2874, 2792, 1635, 1577, 1480, 1418, 1393, 1329, 1241, 1184, 1142, 1125, 1058, 912, 830; ^{1}H-NMR (500 MHz, $CDCl_3$, δ / ppm): 8.35 (1H, *d*, *J* = 5.5 Hz), 8.17 (1H, s), 7.29–7.23 (1H, *m*), 7.05––6.98 (2H, *m*), 6.94 (1H, *d*, *J* = 8.0 Hz), 6.81 (1H, *d*, *J* = 5.5 Hz), 6.74 (1H, *d*, *J* = = 11.0 Hz), 6.60 (1H, *d*, *J* = 11.5 Hz), 3.81–3.73 (2H, *m*), 2.57–2.50 (2H, *m*), 2.46–2.37 (4H, *m*), 1.85–1.77 (2H, *m*), 1.76–1.69 (4H, *m*); ^{13}C-NMR (125 MHz, $CDCl_3$, δ / ppm): 158.79, 150.45, 150.08, 149.09, 134.12, 133.59, 129.47, 129.30, 129.19,129.06, 124.04, 121.08, 114.68, 54.23, 53.89, 48.50, 26.71, 23.37; (+)ESI-HRMS *m/z*: calcd. for [M+H$^+$]: 306.19647. Found: 306.19553.

*5-[3-(Pyrrolidin-1-yl)propyl]-5*H*-dipyrido[4,3-*b*:3',4'-*f*]azepine* (***28***). Yellow oil; IR (ATR, cm^{-1}): 3330, 3028, 2958, 2858, 2803, 1732, 1645, 1580, 1483,

1398, 1335, 1248, 1178, 1063, 929, 831; ^{1}H-NMR (500 MHz, $CDCl_3$, δ / ppm): 8.39 (2H, *d*, *J* = 5.5 Hz), 8.16 (2H, *s*), 6.76 (2H, *d*, *J* = 5.5 Hz), 6.64 (2H, *s*), 3.82–3.75 (2H, *m*), 2.58–2.52 (2H, *m*), 2.47–2.39 (4H, *m*), 1.86–1.79 (2H, *m*), 1.78–1.71 (4H, *m*); ^{13}C-NMR (125 MHz, $CDCl_3$, δ / ppm): 157.08, 150.76, 150.74, 131.19, 128.68, 115.41, 54.24, 53.60, 48.08, 26.42,23.39; (+)ESI-HRMS *m/z*: calcd. for $[M+H^+]$: 307.19172. Found: 307.19048.

*3-(8-Chloro-5*H*-pyrido[4,3-*b*][1]benzazepin-5-yl)*-N,N*-dimethylpropan-1-amine (**29**)*. Yellow oil; IR (ATR, cm^{-1}): 3387, 3026, 2944, 2858, 2817, 2768, 1682, 1578, 1472, 1391, 1327, 1241, 1184, 1132, 1101, 1058, 920, 841; ^{1}H-NMR (500 MHz, $CDCl_3$, δ / ppm): 8.37 (1H, *d*, *J* = 5.5 Hz), 8.18 (1H, *s*), 7.21 (1H, *dd*, *J* = 2.5 Hz, *J* = 8.5 Hz), 6.99 (1H, *d*, *J* = 2.5 Hz), 6.86 (1H, *d*, *J* = 8.5 Hz), 6.80 (1H, *d*, *J* = 5.5 Hz), 6.64 (2H, *s*), 3.79–3.70 (2H, *m*), 2.41–2.30 (2H, *m*), 2.25–2.11 (6H, *m*), 1.76–1.68 (2H, *m*); ^{13}C-NMR (125 MHz, $CDCl_3$, δ / ppm): 158.60, 150.62, 150.42, 147.46, 135.26, 132.73, 130.50, 129.34, 128.98, 128.96, 128.66, 122.27, 114.72, 56.89, 48.29, 45.45, 25.23; (+)ESI-HRMS *m/z*: calcd. for $[M+H^+]$: 314.14185. Found: 314.14336.

*3-(8-Methoxy-5*H*-pyrido[4,3-*b*][1]benzazepin-5-yl)*-N,N*-dimethylpropan-1-amine (**30**)*. Yellow oil; IR (ATR, cm^{-1}): 3381, 2944, 2858, 2819, 2768, 1674, 1634, 1578, 1480, 1394, 1322, 1276, 1244, 1206, 1038, 972, 938, 876; ^{1}H-NMR (500 MHz, $CDCl_3$, δ / ppm): 8.34 (1H, *d*, *J* = 5.5 Hz), 8.17 (1H, *s*), 6.87 (1H, *d*, *J* = 9.0 Hz), 6.85–6.78 (2H, *m*), 6.71 (1H, *d*, *J* = 11.5 Hz), 6.62 (1H, *d*, *J* = 11.5 Hz), 6.57 (1H, *d*, *J* = 3.0 Hz), 3.76 (3H, *s*), 3.73–3.68 (2H, *m*), 2.44–2.36 (2H, *m*), 2.20–2.15 (6H, *m*), 1.79–1.70 (2H, *m*); ^{13}C-NMR (125 MHz, $CDCl_3$, δ / ppm): 159.36, 156.12, 150.53, 150.05, 141.73, 134.76, 133.68, 129.72, 128.82, 121.96, 114.69, 114.37, 114.08, 57.07, 55.47, 48.32, 45.50, 25.40; (+)ESI-HRMS *m/z*: calcd. for $[M + H^+]$: 310.19139. Found: 310.19142.

*[1]Benzothiepino[3,2-*c*]pyridine (**16**)*. Colourless solid; ^{1}H-NMR (500 MHz, $CDCl_3$, δ / ppm): 8.49–8.42 (2H, *m*), 7.49–7.43 (1H, *m*), 7.38–7.29 (3H, *m*), 7.28–7.23 (1H, *m*), 7.13 (1H, *d*, *J* = 12.0 Hz), 6.99 (1H, *d*, *J* = 12.0 Hz); (+)ESI-HRMS *m/z*: calcd. for $[M+H^+]$: 212.05354. Found: 212.05354.

*Pyrido[3',4':6,7]thiepino[3,2-*c*]pyridine (**17**)*. Colourless solid; ^{1}H-NMR (500 MHz, $CDCl_3$, δ / ppm): 8.51 (2H, *d*, *J* = 5.5 Hz), 8.47 (2H, *s*), 7.32 (2H, *d*, *J* = 5.0 Hz), 7.09 (2H, *s*); (+)ESI-HRMS *m/z*: calcd. for $[M+H^+]$: 213.04810. Found: 213.04861.

*8-Chloro[1]benzothiepino[3,2-*c*]pyridine (**31**)*. Colourless solid; m.p.: 132–136 °C; IR (ATR, cm^{-1}): 3965, 3356, 3080, 3048, 3021, 2959, 2928, 2855, 2024, 1989, 1952, 1919, 1894, 1852, 1812, 1754, 1676, 1630, 1569, 1546, 1468, 1395, 1362, 1306, 1273, 1195, 1163, 1099, 1053, 1027, 976, 946; ^{1}H-NMR (500 MHz, $CDCl_3$, δ / ppm): 8.48 (1H, *d*, *J* = 5.0 Hz), 8.46 (1H, *s*), 7.38 (1H, *d*, *J* = = 8.5 Hz), 7.34 (1H, *d*, *J* = 5.0 Hz), 7.29 (1H, *dd*, *J* = 2.0 Hz, *J* = 8.0 Hz), 7.25–7.22 (1H, *m*), 7.03 (2H, *s*); ^{13}C-NMR (125 MHz, $CDCl_3$, δ / ppm): 150.16,

150.03, 144.42, 141.10, 135.08, 134.91, 134.75, 134.06, 131.67, 131.06, 129.68, 129.34, 126.27; (+)ESI-HRMS *m/z*: calcd. for [M+H$^+$]: 246.01387. Found: 246.01318.

*8-Methoxy[1]benzothiepino[3,2-*c*]pyridine* (***32***). Colourless oil; IR (ATR, cm^{-1}): 3597, 3392, 3022, 2928, 2841, 1710, 1591, 1564, 1471, 1389, 1324, 1278, 1243, 1210, 1176, 1153, 1068, 1030, 926, 857, 829; ^{1}H-NMR (500 MHz, $CDCl_3$, δ / ppm); 8.49–8.42 (2H, *m*), 7.38–7.32 (2H, *m*), 7.08 (1H, *d*, *J* = 12.5 Hz), 6.98 (1H, *d*, *J* = 12.0 Hz), 6.87 (1H, *dd*, *J* = 3.0 Hz, *J* = 8.5 Hz), 6.78 (1H, *d*, *J* = 3.0 Hz), 3.79 (3H, *s*); ^{13}C-NMR (125 MHz, $CDCl_3$, δ / ppm): 160.12, 149.96, 149.74, 145.36, 140.92, 135.88, 135.36, 134.14, 130.71, 126.05, 123.70, 115.60, 114.72, 55.43; (+)ESI-HRMS *m/z*: calcd. for [M+H$^+$]: 242.06341. Found: 242.06256.

*8-Fluoro[1]benzothiepino[3,2-*c*]pyridine* (***33***). Colourless solid; m.p.: 110––112 °C; IR (ATR, cm^{-1}): 3336, 2923, 2854, 1740, 1682, 1647, 1598, 1568, 1468, 1391, 1310, 1245, 1205, 1177, 1121, 1058; ^{1}H-NMR (500 MHz, $CDCl_3$, δ / ppm): 8.48 (1H, *d*, *J* = 5.5 Hz), 8.47 (1H, *s*), 7.42 (1H, *dd*, *J* = 5.5 Hz, *J* = 8.5 Hz), 7.35 (1H, *d*, *J* = 5.0 Hz), 7.09–7.01 (3H, *m*), 6.96 (1H, *dd*, *J* = 2.5 Hz, *J* = = 9.0 Hz); ^{13}C-NMR (125 MHz, $CDCl_3$, δ / ppm): 162.95 (*d*, *J* = 247.2 Hz), 150.12, 150.02, 144.73, 141.66 (*d*, *J* = 8.1 Hz), 135.13, 134.92, 134.62 (*d*, *J* = 8.1 Hz), 131.54, 127.88, 126.21, 116.81 (*d*, *J* = 21.8 Hz), 116.18 (*d*, *J* = 22.5 Hz); (+)ESI-HRMS *m/z*: calcd. for [M+H$^+$]: 230.04342. Found: 230.04321.

*8-Chloro-2-methyl-1,2,3,4-tetrahydro[1]benzothiepino[3,2-*c*]pyridine* (***34***). Pale yellow oil. IR (ATR, cm^{-1}): 3012, 2922, 2844, 2784, 2384, 1735, 1636, 1575, 1546, 1461, 1375, 1290, 1263, 1188, 1150, 1128, 1097, 1065, 813; ^{1}H--NMR (500 MHz, $CDCl_3$, δ / ppm): 7.28–7.22 (2H, *m*), 7.16 (1H, *s*), 6.88 (1H, *d*, *J* = 12.5), 6.27 (1H, *d*, *J* = 12.0), 2.99 (2H, *s*), 2.52 (4H, *s*), 2.34 (3H, *s*); ^{13}C--NMR (125 MHz, $CDCl_3$, δ / ppm) 142.04, 135.71, 133.88, 133.42, 133.36, 133.33, 132.48, 129.68, 129.16, 128.24, 58.28, 52.12, 45.15, 34.51; (+)ESI--HRMS *m/z*: calcd. for [M+H$^+$]: 264.06082. Found: 264.06121.

*8-Phenyl[1]benzothiepino[3,2-*c*]pyridine* (***35***). Colourless foam; IR (ATR, cm^{-1}): 3389, 3026, 2925, 2852, 1670, 1565, 1542, 1470, 1389 ,1265, 1174, 1069, 1045, 836; ^{1}H-NMR (500 MHz, $CDCl_3$, δ / ppm): 8.51–8.44 (2H, *m*), 7.59–7.34 (9H, *m*), 7.19 (1H, *d*, *J* = 12.5), 7.03 (1H, *d*, *J* = 12.0); ^{13}C-NMR (125 MHz, $CDCl_3$, δ / ppm): 150.00, 149.90, 144.72, 141.95, 140.00, 139.71, 136.09, 135.40, 133.38, 131.59, 130.71, 128.90, 128.52, 128.41, 127.87, 127.04, 126.27; (+)ESI-HRMS *m/z*: calcd. for [M+H$^+$]: 288.08415. Found: 288.08543.

THE SPECTRA

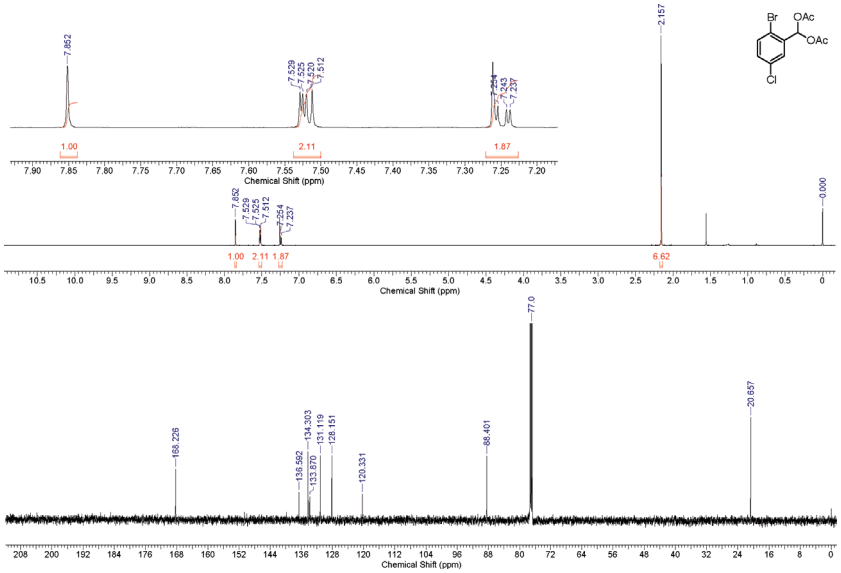

Fig. S-1. The ^{1}H- and ^{13}C-NMR spectra for (2-bromo-5-chlorophenyl)methanediyl diacetate.

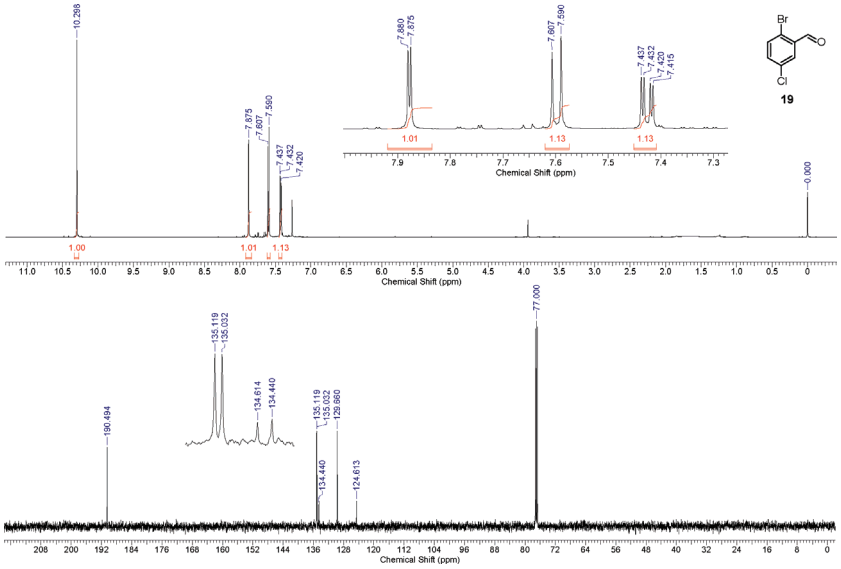

Fig. S-2. The ^{1}H- and ^{13}C-NMR spectra for compound **19**.

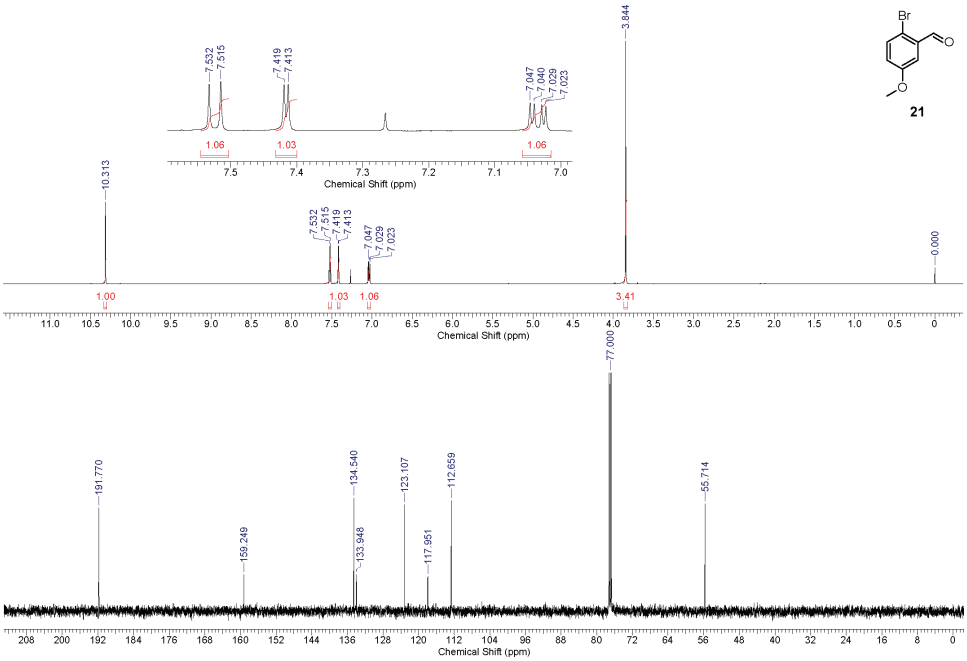

Fig. S-3. The ^{1}H- and ^{13}C-NMR spectra for compound **21**.

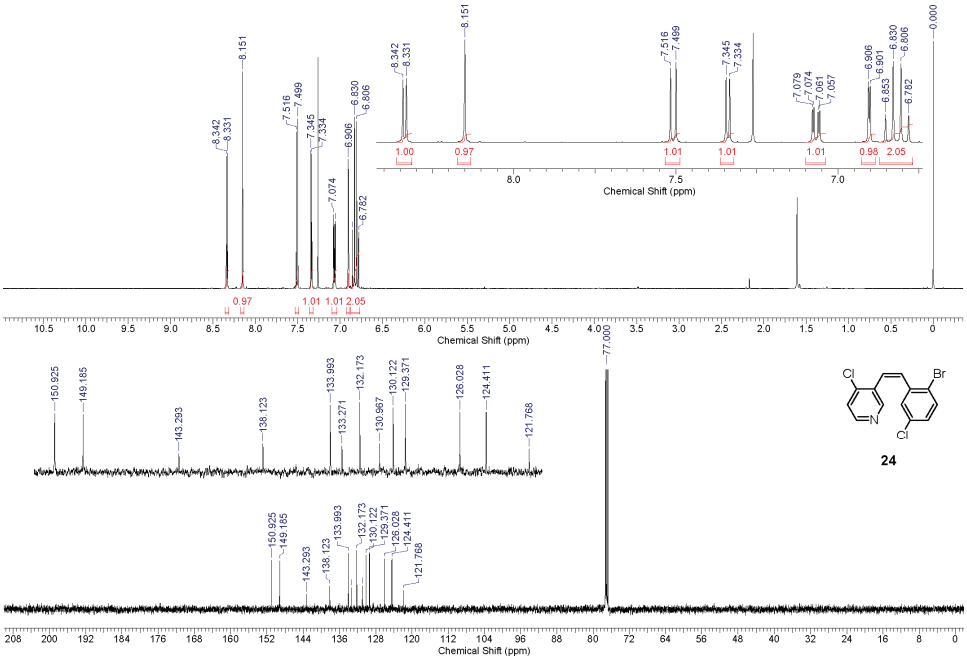

Fig. S-4. The ^{1}H- and ^{13}C-NMR spectra for compound **24**.

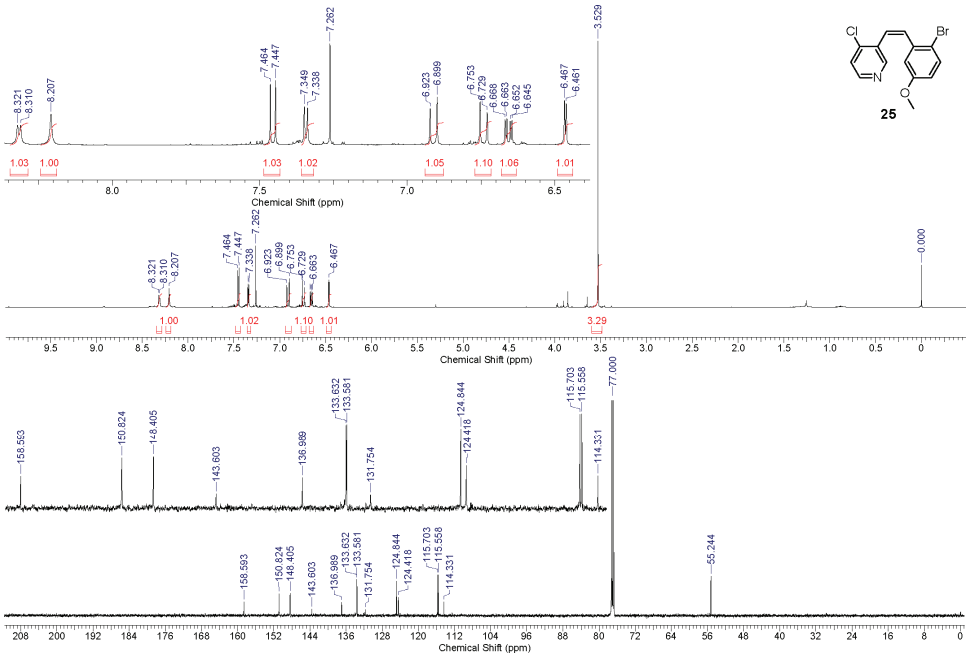

Fig. S-5. The ^{1}H- and ^{13}C-NMR spectra for compound **25**.

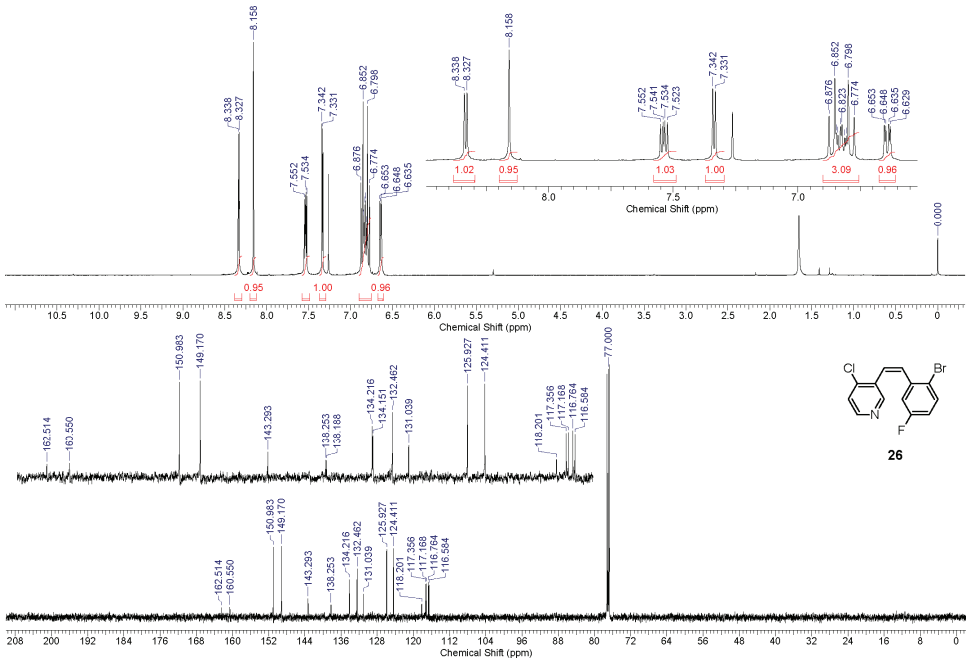

Fig. S-6. The ^{1}H- and ^{13}C-NMR spectra for compound **26**.

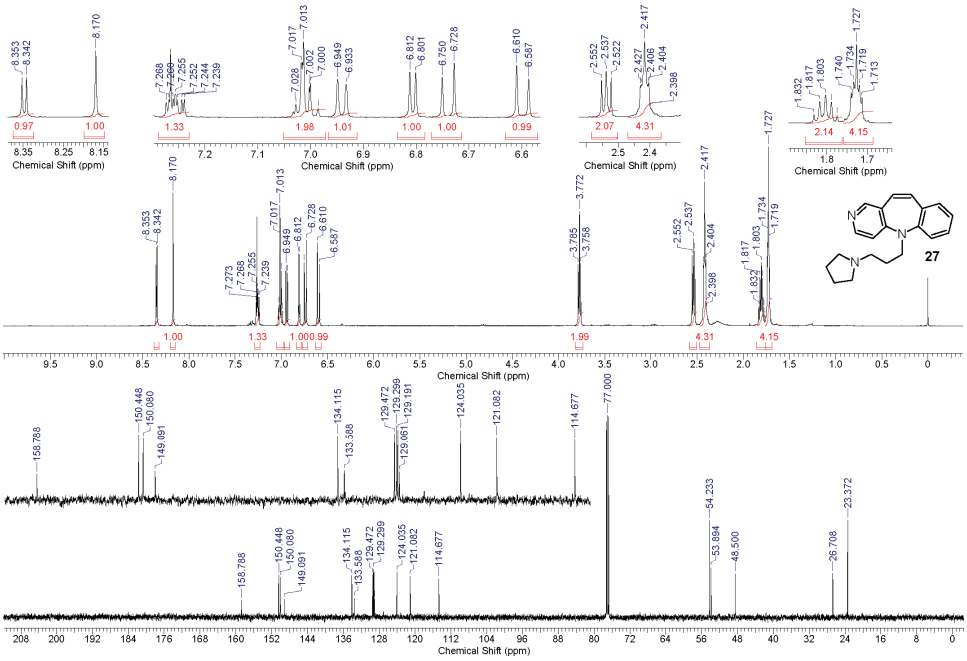

Fig. S-7. The ^{1}H- and ^{13}C-NMR spectra for compound **27**.

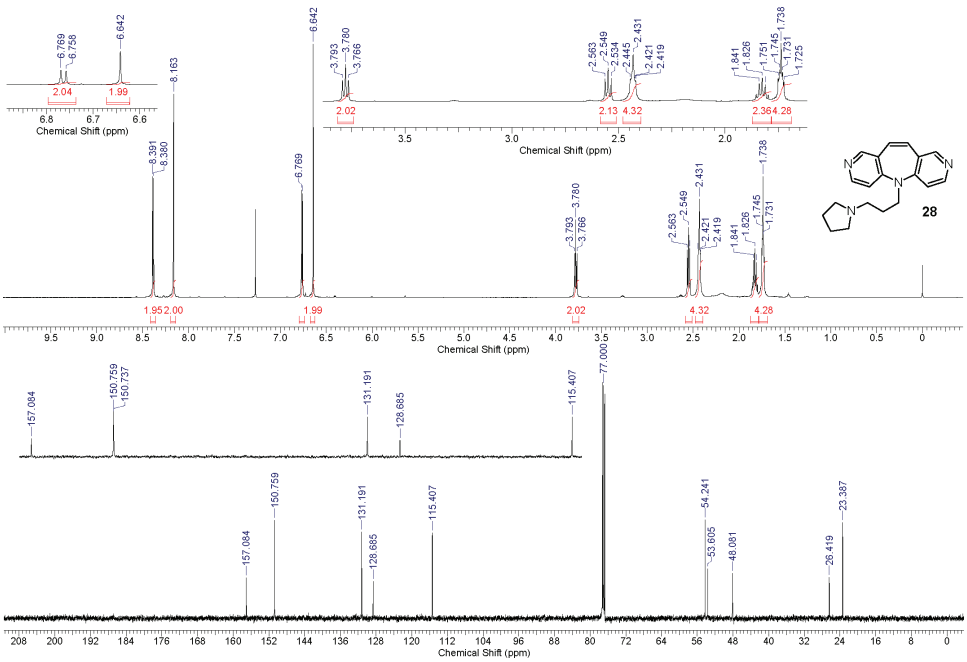

Fig. S-8. The ^{1}H- and ^{13}C-NMR spectra for compound **28**.

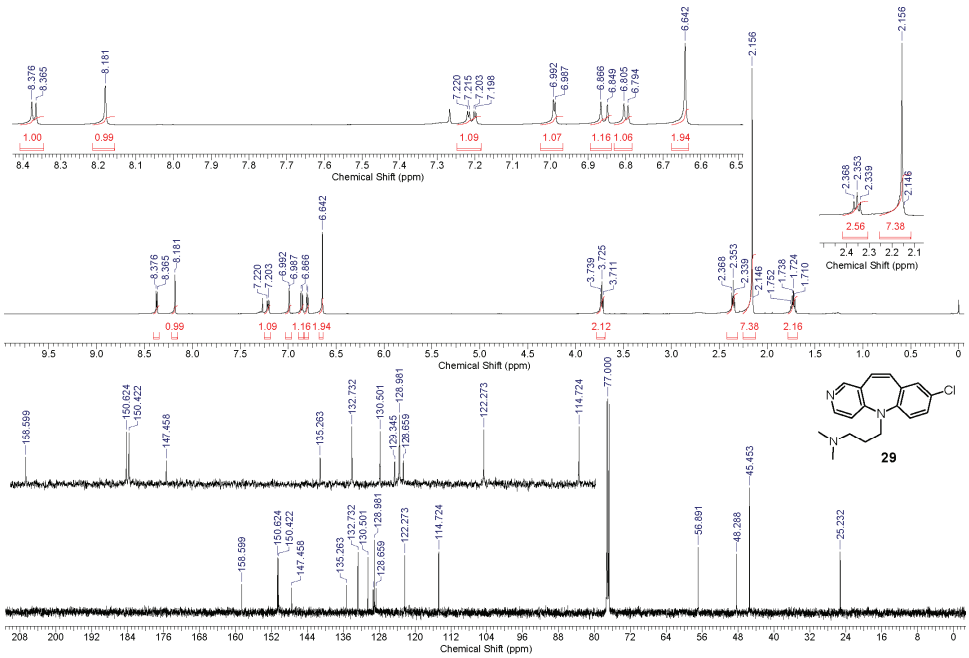

Fig. S-9. The ^{1}H- and ^{13}C-NMR spectra for compound **29**.

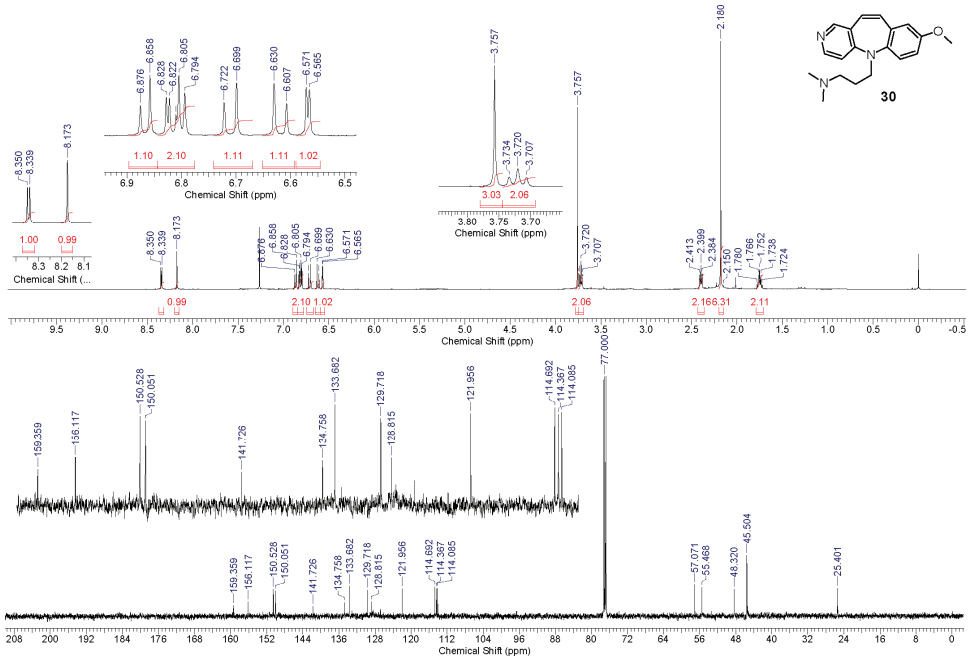

Fig. S-10. The ^{1}H- and ^{13}C-NMR spectra for compound **30**.

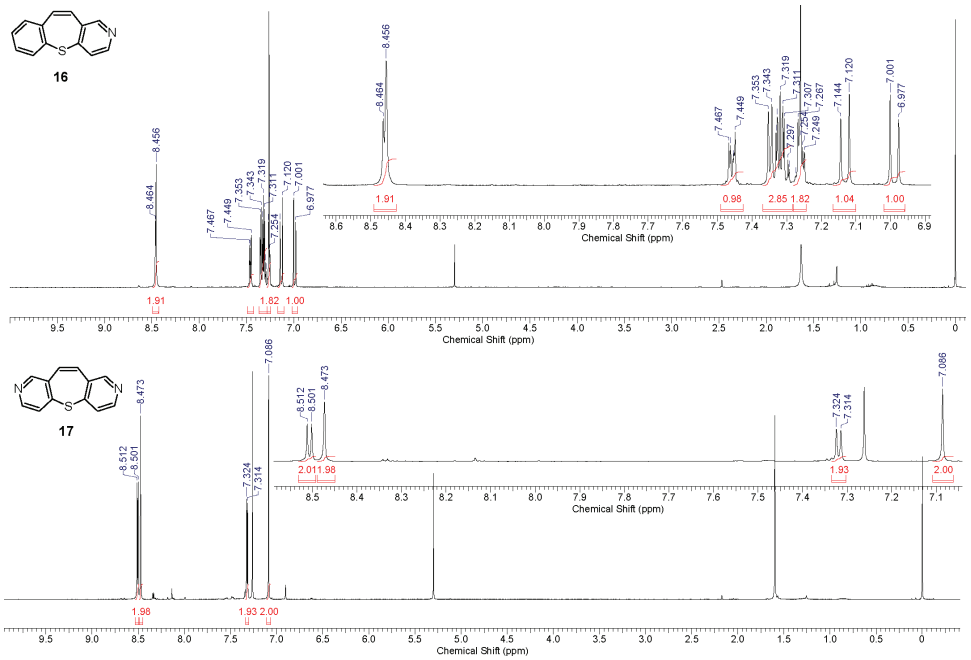

Fig. S-11. The ^{1}H-NMR spectra for compounds **16** and **17**.

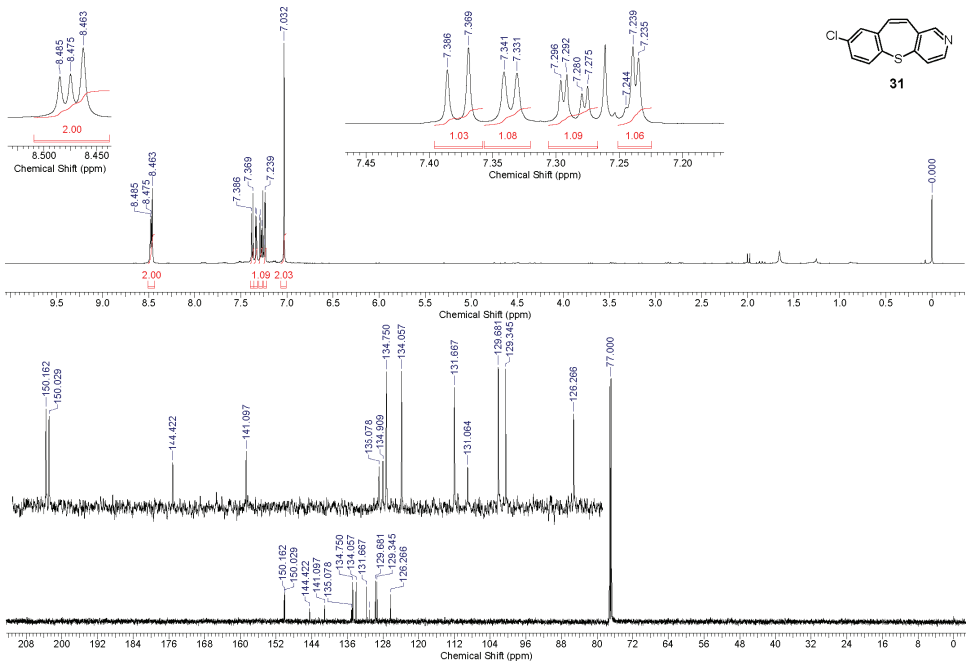

Fig. S-12. The ^{1}H- and ^{13}C-NMR spectra for compound **31**.

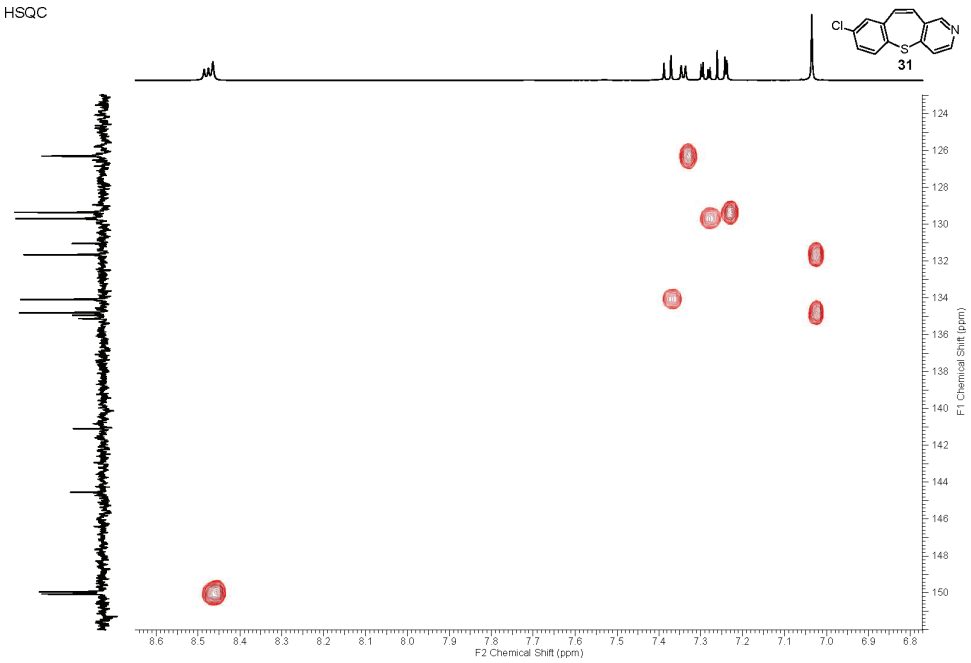

Fig. S-13. 2D ^{1}H-^{13}C HSQC spectrum for compound **31**.

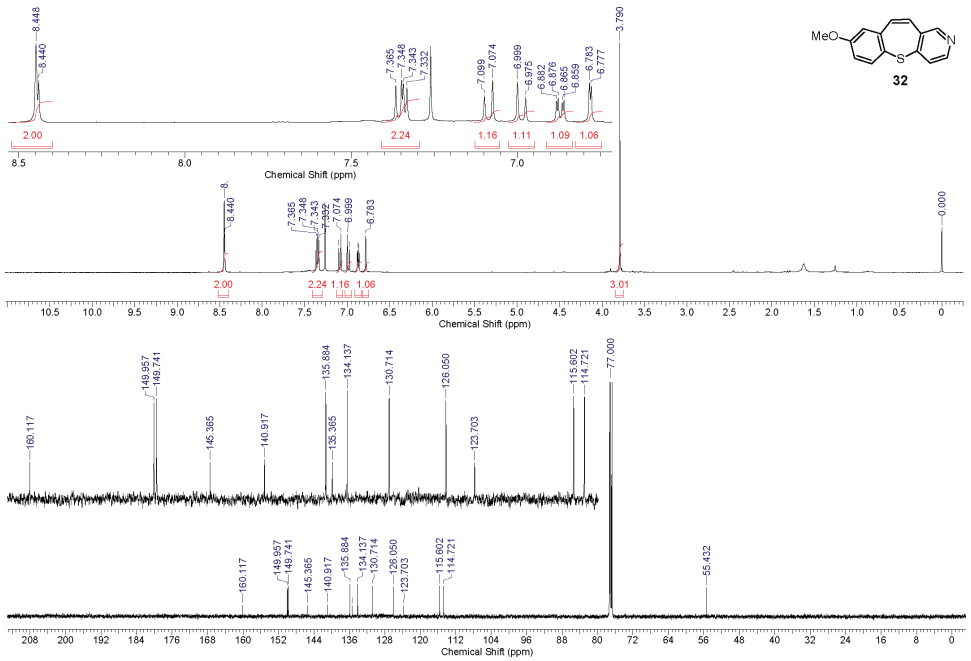

Fig. S-14. The ^{1}H- and ^{13}C-NMR spectra for compound **32**.

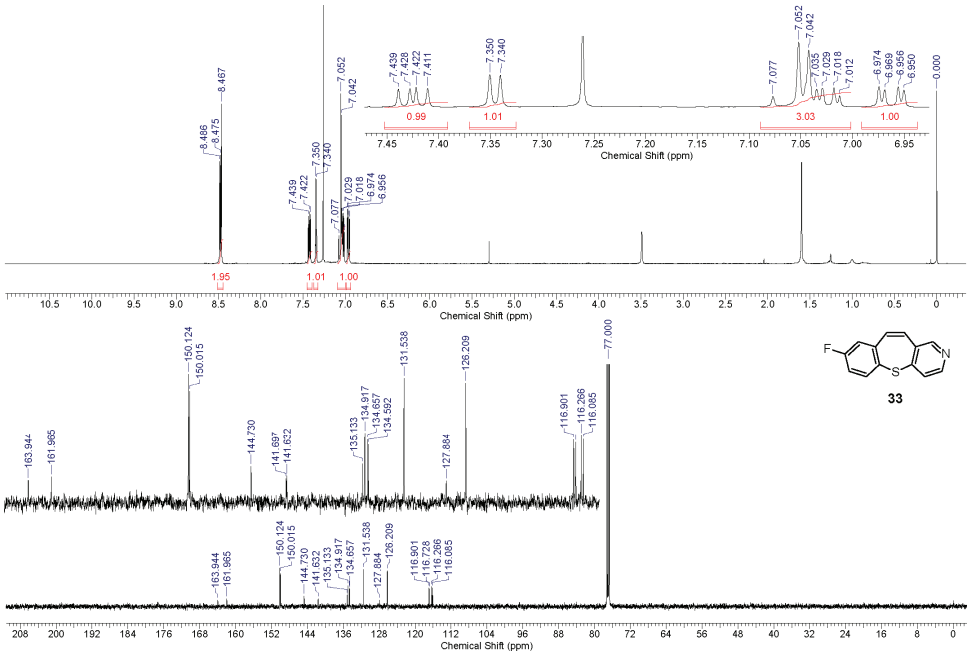

Fig. S-15. The ^{1}H- and ^{13}C-NMR spectra for compound **33**.

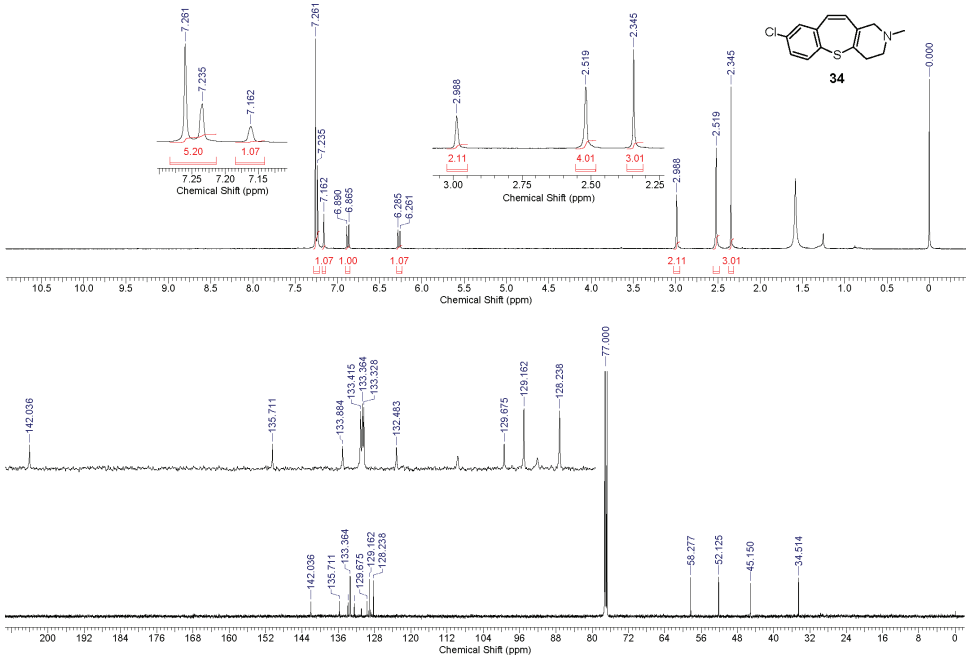

Fig. S-16. The ^{1}H- and ^{13}C-NMR spectra for compound **34**.

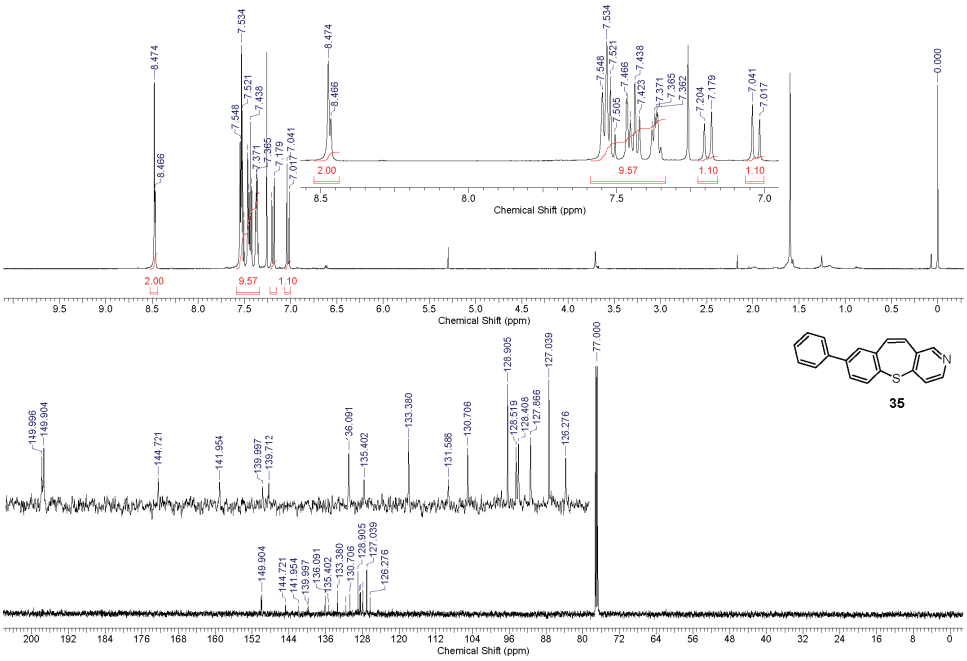

Fig. S-17. The ^{1}H- and ^{13}C-NMR spectra for compound **35**.

HPLC ANALYSES FOR PURITY

Compounds were analyzed for purity (HPLC) using a Agilent 1200 HPLC system equipped with Quat pump (G1311B), injector (G1329B) 1260 ALS, TCC 1260 (G1316A) and detector 1260 DAD VL + (G1315C). All compounds were >95 % pure. The HPLC analyses were performed in diverse systems:

Method A

Zorbax Eclipse Plus C18 4.6×150 mm, 1.8 μ, S.N. USWKY01594 was used as the stationary phase. The eluent was made from the following solvents: 0.2 % formic acid in water (A) and methanol (B). The analysis were performed at the UV max of the compounds (at 250 nm, 254 nm or 270 nm) to maximize selectivity. The compounds were dissolved in methanol; the final concentrations were ≈1 mg ml^{-1}. The flow rate was 0.5 ml min^{-1}.

Compounds **8**–**15**, **27**, **29**, **30** and **34** were eluted using the gradient protocol: 0 – 1 min 95 % A, 1 – 5 min 95 % A → 5 % A, 5 – 14 min 5 % A, 14 – 15 min 5% A → 95 % A, 15 – 16 min 95 % A.

Compounds **16**, **17**, **31**, **32** and **33** were eluted using the gradient protocol: 0 – 1.5 min 95 % A, 1.5 – 5 min 95 % A → 5 % A, 5 – 16 min 5 % A, 16 – 18 min 5 % A → 95 % A.

Compound **35** was eluted using gradient protocol: 0 – 1.5 min 50 % A, 1.5 – 3 min 50 % A → 30 % A, 3 – 6 min 30 % A → 0 % A, 6 – 9 min 0 % A → 50 % A, 9 – 12 min 50 % A.

Method B

Zorbax Eclipse Plus C18 4.6×150 mm, 1.8 μ, S.N. USWKY01594 was used as the stationary phase. The eluent was made from the following solvents: 0.2 % formic acid in water (A) and acetonitrile (B). The analyses were performed at the UV max of the compounds

to maximize selectivity. The compounds were dissolved in methanol; the final concentrations were ≈1 mg ml^{-1}. The flow rate was 0.5 ml min^{-1}.

Compounds **8 – 15**, **27**–**30** and **34** were eluted using the gradient protocol: 0 – 1 min 95 % A, 1 – 6 min 95 % A → 5 % A, 6 – 11 min 5 % A, 11 – 14 min 5 % A → 95 % A, 14 – 15 min 95 % A.

Compounds **31** and **32** were eluted using the gradient protocol: 0 – 1.5 min 95 % A, 1.5 – 5 min 95 % A → 5 % A, 5 – 16 min 5 % A, 16 – 18 min 5 % A → 95 % A, 18 – 21 min 95 % A.

Compounds **16**, **17**, **33** and **35** were eluted using the gradient protocol: 0 – 1.5 min 50 % A, 1.5 – 3 min 50 % A → 30 % A, 3 – 6 min 30 % A → 0 % A, 6 – 9 min 0 % A → 50 % A, 9 – 12 min 50 % A.

Method C

Zorbax Eclipse Plus C18 2.1 × 100 mm, 1.8 μ, was used as the stationary phase. The eluent was made from the following solvents: 0.2 % formic acid in water (A) and acetonitrile (B). The analysis was performed at the UV max of the compound to maximize selectivity. The compound was dissolved in methanol; the final concentrations were ≈1 mg ml^{-1}. The flow rate was 0.5 ml min^{-1}.

Compound **28** was eluted using gradient protocol: 0 – 1 min 95 % A, 1 – 6 min 95 % A→ 5 % A, 6 – 11 min 5 % A, 11 – 14 min 5 % A→ 95 % A, 14 – 15 min 95 % A.

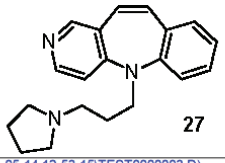

27

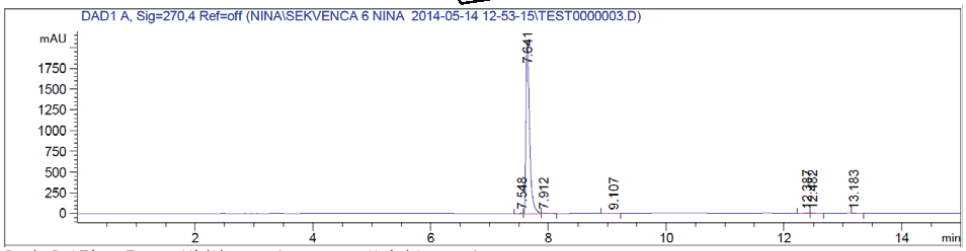

Peak #	RetTime [min]	Type	Width [min]	Area [mAU*s]	Height [mAU]	Area %
1	7.548	BV	0.0421	27.47963	9.67868	0.3071
2	7.641	VV	0.0643	8849.70117	2092.66846	98.8875
3	7.912	VB	0.0695	38.02967	7.71260	0.4249
4	9.107	BB	0.0676	8.57053	1.69131	0.0958
5	12.387	BV	0.0789	10.66416	1.63973	0.1192
6	12.482	VB	0.0758	8.40187	1.31871	0.0939
7	13.183	VB	0.0655	6.41428	1.18783	0.0717

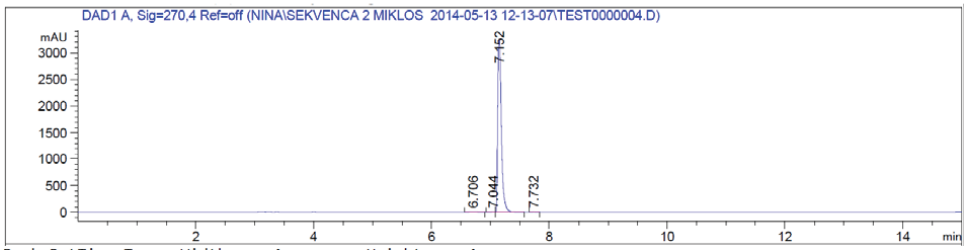

Peak #	RetTime [min]	Type	Width [min]	Area [mAU*s]	Height [mAU]	Area %
1	6.706	BB	0.1018	60.67188	8.06409	0.4295
2	7.044	BV	0.0583	17.64050	4.75640	0.1249
3	7.152	VB	0.0668	1.40376e4	3254.58472	99.3648
4	7.732	BB	0.0534	11.42744	3.18306	0.0809

Fig. S-18. HPLC elution profiles for compound **27**, upper method A and lower method B.

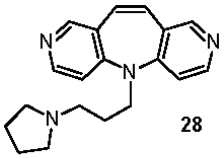

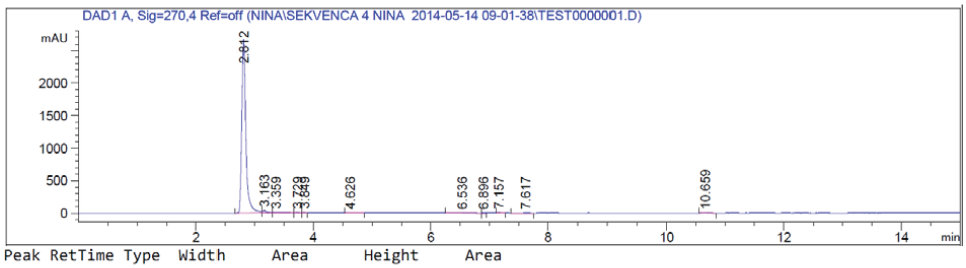

Peak #	RetTime [min]	Type	Width [min]	Area [mAU*s]	Height [mAU]	Area %
1	2.812	BV	0.0720	1.29263e4	2668.47119	96.7264
2	3.163	VV	0.0680	181.72783	36.25947	1.3599
3	3.359	VB	0.1323	77.69334	7.38394	0.5814
4	3.729	BV	0.0746	11.18529	1.79814	0.0837
5	3.849	VB	0.0528	13.06463	3.47869	0.0978
6	4.626	BB	0.0670	12.05556	2.26718	0.0902
7	6.536	BB	0.2034	70.80660	4.10196	0.5298
8	6.896	BV	0.0403	12.08752	4.57284	0.0904
9	7.157	VB	0.0537	30.49500	8.73818	0.2282
10	7.617	BB	0.1465	21.70231	1.85542	0.1624
11	10.659	BB	0.0706	6.65240	1.12362	0.0498

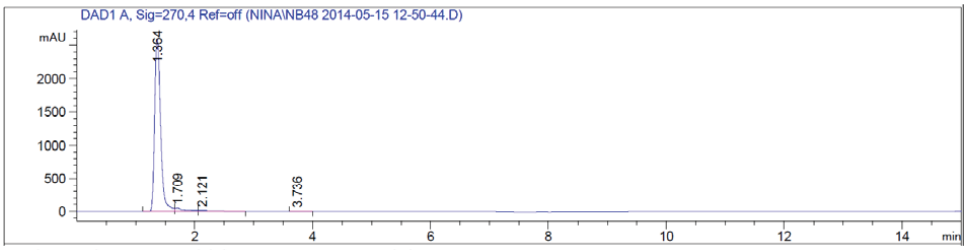

Peak #	RetTime [min]	Type	Width [min]	Area [mAU*s]	Height [mAU]	Area %
1	1.364	BV	0.1094	1.83442e4	2595.84497	96.1463
2	1.709	VV	0.1494	534.30261	46.38500	2.8004
3	2.121	VB	0.1905	181.87314	11.31421	0.9532
4	3.736	BB	0.1143	19.09738	1.97568	0.1001

Fig. S-19. HPLC elution profiles for compound **28**, upper method B and lower method C.

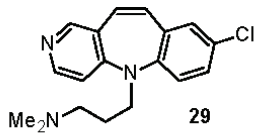

29

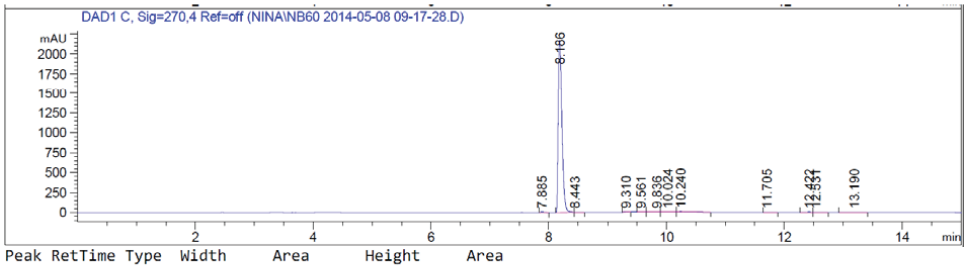

Peak #	RetTime [min]	Type	Width [min]	Area [mAU*s]	Height [mAU]	Area %
1	7.885	BB	0.0521	30.19774	8.46898	0.3108
2	8.186	BV	0.0686	9514.95703	2173.33716	97.9212
3	8.443	VB	0.0594	12.54330	2.71250	0.1291
4	9.310	VV	0.0665	15.16273	3.15939	0.1560
5	9.561	BB	0.0557	8.65833	2.33926	0.0891
6	9.836	BV	0.0888	10.26755	1.43848	0.1057
7	10.024	VV	0.1446	30.93267	2.65173	0.3183
8	10.240	VB	0.1266	49.72878	5.34056	0.5118
9	11.705	BB	0.0903	7.55613	1.07135	0.0778
10	12.422	BV	0.0827	12.88099	2.22059	0.1326
11	12.531	VB	0.0779	10.59624	1.65074	0.1090
12	13.190	BB	0.1318	13.47426	1.24490	0.1387

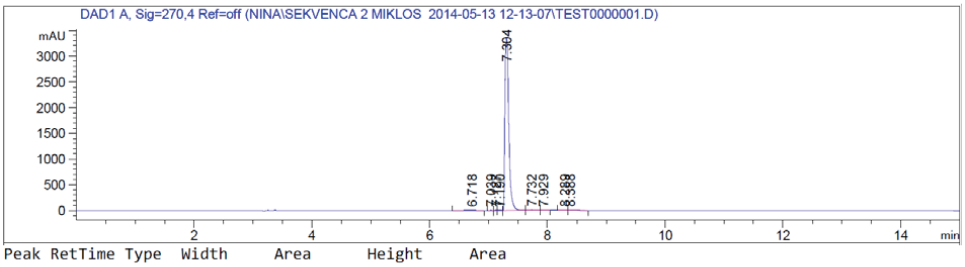

Peak #	RetTime [min]	Type	Width [min]	Area [mAU*s]	Height [mAU]	Area %
1	6.718	BB	0.1330	91.36644	8.49679	0.5849
2	7.039	BV	0.0464	9.06460	2.90784	0.0580
3	7.127	VV	0.0434	9.76251	3.31010	0.0625
4	7.190	VB	0.0506	12.45709	3.53889	0.0798
5	7.304	BV	0.0605	1.53765e4	3353.64990	98.4409
6	7.732	VV	0.1027	58.05438	7.46597	0.3717
7	7.929	VB	0.0614	25.94724	6.25671	0.1661
8	8.289	BV	0.0665	11.27498	2.34898	0.0722
9	8.388	VV	0.0794	25.60482	4.49576	0.1639

Fig. S-20. HPLC elution profiles for compound **29**, upper method A and lower method B.

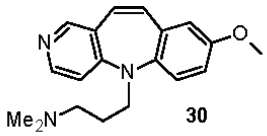

30

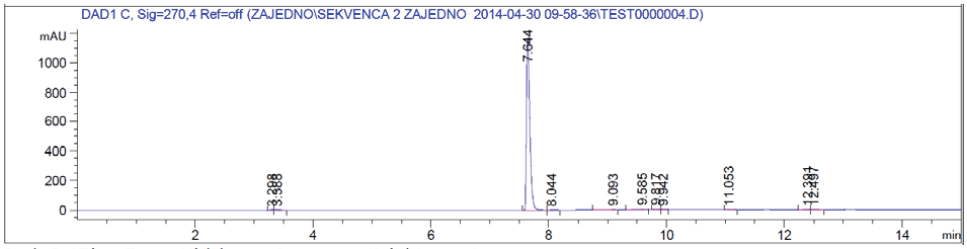

Peak #	RetTime [min]	Type	Width [min]	Area [mAU*s]	Height [mAU]	Area %
1	3.298	BV	0.0541	19.86989	4.44590	0.4148
2	3.388	VB	0.0957	25.92024	3.28044	0.5411
3	7.644	BB	0.0609	4654.91016	1170.44666	97.1709
4	8.044	BB	0.0542	9.56042	2.46893	0.1996
5	9.093	BV	0.0765	14.69546	2.54153	0.3068
6	9.585	BV	0.0967	21.04048	2.86450	0.4392
7	9.817	VV	0.0818	14.01601	2.18601	0.2926
8	9.942	VV	0.0729	7.21489	1.17937	0.1506
9	11.053	BB	0.0598	6.15833	1.36199	0.1286
10	12.391	BV	0.0779	9.03729	1.60000	0.1887
11	12.497	VB	0.0769	8.01088	1.24010	0.1672

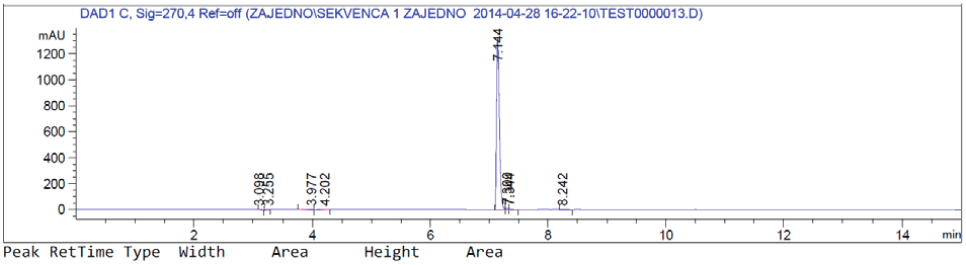

Peak #	RetTime [min]	Type	Width [min]	Area [mAU*s]	Height [mAU]	Area %
1	3.098	BB	0.2107	17.90455	1.00548	0.3835
2	3.255	BV	0.0575	31.74411	8.52148	0.6799
3	3.977	BB	0.1110	37.12119	4.31019	0.7951
4	4.202	BB	0.2120	24.82742	1.37625	0.5318
5	7.144	BV	0.0529	4503.91650	1332.61279	96.4647
6	7.300	VV	0.0456	28.15750	9.09036	0.6031
7	7.344	VB	0.0447	16.08459	5.32594	0.3445
8	8.242	VB	0.0552	9.22391	2.46256	0.1976

Fig. S-21. HPLC elution profiles for compound **30**, upper method A and lower method B.

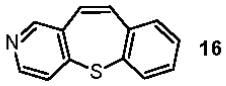

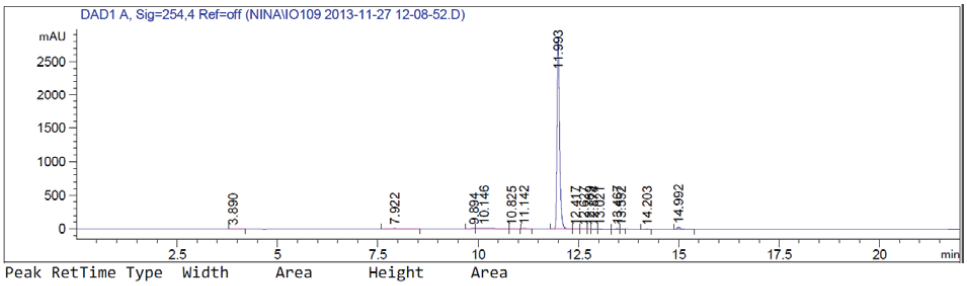

Peak #	RetTime [min]	Type	Width [min]	Area [mAU*s]	Height [mAU]	Area %
1	3.890	BB	0.1354	51.10493	4.46830	0.3845
2	7.922	BB	0.2849	89.93788	3.74178	0.6766
3	9.894	BV	0.0994	17.91653	2.14572	0.1348
4	10.146	VV	0.3010	158.23694	6.43204	1.1905
5	10.825	VB	0.0886	14.11954	2.01784	0.1062
6	11.142	BB	0.0718	47.00090	9.73345	0.3536
7	11.993	BV	0.0664	1.26492e4	2841.25220	95.1628
8	12.417	VB	0.0714	10.71146	2.07020	0.0806
9	12.627	BV	0.0756	13.77031	2.60825	0.1036
10	12.769	VV	0.0645	9.50805	1.83435	0.0715
11	12.874	VV	0.0792	21.27560	3.80838	0.1601
12	13.021	VB	0.0869	7.94873	1.23026	0.0598
13	13.467	BV	0.0704	33.00604	7.07205	0.2483
14	13.552	VV	0.0711	21.05645	4.30051	0.1584
15	14.203	BB	0.0792	6.62382	1.17682	0.0498
16	14.992	BB	0.0836	140.74380	25.42936	1.0588

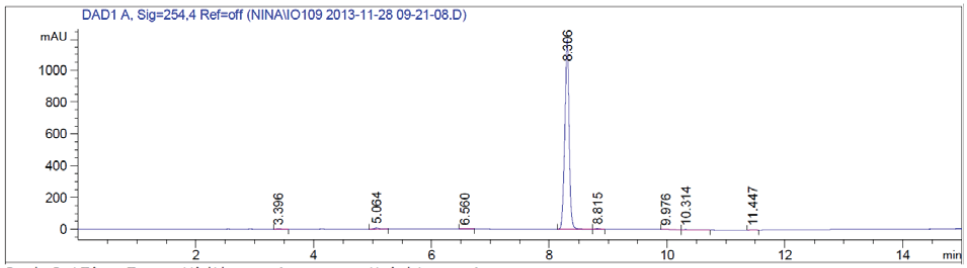

Peak #	RetTime [min]	Type	Width [min]	Area [mAU*s]	Height [mAU]	Area %
1	3.396	BB	0.0720	15.29431	3.13193	0.2476
2	5.064	BB	0.0776	40.54786	7.81269	0.6565
3	6.560	BB	0.0741	6.97794	1.30133	0.1130
4	8.306	BV	0.0744	6071.65381	1201.72729	98.3038
5	8.815	VB	0.0699	17.48453	3.67874	0.2831
6	9.976	BV	0.0849	8.77334	1.47549	0.1420
7	10.314	VB	0.1007	9.81294	1.31997	0.1589
8	11.447	BB	0.0769	5.87038	1.07236	0.0950

Fig. S-22. HPLC elution profiles for compound **16**, upper method A and lower method B.

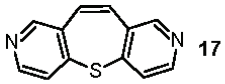

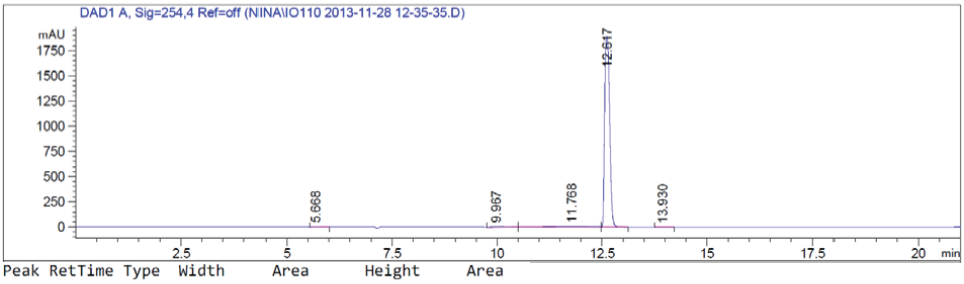

Peak #	RetTime [min]	Type	Width [min]	Area [mAU*s]	Height [mAU]	Area %
1	5.668	BB	0.1665	55.44031	3.93163	0.3390
2	9.967	BB	0.2480	212.26466	10.25258	1.2980
3	11.768	BV	0.8591	528.61047	7.19939	3.2324
4	12.617	VB	0.1346	1.55389e4	1886.19885	95.0201
5	13.930	BB	0.1145	18.06047	1.89800	0.1104

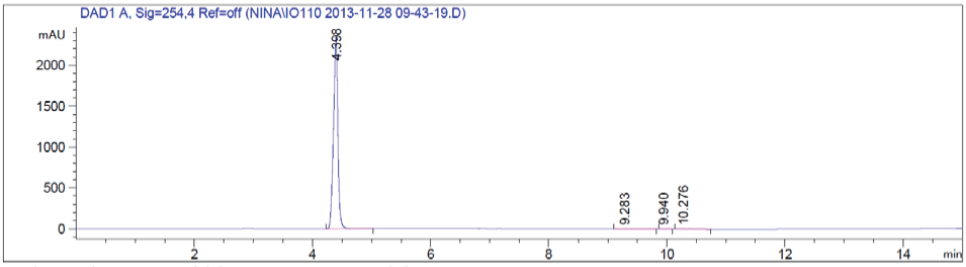

Peak #	RetTime [min]	Type	Width [min]	Area [mAU*s]	Height [mAU]	Area %
1	4.398	BB	0.0756	1.20603e4	2343.01733	99.5661
2	9.283	BB	0.1323	15.04413	1.34216	0.1242
3	9.940	BB	0.0625	6.53773	1.45172	0.0540
4	10.276	BB	0.1134	30.97738	3.47744	0.2557

Fig. S-23. HPLC elution profiles for compound **17**, upper method A and lower method B.

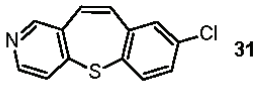

31

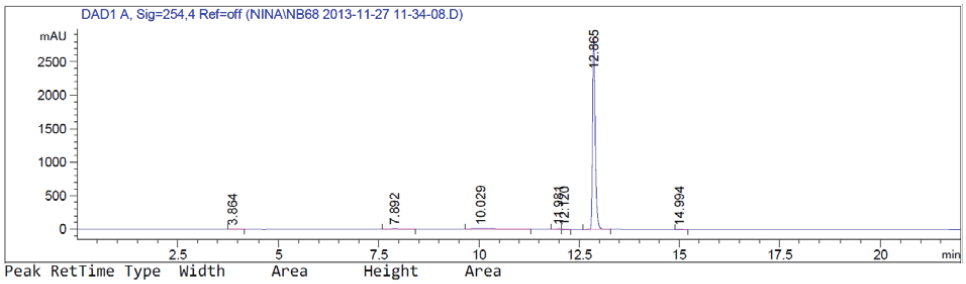

Peak #	RetTime [min]	Type	Width [min]	Area [mAU*s]	Height [mAU]	Area %
1	3.864	BB	0.1363	51.03075	4.51642	0.3738
2	7.892	BB	0.2642	83.32990	3.70753	0.6103
3	10.029	BB	0.5818	165.40530	3.33676	1.2115
4	11.981	BV	0.0749	48.58148	9.53649	0.3558
5	12.120	VB	0.0766	28.84962	5.55861	0.2113
6	12.865	BB	0.0702	1.32392e4	2847.47290	96.9678
7	14.994	BB	0.0845	36.79321	6.60021	0.2695

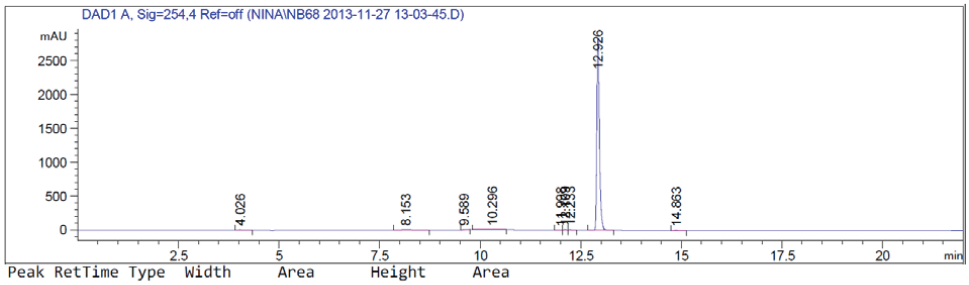

Peak #	RetTime [min]	Type	Width [min]	Area [mAU*s]	Height [mAU]	Area %
1	4.026	BB	0.1429	54.69809	4.53009	0.4222
2	8.153	BB	0.2723	87.95848	3.78935	0.6789
3	9.589	BB	0.0896	7.88486	1.05052	0.0609
4	10.296	BB	0.2664	62.62362	2.76284	0.4834
5	11.998	BV	0.0696	7.87534	1.45576	0.0608
6	12.109	VV	0.0690	44.50266	9.61065	0.3435
7	12.233	VB	0.0706	32.70956	6.51745	0.2525
8	12.926	BB	0.0676	1.26211e4	2826.88281	97.4177
9	14.863	BB	0.0809	36.30520	6.78889	0.2802

Fig. S-24. HPLC elution profiles for compound **31**, upper method A and lower method B.

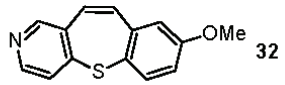

32

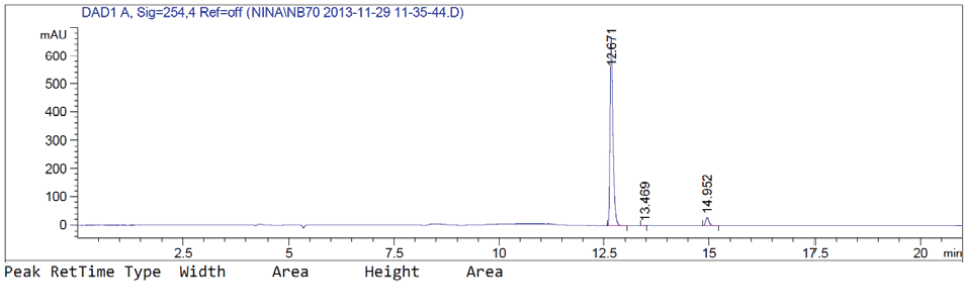

Peak #	RetTime [min]	Type	Width [min]	Area [mAU*s]	Height [mAU]	Area %
1	12.671	VB	0.0719	3203.70923	668.97974	95.0268
2	13.469	BV	0.0602	5.36811	1.07582	0.1592
3	14.952	BB	0.0843	162.29872	28.98040	4.8140

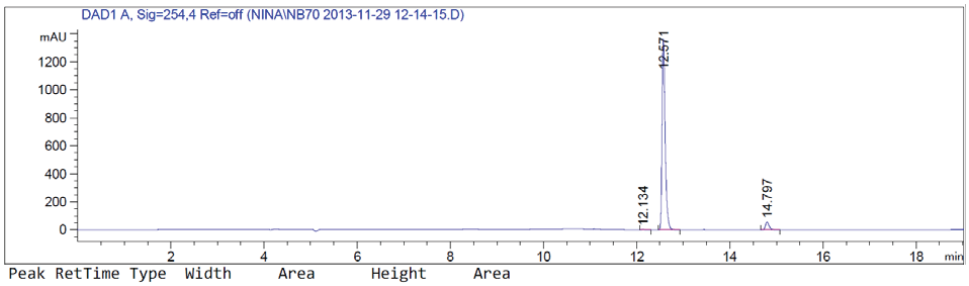

Peak #	RetTime [min]	Type	Width [min]	Area [mAU*s]	Height [mAU]	Area %
1	12.134	BB	0.0664	7.48816	1.63641	0.1128
2	12.571	VV	0.0695	6308.89600	1362.75183	95.0506
3	14.797	BB	0.0826	321.02032	58.44611	4.8365

Fig. S-25. HPLC elution profiles for compound **32**, upper method A and lower method B.

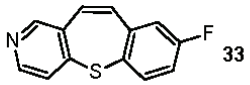

33

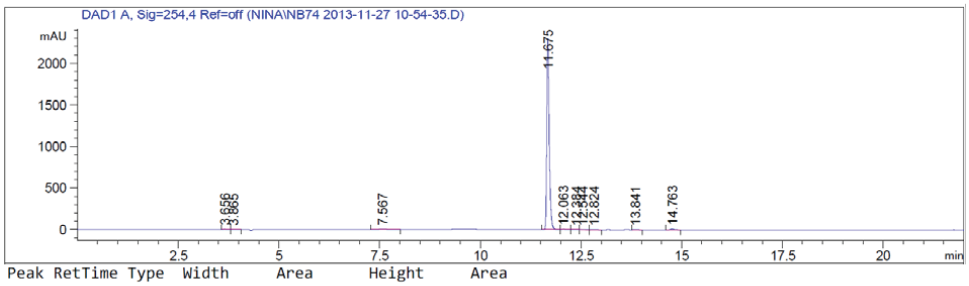

Peak #	RetTime [min]	Type	Width [min]	Area [mAU*s]	Height [mAU]	Area %
1	3.656	BV	0.1137	37.60769	4.07236	0.3791
2	3.865	VB	0.0988	15.03811	1.86089	0.1516
3	7.567	BB	0.2690	66.57471	2.90348	0.6711
4	11.675	VV	0.0635	9657.76074	2298.79932	97.3485
5	12.063	VB	0.0686	28.64441	6.06960	0.2887
6	12.384	BV	0.0865	7.78985	1.06921	0.0785
7	12.544	VB	0.0897	11.56906	1.54753	0.1166
8	12.824	BB	0.0816	12.90930	2.07346	0.1301
9	13.841	BB	0.0744	23.91412	4.90121	0.2411
10	14.763	BB	0.0788	59.00208	11.42182	0.5947

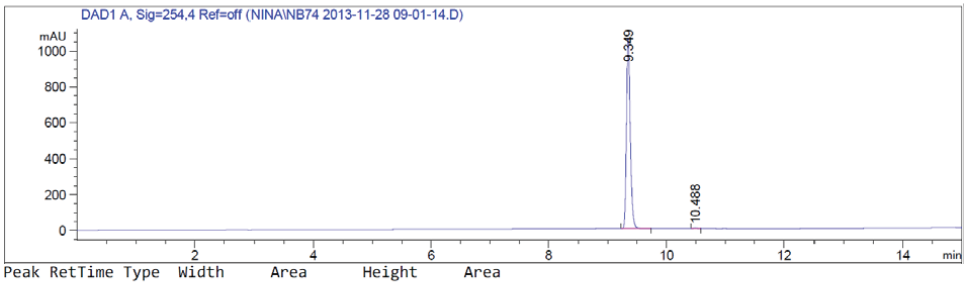

Peak #	RetTime [min]	Type	Width [min]	Area [mAU*s]	Height [mAU]	Area %
1	9.349	BB	0.0681	4770.22705	1057.27808	99.6944
2	10.488	BV	0.0546	14.62429	3.86562	0.3056

Fig. S-26. HPLC elution profiles for compound **33**, upper method A and lower method B.

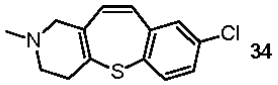

34

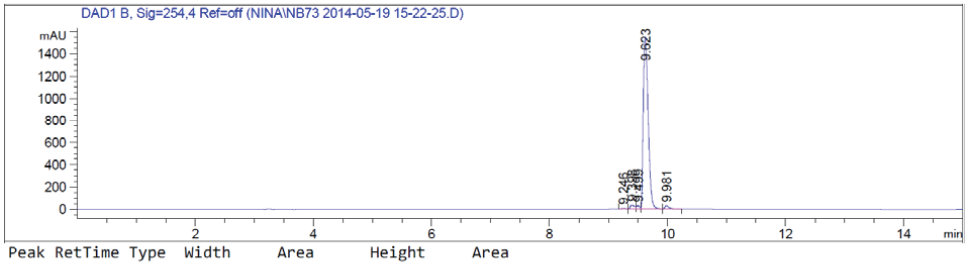

Peak #	RetTime [min]	Type	Width [min]	Area [mAU*s]	Height [mAU]	Area %
1	9.246	BB	0.0604	19.41837	4.36622	0.2094
2	9.398	BV	0.0747	160.53960	32.47451	1.7309
3	9.499	VV	0.0559	100.91060	27.13669	1.0880
4	9.623	VB	0.0919	8867.87793	1546.94482	95.6141
5	9.981	BB	0.0709	125.90913	26.26822	1.3576

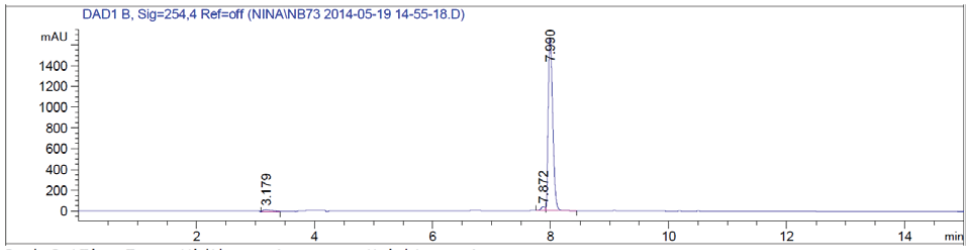

Peak #	RetTime [min]	Type	Width [min]	Area [mAU*s]	Height [mAU]	Area %
1	3.179	BV	0.1546	260.14404	21.73965	2.7939
2	7.872	BV	0.0652	176.65594	38.40658	1.8972
3	7.990	VB	0.0842	8874.45410	1664.73474	95.3089

Fig. S-27. HPLC elution profiles for compound **34**, upper method A and lower method B.

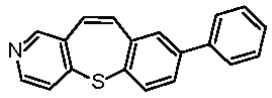

35

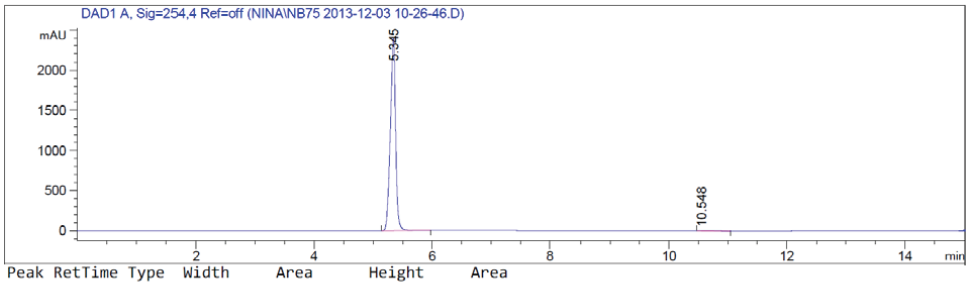

Peak #	RetTime [min]	Type	Width [min]	Area [mAU*s]	Height [mAU]	Area %
1	5.345	BB	0.0900	1.47841e4	2396.31665	99.9182
2	10.548	BB	0.0798	12.10475	2.17994	0.0818

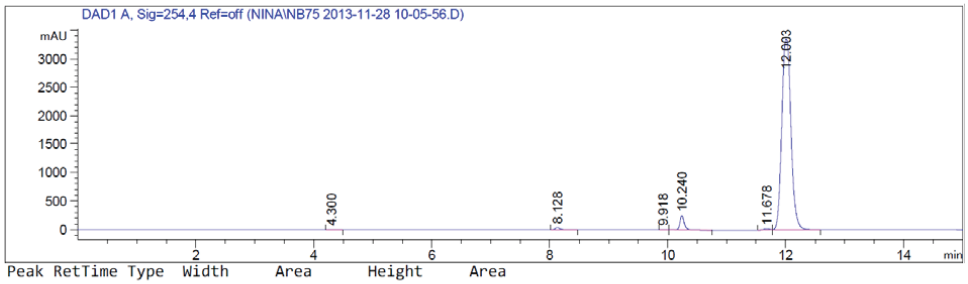

Peak #	RetTime [min]	Type	Width [min]	Area [mAU*s]	Height [mAU]	Area %
1	4.300	BB	0.0694	12.09601	2.45778	0.0320
2	8.128	BB	0.0751	189.58134	37.76797	0.5013
3	9.918	BB	0.0583	5.52080	1.30700	0.0146
4	10.240	BB	0.0742	1236.32520	249.91795	3.2690
5	11.678	BV	0.1044	136.08669	20.12759	0.3598
6	12.003	VB	0.1280	3.62400e4	3355.45898	95.8233

Fig. S-28. HPLC elution profiles for compound **35**, upper method A and lower method B.

Journal of the Serbian Chemical Society
JSCS-info@shd.org.rs • www.shd.org.rs/JSCS
J. Serb. Chem. Soc. *80* (7) 853–866 (2015)
JSCS–4764
UDC 547.9+544.473:577.15+547.918+542.913+66.094.941
Original scientific paper

Ultrafast synthesis of isoquercitrin by enzymatic hydrolysis of rutin in a continuous-flow microreactor

JUN WANG[1,2], AN GONG[2], SHUANGSHUANG GU[2], HONGSHENG CUI[2] and XIANGYANG WU[1]*

[1]*School of Environment and Safety Engineering, Jiangsu University, Zhenjiang 212013, P. R. China and* [2]*School of Biotechnology, Jiangsu University of Science and Technology, Zhenjiang 212018, P. R. China*

(Received 15 September, revised 6 November, accepted 13 November 2014)

Abstract: Isoquercitrin is a rare flavonol glycoside with a wide range of biological activities and is a key synthetic intermediate for the production of enzymatically modified isoquercitrin. In order to establish an ultrafast bioprocess for obtaining isoquercitrin, a novel continuous flow biosynthesis of isoquercitrin using the hesperidinase-catalyzed hydrolysis of rutin in a glass–polydimethylsiloxane (PDMS) microreactor was first performed. Using the developed microchannel reactor (200 μm width, 50 μm depth and 2 m length) with one T-shaped inlet and one outlet, the maximum yield of isoquercitrin (98.6 %) was achieved in a short time (40 min) under the following optimum conditions: rutin concentration at 1 g L^{-1}, hesperidinase concentration at 0.1 g mL^{-1}, reaction temperature 40 °C, and a flow rate of 2 μL min^{-1}. The value of the activation energy, E_a, of the enzymatic reaction was 4.61 kJ mol^{-1}, and the reaction rate and volume productivity were approximately 16.1-fold and 30 % higher, respectively, than those in a batch reactor were. Thus, the use of a continuous-flow microreactor for the enzymatic hydrolysis of rutin is an efficient and simple approach to achieve a relatively high yield of isoquercitrin.

Keywords: biocatalysis; continuous flow; hesperidinase; isoquercitrin; microreactor.

INTRODUCTION

Isoquercitrin is a rare flavonol glycoside with a wide range of biological activities and is a key synthetic intermediate for the production of enzymatically modified isoquercitrin (EMIQ), a new multiple food additive. Due to its significant economic benefits and ecological acceptability when compared extraction from natural sources and chemical synthesis,[1] there is a respectable number of reports indicating that isoquercitrin can be efficiently synthesized from rutin

* Corresponding author. E-mail: wuxy@ujs.edu.cn or jimwang_js@hotmail.com
doi: 10.2298/JSC150914112W

using an enzymatic hydrolysis process under suitable reaction conditions.[2] Recently, several methods for the transformation of rutin to isoquercitrin have been investigated, including acid hydrolysis,[3] heating,[4] microbial transformation,[5] and enzymatic transformation techniques.[6] Among these methods, the biotransformation of rutin to isoquercitrin using selective hydrolysis would be a feasible procedure if the transformation could be performed at a reasonable cost.

The application of commercial hesperidinase as a biocatalyst in the biosynthesis of isoquercitrin by the selective biotransformation of rutin has many advantages when compared with crude and recombinant enzymes. Hesperidinase is more technically feasible for biological manufacturing approaches by controlling the pH instead of the temperature.[3,7] Consecutively, using an ionic liquid as a novel co-solvent in the [Bmim][BF_4]–glycine–sodium hydroxide buffer (pH 9; 10:90, *V*/*V*) to improve the isoquercitrin synthesis could allow for greater dissolution of the substrates and exercise a significant effect on the conversion, yield and selectivity of the enzymatic reaction system. These results indicated that ionic liquids could effectively enhance the selective synthesis of isoquercitrin and that the reaction process is simple and eco-friendly.[4,8] In addition, the reaction time necessary to achieve the highest isoquercitrin yield of 91.41 % was reduced from 30 to 10 h, while the conversion of rutin and the yield of isoquercitrin were increased by 1.67-fold and 2.33-fold, respectively.[9] However, the industrial production of isoquercitrin is hindered by a low reaction rate in a batch bioreactor. Therefore, a longer reaction time would significantly increase the overall production cost of preparing isoquercitrin. For this reason, a better method for a high-efficiency synthesis of isoquercitrin over a short time needs to be developed.

Due to the rapid heat transfer and mixing in microreactors, reactions can be performed significantly faster than those in batch reactors, typically with increases in both yield and selectivity.[10] Recently, the use of microreactor technologies within the scope of bioprocesses as process intensification and production platforms is gaining momentum.[11,12] Compared to traditional batch reactors, this trend can be ascribed to a particular set of characteristics of microreactors, namely the enhanced mass and heat transfer, combined with easier handling and smaller volumes.[13] Haswell and co-workers demonstrated that the aldol reaction between aldehyde and silyl enol ether in the presence of tetrabutyl ammonium fluoride (TBAF) reaches completion in only 20 min when using a microreactor, *versus* 24 h in a typical reactor.[14] Herein, miniaturized devices are gaining widespread use in biocatalysis because this approach contributes to the rationalization of process development with a significant reduction in the work force, in the quantity of reagents required and in waste production, concomitantly contributing to a significant cost reduction.[15] These microreactors have been shown to outperform conventional, large-scale vessels operating in the batch mode, given the

favorable mass and heat transfer characteristics due to a large area to volume ratio and the possibility of operating in a continuous mode.[16] Under the correct conditions, microreactors can also offer better selectivity, improved yields over shorter periods, increased process control, greater safety, and flexible production.[17] Kanno and co-workers showed that an enzyme-catalyzed reaction performed homogeneously in a flow could yield higher conversions than that in the batch counterpart.[18] In this case, a solution of α-galactosidase in phosphate buffer at pH 8 was combined with a similarly buffered solution of *p*-nitrophenyl-α-D-galactopyranoside (PNPGal) in a 200 μm×200 μm microreactor. The authors were able to show that the hydrolysis in the microreactor was 5-fold faster than that in the analogous batch reaction performed in a micro-test tube.[19] However, no report has hitherto been published detailing the use of a continuous-flow microreactor to significantly enhance the hesperidinase-catalyzed synthesis of isoquercitrin.

The purpose of this study was to set up a continuous biocatalysis system for the selective and effective biotransformation of rutin to isoquercitrin in a glass–PDMS microreactor. The effects of the channel length of the microreactor, reaction temperature, rutin concentration and enzyme concentration on isoquercitrin yield were investigated. In addition, the activation energy value E_a of the enzymatic reaction was determined.

MATERIALS AND METHODS

Materials

Hesperidinase (contains both α-L-rhamnosidase and β-D-glucosidase activities, ≥1 units g^{-1} solid) produced by *Aspergillus niger* and standard isoquercitrin were purchased from Sigma (St. Louis, MO, USA). The ionic liquid 1-butyl-3-methylimidazolium tetrafluoroborate ([Bmim][BF_4]) was purchased from Shanghai Cheng-Jie Chemical Co. (Shanghai, China) and had a residual chloride content of less than 50 ppm. All the reagents used were of analytical grade except methanol and acetonitrile, both of which were of HPLC-grade (purchased from Tedia Co. (Fairfield, OH, USA)). All other solvents and reagents were of analytical grade. Water was purified using an Elga Purelab Option-Q purification system (Elga Labwater, High Wycombe, UK) and had a resistivity of not less than 18.0 MΩ cm. This water was used for cleaning procedures and in the preparation of all buffer solutions. All aqueous solutions were prepared with ultrapure water and filtered through a 0.45 μm membrane filter.

Hesperidinase-catalyzed synthesis of isoquercitrin in a continuous-flow microreactor

Hesperidinase-catalyzed synthesis of isoquercitrin was realized in a glass–PDMS microreactor with rectangular microchannels. The microreactor developed by the laser burn technology had a T-shaped inlet and an outlet channel. The main channel dimension was 200 μm wide, 50 μm deep and 2 m long (Fig. 1). The reaction substrate (rutin at pH 9 in glycine––sodium hydroxide buffer) and an enzyme solution containing 10 % [Bmim][BF_4] were both pumped into the microchannel by a two-channel syringe pump. The flow rates of the two phases were the same.

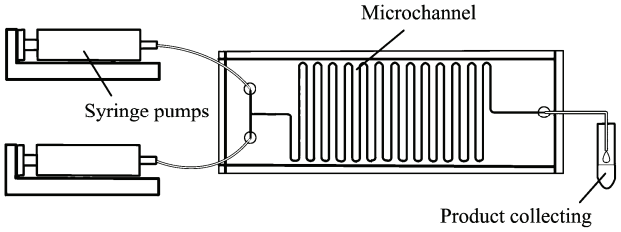

Fig. 1. Ultrafast synthesis of isoquercitrin through the enzymatic hydrolysis of rutin in a microreactor.

A scheme of isoquercitrin synthesis using hesperidinase-catalyzed hydrolysis of rutin is presented in Fig. 2, which shows the chemical structures of rutin, isoquercitrin and L-rhamnose.

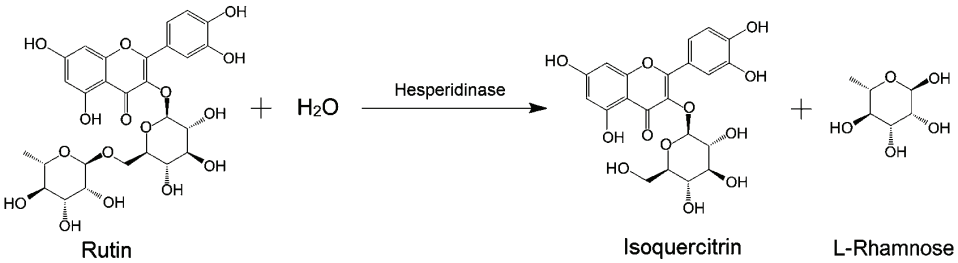

Fig. 2. Scheme of isoquercitrin synthesis using hesperidinase-catalyzed hydrolysis of rutin.

HPLC analysis and LC-MS analysis

HPLC quantitative analyses were performed using a constant flow pump (2PB0540, Beijing Satellite Factory, Beijing, China) with a UV–Vis detector (L-7420, Techcomp Co., Shanghai, China) and an N-2000 workstation (Hangzhou Mingtong S&T Ltd., Hangzhou, China). An Alltima C_{18} column (250 mm×4.6 mm, i.d.; 5 μm; from W. R. Grace & Co., Deerfield, IL, USA) was used, and the column was maintained at 30 °C. The separation and determination of rutin and isoquercitrin using the HPLC/UV method was performed on the Alltima C_{18} column with a mobile phase consisting of acetonitrile:0.02 % phosphoric acid solution (20:80, *V*/*V*) at a flow rate of 1.0 mL min^{-1}. Rutin and isoquercitrin were detected at 360 nm. All solutions were filtered through a 0.45 μm filter before injection. All of the experiments were performed in triplicate.

The isoquercitrin yield of the hesperidinase-catalyzed isoquercitrin synthesis was calculated using the following equation:

$$\text{Isoquercitrin yield (\%)} = \frac{\text{Moles of isoquercitrin}}{\text{Initial moles of rutin}} \times 100 \quad (1)$$

LC-MS was performed on a Thermo Fisher system. The LC equipment comprised a Finnigan MAT Spectra System P4000 pump, an autosampler with a 50 μL loop, a UV6000 LP diode array detector (DAD) and a Finnigan AQA mass spectrometer. LC separation was performed on the Alltima C_{18} column (250 mm×4.6 mm, i.d.; 5 μm). The mobile phases consisted of 0.1 % formic acid in water (A) and 0.1 % formic acid in acetonitrile (B). Separation was performed under the following conditions: 0–35 min, 6–100 % B; 35–40 min, back to 6

% B. The column was equilibrated for 15 min prior to each analysis. The wavelength range of the DAD was 200 to 400 nm. The flow rate was 1.0 mL min^{-1} for LC, and the column remained at 40 °C during DA detection. Electrospray ionization (ESI) was performed using nitrogen to assist nebulization (1.0 mL min^{-1} flow rate). Selected ion monitoring (SIM) in the negative ion mode with 1.6 kV capillary voltage was used, and the temperature of the curved desolvation line (CDL) and heat block were both set at 200 °C. The data were processed using Xcalibur 1.2 software. The intense peaks at *m*/*z* 463.17 in the ESI-MS spectra under negative ion mode corresponded to the deprotonated $[M–H]^-$ of isoquercitrin.[9]

Kinetic analyses

To study the kinetics of the enzymatic synthesis of isoquercitrin, the reactions were performed at different temperatures. The temperature ranged from 25 to 40 °C because the hesperidinase could exhibit its optimal activity at 40 °C and a temperature higher than 40 °C might deactivate the enzyme. The reaction rates were calculated according to:

$$k = \ln\frac{a}{(a-x)}\frac{1}{t} \quad (2)$$

where k is the reaction rate constant (min^{-1}), a is the initial concentration of substrate (μmol L^{-1}) and x is the concentration of isoquercitrin at time t, where t is the reaction time.

Statistical analyses

Triplicate experiments were performed for each investigated parameter. The standard deviation of the values was calculated to check the reliability of the results. The differences in mean values were evaluated using the analysis of variance (ANOVA) method. Significance was determined at the 95 % level of probability.

RESULTS AND DISCUSSION

The effect of microchannel length

The continuous-flow microreactor in this study consisted of channel diameters of 50 μm deep and 200 μm wide. The effects of the microreactor channel length on isoquercitrin yield using a continuous-flow microreactor at different flow rates are shown in Fig. 3A. Increasing the channel length from 0.5 to 2 m had a beneficial effect on isoquercitrin yield. When the microfluid flow rate was 2 μL min^{-1}, the channel length was 2 m, and the residence time was 40 min, a maximum yield of 34.5 % was achieved. These results indicated that the shallow depth of the microreactor channels provided for very short diffusion lengths of reaction mixtures and induced the microfluid under laminar flow condition.[20] This is one of the great advantages of using microscale reactors for rapid reactions.

These results sufficiently confirmed that reducing the flow rate to induce a prolonged residence time would facilitate enzymatic reactions. However, when the liquid flow rate was too fast, the reaction droplets of hesperidinase increased friction with the inner wall of the channel. This phenomenon prompted the increased shear stress and local overheating and deactivated the enzyme.[21] Therefore, the yield of isoquercitrin was reduced.

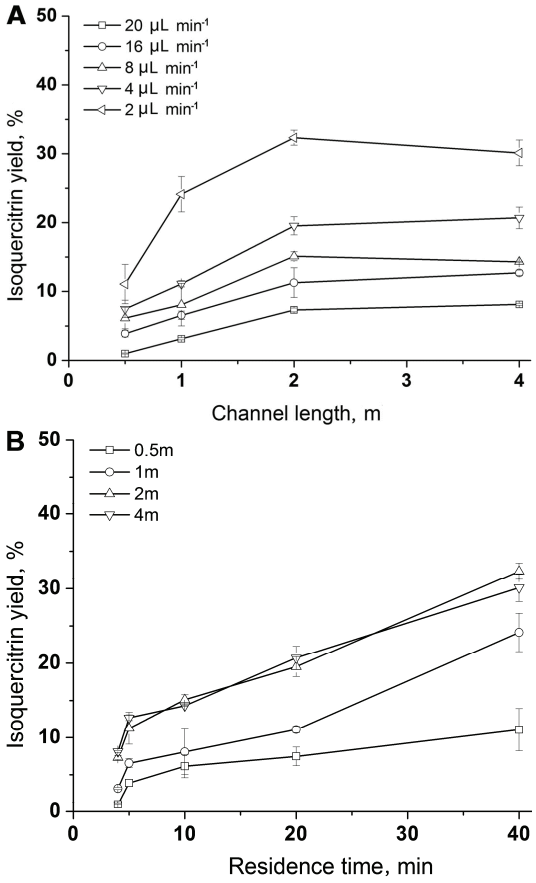

Fig. 3. Using the continuous-flow microreactor developed to synthesize isoquercitrin by the enzymatic hydrolysis of rutin. A) Effects of the channel length of the microreactor on the isoquercitrin yield at different flow rates; B) effects of residence time on the isoquercitrin yield. Reaction temperature: 40 °C; rutin concentration: 1 g L^{-1}; hesperidinase concentration: 0.01 g mL^{-1}.

The effects of residence time on the efficiency of isoquercitrin synthesis are shown in Fig. 3B. Using a 2 m long channel, the residence time (4–40 min) of the reaction mixture in the microreactor was tuned by varying the flow rates (20–2 μL min^{-1}). As expected, the reaction appeared to be favored by an increase in the residence time. When the enzymatic reaction was conducted at 20 μL min^{-1}, only a 29.0 % yield was obtained, while at 2 μL min^{-1}, a maximum yield of 34.5 % was achieved. Thus, a 2 m long channel was chosen for further experiments.

The effect of reaction temperature

The effects of temperature on isoquercitrin yield using a continuous-flow microreactor at different flow rates are shown in Fig. 4A. The isoquercitrin yield initially increased with temperatures ranging from 25 to 40 °C, whereas higher temperatures led to a decline in isoquercitrin yield and enzyme denaturation, which lowered the efficiency of enzymatic hydrolysis. The yield had a similar

tendency at different flow rates. An optimal temperature of 40 °C at 2 μL min^{-1} was chosen to promote the maximum yield of isoquercitrin.

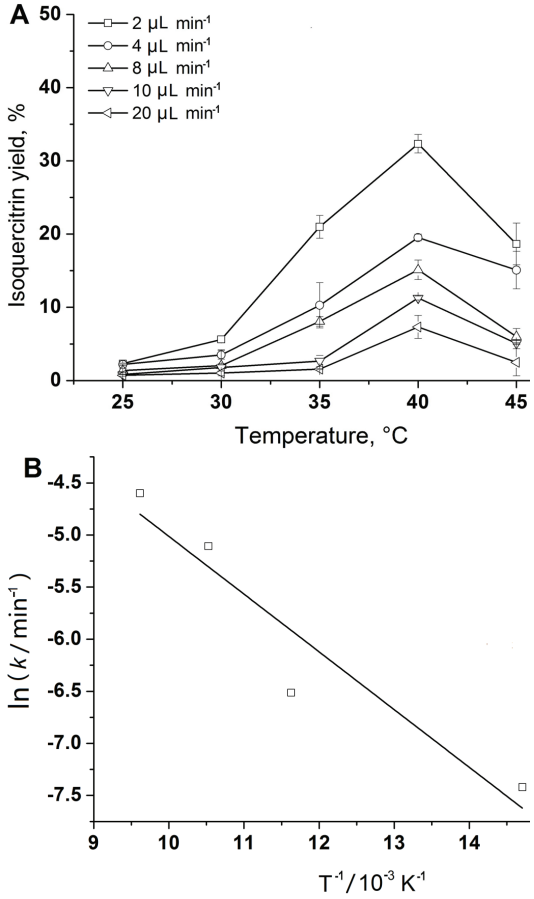

Fig. 4. A) Effects of temperature on the isoquercitrin yield and B) the Arrhenius plot of ln k *vs.* T^{-1} using the developed continuous-flow microreactor at different flow rates at 40 °C. Rutin concentration: 1 g L^{-1}; hesperidinase concentration: 0.01 g mL^{-1}.

An analysis was performed to study the effects of temperature on reaction rate and energy of activation in the enzymatic synthesis of isoquercitrin. Depending on the reaction rate constant values at various reaction temperatures, the value of energy of activation could be further estimated according to the Arrhenius equation:

$$\ln k = \frac{E_a}{RT} + \ln A \tag{3}$$

where k is the reaction rate constant, A is the frequency factor and E_a is the energy of activation.

An Arrhenius plot made based on ln k *vs.* the reciprocal of temperature is shown in Fig. 4B. The reaction rate increased with increasing temperature. In

addition, the activation energy E_a could be obtained from the slope of the straight line. Thus, when the flow rate was 2 μL min^{-1}, the E_a of the reaction was calculated to be 4.61 kJ mol^{-1}. E_a represents the ability of the enzymatic reaction to overcome the original "energy barrier". In this continuous-flow microreactor, the E_a value is relatively small, and the enzymatic reaction occurs more easily. These results suggest that heat transfer was compromised in the developed microreactor with rectangular microchannels and that local temperature changes were significant. Heat transfer was enhanced as the flow rate increased; therefore, the heat dissipates faster from the active site of the enzyme,[22] which subsequently decreased the yield of isoquercitrin when the temperature exceeded 40 °C.

The effect of rutin concentration

The effects of the rutin concentration on isoquercitrin yield using a microreactor at different flow rates are shown in Fig. 5A. As expected, the yield of isoquercitrin increased with increasing inlet substrate concentration and lowering the flow rate. At inlet concentrations of rutin of 1 g L^{-1}, a yield of isoquercitrin of

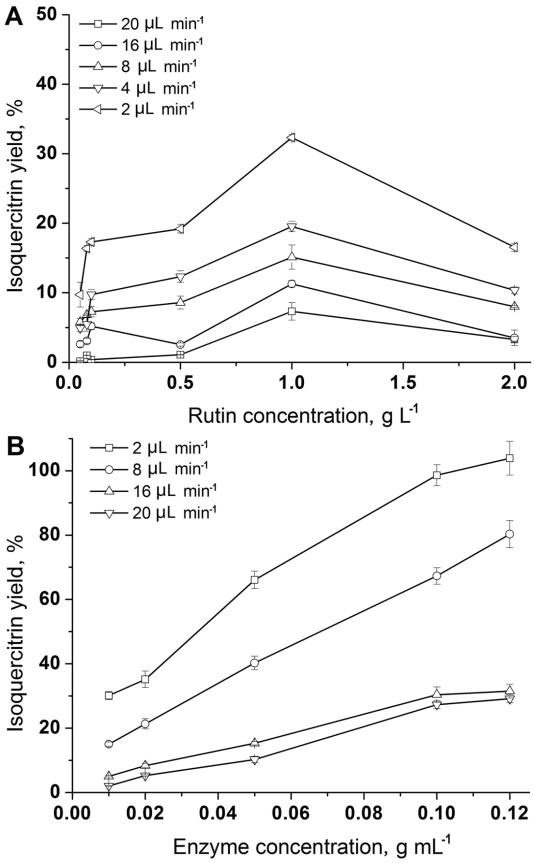

Fig. 5. A) Effects of rutin concentration and B) enzyme concentration on the isoquercitrin yield using the developed continuous-flow microreactor at different flow rates. Reaction temperature: 40 °C; A) hesperidinase concentration: 0.01 g mL^{-1}; B) rutin concentration: 1.0 g L^{-1}.

approximately 34.5 % was obtained after 40 min. However, further increasing the inlet concentration to 2 g L^{-1} decreased the yield of isoquercitrin significantly. The reasons mainly include two aspects: 1) the hesperidinase concentration in this experiment was very limited, resulting in an enzyme that could not fully contact with the substrate; 2) substrate inhibition was present and enzyme denaturation was detected at a high substrate concentrations. In addition, higher substrate concentrations caused clogging in continuous flow reactors.[23] The inlet concentration of rutin used in the microreactor was in agreement with a previous study.[9] However, some studies reported that the inlet substrate concentrations used in a microreactor were 10 times lower than those in a batch reactor.[24]

Hence, the presented microreactor technology is economically feasible for the large-scale production of isoquercitrin without reducing the substrate concentration of rutin. Usually, substrate inhibition and product degradation were two possible reasons for the decrease in isoquercitrin conversion when the concentration of rutin was higher. Hypothetically, when the concentration of rutin is 1 g L^{-1}, a higher isoquercitrin yield should be obtained. However, if isoquercitrin is abundantly produced and the substrate concentration is appropriately increased, the yield and efficiency should be greatly improved. Thus, 1 g L^{-1} of rutin was chosen as a suitable substrate concentration for further study.

The effect of hesperidinase concentration

The effects of the hesperidinase concentration on isoquercitrin yield with different flow rates are shown in Fig. 5B. Under identical conditions of temperature and substrate concentration, the effect of the concentration of hesperidinase in the range of 0.01 to 0.12 g mL^{-1} on isoquercitrin yield at different flow rates was observed. An increase in the concentration of hesperidinase up to 0.1 g mL^{-1} had a positive effect on the isoquercitrin yield. When the concentration of hesperidinase was 0.1 g mL^{-1}, the yield of isoquercitrin was near 98.6 %. Further increases in the enzyme concentration up to 0.12 g mL^{-1} increased the yield of isoquercitrin only slightly. Hence, from an economic perspective, the best hesperidinase concentration was 0.1 g mL^{-1}.

The enzyme concentration plays an important role in enzymatic syntheses,[25] and the number of active sites in a particular enzyme can affect the reaction rate.[26] In addition, the separation of the product can be easily attained using triacetin as an organic phase to extract isoquercitrin from the reaction mixture after completion of the enzymatic reaction.[27] As expected, the yield under steady-state conditions increased with decreasing flow rate. A yield of approximately 98.6 % was achieved at an inlet rutin concentration of 1 g mL^{-1} and a flow rate of 2 μL min^{-1}. The aqueous phase with the hesperidinase and unreacted rutin could be recycled, which makes this process much more economic.

The effect of flow rate and residence time

To investigate the effect of flow rate on the hesperidinase-catalyzed synthesis of isoquercitrin by the enzymatic hydrolysis of rutin, five different flow rates, *i.e.*, 2, 4, 8, 16 and 20 μL min^{-1}, were selected for testing. As shown in Figs. 3A, 4A, 5A and 5B, different isoquercitrin yields were obtained at various flow rates. In every figure, a flow rate of 2 μL min^{-1} resulted in a higher isoquercitrin yield than those obtained at the other rates. As the flow rate was further increased, the isoquercitrin yield was clearly reduced and reached the lowest yield at 20 μL min^{-1}. In particular, Fig. 5B shows that the isoquercitrin yield was the highest, up to 98.6 %, at a flow rate of 2 μL min^{-1}.

By using longer channels and reducing the flow rate, the residence time increases. Longer residence times allow a more complete, full contact between substrates and enzymes. However, increasing the channel length from 2 m to 4 m did not obviously change the isoquercitrin yield, possibly because the stability of hesperidinase was lower at longer channel lengths. In addition, the pressure would increase with a further reduction in the channel dimension, and this is disadvantageous to the actual operation.

Under different flow rates in a 4 m long microreactor with rectangular microchannels, the faster the flow rate, the longer was the residence time of the hesperidinase-catalyzed synthesis of isoquercitrin by enzymatic hydrolysis of rutin. In this microreactor, flow rates ranging from 2 to 20 μL min^{-1} were employed, and the corresponding residence time was decreased from 2.5 h to 15 min. The isoquercitrin yield increased as the residence time was extended, which was most likely due to the increase in the mass transfer of the substrate towards hesperidinase molecules because of the increase in the reaction time.[28,29] As the residence time increased, interactions between the substrate and enzyme increased, resulting in a higher yield of isoquercitrin. This result indicates that the flow rate is a vitally important factor for the operation of a microreactor with rectangular microchannels. At low flow rates, the increased residence time in the reaction system allowed for the completion of the enzymatic synthesis reaction.[30] At high flow rates, the residence time was most likely not long enough for the completion of enzymatic synthesis because the synthesis of isoquercitrin was not fast enough to complete the enzymatic reaction in such a short time.

Comparing the technology between the microreactor and the batch reactor

A maximum isoquercitrin yield of 98.6 % was obtained in the continuous-flow microreactor after 40 min, which was 16.1-fold faster than the yield of 91.4 % in the batch reactor (10 h, Table I). The calculated volume productivity at a rutin inlet concentration of 1 g L^{-1} was 3.23 μM min^{-1} at a residence time of 40 min, which was more than 1.2-fold higher than that reported within the batch reactor,[9] where the highest volume productivity was 2.49 μM min^{-1}. Thus, the

volume productivity in the microreactor was 30 % higher than that in the batch reactor. Herein, although isoquercitrin production in a specific time was lower than that in a conventional reactor, the reaction time in the microreactor was 14 times lower than that in a batch reactor. Considering these two factors, biocatalysis technology in the microreactor could be a feasible industrial tool in the future.

TABLE I. Comparative results for the hesperidinase-catalyzed transformation of rutin to produce isoquercitrin in different reactors

Reactor	Substrate concentration, g L^{-1}	Enzyme (concentration) g mL^{-1}	Reaction time, h	Isoquercitrin yield, %	Volume productivity, μM min^{-1}	Ref.
Micro-reactor[a]	1	Hesperidinase (0.10)	0.67	98.60±3.25	3.23	This work
Batch reactor[b]	1	Hesperidinase (0.05)	10	91.46±0.55	2.49	Wang *et al.*[3]
Batch reactor[c]	0.92	Crude enzyme extract of *A. niger* (–)	4	–	–	You *et al.*[1]
Batch reactor[d]	0.46	Naringinase (0.05)	6	61	–	Vila-Real *et al.*[31]

[a]reaction conditions: rutin concentration 1 g L^{-1}, reaction temperature 40 °C, flow rate 2 μL min^{-1} for 40 min, [Bmim][BF_4]–buffer (pH 9.0), 10:90, *V*/*V*, as the reaction medium; [b]reaction conditions: rutin concentration 1 g L^{-1}, reaction temperature 40 °C, 120 rpm for 10 h, [Bmim][BF_4]–buffer (pH 9.0), 10:90, *V*/*V*, as the reaction medium; [c]reaction conditions: rutin concentration 0.92 g L^{-1}, reaction temperature 60 °C, 50 μL of crude enzyme extract of *A. niger* was resuspended in a reaction system; [d]reaction conditions: rutin concentration 0.46 g L^{-1}, reaction temperature 60 °C for 6 h in a 20 mmol L^{-1} citrate buffer system

As shown in Table I, You *et al.*[1] obtained isoquercitrin using a crude enzyme extract of *Aspergillus niger* in 4 h. The reaction time and the substrate concentration were 7.97-fold longer and 0.92-fold lower, respectively, than those in the microreactor. In addition, the results of Vila-Real *et al.*[31] indicated that isoquercitrin was obtained using the enzymatic hydrolysis of rutin with a production yield of 61 % under the conditions of 0.05 g mL^{-1} naringinase and 0.46 g L^{-1} rutin in 6 h. The isoquercitrin yield and rutin concentration were 37.6 % and 2.18-fold lower, respectively, than those in the microreactor, and the reaction time was much longer than that in the microreactor. This is due to the increased specific interfacial area and the reduced diffusion length in the microreactor, both improving the mass transfer rates in the reaction.[32] These results imply that to determine the suitable performance of a continuous-flow microreactor on an industrial scale, a numbering up approach with parallel microreactors could be adopted. Generally, the developed multi-channel microreactors and other similar multi-input microreactors are more inclined to the demands of industrial production.[33,34] The higher the number of channels, the greater the injection volume

of the substrates. The volume productivity of products would be significantly increased.[35] Thus, a shorter reaction time would significantly decrease the overall production costs of preparing isoquercitrin.

Due to the rapid heat transfer and mixing in microreactors, the reactions could be performed significantly faster than those in batch modes, typically with increases in both yield and selectivity.[32] When examining rapid reactions that allowed for equivalent reaction times in flow and batch modes, the yield was improved.[36] In addition to high yields, microreactors provide environments for highly selective chemistry, most likely due to the precise temperature control. When compared to a batch reactor, the microreactor had a higher efficiency.[37] This improvement could be attributed to two factors:[38] 1) the surface-to-volume ratio in the microreactors is much higher than in batch reactors, which increases the enzyme active sites available to the reactants at any time; and 2) the volume of the microreactor is so limited that the reactants are forced to be in contact with enzyme active sites because the diffusion paths in microreactors are much smaller. Another advantage of using the developed microreactor is that the biocatalytic reaction could be performed continuously in the preparation of isoquercitrin. In summary, the developed biocatalysis method using a continuous-flow microreactor in a shorter time (40 min) could produce a comparable amount of isoquercitrin as in a batch reactor (10 h). Thus, the bioprocess is much more economical in the industrial preparation of isoquercitrin and other precious natural medicines.[39] Thus, the novel approach using a continuous-flow microreactor used to synthesize isoquercitrin through the enzymatic hydrolysis of rutin was both efficient and simple.

CONCLUSIONS

An efficient and rapid process for isoquercitrin production using the hesperidinase-catalyzed hydrolysis of rutin was successfully developed in a continuous-flow microchannel reactor. The maximum isoquercitrin yield of 98.6 % and a volume productivity of 3.23 μmol L^{-1} min^{-1} were obtained under the following optimum conditions: a flow rate of 2 μL min^{-1} (residence time of 40 min), a rutin concentration of 1 g L^{-1}, a hesperidinase concentration of 0.1 g mL^{-1}, and a temperature of 40 °C. The value of the activation energy E_a of the enzymatic reaction was 4.61 kJ mol^{-1} at 2 μL min^{-1}. The enzymatic reaction rate in the developed microreactor was approximately 26-fold higher than that in a batch reactor. Thus, the novel approach using a continuous-flow microreactor for the synthesis of isoquercitrin through the enzymatic hydrolysis of rutin was both efficient and simple. Moreover, this microtechnology could also be applied in the effective synthesis of other precious natural medicines.

Acknowledgements. This work was supported by the China Postdoctoral Science Foundation Funded Projects (2013T60505, 2012M510124), the Postdoctoral Science Foundation

Funded Project of Jiangsu University (1143002085), and the Qing Lan Project of Jiangsu Province (2014).

ИЗВОД

БРЗА СИНТЕЗА ИЗОКВЕРЦИТРИНА ЕНЗИМСКОМ ХИДРОЛИЗОМ РУТИНА У МИКРОРЕАКТОРУ СА НЕПРЕКИДНИМ ПРОТОКОМ

JUN WANG[1,2], AN GONG[2], SHUANGSHUANG GU[2], HONGSHENG CUI[2] и XIANGYANG WU[1]

[1]*School of the Environment and Safety Engineering, Jiangsu University, Zhenjiang 212013, P R China и*
[2]*School of Biotechnology, Jiangsu University of Science and Technology, Zhenjiang 212018, P.R. China*

Изокверцитрин је ретки флавонолни гликозид широког опсега биолошких активности и кључни је интермедијер у синтези ензимски модификованог изокверцитрина. Да би се успоставио изузетно брз поступак за добијање изокверцитрина, коришћен је биореактор од стакла и полидиметилсилоксана са сталним протоком, а рутин је хидролизован хесперинидазом. Применом новог микроканалног реактора (ширине 200 μm, дубине 50 μm и дужине 2 m), са једним улазом Т облика и једним излазом, максимални принос изокверцитрина (98,6 %) је добијен у кратком времену (40 min), под следећим оптималним условима: концентрација рутина 1 g L^{-1}, концентрација хесперинидазе 0,1 g mL^{-1}, реакциона температура 40 °C и проток 2 μL min^{-1}. Енергија активације за ензимску реакцију је била 4,61 kJ mol^{-1}, а брзина реакције и запремински принос су биле 16,1 пута, односно за 30 % веће него у стандардном реактору. Дакле, примена микрореактора са сталним протоком за синтезу изокверцитрина ензимском хидролизом рутина је ефикасан и једноставан поступак.

(Примљено 15. септембра, ревидирано 6. новембра, прихваћено 13. новембра 2014)

REFERENCES

1. H. J. You, H. J. Ahn, G. E. Ji, *J. Agric. Food Chem.* **58** (2010) 10886
2. K. Valentová, J. Vrba, M. Bancířová, J. Ulrichová, V. Křen, *Food Chem. Toxicol*. **68** (2014) 267
3. J. Wang, L. Zhao, G. Sun, Y. Liang, F. A. Wu, Z. Chen, S. Cui, *Afr. J. Biotechnol*. **10** (2013) 1460
4. L. Weignerová, P. Marhol, D. Gerstorferová, V. Křen, *Bioresour. Technol*. **115** (2012) 222
5. J. Tamayo-Ramos, M. Flipphi, E. Pardo, *Microb. Cell Fact.* **11** (2012) 26
6. D. Gerstorferová, B. Fliedrová, P. Halada, P. Marhol, V. Křen, L. Weignerová, *Process Biochem*. *(Oxford, UK)* **47** (2012) 828
7. J. Wang, M. Wang, F. Wu, Z. Chen, S. Cui, *J. Med. Plants Res*. **6** (2012) 1130
8. W. Lou, M. Zong, H. Wu, R. Xu, *Chin. J. Chem. Eng.* **12** (2004) 87
9. J. Wang, G. Sun, L. Yu, F. Wu, X. J. Guo, *Bioresour. Technol.* **128** (2013) 156
10. C. Wiles, P. Watts, S. Haswell, E. Pombo-Villar, *Tetrahedron* **61** (2005) 10757
11. F. Lévesque, P. H. Seeberger, *Angew. Chem. Int. Ed.* **51** (2012) 1706
12. G. Chen, J. Yue, Q. Yuan, *Chin. J. Chem. Eng.* **16** (2008) 663
13. A. Nagaki, D. Ichinari, J. Yoshida, *Chem. Commun*. **49** (2013) 3242
14. C. Wiles, P. Watts, S. Haswell, E. Pombo-Villar, *Lab Chip* **1** (2001) 100
15. M. P. Marques, P. Fernandes, *Molecules* **16** (2011) 8368
16. T. Inoue, K. Ohtaki, S. Murakami, S. Matsumoto, *Fuel Process Technol*. **108** (2013) 8
17. A. Pohar, I. Plazl, P. Žnidaršič-Plazl, *Lab Chip* **9** (2009) 3385
18. K. Kanno, H. Maeda, S. Izumo, M. Ikuno, K. Takeshita, A. Tashiro, M. Fujii, *Lab Chip* **2** (2002) 15

19. B. Mason, K. Price, J. Steinbacher, A. Bogdan, D. McQuade, *Chem. Rev*. **107** (2007) 2300
20. J. Yang, F. Lu, L. Kostiuk, D. Kwok, *J. Micromech. Microeng*. **13** (2003) 963
21. K. Sakai-Kato, M. Kato, T. Toyo'Oka, *Anal. Chem.* **75** (2003) 388
22. B. Chen, H. Liu, Z. Guo, J. Huang, M. Wang, X. Xu, L. Zheng, *J. Agric. Food Chem*. **59** (2011) 1256
23. J. Lawrence, B. O'Sullivan, G. Lye, R. Wohlgemuth, N. Szita, *J. Mol. Catal., B* **95** (2013) 111
24. G. Stojkovič, P. Žnidaršič-Plazl, *Process Biochem*. *(Oxford, UK)* **47** (2012) 1102
25. A. Mimi Sakinah, A. Ismail, R. Illias, A. Zularisam, O. Hassan, T. Matsuura, *Sep. Purif. Technol.* **124** (2014) 61
26. G. Tian, S. Xiang, R. Noiva, W. Lennarz, H. Schindelin, *Cell* **124** (2006) 61
27. C. Stalikas, *J. Sep. Sci*. **30** (2007) 3268
28. G. Greenway, S. Haswell, D. Morgan, V. Skelton, P. Styring, *Sens. Actuators, B* **63** (2000) 153
29. Y. Wang, X. Zhang, A. Wang, X. Li, G. Wang, L. Zhao, *Chem. Eng. J*. **235** (2014) 191
30. S. Mohr, K. Fisher, N. Scrutton, N. Goddard, P. Fielden, *Lab Chip* **10** (2010) 1929
31. H. Vila-Real, A. J. Alfaia, M. R. Bronze, A. R. Calado, M. H. Ribeiro, *Enzyme Res*. (2011) 4760
32. V. Skelton, G. Greenway, S. Haswell, P. Styring, D. Morgan, B. Warrington, S. Wong, *Analyst* **126** (2001) 11
33. P. B. Wojciech, V. Willem, N. David, *Lab Chip* **7** (2007) 1717
34. J. Wagner, T. Kirner, G. Mayer, J. Albert, J. M. Kohler, *Chem. Eng. J.* **101** (2004) 251
35. W. Ehfreld, V. Hessel, H. Lowe, *Microreactors: New Technology for Modern Chemistry*, Wiley–VCH, Weinheim, Germany, 2000
36. S. Taghavi-Moghadam, A. Kleemann, G. Golbig, *Org. Process Res. Dev*. **5** (2001) 652
37. C. Basheer, F. S. Jahir Hussain, H. K. Lee, S. Valiyaveettil, *Tetrahedron Lett.* **45** (2004) 7297
38. J. Wang, S. S. Gu, H. S. Cui, X. Y. Wu, F. A. Wu, *Bioresour. Technol.* **158** (2014) 39
39. T. D. Zeng, D. Wheeler, A. V. Desai, B. Oenal, D. E. Reichert, P. A. Kenis, *Lab Chip* **24** (2010) 3387.

Journal of the Serbian Chemical Society
JSCS-info@shd.org.rs • www.shd.org.rs/JSCS
J. Serb. Chem. Soc. 80 (7) 867–875 (2015)
JSCS–4765
UDC 546.562+546.732:548.7+547.772+547.857.8
Original scientific paper

Synthesis and crystal structure of Cu(II) and Co(II) complexes with the 1,3-dimethylpyrazole-5-carboxylic acid ligand

ŽELJKO K. JAĆIMOVIĆ[1], MILICA KOSOVIĆ[1], SLAĐANA B. NOVAKOVIĆ[2]*, GERALD GIESTER[3] and ANA RADOVIĆ[4]

[1]*Faculty of Metallurgy and Technology, University of Montenegro, Podgorica, Montenegro,* [2]*Vinča Institute of Nuclear Sciences, Laboratory of Theoretical Physics and Condensed Matter Physics, University of Belgrade, P. O. Box 522, 11001 Belgrade, Serbia,* [3]*Institut für Mineralogie und Kristallographie, Fakultät für Geowissenschaften, Geographie und Astronomie, University of Vienna, Althanstraße 14, A-1090 Vienna,, Austria and* [4]*Accreditation Body of Montenegro, Jovana Tomaševića 1, 81000 Podgorica, Montenegro*

(Received 22 July, revised 30 December 2014, accepted 30 January 2015)

Abstract: In the reaction of 1,3-dimethylpyrazole-5-carboxylic acid (HL) with $M(OAc)_2 \cdot 4H_2O$, (M = Cu or Co), two novel complexes were prepared, the square-planar $[CuL_2(H_2O)_2]$ and the octahedral $[CoL_2(MeOH)_4]$. The crystal structures were determined by single-crystal X-ray diffraction. In both complexes, the deprotonated acid displays monodentate coordination to the metal ions. According to the results of a CSD survey, this is the first structural report on the metal complexes with an N^1-substituted pyrazole-5-carboxylic ligand.

Keywords: pyrazole-based ligand; transition metal complex; crystal structure.

INTRODUCTION

Pyrazole-based compounds and their transition metal complexes have attracted considerable research interest because of their potentially beneficial biological properties. The wide biological activity of this class of compounds (anticancer, antimicrobial, antiviral, anti-inflammatory and others) is described in several reviews.[1] Apart from the investigation of the biological activity of pyrazole derivatives, they have been extensively used as ligands or synthons in coordination chemistry[2] and crystal engineering including the metal organic frameworks.[3] The most of these valuable functions of pyrazole ligands originate in their various bonding modes to metal ions that can be further influenced and rationally designed by the attachment of substituents with additional coordination sites.[3–5] Another important property of pyrazole derivatives is the presence of hydrogen bonding sites, either on the pyrazole ring (pyrrolic N–H donor and pyridinic N

* Corresponding author. E-mail: snovak@vin.bg.ac.rs
doi: 10.2298/JSC140722009J

acceptor) or its substituents, which facilitates molecular association into the hydrogen-bonded supramolecular structures.

Ligands derived from pyrazole-5-carboxylic acid also display various bonding modes as they can coordinate in mono- or dianionic form through the pairs of *N*- and *O*-donors from the heterocyclic ring and carboxyl groups. Despite this coordination variety, the Cambridge Structural Databank (CSD)[6] does not contain information about metal complexes with N^1-substituted derivatives of pyrazole-5-carboxylic acid. Herein, the syntheses, IR characterization and crystal structures of Cu(II) and Co(II) complexes with 1,3-dimethylpyrazole-5-carboxylate (Scheme 1) are presented, whereby the X-ray experiments revealed the not very common monodentate coordination of this pyrazole-5-carboxylic acid based ligand.

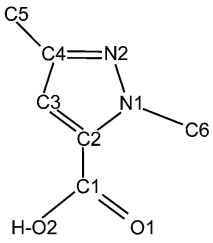

Scheme 1. 1,3-Dimethylpyrazole-5-carboxylic acid (HL) with atom numbering.

EXPERIMENTAL

Preparation of the complexes

The $[CuL_2(H_2O)_2]$ complex was synthesized in the reaction of a warm methanolic solution (10 cm^3 CH_3OH) of 0.25 mmol (0.049 g) $Cu(OAc)_2 \cdot 4H_2O$ with a warm methanolic solution (5 cm^3 CH_3OH) of 0.5 mmol (0.070 g) 1,3-dimethylpyrazole-5-carboxylic acid (HL) mixed in a 1:2 mole ratio. After two days, the blue single crystal product was filtered off and washed with methanol. The yield was 84.29 % (0.080 g).

The $[CoL_2(MeOH)_4]$ complex was synthesized in the reaction of a warm methanolic solution (3 cm^3 CH_3OH) of 0.125 mmol (0.031 g) $Co(OAc)_2 \cdot 4H_2O$ with a warm methanolic solution (3 cm^3 CH_3OH) of 0.25 mmol (0.035 g) 1,3-dimethylpyrazole-5-carboxylic acid (HL) mixed in a 1:2 mole ratio. After two days, the single crystal product was filtered off and washed with methanol. Yield was 32.75 % (0.019 g). The synthesis resulted in the mixture of reactants, HL and $Co(OAc)_2 \cdot 4H_2O$, and a very small amount of the $[CoL_2(MeOH)_4]$ complex. After filtering off, the purple crystals of the complex were mechanically separated for IR and X-ray analysis.

For both syntheses, the 1,3-dimethylpyrazole-5-carboxylic acid was used as purchased from Sigma–Aldrich.

Infrared spectra

The infrared spectra (IR) of the synthesized complexes and corresponding uncoordinated ligand were recorded as KBr pellet on a Thermo Nicolet Nexus 670 FT-IR instrument in the wavenumber range of 4000–400 cm^{-1}. As expected, the IR spectra of complexes show rather similar features, especially concerning the position of the relevant absorption band $\nu(COO^-)$. The spectrum of the uncoordinated ligand displayed ν(COOH) at 1712.27 cm^{-1}, while in spectra of the complexes, the band was replaced with $\nu_{as}(COO^-)$ at *ca*. 1600 cm^{-1} and $\nu_s(COO^-)$

at *ca*. 1350 cm^{-1}. The approximate $\Delta\nu$ of 250 cm^{-1} is in accordance with monodentate coordination of the carboxyl ligand.[7] IR (cm^{-1}): 2926.26, 2578.64, 2481.96, 1712.27, 1542.66, 1471.80, 1245.67; $[CuL_2(H_2O)_2]$: 3434.32, 2926.48, 1600.12, 1538.44, 1460.62, 1354.18, 1293.23; $[CoL_2(MeOH)_4]$: 3380.68, 2927.31, 1605.24, 1536.72, 1459.10, 1350.08, 1287.29.

X-ray crystal structure determination

The diffraction data from selected single crystals of $[CuL_2(H_2O)_2]$ and $[CoL_2(MeOH)_4]$ were collected at 200 and 150 K, respectively on a Nonius Kappa CCD diffractometer equipped with a monocapillary optics collimator, MoK_α radiation (λ = 0.71073 Å). The data were corrected for absorption by evaluation of multi-scans. The crystal structure was solved by direct methods, using SHELXS and refined with SHELXL.[8] The H atoms attached to C atoms were placed at geometrically calculated positions with the C–H distances fixed to 0.93 and 0.96 Å from aromatic and methyl C atoms, respectively. The corresponding isotropic displacement parameters of the hydrogen atoms were equal to $1.2U_{eq}$ and $1.5U_{eq}$ of the parent C atoms. The H atoms attached to O atoms were located in the final electron density maps and refined isotropically. The geometrical calculations were performed with PARST[9] and PLATON.[10] The programs ORTEP[11] and Mercury[12] were used for molecular graphics. The details of the X-ray structural analysis are given in Table S-I of the Supplementary material to this paper.

RESULTS AND DISCUSSION

Coordination modes of pyrazole-5-carboxylic acid ligands in metal complexes extracted from CSD

The CSD analysis[6] focused only on the donor abilities of the pyrazole-5--carboxylic acid ligands (with four potential coordination sites in total) and hence, the crystal structures of complexes with derivatives comprising additional donor sites were not considered. In the complex compounds extracted from CSD, the pyrazole-5-carboxylic ligands displayed seven different ways of coordination. In over 70 % of the structures (40 of 56 extracted), the ligands derived from pyrazole-5-carboxylic acid coordinate only as N^1, *O* bidentates forming the five membered chelate rings. The coordination of the remaining donors leads to the formation of bi- or polynuclear metal complexes, while the formation of a chelate ring is still preferential. There are only two examples of monodentate coordination of pyrazole-5-carboxylic ligands.[13,14] In both of these complexes, the monodentate coordination can be related to the possible steric hindrance between the ligands in the coordination spheres of the corresponding metal ions. Up to now, the crystal structures of complexes with N^1-substituted derivatives of pyrazole-5-carboxylic acid have not been reported.

In the case of the ligand present in the title complexes (Scheme 1), the methyl substituent on the N^1-pyrazole prevents the most frequently occurring chelating form and confines the coordination to the carboxyl oxygen donor. Moreover, the steric hindrance that this substituent produces on the third donor site, N^2-pyrazole, significantly reduces the coordination ability of this donor, consequently monodentate coordination could be expected. It should be men-

tioned that the crystal structures of complexes comprising N^2-substituted pyrazole-5-carboxylic ligands are also scarce in the literature. In several reported cases with phenyl substituents on pyrazole N^2, the corresponding ligands coordinate in the N^1O-chelating mode.[15]

Description of crystal structures

The $[CuL_2(H_2O)_2]$ complex crystallizes in the space group $P2_1/c$. The Cu atom is placed in a nearly ideal square planar environment formed by pairs of oxygen donors from the deprotonated carboxylic acid and H_2O molecules, Fig. 1a. The lengths of the two types of Cu−O bonds coincide within the s.u. values, while the angle O2−Cu1−O1w of 91.09(6)° actually shows the largest deviation from the ideal square-planar geometry (Table S-II of the Supplementary material). The Cu(II) ion lies on an inversion center. The Cu−O1w and Cu−O1 bond lengths are within the ranges of previously reported square-planar Cu(II) complexes comprising monodentately-coordinated carboxyl and H_2O ligands.[16] In comparison to the crystal structure of the uncoordinated 1,3-dimethylpyrazole-5--carboxylic acid (HL),[17] the geometry of the coordinated ligand is slightly altered (Table S-II). Apart from the expected changes in the carboxyl fragment due to the acid deprotonation, the dihedral angle between COO^- and pyrazole planes increases upon the ligand coordination form 4.0 to 8.7(2)°. Concerning the coordination plane of the four oxygen donors, the pyrazole ring is rotated by 69.2(1)°.

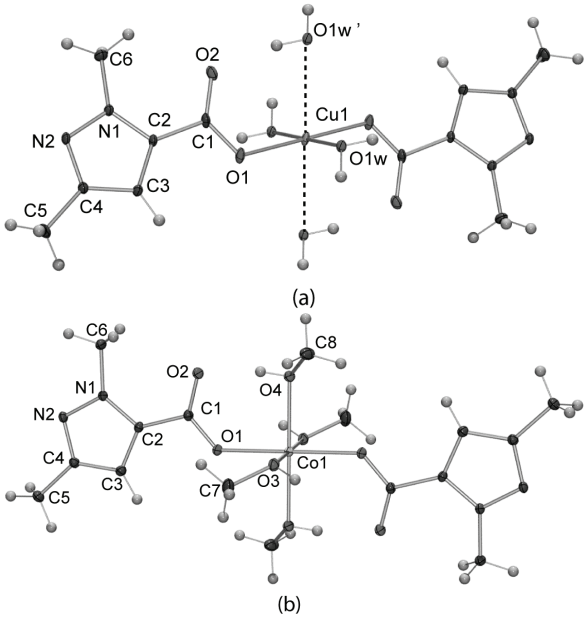

Fig. 1. Molecular structures of: a) $[CuL_2(H_2O)_2]$ with indicated positions of pseudo-coordinated O1w atoms (dashed lines) and b) $[CoL_2(MeOH)_4]$, independent molecule A. The displacement ellipsoids are drawn at the 40 % probability level.

Two types of rather strong hydrogen bonds having H···A distances shorter than 2.0 Å stabilize the crystal structure of the $[CuL_2(H_2O)_2]$ complex (Table I). The O1w−H1w···O1 interaction between the H_2O molecule and the uncoordinated carboxyl oxygen atom links the complex units into a chain extending along the *a* axis (Fig. 2a). It should be noticed that within this chain, each H_2O oxygen atom is closely adjacent to the Cu(II) ions of the neighboring complex unit. The Cu1···O1w^i ($i = x–1, y, z$) distance is 2.802(1) Å, which is significantly shorter than the sum of the van der Waals radii of these two atoms (3.84 Å).[18] Taking into account these short Cu···O1w^i contacts, the environment of each Cu(II) ion could be described as pseudo-octahedral. The positions of pseudo-coordinated O1w^i atoms are shown in Fig. 1a. The angles formed between the atom O1w^i and the O2 and O1w donor atoms from the Cu(II) coordination sphere are 87.9 and 105.8°, respectively. The separation distance between two Cu(II) in the chain is 3.826(1) Å and coincides with the length of the shortest *a* axis. Both H_2O molecules coordinated to Cu(II) further engage as hydrogen bonding donors to the non-substituted pyrazole *N* atoms of the neighboring chain (O1w−H2w···N2), leading to cross-linkage and the formation of a three-dimensional network. A fragment of this three-dimensional crystal packing is shown in Fig. 2a.

TABLE I. The geometry of hydrogen bonding (Å, °) for the Cu(II) and Co(II) complexes; symmetry codes for $[CuL_2(H_2O)_2]$: i) $x+1, y, z$; ii) $–x+1, y–1/2, –z+1/2$; symmetry codes for $[CoL_2(MeOH)_4]$: i) x, y, z; ii) $x, y–1, z$

Structure	*D*–H···*A*	*D*–H	*D*···*A*	H···*A*	*D*–H···*A*
$[CuL_2(H_2O)_2]$	O1w−H1w···O3^i	0.81(3)	2.611(2)	1.82(3)	165(3)
	O1w−H2w···N2^{ii}	0.83(3)	2.716(2)	1.89(3)	170(4)
$[CoL_2(MeOH)_4]$	O4a−H4a···O2a^i	0.79(3)	2.587(2)	1.83(3)	160(3)
	O4b−H4b···O1b^i	0.82(3)	2.582(2)	1.78(3)	167(3)
	O3a−H3a···N2a^{ii}	0.73(3)	2.707(3)	1.98(3)	175(3)
	O3b−H3b···N2b^{ii}	0.79(3)	2.765(2)	1.97(3)	177(3)

The second complex $[CoL_2(MeOH)_4]$ crystallizes in space group *P*-1, with the asymmetric unit containing two halves of the corresponding crystallographically independent complex molecules (A and B). The two Co(II) ions, which are placed in the inversion centers (0,0,0 and 0.5,0.5,0.5), adopt deformed octahedral coordination geometry (Table S-II) built by two monodentately coordinated L ligands and four molecules of methanol, Fig. 1b. The Co−O1 coordination bonds in the two independent molecules are of similar lengths, while the dihedral angles between the carboxyl and pyrazole planes are 8.6(2) and 3.5(2)° for molecules A and B, respectively. The bonds within the L ligand show only small variations with respect to the uncoordinated molecule[17] and the same ligand in the Cu(II) complex. Comparison of the monodentate coordination of the L

ligand to the Co(II) and Cu(II) ions in the two complexes revealed a pronounced difference between the Cu1−O1−C1 and each of the two Co1−O1−C1 angles (9.3° on average) (Table S-II). In both molecules of $[CoL_2(MeOH)_2]$, the carboxyl group of L is placed in the level of vicinal MeOH ligand and engages in strong intramolecular (O4−H4···O2) hydrogen bonding (Table I). This is in contrast to the Cu(II) complex in which a carboxyl group points away from the vicinal ligand to engage in intermolecular O−H···O interaction.

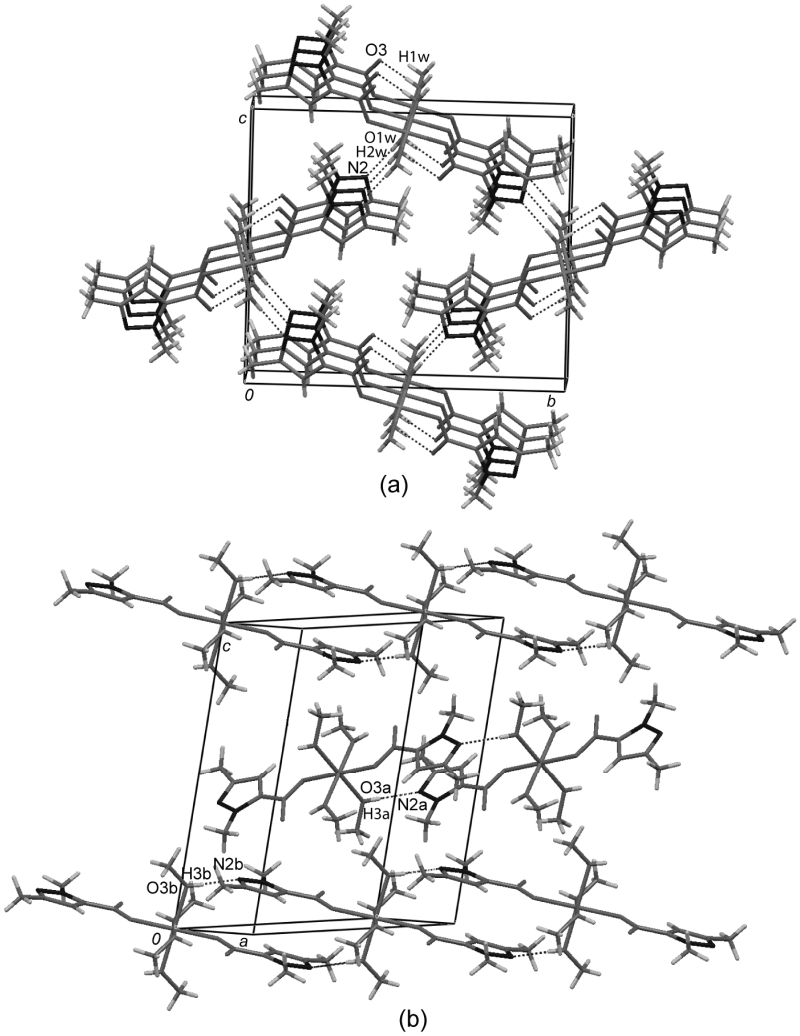

Fig. 2. Crystal packing of: (a) $[CuL_2(H_2O)_2]$ and (b) $[CoL_2(MeOH)_4]$. Intermolecular interactions are indicated by dashed lines.

The MeOH ligands mostly contribute to the dissimilarity of the two independent $[CoL_2(MeOH)_4]$ molecules. Thus, the Co−O coordination bonds involving MeOH ligands (Table S-II) are both longer in molecule B by 0.04Å on average. A closer comparison of the coordinated MeOH also showed marked differences in the orientation of their methyl groups. Considering the MeOH ligands that form strong intramolecular hydrogen bonds, it could be observed that their C8 methyl atoms deviate from corresponding O1/O1′/O4/O4′ planes by 0.18(1) and 0.96(1) Å in A and B, respectively. In both type of molecules another pair of MeOH serves as donor in the O3−H3···N2 intermolecular hydrogen bond to the pyrazole acceptor from the neighboring molecule (Table I). These interactions lead to the formation of two distinct chains composed of the same type of molecules, A or B. Both chains run in the direction of the *b* axis; the mutual inclination between the pyrazole rings belonging to different chains is 47.4(1)°. The chains composed of A and B molecules mutually interact by van der Waals interactions (Fig. 2b).

CONCLUSION

The report describes the synthesis, IR characterization and crystal structures of Cu(II) and Co(II) complexes with 1,3-dimethylpyrazole-5-carboxyle ligand (HL), the square-planar $[CuL_2(H_2O)_2]$ and the octahedral $[CoL_2(MeOH)_4]$. The presence of a methyl substituent on the N^1 atom of HL prevents bidentate coordination common for pyrazole-5-carboxylic acid-based ligands; therefore, in both complexes the ligand is monodentately coordinated to the metal ion. The crystal structures of the complexes are stabilized by extensive O−H···O and O−H···N hydrogen bonds, in which H_2O and methanol ligands play a significant role as hydrogen bonding donors.

SUPPLEMENTARY DATA

Crystallographic data of the structural analysis have been deposited with the Cambridge Crystallographic Data Centre CCDC No. 1015253 and 1015254. The data are available free of charge *via* www.ccdc.cam.ac.uk/data_request/cif (or from the CCDC, 12 Union Road, Cambridge CB2 1EZ, UK; +44 1223 336033; e-mail: deposit@ccdc.cam.ac.uk). The crystallographic data, and selected bond lengths and angles for the Cu and Co complexes are given in Tables S-I and S-II, respectively, of the Supplementary material to this paper, which is available electronically from http://www.shd.org.rs/JSCS/ or from the corresponding author on request.

Acknowledgement. S. B. N. thanks the Ministry of Education and Science of the Republic of Serbia (Project No. 172014 and 172035) for financial support. Ž. J. and M. K. thank to the Ministry of Science of the Republic of Montenegro/Natonal project for the financial support.

ИЗВОД

СИНТЕЗА И КРИСТАЛНА СТРУКТУРА КОМПЛЕКСА Cu(II) И Co(II) СА 1,3-ДИМЕТИЛ-ПИРАЗОЛ-5-КАРБОКСИЛНОМ КИСЕЛИНОМ

ЖЕЉКО К. ЈАЋИМОВИЋ[1], МИЛИЦА КОСОВИЋ[1], СЛАЂАНА НОВАКОВИЋ[2], GERALD GIESTER[3] и АНА РАДОВИЋ[4]

[1]Металуршко–технолошки факултет Универзитета у Црној Гори, Подгорица , Црна Гора, [2]Институт за нуклеарне науке „Винча“, Лабораторија за физику кондензоване материје,Универзитет у Београду, п. пр. 522, 11001 Београд, [3]Institut für Mineralogie und Kristallographie, Fakultät für Geowissenschaften, Geographie und Astronomie, University of Vienna Althanstraße 14, A-1090 Vienna, Austria и [4]Акредитационо тело Црне Горе, Јована Томашевића 1, 81000 Подгорица, Црна Гора

У реакцији 1,3-диметилпиразол-5-карбоксилне киселине (HL) и $M(OAc)_2{\cdot}4H_2O$ (M = Cu или Co) синтетисана су два нова комплекса, квадратно-планарни $[CuL_2(H_2O)_2]$ и октаедарски $[CoL_2(MeOH)_4]$. Некоординовани лиганд и синтетисани комплекси су окарактерисани инфрацрвеним спектрима. Кристалне стуктуре комплекса су одређене рендгенском стуктурном анализом. У оба комплекса депротонована киселина се координује за јон метала као монодентатни лиганд. Према резултатима претраге Кембричке банке података ово је први стуктурни опис комплекса метала са N^1-супституисаним дериватом пиразол-5-карбоксилне киселине.

(Примљено 22. јула, ревидирано 30. децембра 2014, прихваћено 30. јануара 2015)

REFERENCES

1. a) J. M. Alex, R. Kumar, *J. Enzyme Inhib. Med. Chem.* **29** (2014) 427; b) V. Kumar, K. Kaur, G. K. Gupta, A. K. Sharma, *Eur. J. Med. Chem.* **69** (2013) 735; c) F. Chimenti, A. Bolasco, F. Manna, D. Secci, P. Chimenti, A. Granese, O. Befani, P. Turini, R. Cirilli, F. La Torre, S. Alcaro, F. Ortuso, T. Langer, *Curr. Med. Chem*. **13** (2006) 1411
2. Ž. K. Jaćimović, G. A. Bogdanović, B. Holló, V. M. Leovac, K. Mészáros Szécsényi, *J. Serb. Chem. Soc*. **74** (2009) 1259, and references therein
3. a) S. Bhattacharya, A. Goswami, B. Gole, S. Ganguly, S. Bala, S. Sengupta, S. Khanra, R. Mondal, *Cryst. Growth Des.* **14** (2014) 2853; b) T.-J. Won, J. K. Clegg, L. F. Lindoy, J. C. McMurtrie, *Cryst. Growth Des.* **7** (2007) 972
4. A. M. Halcrow, *Dalton Trans*. (2009) 2059
5. R. Mukherjee, *Coord. Chem. Rev*. **203** (2000) 151
6. F. H. Allen, *Acta Crystallogr., B* **58** (2002) 380. CSD version 5.35 updates (May 2014)
7. K. Nakamoto, *Infrared and Raman Spectra of Inorganic and Coordination Compounds*, *Part B*, Wiley–Interscience, New York, 2009, p 271
8. G. M. Sheldrick, *Acta Crystallogr.*, *A* **64** (2008) 112
9. M. Nardelli, *Comput. Chem*. *(Oxford, UK)* **7** (1983) 95
10. A. L. J. Spek, *J. Appl. Crystallogr*. **36** (2003) 7
11. L. J. Farrugia, *J. Appl. Crystallogr*. **30** (1997) 565
12. C. F. Macrae, P. R. Edgington, P. McCabe, E. Pidcock, G. P. Shields, R. Taylor, M. Towler, J. van de Streek, *J. Appl. Crystallogr*. **39** (2006) 453
13. V. Chandrasekhar, R. Thirumoorthi, R. K. Metre, B. Mahanti *J. Organomet. Chem.* **696** (2011) 600
14. Z.-P. Li, Y.-H. Xing, C.-G. Wang, J. Li, Y.-Z. Cao, X.-Q. Zeng, M.-F. Ge, S.-Y. Niu, *Z. Anorg. Allg. Chem.* **635** (2009) 2601

15. a) Y. Chen, C.-B. Liu, Y.-N. Gong, J.-M. Zhong, H.-L. Wen, *Polyhedron* **36** (2012) 6; b) H. Liu, C.-B. Liu, Y.-N. Gong, Y.-H. Wang, H.-L. Wen, *Chin. J. Chem.* **31** (2013) 407
16. a) R. Lamann, M. Hulsen, M. Dolg, U. Ruschewitz, *Z. Anorg. Allg. Chem.* **638** (2012) 1424; b) Y. Kani, M. Tsuchimoto, S. Ohba, *Acta Crystallogr*., *C* **56** (2000) e79
17. E. Foresti Serantoni, R. Mongiorgi, L. Riva di Sanseverino, *Atti Accad. Naz. Lincei Cl. Sci. Fis. Mat. Nat, Rend.* **54** (1973) 787
18. A. Bondi, *J. Phys. Chem*. **68** (1964) 441.

Journal of the Serbian Chemical Society
JSCS@tmf.bg.ac.rs • www.shd.org.rs/JSCS
J. Serb. Chem. Soc. 80 (7) S246–S247 (2015) *Supplementary material*

SUPPLEMENTARY MATERIAL TO

Synthesis and crystal structure of Cu(II) and Co(II) complexes with 1,3-dimethyl-pyrazole-5-carboxylic acid ligand

ŽELJKO K. JAĆIMOVIĆ[1], MILICA KOSOVIĆ[1], SLAĐANA B. NOVAKOVIĆ[2]*, GERALD GIESTER[3] and ANA RADOVIĆ[4]

[1]*Faculty of Metallurgy and Technology, University of Montenegro, Podgorica, Montenegro,* [2]*Vinča Institute of Nuclear Sciences, Laboratory of Theoretical Physics and Condensed Matter Physics, University of Belgrade, P. O. Box 522, 11001 Belgrade, Serbia,* [3]*Institut für Mineralogie und Kristallographie, Fakultät für Geowissenschaften, Geographie und Astronomie, University of Vienna, Althanstraße 14, A-1090 Vienna,, Austria and* [4]*Accreditation Body of Montenegro, Jovana Tomaševića 1, 81000 Podgorica, Montenegro*

J. Serb. Chem. Soc. 80 (7) (2015) 867–875

TABLE S-I. Crystallographic data for Cu(II) and Co(II) complexes

Parameter	$[CuL_2(H_2O)_2]$	$[CoL_2(MeOH)_4]$
Molecular formula	$C_{12}H_{18}N_4O_6Cu$	$C_{16}H_{30}N_4O_8Co$
Formula weight	377.84	465.37
Temperature, K	200(1)	150(1)
Wavelength, Å	0.71073	0.71073
Crystal system	Monoclinic	Triclinic
Space group	$P2_1/c$	P-1
Unit cell dimensions		
a / Å	3.8258(8)	8.3416(17)
b / Å	15.3819(15)	9.6067(19)
c / Å	13.1874(12)	14.497(3)
α / °	90	102.83(3)
β / °	97.337(3)	91.81(3)
γ / °	90	103.97(3)
V / Å^3	769.70(19)	1094.7(4)
Z	2	2
μ / mm^{-1}	1.456	1.412
F(000)	390	490
D_{calc} / g cm^{-3}	1.630	0.831
Crystal size / mm^3	0.42 × 0.24 × 0.22	0.28 × 0.15 × 0.13
θ range for data collection, °	4.09–30.03	3.67–30.39
Reflections collected	4368/116	12527/289

* Corresponding author. E-mail: snovak@vin.bg.ac.rs

TABLE S-I. Continued

Parameter	$[CuL_2(H_2O)_2]$	$[CoL_2(MeOH)_4]$
Independent reflections/parameters	2251	6484
Reflections for $I > 2\sigma(I)$	1835	4590
R_{int}	0.0144	0.0357
Goodness-of-fit on F^2	1.046	1.037
R_1, wR_2 [$I > 2\sigma(I)$]	0.0288, 0.0772	0.0420, 0.0933
Largest ΔF peak and hole, e Å^{-3}	0.36 / −0. 35	0.37 / −0.49

TABLE S-II. Selected bond lengths (Å) and angles (°) for the Cu(II) and Co(II) complexes

Bond	HL[1]	$[CuL_2(H_2O)_2]$	$[CoL_2(MeOH)_2]$	
			A	B
Cu1−O1/Co1−O1	–	1.950(1)	2.075(1)	2.072(1)
Cu1−O1w	–	1.953(2)	–	–
Co1−O3	–	–	2.066(2)	2.121(2)
Co1−O4	–	–	2.071(2)	2.104(1)
C1−O1	1.331	1.273(2)	1.270(2)	1.267(2)
C1−O2	1.205	1.245(2)	1.244(2)	1.252(2)
C1−C2	1.471	1.493(2)	1.496(3)	1.494(2)
C2−C3	1.401	1.377(2)	1.375(3)	1.387(3)
C3−C4	1.382	1.392(2)	1.400(3)	1.389(3)
N2−C4	1.353	1.337(2)	1.334(3)	1.340(2)
N1−N2	1.350	1.347(2)	1.360(2)	1.359(2)
N1−C6	1.470	1.458(2)	1.454(3)	1.458(2)
N1−C2	1.355	1.361(2)	1.361(2)	1.354(2)
C4−C5	1.501	1.500(2)	1.498(3)	1.501(3)
Angle, °				
O1−Cu−O1w	–	88.91(6)	–	–
O1−Co−O3	–	–	90.55(7)	93.22(6)
O1−Co−O4	–	–	88.38(7)	91.29(6)
O3−Co−O4	–	–	92.07(9)	91.43(6)
Cu1−O1−C1/Co1−O1−C1	–	120.36(12)	130.7(12)	128.34(12)
O1−C1−O2	124.7	126.54(16)	126.67(17)	126.01(17)
O1−C1−C2	110.9	114.44(15)	113.51(16)	114.79(16)
O2−C1−C2	124.4	119.02(15)	119.82(16)	119.20(16)
C1−C2−C3	129.2	129.74(15)	128.49(17)	128.37(17)
C1−C2−N1	124.4	123.69(15)	124.83(17)	125.22(16)

REFERENCES

1. E. Foresti Serantoni, R. Mongiorgi, L. Riva di Sanseverino, *Atti Accad. Naz. Lincei Cl. Sci. Fis. Mat. Nat, Rend.* **54** (1973) 787.

Journal of the Serbian Chemical Society
JSCS-info@shd.org.rs • www.shd.org.rs/JSCS
J. Serb. Chem. Soc. 80 (7) 877–888 (2015)
JSCS–4766
UDC 547.514.72+546.732:547.521+519.677:544.112–185
Original scientific paper

Nucleus-independent chemical shift profiles along the intrinsic distortion path for Jahn–Teller active molecules. Study on the cyclopentadienyl radical and cobaltocene

LJUBICA ANDJELKOVIĆ[1], MARKO PERIĆ[1#], MATIJA ZLATAR[1] and MAJA GRUDEN-PAVLOVIĆ[2*#]

[1]*Center for Chemistry, ICTM, University of Belgrade, Njegoševa 12, 11001 Belgrade, Serbia and* [2]*Faculty of Chemistry, University of Belgrade, Studentski Trg 12–16, 11001 Belgrade, Serbia*

(Received 7 November 2014, revised 11 March, accepted 12 March 2015)

Abstract: The aromatic/anti-aromatic behavior of the cyclopentadienyl anion (Cp^-), bis(η^5-cyclopentadienyl)iron(II) ($Fe(Cp)_2$), as well as of the Jahn–Teller (JT) active cyclopentadienyl radical ($Cp^\bullet$) and bis(η^5-cyclopentadienyl)-cobalt(II) ($Co(Cp)_2$) were investigated using density functional theory (DFT) calculations of the nuclear independent chemical shifts (*NICS*). According to the *NICS* values, pentagon ring in $Fe(Cp)_2$ is more aromatic than that of the isolated Cp^-. The *NICS* parameters were scanned along the Intrinsic Distortion Path (IDP) for $Cp^\bullet$ and $Co(Cp)_2$ showing anti-aromaticity, which decreased with increasing deviation from the high symmetry D_{5h} to the low symmetry (LS) C_{2v}. Changes in the *NICS* values along the IDP revealed that $Co(Cp)_2$ in the LS nuclear arrangement has aromatic character, in contrast to the case of $Cp^\bullet$.

Keywords: vibronic coupling; DFT; aromaticity; metallocene.

INTRODUCTION

Aromaticity, an intuitive concept in chemistry and physics, is considered as a property of systems that are thermodynamically stabilized due to cyclic electron delocalization. The delocalized electronic structure of aromatic compounds yields enhanced planarity, equalized bond lengths, enhanced stability due to the resonance, favoring substitution instead of addition that would be typical for isolated double bonds, and the ability to sustain ring currents when exposed to external magnetic fields. Contrary to the concept of aromaticity, the Jahn–Teller (JT) effect[1,2] induces unequalization of bond lengths, leading to the stabilization

* Corresponding author. E-mail: gmaja@chem.bg.ac.rs
# Serbian Chemical Society member.
doi: 10.2298/JSC141107025A

of a system upon distortion. The connection of aromaticity and the JT effect is of utmost importance, since both effects have been very useful in the characterization and interpretation of the structure, stability and reactivity of many molecules. For this reason, computational chemists seek the origin, explanation and understanding of these two phenomena. According to The Hückel molecular orbital (MO) theory,[3,4] species with $4n + 2$ π electrons are aromatic, whereas structures with $4n$ π electrons are defined as anti-aromatic. Structures with $4n+1$ π electrons with unpaired electrons in degenerate orbitals are JT active species, and are supposed to show anti-aromaticity.[5–8] Bearing in mind that the JT theorem states that a molecule with a degenerate ground electronic state distorts along non-totally symmetric vibrational coordinates, and in such a way removes the degeneracy and lowers the energy, the question naturally arises: How does the JT distortion influence the aromaticity/anti-aromaticity? Although it is well known that different criteria of aromaticity may lead to different overall conclusions,[9] nucleus-independent chemical shifts (*NICS*) provide a widely accepted quantitative measure of aromaticity/anti-aromaticity.[10,11] Furthermore, a scan of the *NICS* parameters along the intrinsic distortion path (IDP)[12–14] was found to be the method of choice in the analysis of the aromatic behavior of JT active species,[7,8,15] since the distortion path provides direct insight into the microscopic origin, mechanism and consequences of distortion.[13,14]

A detailed density functional theory (DFT) computational analysis was performed to investigate the aromaticity of the cyclopentadienyl anion (Cp^-), bis(η^5--cyclopentadienyl)iron(II) ($Fe(Cp)_2$), the cyclopentadienyl radical ($Cp^\bullet$) and bis(η^5-cyclopentadienyl)cobalt(II) ($Co(Cp)_2$). In spite of their relatively simple composition, the aromaticity of the JT active $Cp^\bullet$ and $Co(Cp)_2$ have not been fully rationalized so far. Therefore, the aim of this work was also to understand the influence of the JT effect on the aromatic behavior of these species. The *NICS* were determined for the reference non-JT active species, Cp^- and $Fe(Cp)_2$, and molecules prone to the JT effect, $Cp^\bullet$ and $Co(Cp)_2$. In order to preserve chemically important features, an analysis of the full *NICS* profile of $Cp^\bullet$ and $Co(Cp)_2$ along the IDP was performed.

METHODOLOGY

All the DFT calculations were realized using the Amsterdam Density Functional program package, ADF2013.01.[16-18] Geometry optimization of all the investigated molecules was performed using the local density approximation (LDA) characterized by the Vosko–Willk––Nusair (VWN) parametrization,[19] as well as using general gradient approximations (GGA), such as BP86,[20,21] PW91,[22] OPBE,[23] and S12g,[24] and hybrids B3LYP[25,26] and S12h.[24] All electron triple-zeta Slater-type orbitals (STO) plus one polarization function (TZP) basis set were used for all atoms. All calculations were spin-unrestricted. Analytical harmonic frequencies[27,28] were calculated in order to ascertain that the low symmetry (LS) structures correspond to the stationary points on the potential energy surfaces. Calculations of the *NICS* values were performed at the B3LYP/6-311+G* level of theory using the Gaussian 09W

program package using LDA optimized geometries.[21,29-31] The *NICS* parameters were calculated for ghost atoms located at the center of Cp^- and $Cp^\bullet$. In order to obtain the full profile of aromatic/anti-aromatic behavior, calculations of the *NICS* parameters were performed from 0 Å to 5 Å, in steps of 0.5 Å. In order to avoid the influence of the magnetic field of the central metal ion in metallocenes, the first *NICS* value was calculated 1 Å above the metal ion along the *z*-axis. For JT active species in a high symmetry (HS) nuclear arrangement, the *NICS* values were calculated imposing HS (D_{5h}) nuclear arrangement and LS (C_{2v}) of electron density. The *NICS* parameters for JT active species, $Cp^\bullet$ and $Co(Cp)_2$, were scanned along the IDP.

Intrinsic distortion path – IDP

The IDP method[12-14] is based on the fact that all the information about the vibronic coupling at the HS nuclear arrangement is also contained in the distorted LS minimum energy structure. Hence, the distortion is given as a superposition of all totally symmetric normal modes in the LS point group, linking the HS configuration with the LS structure. Every point on the potential energy surface can be represented by a 3*N* dimensional vector, *N* being the number of atoms, $\vec{R}_X$, using mass-weighted generalized coordinates relative to the origin. The geometry of the LS energy minimum obtained by DFT calculations was chosen to be the origin of the configuration space, $\vec{R}_{LS} = 0$. Within the harmonic approximation, it is possible to express $\vec{R}_X$ as a linear combination of N_{a1} totally symmetric normal coordinates in the LS:

$$\vec{R}_X = \sum_{k=1}^{N_{a1}} \omega_{Xk} \vec{Q}_k \tag{1}$$

where ω_{Xk} are weighting factors that represent the contribution of the displacements along the different totally symmetric normal coordinates to $\vec{R}_X$; $\vec{Q}_k$ are mass-weighted totally symmetric normal coordinates, which are the eigenvectors of the Hessian, obtained from the DFT frequency calculations in the LS minimum energy conformation. The corresponding eigenvalues are λ_k.

Within this model, the energy of any nuclear configuration $\vec{R}_X$, E_X, relative to the LS energy minimum, is expressed as the sum of the energy contributions of all the LS totally symmetric normal modes:

$$E_X = \sum_{k=1}^{N_{a1}} E_k = \frac{1}{2} \sum_{k=1}^{N_{a1}} \omega_{Xk}^2 \vec{Q}_k^2 \lambda_k \tag{2}$$

The force at any given point ($\vec{R}_X$), $\vec{F}_{Xk}$ is defined as a derivate of the energy over Cartesian coordinates and in the HS point, it indicates the main driving force for the JT distortion. The total force is represented as a vector sum of the individual forces:

$$\vec{F}_{X_{tot}} = \frac{1}{2} \sum_{k=1}^{N_{a1}} \omega_{Xk} \lambda_k M^{1/2} \vec{Q}_k = \sum_{k=1}^{N_{a1}} \vec{F}_{Xk} \tag{3}$$

where *M* is a diagonal $3N \times 3N$ matrix with atomic masses in triplicate as elements (m_1, m_1, m_1, m_2,…, m_n), and enables the calculation of the IDP exactly from the HS to the LS point. The above details about IDP can be found elsewhere.[12-14]

RESULTS AND DISCUSSION

The planar Cp^- in its singlet state with D_{5h} symmetry was optimized using several different levels of theory. All chosen exchange correlation (XC) functionals reproduced experimental geometrical parameters with sufficient accuracy,[32] Table I. The $Fe(Cp)_2$ molecule has two possible conformations, eclipsed D_{5h} and staggered D_{5d}. According to previous studies, the D_{5h} conformation is the global minimum on the potential energy surface.[33–38] The calculated bond lengths, Table I, are in excellent agreement with the experimental data,[39] and with earlier theoretical investigations.[40] Since all the functionals reproduced geometrical parameters with good accuracy, the *NICS* were computed at the B3LYP/6-311+G* level, using geometries obtained with the simplest LDA functional. Calculated *NICS* values for Cp^- and $Fe(Cp)_2$ are given in Table II. Previous sophisticated computational studies provide a rather satisfactory insight into the nature of the aromaticity of Cp^- and revealed that Cp^- is aromatic, which is in accordance with the herein presented results.[41–46] It is important to emphasize that the *NICS* parameters for Cp^- were computed at the center of the pentagon and at various distances from the center of the ring. In the case of $Fe(Cp)_2$, the starting point for the *NICS* calculation was 1 Å above the central metal ion following the *z*-axis. The *NICS* value calculated at 1.6 Å represent the *NICS* in the center of the pentagon ring of the cyclopentadienyl ligand. According to the results, both molecules show aromatic character, and $Fe(Cp)_2$ is more aromatic,

TABLE I. Selected bond lengths (Å) for the stationary points of the investigated molecules, calculated with different XC functionals

Molecule	Bond	LDA	BP86	PW91	OPBE	S12g	B3LYP	S12h	Exp.
Cp^- (D_{5h}, $^1A_1'$)	C–C	1.406	1.420	1.417	1.413	1.414	1.410	1.404	1.413[32]
$Fe(Cp)_2$ (D_{5h}, $^1A_1'$)	Fe–C	2.004	2.055	2.049	2.006	2.033	2.082	2.048	2.03[39]
	C–C	1.422	1.434	1.432	1.429	1.429	1.422	1.417	1.43[39]
$Cp\cdot$ (C_{2v}, $^2B_1$)	C–C	1.364	1.374	1.372	1.370	1.371	1.365	1.360	–
		1.424	1.439	1.436	1.432	1.432	1.432	1.426	
$Cp\cdot$ (C_{2v}, $^2A_2$)	C–C	1.455	1.471	1.468	1.462	1.463	1.465	1.457	–
		1.390	1.402	1.400	1.397	1.397	1.394	1.389	
$Co(Cp)_2$ (C_{2v}, $^2B_1$)	Co–C	2.029	2.091	2.084	2.038	2.070	2.129	2.092	2.119[50]
		2.070	2.134	2.128	2.080	2.112	2.175	2.137	
		2.098	2.155	2.149	2.108	2.135	2.185	2.151	
	C–C	1.434	1.447	1.445	1.441	1.441	1.435	1.429	1.429[50]
		1.415	1.426	1.424	1.421	1.421	1.415	1.409	
		1.402	1.412	1.410	1.408	1.408	1.400	1.396	
$Co(Cp)_2$ (C_{2v}, $^2A_2$)	Co–C	2.090	2.150	2.143	2.101	2.129	2.184	2.149	2.119[50]
		2.047	2.111	2.104	2.056	2.089	2.153	2.115	
		2.022	2.083	2.076	2.031	2.062	2.118	2.083	
	C–C	1.406	1.416	1.414	1.412	1.412	1.404	1.400	1.429[50]
		1.426	1.438	1.436	1.432	1.432	1.427	1.421	
		1.438	1.450	1.448	1.444	1.444	1.439	1.432	

Table II.[41–49] The isolated Cp^- ring has a *NICS* value of –12.52 ppm in the center, Table II. When two Cp^- rings are placed at the distance which they have in the $Fe(Cp)_2$ molecule (3.2 Å), the *NICS* parameter calculated at the center of one 5-membered ring was –12.13 ppm. Hence, the difference between the *NICS* parameters for the isolated Cp^- and for the Cp^- fragment in $Fe(Cp)_2$ is caused by the presence of the central metal ion.

TABLE II. Calculated *NICS* values (ppm) for Cp^- and $Fe(Cp)_2$ using LDA optimized geometries at various distances (Å) from the center of the molecules (for $Fe(Cp)_2$, the *NICS* calculated at 1.6 Å corresponds to the *NICS* value at the center of the Cp^- ligand)

Distance, Å	*NICS*	$NICS_{zz}$
	Cp^-	
0.0	–12.52	–15.95
1.0	–9.44	–33.70
2.0	–3.97	–17.86
3.0	–1.63	–7.87
4.0	–0.77	–3.87
5.0	–0.40	–2.13
	$Fe(Cp)_2$	
1.0	–103.47	–65.35
1.6	–42.14	–29.40
2.0	–31.15	–29.73
3.0	–9.46	–29.07
4.0	–2.44	–13.37
5.0	–0.95	–6.38

It is worth noting that $Cp^\bullet$ and $Co(Cp)_2$ have a hole and an unpaired electron, respectively, in a doubly degenerate highest occupied molecular orbital. Since it was previously shown that the eclipsed conformation is more stable and the JT effect does not depend on the rotation of the rings,[51] the discussion will be limited only to $Co(Cp)_2$ in the eclipsed conformation. The ground electronic state of the investigated species in D_{5h} symmetry is $^2E_1''$, which couples with the doubly degenerate vibration, e_2'. According to group theory considerations, the descent in symmetry goes from the D_{5h} to the C_{2v} point group, and thus, the state $^2E_1''$ splits into $^2A_2$ and $^2B_1$. The average bond distances for the distorted LS structures of $Cp^\bullet$ calculated at different levels of theory are consistent, Table I. The calculated bond lengths for $Co(Cp)_2$ are in accordance with experiments,[50] regardless of the choice of selected XC functional, Table I. Recently, the JT distortion in these molecules was analyzed in detail using a multideterminental DFT approach and the IDP method.[12,14,51–53] The calculated JT parameters of $Cp^\bullet$ and $Co(Cp)_2$ using a multideterminental DFT approach are given in Table III. The results for $Cp^\bullet$ obtained by Miller *et al.*, who used dispersed fluorescence spectroscopy, are considered to be the benchmark (E_{JT} = 1237 cm^{-1}).[54] The pre-

TABLE III. Results of the DFT calculations performed to analyze the JT effect in $Cp^{\bullet}$ and $Co(Cp)_2$; the energies are given in eV; the JT parameters E_{JT} and Δ are given in cm^{-1} and R_{JT} in $(amu)^{1/2}$Å

Molecule	Symmetry	LDA	BP86	PW91	OPBE	S12g	B3LYP	S12h
$Cp^{\bullet}$	D_{5h}, $^2E_1''$	–64.674	–59.989	–61.008	–60.966	–61.624	–67.948	–72.863
	D_{5h}, $^2A_2$	–64.653	–60.031	–61.042	–61.018	–61.658	–68.369	–73.402
	D_{5h}, $^2B_1$	–64.653	–60.031	–61.042	–61.018	–61.658	–68.369	–73.402
	C_{2v}, $^2A_2$	–64.808	–60.192	–61.203	–61.179	–61.817	–68.578	–73.596
	C_{2v}, $^2B_1$	–64.808	–60.192	–61.205	–61.179	–61.817	–68.578	–73.596
	E_{JT}, $^2A_2$	1244.5	1301.8	1294.5	1300.2	1281.6	1685.7	1567.9
	E_{JT}, $^2B_1$	1244.5	1301.0	1312.3	1301.0	1284.0	1688.1	1568.8
	Δ	0.0	–0.8	–17.7	–1.6	–2.41	0.0	0.8
	R_{JT}, $^2A_2$	0.25	0.26	0.26	0.26	0.26	0.27	0.27
	R_{JT}, $^2B_1$	0.25	0.26	0.26	0.26	0.26	0.27	0.27
$Co(Cp)_2$	D_{5h}, $^2E_1''$	–142.290	–130.675	–133.049	–133.385	–134.525	–149.601	–161.584
	D_{5h}, $^2A_2$	–142.261	–130.690	–133.061	–133.381	–134.528	–150.140	–162.247
	D_{5h}, $^2B_1$	–142.261	–130.690	–133.061	–133.381	–134.528	–150.140	–162.246
	C_{2v}, $^2A_2$	–142.362	–130.785	–133.156	–133.485	–134.626	–150.230	–162.345
	C_{2v}, $^2B_1$	–142.362	–130.785	–133.156	–133.485	–134.626	–150.231	–162.344
	E_{JT}, $^2A_2$	813.8	762.2	761.4	838.0	783.9	727.5	791.2
	E_{JT}, $^2B_1$	813.8	761.4	759.8	839.6	785.6	729.1	785.6
	Δ	0.0	0.0	1.6	–1.6	0.0	–2.4	13.7
	R_{JT}, $^2A_2$	0.35	0.34	0.34	0.35	0.34	0.34	0.34
	R_{JT}, $^2B_1$	0.35	0.34	0.34	0.35	0.34	0.34	0.34

sent calculations at the LDA level gave a value of 1244 cm^{-1}, which is in great accordance with the experimentally obtained one, although all other XC functionals also give satisfactory results, Table III. The values of the JT stabilization energies in $Co(Cp)_2$, Table III, are in agreement with the value of 1050 cm^{-1} estimated from its solid state EPR spectra.[55] For both investigated JT active molecules, the warping barrier is close to zero, independent of the level of theory (Table III). The different ground states obtained by different XC functionals (Table III) are due to the very small warping barriers, which are within the range of the accuracy of the calculation. Furthermore, IDP analysis gave a deeper insight into the vibronic coupling in these JT active molecules.[14,53] In both molecules, it is possible to distinguish two distinct regions on the potential energy profile. In the first region, the energy changes faster, and most of the E_{JT} is achieved after 40 % of the path. In the second region, the change of the energy is small, the adiabatic potential energy surface is flat and the molecule just relaxes towards the global minimum. Three vibrations are most important for the distortion in Cp: C–C stretch, C–C–C bend, and C–C–H bend. These three modes were experimentally found to be the most significant.[54] In the case of $Co(Cp)_2$, the out-of-plane ring deformation and C–H wagging (the out-of-plane C–H bending), are the most important for the JT distortion. Although the JT effect in $Cp^{\bullet}$

and $Co(Cp)_2$ has often been studied,[54–56] the influence of the vibronic coupling on their aromatic character has not been investigated. The question is whether the distortion has a significant impact on the change of aromaticity. In $Cp^{\bullet}$ and $Co(Cp)_2$, the degeneracy of the $^2E_1''$ state is broken by the JT distortion that stabilizes the system. Therefore, the *NICS* parameters were computed at the LDA optimized geometries for both the HS and LS points on the potential energy surfaces. Observing the *NICS* values at the HS point of $Cp^{\bullet}$, a high anti-aromatic character is noticeable, Table IV. The calculated parameters for the global minimum of $Cp^{\bullet}$ show that it still possesses anti-aromatic character,[5] but much weaker than in the HS point, Table IV. Moving from the center of the pentagon ring along the *z*-axis, the *NICS* indices decrease. In the case of $Co(Cp)_2$, it is evident that molecule at the HS point has high anti-aromatic character, Table V. In the global minimum structure, $Co(Cp)_2$ shows σ aromaticity and π anti-aromaticity according to the *NICS* and $NICS_{zz}$ values, Tables IV and V.

TABLE IV. Calculated *NICS* values (ppm) for $Cp^{\bullet}$ using LDA optimized geometries at HS and LS geometries at various distances (Å) from the center of the ring; the *NICS* values for both LS structures are the same

Electronic state	Distance, Å	*NICS*	$NICS_{zz}$
	$Cp^{\bullet}$ (D_{5h})		
$^2B_1/^2A_2$	0.0	86.88	273.95
	1.0	72.10	217.30
	2.0	21.36	61.38
	3.0	6.65	18.12
	4.0	2.69	7.06
	5.0	1.34	3.40
	$Cp^{\bullet}$ (C_{2v})		
$^2B_1/^2A_2$	0.0	20.78	77.09
	1.0	14.79	45.84
	2.0	3.58	8.00
	3.0	0.91	0.87
	4.0	0.31	–0.12
	5.0	0.13	–0.22

Since dependence of the *NICS* parameters on the distortion, $\vec{R}_X$ / $\vec{R}_{JT}$, and distances (Å) from the center of the molecules gives a more detailed picture, the *NICS* parameters were monitored along the IDP path for $Cp^{\bullet}$ and $Co(Cp)_2$, Fig. 1 and 2, respectively. The *NICS* parameters were scanned only for the $^2B_1$ state, since those computed for the $^2A_2$ state were almost the same. Due to the non-totally symmetric electron density, both molecules in D_{5h} possess strong anti-aromatic character. Near the point of electron degeneracy, *i.e.*, near the HS nuclear arrangement, the HOMO–LUMO gap is substantially small, thus the *NICS* parameters have large positive values in the first region of the IDP (Figs. 1

TABLE V. Calculated *NICS* values (ppm) for $Co(Cp)_2$ using LDA optimized geometries at HS and LS geometries at various distances (Å) from central metal ion. The *NICS* value calculated at 1.7 Å corresponds to the *NICS* parameter in the center of the pentagon in $Co(Cp)_2$; The *NICS* values for both LS structures are the same

Electronic state	Distance, Å	*NICS*	$NICS_{zz}$
	$Co(Cp)_2$ (D_{5h})		
$^2B_1/^2A_2$	1.0	302.49	1135.98
	1.7	67.59	281.61
	2.0	42.20	182.76
	3.0	24.86	73.78
	4.0	9.80	24.48
	5.0	4.04	9.32
	$Co(Cp)_2$ (C_{2v})		
$^2B_1/^2A_2$	1.0	–3.91	209.45
	1.7	–10.86	42.41
	2.0	–11.11	21.41
	3.0	–1.64	–5.91
	4.0	–0.10	–5.08
	5.0	–0.04	–2.92

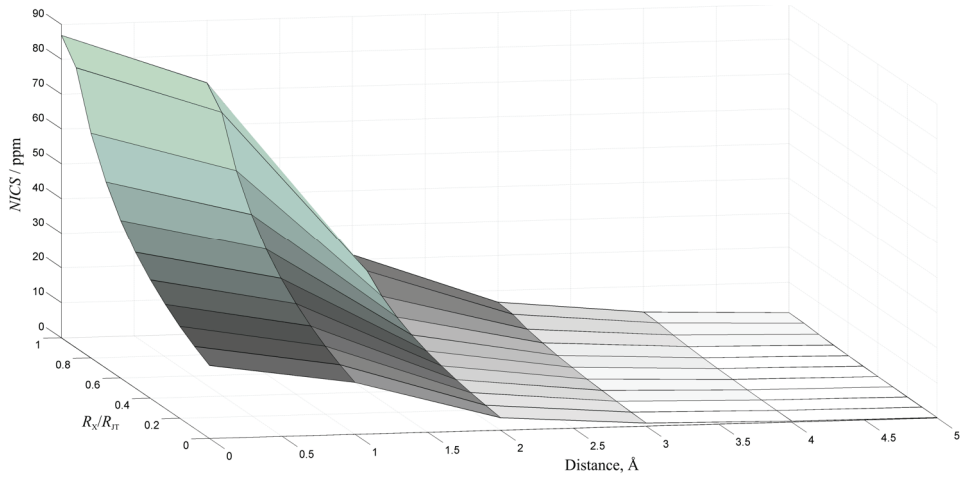

Fig. 1. Schematic plot of the *NICS* values along the IDP for $Cp^{\bullet}$ (from D_{5h} to C_{2v}), $^2B_1/^2A_2$ electronic states.

and 2). Going toward the global minimum point on the potential energy surface, the *NICS* values decrease and hence, the initially strong anti-aromatic character lowers, and finally, in the case of $Co(Cp)_2$, the *NICS* indices become negative, Figs. 1 and 2. It is worth noting that the negative *NICS* values in $Co(Cp)_2$ occur after 40 % of the IDP, where most of the JT stabilization is attained. The driving force responsible for the removal of orbital degeneracy leads to an enlargement of the HOMO–LUMO gap. Considering $Cp^{\bullet}$, for both the HS and LS nuclear arrange-

ment, the calculations revealed that the *NICS* decrease gradually along the *z*-axis, Fig. 1. Moving apart along the *z*-axis in the HS configuration of $Co(Cp)_2$, an abrupt decrease in the *NICS* parameters was observed until a distance of 1.7 Å (center of pentagon ring), Fig. 2. Going even further, the *NICS* parameters show a smooth decreasing trend, as expected.

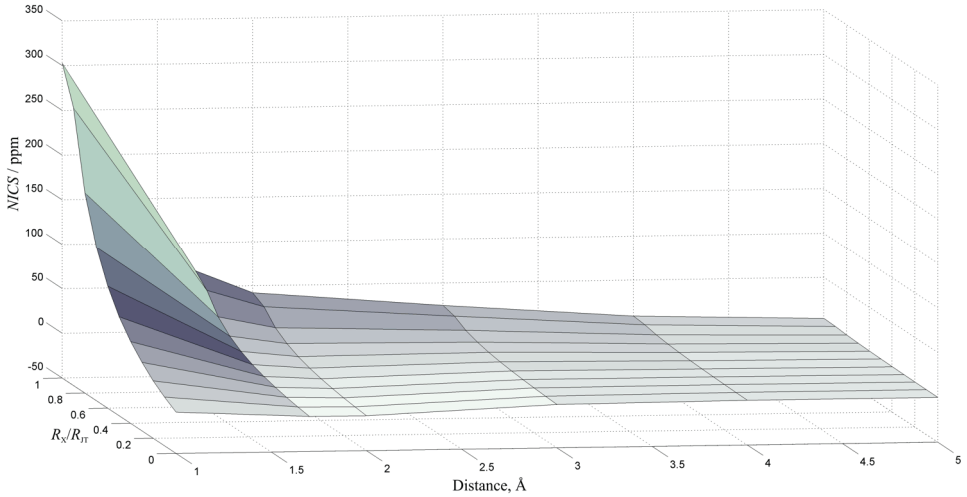

Fig. 2. Schematic plot of the *NICS* values along the IDP for $Co(Cp)_2$ (from D_{5h} to C_{2v}), $^2B_1/^2A_2$ electronic states.

CONCLUSIONS

Aromaticity is one of the oldest and most fundamental concepts in chemistry. The nature of aromatic compounds is very attractive, thus these species are among the most desirable synthetic targets. Since aromaticity is still awaiting comprehensive investigation, a detailed analysis of the *NICS* parameters, as one of the most widely used and efficient magnetic criteria, was performed in Cp^-, $Fe(Cp)_2$, $Cp^\bullet$ and $Co(Cp)_2$ by the means of DFT.

The calculations revealed that Cp^- and $Fe(Cp)_2$ are highly aromatic molecules. According to the *NICS*, the Cp^- ring in $Fe(Cp)_2$ is far more aromatic than the isolated Cp^-, showing the impact of the Fe^{2+}. In other words, these results would be highly attractive in applied sciences for the design of new advanced materials with desired properties, and the understanding of electronic structure, chemical bonding and properties in a moiety of aromatic species.

A thorough study of the influence of the JT effect on the aromaticity is presently of the utmost importance due to the increasing development of material chemistry, and substantial differences in aromatic/anti-aromatic behavior of JT active molecules. Thus, finding a method of choice to determine both chemically relevant phenomena is essential since they lead to the different reaction pathways

and the connection of aromaticity and vibronic coupling demands tremendous caution. For this purpose, the monitoring of the *NICS* along the IDP was performed. Similarly to the previous studies,[7,8,15] the anti-aromaticity decreases with increasing deviation from the high symmetry D_{5h} structures to the low symmetry C_{2v} global minimum structures, confirming that the JT distortion represents a mechanism for reducing anti-aromatic character. In the LS structure of $Co(Cp)_2$, the *NICS* become even negative, revealing aromatic character, in contrast to $Cp^{\bullet}$.

Acknowledgement. This work was financially supported by the Ministry of Education, Science and Technological Development of the Republic of Serbia (Grant No. 172035).

И З В О Д

ПРОФИЛ ХЕМИЈСКИХ ПОМЕРАЊА НЕЗАВИСНИХ ОД ЈЕЗГРА ДУЖ СВОЈСТВЕНОГ ПУТА ДИСТОРЗИЈЕ ЗА МОЛЕКУЛЕ ПОДЛОЖНЕ ЈАН–ТЕЛЕРОВОЈ ДИСТОРЗИЈИ. ПРОУЧАВАЊЕ ЦИКЛОПЕНТАДИЕНИЛ РАДИКАЛА И КОБАЛТОЦЕНА.

ЉУБИЦА АНЂЕЛКОВИЋ[1], МАРКО ПЕРИЋ[1], МАТИЈА ЗЛАТАР[1] и МАЈА ГРУДЕН-ПАВЛОВИЋ[2]

[1]Центар за хемију, ИХТМ, Универзитет у Београду, Његошева 12, 11001 Београд и [2]Хемијски факултет, Универзитет у Београду, Студентски трг 16, 11001 Београд

Ароматичност/антиароматичност циклопентадиенил анјона (Cp^-), бис(η^5-циклопентадиенил)гвожђа(II) ($Fe(Cp)_2$), као и, циклопентадиенил радикала ($Cp^{\bullet}$) и бис(η^5-циклопентадиенил)кобалта(II) ($Co(Cp)_2$), молекула подложних Јан–Телеровој дисторзији, испитивана је коришћењем теорије функционала густине (DFT) за израчунавање хемијских померања независних од језгра (*NICS*). На основу израчунатих хемијских померања, петочлани прстен у $Fe(Cp)_2$ је ароматичнији него изоловани Cp^-. *NICS* вредности, праћене дуж својственог пута дисторзије за $Cp^{\bullet}$ и $Co(Cp)_2$, указују на антиароматичност испитиваних врста, која се смањује са снижењем симетрије од D_{5h} до C_{2v}. Промене у *NICS* параметрима дуж пута дисторзије показују да $Co(Cp)_2$ у ниској симетрији поседује ароматични карактер, за разлику од $Cp^{\bullet}$.

(Примљено 7. новембра 2014, ревидирано 11. марта, прихваћено 12. марта 2015)

REFERENCES

1. H. A. Jahn, E. Teller, *Proc. R. Soc. London, Ser. A* **161** (1937) 220
2. I. B. Bersuker, *The Jahn–Teller Effect*, Cambridge University Press, New York, 2006
3. E. Hückel, *Z. Phys.* **70** (1931) 204
4. E. Hückel, *Z. Phys.* **78** (1932) 628
5. A. D. Allen, T. T. Tidwell, *Chem. Rev.* **101** (2001) 1333
6. A. C. Tsipis, *Phys. Chem. Chem. Phys*. **11** (2009) 8244
7. Lj. Andjelković, M. Perić, M. Zlatar, S. Grubišić, M. Gruden-Pavlović, *Tetrahedron Lett*. **53** (2012) 794
8. M. Perić, Lj. Andjelković, M. Zlatar, C. Daul, M. Gruden-Pavlović, *Polyhedron* **80** (2014) 69
9. Z. Chen, C. S. Wannere, C. Corminboeuf, R. Puchta, P. von Ragué Schleyer, *Chem. Rev.* **105** (2005) 3842
10. P. von Ragué Schleyer, C. Maerker, A. Dransfeld, H. Jiao, N. J. R. van Eikema Hommes, *J. Am. Chem. Soc.* **118** (1996) 6317

11. H. Jiao, P. von Ragué Schleyer, *Angew. Chem. Int. Ed. Eng.* **35** (1996) 2383
12. M. Zlatar, C.-W. Schläpfer, C. Daul, in *The Jahn–Teller-Effect Fundamentals and Implications for Physics and Chemistry*, H. Koeppel, D. R. Yarkoni, H. Barentzen, Eds., Springer Series in Chemical Physics, Vol. 97, Springer, Berlin Heidelberg, 2009, Ch. 1, p. 131
13. H. Ramanantoanina, M. Zlatar, P. García-Fernández, C. Daul, M. Gruden-Pavlović, *Phys. Chem. Chem. Phys.* **15** (2013) 1252
14. M. Gruden-Pavlović, P. García-Fernández, Lj. Andjelković, C. Daul, M. Zlatar, *J. Phys. Chem., A* **115** (2011) 10801
15. M. Perić, Lj. Andjelković, M. Zlatar, A. S. Nikolić, C. Daul, M. Gruden-Pavlović, *Monatsh. Chem.* **144** (2013) 817
16. ADF2013.01. SCM, *Theoretical Chemistry*, Vrije Universiteit, Amsterdam, http://www.scm.com, accessed in July, 2015
17. C. F. Guerra, J. G. Snijders, G. te Velde, E. J. Baerends, *Theor. Chem. Acc.* **99** (1998) 391
18. G. te Velde, F. M. Bickelhaupt, S. J. A. van Gisbergen, C. F. Guerra, E. J. Baerends, J. G. Snijders, T. Ziegler, *J. Comput. Chem.* **22** (2001) 931
19. S. Vosko, L. Wilk, M. Nusair, *Can. J. Phys.* **58** (1980) 1200
20. A. D. Becke, *Phys. Rev., B* **38** (1988) 3098
21. J. P. Perdew, *Phys. Rev., B* **33** (1986) 8822
22. J. P. Perdew, in *Electronic Structure of Solids '91*, P. Ziesche, H. Eschrig, Eds., Akademie Verlag, Berlin, 1991, p. 11
23. M. Swart, A. W. Ehlers, K. Lammertsma, *Mol. Phys.* **102** (2004) 2467
24. M. Swart, *Chem. Phys. Lett.* **580** (2013) 166
25. A. D. Becke, *J. Chem. Phys.* **98** (1993) 5648
26. C. Lee, W. Yang, R. G. Parr, *Phys. Rev., B* **37** (1988) 785
27. A. Bérces, R. M. Dickson, L. Fan, H. Jacobsen, D. Swerhone, T. Ziegler, *Comput. Phys. Commun.* **100** (1997) 247
28. H. Jacobsen, A. Bérces, D. Swerhone, T. Ziegler, *Comput. Phys. Commun.* **100** (1997) 263
29. *Gaussian 09*, Revision A.01, Gaussian, Inc., Wallingford, CT, 2009
30. A. D. Becke, *J. Chem. Phys.* **84** (1986) 4524
31. J. P. Perdew, W. Yue, *Phys. Rev.* **33** (1986) 8800
32. R. E. Dinnebier, U. Behrens, F. Olbrich, *Organometallics* **16** (1997) 3855
33. N. Mohammadi, A. Ganesan, C. T. Chantler, F. Wang, *J. Organomet. Chem.* **713** (2012) 51
34. H. Koch, P. Jørgensen, T. Helgaker, *J. Chem. Phys.* **104** (1996) 9528
35. U. Hohm, D. Goebel, S. Grimme, *Chem. Phys. Lett.* **272** (1997) 328
36. K. Pierloot, B. J. Persson, B. O. Roos, *J. Phys. Chem.* **99** (1995) 3465
37. A. Haaland, J. E. Nilsson, *Acta Chem. Scand.* **22** (1968) 2653
38. M. Swart, *Inorg. Chim. Acta* **360** (2007) 179
39. E. A. Seibold, L. E Sutton, *J. Chem. Phys.* **23** (1955) 1967
40. S. Coriani, A. Haaland, T. Helgaker, P. Jørgensen, *ChemPhysChem* **7** (2006) 245
41. J. Oscar, C. Jiménez-Halla, E. Matito, J. Robles, M. Sola, *J. Organomet. Chem.* **691** (2006) 4359
42. T. M. Krygowski, M. K. Cyrański, *Chem. Rev.* **101** (2001) 1385
43. V. I. Minkin, M. N. Glukhovtsev, B. A. Simkin, *Aromaticity and Antiaromaticity: Electronic and Structural Aspects*, Wiley, New York, 1994
44. V. Ya. Lee, A. Sekiguchi, *Angew. Chem., Int. Ed.* **46** (2007) 6596

45. H. Jiao, P. von Ragué Schleyer, Y. Mo, M. A. McAllister, T. T. Tidwell, *J. Am. Chem. Soc.* **119** (1997) 7075
46. L. Nyulászi, P. von Ragué Schleyer, *J. Am. Chem. Soc.* **121** (1999) 6872
47. M. Laskoski, W. Steffen, M. D. Smith, U. H. F. Bunz, *Chem. Commun.* (2001) 691
48. D. E. Bean, P. W. Fowler, M. J. Morris, *J. Organomet. Chem.* **696** (2011) 2093
49. T. N. Gribanova, R. M. Minyaev, V. I. Minkin, *Open Org. Chem. J.* **5** (2011) 62
50. M. Yu. Antipin, R. Boese, N. Augart, G. Schmid, *Struct. Chem.* **4** (1993) 91
51. M. Zlatar, C.-W. Schläpfer, E. P. Fowe, C. Daul, *Pure Appl. Chem*. **81** (2009) 1397
52. L. Andjelković, M. Gruden-Pavlović, C. Daul, M. Zlatar, *Int. J. Quantum Chem.* **113** (2013) 859
53. M. Zlatar, M. Gruden-Pavlović, C.-W. Schläpfer, C. Daul, *J. Mol. Struc. THEOCHEM* **954** (2010) 86
54. B. E. Applegate, J. Bezant, T. A. Miller, *J. Chem. Phys.* **114** (2001) 4869
55. J. H. Ammeter, L. Zoller, J. Bachmann, P. Baltzer, E. R. Bucher, E. Deiss, *Helv. Chim. Acta* 64 (1981) 1063
56. B. E. Applegate, T. A. Miller, *J. Chem. Phys*. **114** (2001) 4855.

Journal of the Serbian Chemical Society
JSCS-info@shd.org.rs • www.shd.org.rs/JSCS
J. Serb. Chem. Soc. 80 (7) 889–902 (2015)
JSCS–4767
UDC 546.766+541.183+66.095.26+544.713.432
Original scientific paper

The adsorption behavior and mechanistic investigation of Cr(VI) ions removal by poly(2-(dimethylamino)ethyl methacrylate)/poly(ethyleneimine) gels

ZHENGBO HOU, WEIXIA ZHU, HANG SONG, PENGFEI CHEN and SHUN YAO*

School of Chemical Engineering, Sichuan University, Chengdu, 610065, China

(Received 14 July, revised 24 December 2014, accepted 4 March 2015)

Abstract: The composite hydrogels based on 2-(dimethylamino)ethyl methacrylate (DMAEMA) and polyethyleneimine (PEI) were prepared by amino radical polymerization and confirmed by Fourier transform infrared (FTIR) spectroscopy and elemental analysis. Then adsorption behavior and mechanism of Cr(VI) ions adsorption on the obtained materials were investigated by scanning electron microscopy, zeta potential determination and thermogravimetric analysis, *etc*. The adsorption process was found to follow pseudo-second order kinetics and the Langmuir model, and the maximum adsorption capacity of Cr(VI) ions reached 122.8 mg g^{-1}. X-ray photoelectron spectroscopy (XPS) and pH analysis revealed that the Cr(VI) ions were adsorbed into the gels through the electrostatic interaction mechanism, and SO_4^{2-} in the solution had a great effect on the adsorption process. In addition, a high pH and ionic strength could reduce the uptakes of the adsorbate, which could be used for desorption of Cr(VI) ions from the gels.

Keywords: 2-(dimethylamino)ethyl methacrylate; polyethyleneimine; adsorption; Cr(VI); polymerization.

INTRODUCTION

At present, many techniques, such as chemical reduction, adsorption, electrolysis, ion exchange, precipitation *etc*., are employed to remove Cr(VI) ions from wastewater.[1–3] Cr(VI) ions are more toxic than Cr(III).[4] Among the reported traditional techniques, adsorption is an effective method due to the advantages of high selectivity, no secondary pollution, easy operation and the possibility of adsorbent recycling. Various adsorbents have been used to remove Cr(VI), such as macroporous 1,2-ethylenediamine-aminated polystyrene particles.[5] crosslinked cassava residue xanthate,[6] functionalized ordered mesoporous carbon,[7] hard walnut shell,[8] β-FeOOH-coated sand,[9] nitrogen-enriched activated

* Corresponding author. E-mail: cusack@scu.edu.cn
doi: 10.2298/JSC140701024H

carbon from waste medium density fiberboard,[10] a chitosan-coated fly ash composite,[11] iron(III)-impregnated sorbent prepared from sugarcane bagasse,[12] *etc*. Their maximum adsorption capacities were 100.06, 37.76, 68.21, 80.24, 0.060––0.076, 89.21, 33.00 and 13.72 mg g^{-1}, respectively. At present, the exploration for new practical, economic and efficient adsorbents for the removal of Cr(VI) ions is still meaningful and necessary.

In recent years, hydrogels prepared from 2-(dimethylamino)ethyl methacrylate (DMAEMA) and its co-polymers have attracted much interest due to their pH and thermal sensitivity.[13,14] A large number of research reports were concerned with more special environment sensitivities and their applications for water treatment.[15–17] Poly-DMAEMA exhibited a high adsorption capacity (70 mg g^{-1}) for Cr(VI).[18,19] Polyethyleneimine (PEI) is a water-soluble polyamine with many nitrogen atoms of amino groups on its macromolecular chains, which could interact effectively with some kinds of pollutants. Therefore, the copolymerization of PDMAEMA and PEI was expected to provide a material with a high adsorption capacity for the removal of Cr(VI) ions from aqueous solution.

In this study, PEI macromolecules were grafted onto PDMAEMA *via* free radical polymerization on the amine nitrogen atoms, yielding PEI/PDMAEMA for the first time as a novel cationic composite material for the adsorption of anions. The adsorption properties of Cr(VI) ions on the PEI/PDMAEMA were studied thoroughly. It was expected that this PEI/PDMAEMA material would possess satisfactory adsorption capacity and rate for Cr(VI) ions in water.

EXPERIMENTAL

Materials

2-(Dimethylamino)ethyl methacrylate (DMAEMA) monomer, *N*,*N*′-methylenebisacrylamide (MBAA) cross-linker, and azobisisobutyronitrile (AIBN) initiator were purchased from Puguang Industrial Co., Ltd. (each of purity >99 % , Shanghai, China). Branched polyethyleneimine (PEI) ($\bar{M}_w$ = 1800 g mol^{-1}, 25 % aqueous solution, the content of primary, secondary and tertiary amino groups were 35, 35 and 30 %, respectively) was obtained from Mengde Electroplate Chemistry Co. (specific electro-plating class, Jiangsu, China). K_2CrO_4 was provided by Jingqiu Chemistry Factory (AR, Beijing, China).

Preparation of the adsorbents

The polymerization procedures for DMAEMA monomer and MBAA cross-linker were studied in a previous study.[19] For each polymerization, first, 3.144 g DMAEMA, 0.154 g MBAA, and 0.050 g AIBN were dissolved in 3 mL of ethanol solution and the PEI solution was diluted with distilled water to prepare a solution with the mass concentration (0–5 wt. %). Then, the ethanolic mixture was added into 18 mL PEI solution of different concentrations and stirred under a nitrogen atmosphere for 10 min. Afterwards the solutions were immediately poured into tubes with 6 mm inner diameter, which were sealed and submerged in thermostatic water bath for 3 h at different temperatures. Finally, the PEI/PDMAEMA gels were rapidly cooled to room temperature and cut into 3-mm thick slices for further use. The

composite materials prepared with 0, 3 and 5 wt. % PEI solution were marked as ED 0, ED 3 and ED 5, respectively.

The amount of PEI in the adsorbent (graft yield, *GY*) was determined by element analysis. According to the content of elements, *GY* could be calculated as follows:

$$GY(\%) = \frac{W_{\mathrm{PEI}}}{W_{\mathrm{PDMAEMA}}} \times 100 \quad (1)$$

where W_{PEI} and W_{PDMAEMA} are the PEI and PDMAEMA weight percentage in the PEI/ /PDMAEMA material, respectively, which were calculated from the results of the element analysis.

Characterization of the PDMAEMA and PEI/PDMAEMA

The FTIR spectra of PDMAEMA and PEI/PDMAEMA were recorded on Spectrum One FTIR spectrometer (Perkin–Elmer, USA) as KBr discs. The zeta potential analysis was performed using a PALS Zeta Potential Analyzer, version 3.43 (Brookhaven Instruments, USA). Elemental analyses were accomplished with 2400 Series II CHNS/O elemental analyzer (PerkinElmer, USA). The DTG curves were obtained using a FRC/T-2 thermal analyzer (Optical Instruments Factory, Beijing, China) at a heating rate of 10 °C min^{-1} under a nitrogen atmosphere. The morphology of the dried composite materials after drying under vacuum at 50 °C for 24 h was observed using a JEM-100CX-II scanning electron microscope (SEM). (JEOL, Japan). X-ray photoelectron spectroscopy (XPS) data were obtained with an ESCALab220i-XL electron spectrometer (VG Scientific, USA) using 300 W AlK_{α} radiation. To compensate for surface charge effects, the binding energies were calibrated using the C1s hydrocarbon peak at 284.8 eV.

The hydrogels were immersed in water to reach a swollen equilibrium at 40 °C. Afterwards, they were withdrawn and weighed after the removal of excess surface water. Equilibrium Swelling Ratio (*ESR*) is the moisture content to dry weight of hydrogel ratio:

$$ESR = \frac{W_{\mathrm{s}} - W_{\mathrm{d}}}{W_{\mathrm{d}}} \quad (2)$$

where W_{s} is the weight of the swollen gel at the desired time and W_{d} is the weight of the dried gel.

Adsorption of Cr(VI) ions

A certain amount of $\mathrm{K_2CrO_4}$ was dissolved in redistilled water to obtain the stock solution. The concentrations of Cr(VI) were determined by TU1810SPC UV–Vis spectrophotometer (Puxitongyong Instrument Co., Ltd., China) at 540 nm. For each adsorption experiment, the stock solution was diluted to desired concentration (c_0, 25–225 mg L^{-1}), and then the adsorbents were immersed into the conical flasks containing the diluted solution. Finally, the conical flasks were placed in a shaking bed at different temperatures for desired time, and the concentration in supernatant was determined as c_t. In addition, the solution pH was adjusted by 1 mol L^{-1} HCl or 1 mol L^{-1} NaOH and monitored by a digital pH meter (Yulong Instrument Co., Ltd., China).The adsorption amount of Cr(VI) (Q, mg g^{-1}) was calculated according to the following equation:

$$Q = \frac{V(c_0 - c_t)}{W_{\mathrm{PEI/PDMAEMA}}} \quad (3)$$

where V (mL) and $W_{PEI/PDMAEMA}$ (g) stand for the solution volume and the mass of the adsorbent, respectively.

Desorption of Cr(VI) ions

Firstly, the sorbents were immersed in 150 mg L^{-1} of Cr(VI) solution at pH 2.0 for 4 h to reach equilibrium, respectively. The adsorption amount (Q_a, mg g^{-1}) of Cr(VI) ions, was calculated by Eq. (3). Then the sorbents were filtered and soaked in 10 mL of 0.1 mol L^{-1} NaOH solution for 24 h at room temperature. Finally, the concentration of Cr(VI) ions in the eluent was determined, and the amount of desorption was denoted by Q_d (mg g^{-1}). The desorption ratio was defined by the following equation:

$$\text{Desorption ratio } (\%) = \frac{Q_d}{Q_a} \times 100 \quad (4)$$

RESULTS AND DISCUSSION

Preparation process and characterization of PEI/PDMAEMA

As a very popular azo-initiator in polymerization processes, azobisisobutyronitrile (AIBN) can easily produce nitrogen gas and radicals through splitting reaction. Polyethyleneimine (PEI) possesses many free amino groups. When they interact with the radicals of the AIBN initiator, the amino group will lose a proton. As the result, a nitrogen radical ($N^{\bullet}$) together with 2-cyano-2-propyl radical ($C^{\bullet}$) could be obtained. Then, the former ($N^{\bullet}$) could initiate the copolymerization of DMAEMA to form PEI/PDMAEMA. The role of amine in vinyl radical polymerizations was summarized and analyzed in a previous study.[20] In addition, the latter ($C^{\bullet}$) could either produce the polymerization among the monomer or abstract a hydrogen atom from the PEI, resulting in the copolymerization of DMAEMA and PEI. The related copolymerization process is shown in Scheme 1.

The ultrasound-assisted (at room temperature) and the Soxhlet extraction methods with 95 % ethanol were first used to verify the copolymerization of PEI on the polymer network. There was no or negligible residual remains in the extracted liquid after the removal of solvent under vacuum. The results indicated that PEI had been successfully grafted onto the network and the copolymerization product was stable. Furthermore, the formation of ED 0 and ED 5 could be further proved by FTIR spectroscopy according to an analysis similar to that in previous reports.[21–24] All of the IR spectra are shown in Fig. 1.

Moreover, zeta potential analysis was used to characterize the PEI/ /PDMAEMA products. The zeta potential of ED 0 was only +7.25 mV, but for ED 5, it became +20 mV in pH 2 hydrochloric acid buffer solution. This could be interpreted as proof of the incorporation of PEI, which contains many amino functional groups. In order to analyze the content of nitrogen before and after introduction of PEI, the ED 0, ED 3 and ED 5 materials were characterized by elemental analysis (Table I). Compared with ED 0 and ED 3, ED 5 had a higher content of nitrogen. According to elemental analysis, the amount of PEI in the ED 5 was calculated to be 5.93 %.

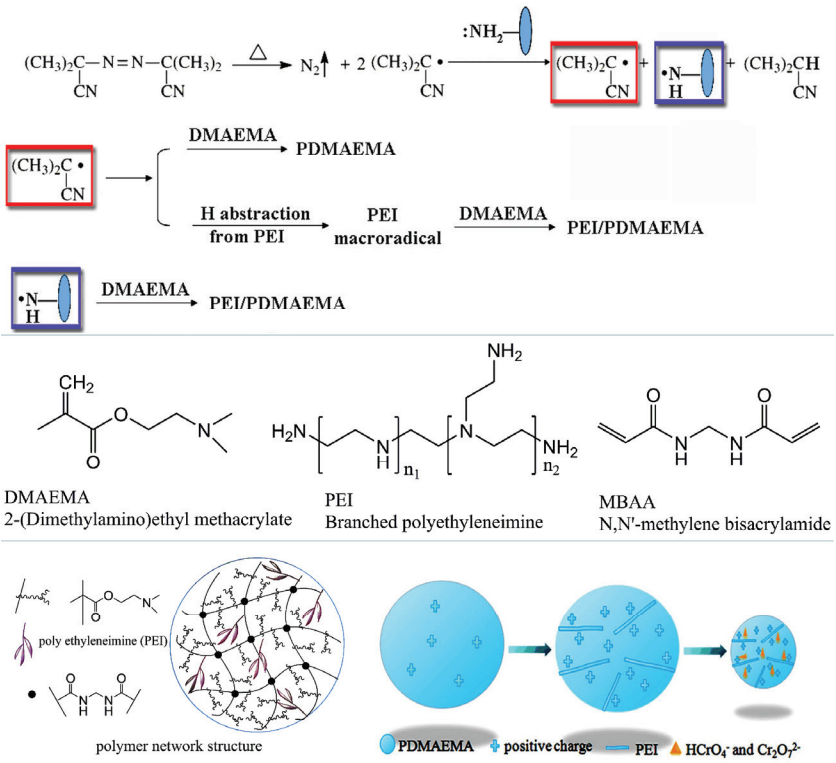

Scheme 1. Copolymerization process of PEI/PDMAEMA gels and adsorption of Cr(VI).

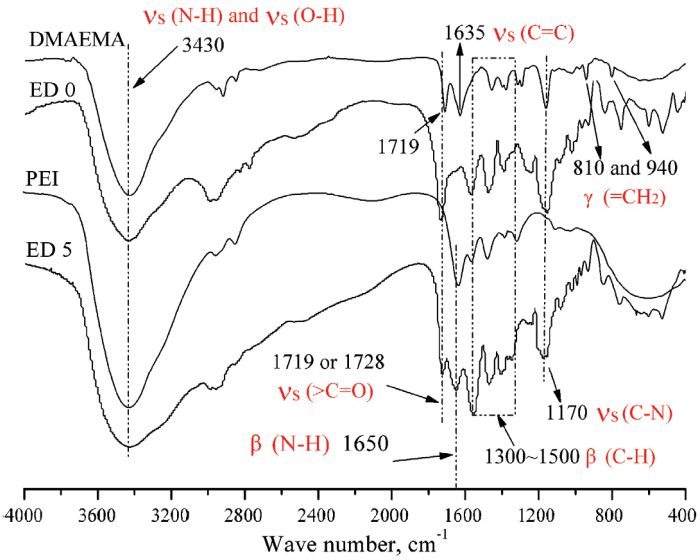

Fig. 1. FTIR spectra of PEI, DMAEMA, PEI/PDMAEMA (ED 5) and PDMAEMA (ED 0).

TABLE I. Elemental analysis (%) of ED 0, ED 3 and ED 5

Material	Element				GY_{PEI} / %
	C	H	N	O	
ED 0	58.50	13.22	6.81	21.47	–
ED 3	58.67	12.01	8.11	21.21	3.76
ED 5	58.60	10.08	9.32	22.00	5.93

The thermal stability of the PEI, ED 0 and ED 5 gels were examined by thermal analysis (Fig. 2). The removal of physically adsorbed and interlayer water occurred up to 150 °C, and the raw PEI sample lost its 75 % weight in this temperature range. In the second stage, a significant weight loss of 44.68 % could be attributed to the decomposition of the functional amino-groups on the composite material when the temperature ascended to 300 °C. As shown in the differential thermogravimetric (DTG) curves, the rate of mass loss reached its maximum at 281 °C for ED 0, but was postponed by 20 °C after incorporation of PEI. In the last stage, a smaller mass loss of 14.83 % in the 300–400 °C range was associated with degradation of the carbon skeletons, and the fastest decomposition rate appeared at 413 °C. These results implied that the ED 5 gel was successfully prepared and ED 5 could be applied in higher temperature system.

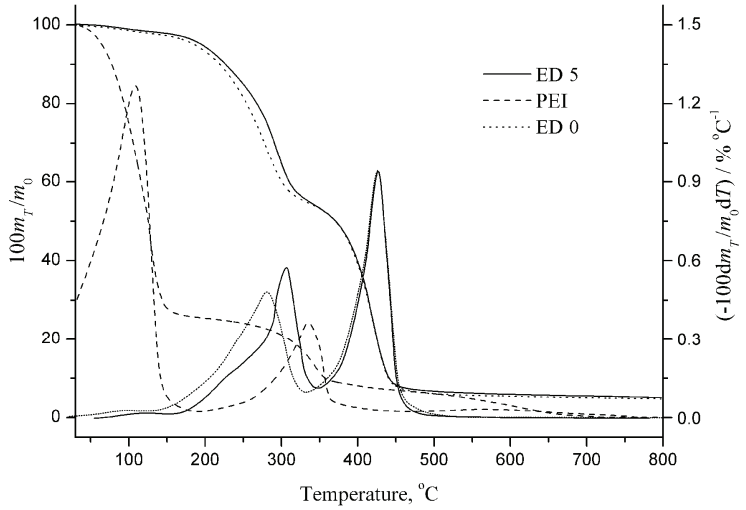

Fig. 2. Thermogravimetric and differential thermogravimetric curves of PEI, ED 0 and ED 5.

Equilibrium swelling ratios (ESR) of PEI/PDMAEMA

The swelling behavior of the hydrogels in water at different temperatures is shown in Fig. 3. As is clearly shown, the ESR of ED 0 and the ED 5 gels

decreased with increasing temperature and exhibited a marked inflexion when the temperature reached the special critical point, which is consistent with the lower critical solution temperature[25–27] (LCST: around 40 °C and 65 °C for ED 0 and ED 5, respectively). Figure 3 also shown the ESR of ED 5 immersed in buffer solution as a function of pH value. The gel in the buffer solution with the low pH value presented higher swelling ratios than those of the gel in the alkaline solution. The results could be explained by the following reason: the free electron pair of the amino group conjugated with the carboxyl in the DMAEMA units when the gel was immersed in water. However, this coordination was severely weakened in the acidic solution because of protonation of the tertiary amino groups.[27]

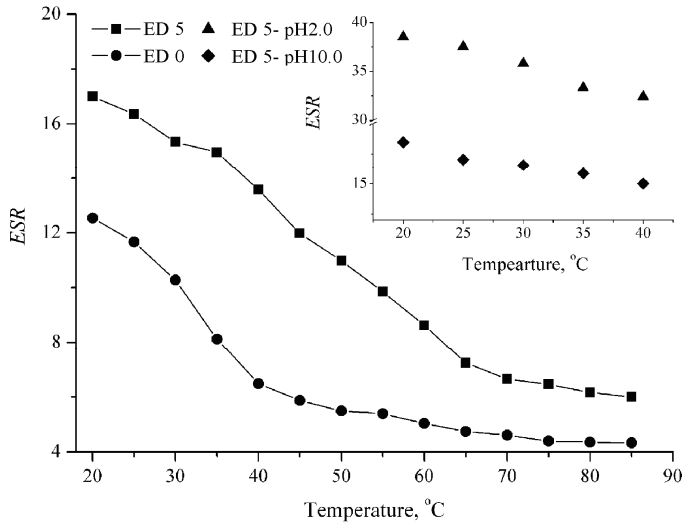

Fig. 3. Equilibrium swelling ratios of ED 0 and ED 5 gels in purified water and ED 5 in acid or alkali solution at different temperatures.

Adsorption kinetics of Cr(VI) ions

Adsorption duration is an important factor affecting the adsorption process and amount. The optimal duration of adsorption was investigated, and the results (Fig. S-1 of the Supplementary material to this paper) showed that the introduction of PEI onto PDMAEMA gels had a significant effect on the adsorption behavior of Cr(VI). When the concentration of PEI was increased to 5 %, the amount of adsorbed Cr(VI) ions increased to 122.8 mg g^{-1} and the adsorption rate was obviously improved, *e.g.*, the adsorption by ED 5 reached complete saturation after 120 min, but for ED 0, 180 min were needed. A high adsorption rate is desirable to provide for a short contact time between the metal solution and the adsorbent in an actual process.[28] Furthermore, the influence of tempe-

rature in the preparation process could be ascribed to a change in the degree of crosslinking. The higher the reaction temperature was, the faster was the reaction rate, and the denser was the degree of crosslinking in the network. As the result, the inflexibility of polymer became stronger and the elasticity became weaker. It was very difficult for Cr(VI) anions to be adsorbed by the internal active site with a too high degree of crosslinking.

The kinetic model provides information regarding the mechanism and thus the adsorption data were correlated with the pseudo-first order kinetic model and pseudo-second order kinetic model.[29]

The adsorption kinetic parameters are summarized in Table II. It was found that the theoretical $Q_{e,cal}$ values for the adsorbate were very close to the experimental Q_{eq} values in the case of the pseudo-second order kinetics. Furthermore, all the linear fitting coefficients (R^2) of the pseudo-second order kinetics were above 0.99, which were slightly higher than were those of the pseudo-first order kinetics. Thus, the pseudo-second order equation fitted well with the experimental data and could describe the adsorbent behavior well.

TABLE II. The adsorption kinetic parameters of Cr(VI) ions onto the gels; $Q_{e,exp}$: the equilibrium adsorption amount of Cr(VI) (experimental data); k_1: the adsorption rate constant for the pseudo-first order model; $Q_{e,cal}$: the equilibrium adsorption amount of Cr(VI) (calculated data); k_2: the adsorption rate constant for the pseudo-second order model

Sample	$Q_{e,exp}$ mg g^{-1}	Pseudo-first order model			Pseudo-second order model		
		$k_1\times10^{-3}$ min^{-1}	$Q_{e,cal}$ mg g^{-1}	R^2	$k_2\times10^{-3}$ g mg^{-1}	$Q_{e,cal}$ mg g^{-1}	R^2
ED 0	73.17	16.31	71.30	0.9508	0. 2929	81.94	0.9932
ED 3	95.34	22.98	87.91	0.9637	0.4276	102.1	0.9974
ED 5	122.8	25.42	88.12	0.9643	0.6052	128.0	0.9991
75 °C	91.86	29.75	116.3	0.8881	0.4094	99.41	0.9967
85 °C	122.8	25.37	88.12	0.9643	0.6047	128.0	0.9991
95 °C	85.03	15.59	68.44	0.9867	0.3897	92.25	0.9982

Adsorption isotherm of Cr(VI) ions

Adsorption isotherm is one of the important parameters for understanding the adsorption behavior and mechanism. The adsorption equilibrium curves are shown in Fig. S-2 of the Supplementary material, and the Langmuir and Freundlich isotherm models were used to fit the equilibrium data.[30–33]

As shown in Table III, the values of $Q_{e,cal}$ derived from the Langmuir model increased with increasing temperature up to 40 °C but decreased with further increasing of the temperature. This could be explained as follows: the elevated temperature enhanced the deprotonation of amino-groups and resulted in a weaker interaction between the amino groups and Cr(VI) ions.[16] In addition, from the comparison of R^2, R_L and k values, it was found that the Langmuir model could fit much better with the experiment data. Overall speaking, the

Langmuir isotherm gave a better fit to the experimental data than the Freundlich isotherm. The results indicated insights on the monolayer coverage of PEI/ /PDMAEMA composite and that there were no side interactions among the adsorbates. Furthermore, the site-specific interactions took place between the binding sites and anions, and the adsorbent surface was homogeneous.

TABLE III. The adsorption isotherms parameters of Cr(VI) ions onto the ED 5; K_L: the constant of the Langmuir isotherm; R_L: the separation factor of Langmuir isotherm (favorable ($0 < R_L < 1$), unfavorable ($R_L > 1$), linear relationship ($R_L = 1$) and irreversible ($R_L = 0$)[30-32]); K_F: the constant of the Freundlich isotherm; k: the slope of Freundlich isotherm model (Langmuir isotherm ($k < 1$), Freundlich isotherm ($k > 1$)[32-34])

T / °C	Langmuir model				Freundlich model		
	K_L / 10^2 L mg^{-1}	$Q_{e,cal}$ / mg g^{-1}	R^2	R_L	K_F / mg g^{-1}	k	R^2
30	2.719	146.2	0.9915	0.4238–0.1379	11.23	0.4980	0.9802
40	5.366	172.7	0.9879	0.2715–0.0749	19.41	0.4771	0.8967
50	3.745	159.0	0.9943	0.3481–0.1040	15.36	0.4755	0.9764
60	3.063	153.1	0.9981	0.3950–0.1243	12.12	0.5035	0.9718

Effect of initial pH value on the adsorption process

The pH value influences the distribution of Cr(VI) ions species, Fig. 4 (main forms: $H_2Cr_2O_7$ (pH < 1), $HCrO_4^-$ and $Cr_2O_7^{2-}$ (1 < pH < 6) and CrO_4^{2-} (pH > > 6)). For PEI/PDMAEMA, the pH value affects the protonation and deprotonation of amino groups, which are the active adsorption sites for anions. The maximum amount of Cr(VI) ions adsorption onto ED 5 and ED 0 were both obtained at pH 2.0. With increasing pH values, the interaction between anions and amine groups weakened because of the deprotonation of the amino groups and the competition of OH^-. However, when the pH value was below 2.0, the uptake of

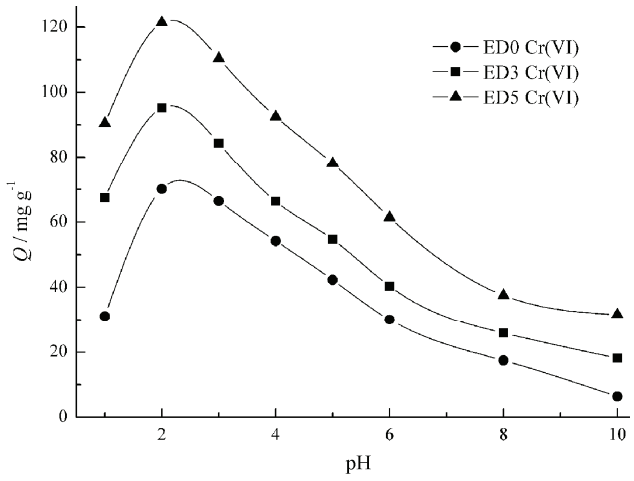

Fig. 4. The effects of pH on the adsorption of Cr(VI) ions onto the gels at 40 °C.

Cr(VI) ions decreased because the Cr(VI) ions converted into $H_2Cr_2O_7$, which unfavorably interacted with the protonated amine groups. Furthermore, when the pH value was 10.0, the Cr(VI) uptake was still up to 32 mg g^{-1} onto the ED 5. It could be concluded that the adsorption amount reached maximum values around a pH value of 2.0, and the working pH range of the composite adsorbent for Cr(VI) ions was obviously improved due to the introduction of PEI.

Effects of ionic strength and species on the adsorption process

The results are shown in Fig. S-3 of the Supplementary material. The adsorption capacities of the gels remarkably decreased with increasing concentration of NaCl because of the competition between Cl^- and the anionic adsorbents. The effect of ionic species could be divided into two groups: cationic group (NaCl, KCl and NH_4Cl) and anionic group (NaCl, $NaNO_3$ and Na_2SO_4). The results showed that the effects of ions (Na^+, K^+, NH_4^+, Cl^- and NO_3^-) on the adsorption process were not obvious. Comparatively speaking, the SO_4^{2-} had a great effect on the adsorption process. This could be summarized as the competition between Cr(VI) and SO_4^{2-}.

Morphology and XPS analysis

Figure 5 shows the SEM images of ED 0, ED 5 and ED 5 after adsorption of Cr(VI). These samples were coated with a thin layer of gold and examined by

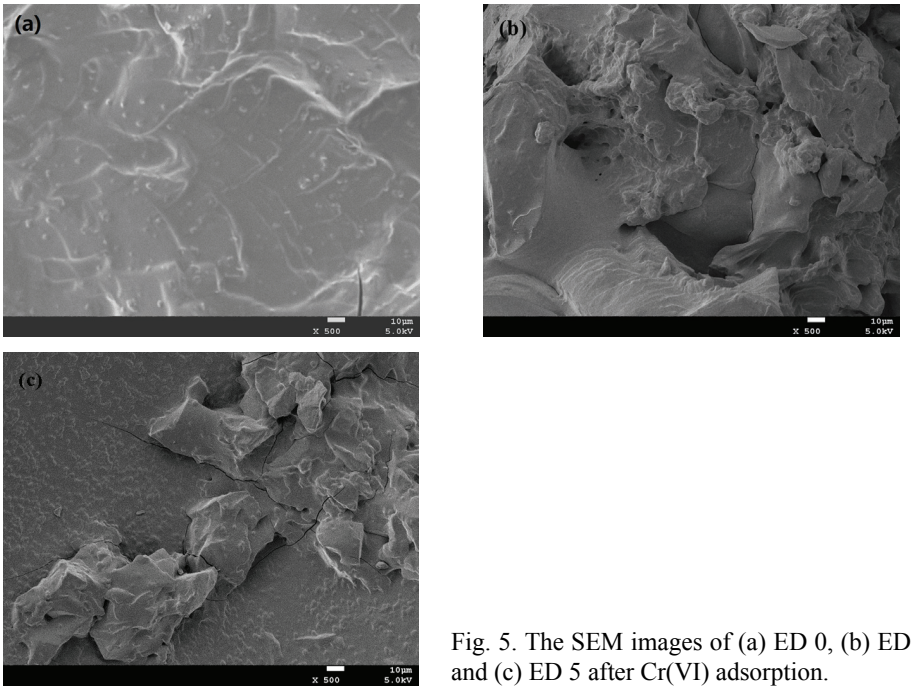

Fig. 5. The SEM images of (a) ED 0, (b) ED 5 and (c) ED 5 after Cr(VI) adsorption.

SEM. After the introduction of PEI on the polymer, there were no significant changes in the morphology of the gels. However, clearly ragged topographies appeared after Cr(VI) ions adsorption, which was relevant to the formation of bubbles during the adsorption process.

The XPS spectra of the ED 5 composite material before and after Cr(VI) adsorption are shown in Fig. 6a. Before adsorption, only the peaks at the binding energies of *ca*. 284.8, 399.5 and 532.4 eV, corresponding to C, N and O, res-

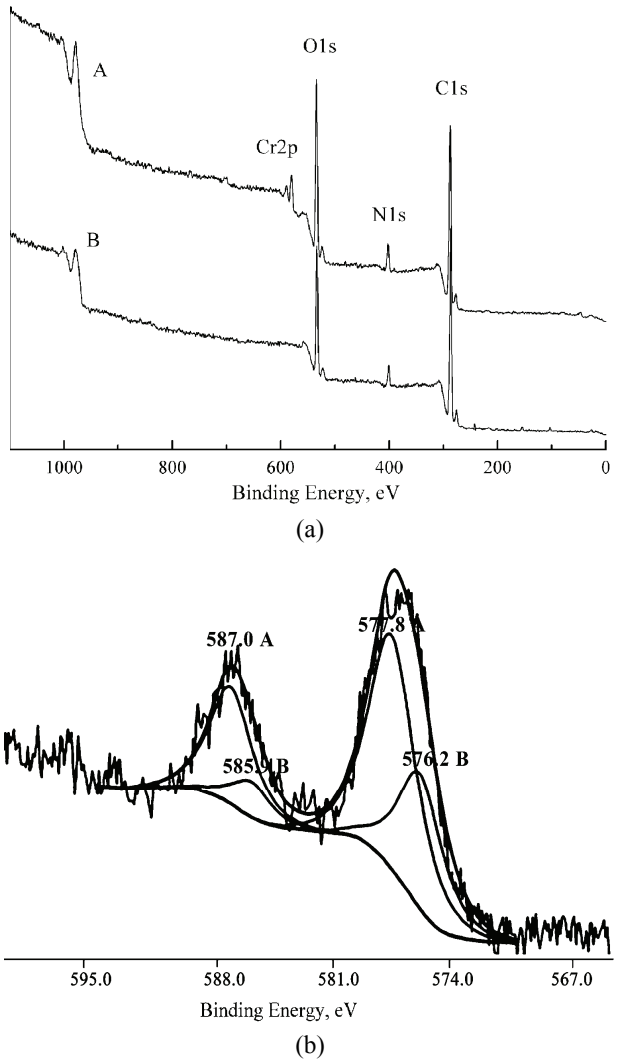

Fig. 6. a) The XPS spectra of ED 5 composite material before (A) and after (B) Cr(VI) adsorption; b) the results of a meticulous XPS analysis of the ED 5 composite material for (A) $Cr_2O_7^{2-}$ and (B) $HCrO_4^-$ adsorption.

pectively, could be found in the XPS spectrum of ED 5. After adsorption, new significant bands corresponding to Cr(VI) appeared at binding energy of *ca*. 577.2 and 586.8 eV. The result confirmed that Cr(VI) had been adsorbed onto ED 5. Furthermore, a meticulous XPS analysis was performed using fitting software and the results were presented in Fig. 6b. The main peak of *ca*. 277.5 eV was made up of 577.8 and 576.2 eV peaks, which indicated that the forms of the adsorbed Cr(VI) ions were $HCrO_4^-$ and $Cr_2O_7^{2-}$.[35] This conclusion was in accord with the fact that $HCrO_4^-$ and $Cr_2O_7^{2-}$ exist mainly in the pH range of 1.0–6.0.

Desorption of Cr(VI) ions

According to repeated experiments, the pH value of the solution could obviously affect the interaction between anionic adsorbates and the amine groups in the composite materials. Thus, 0.1 mol L^{-1} NaOH solution was chosen for the desorption process. The results showed 96.3 % of Cr(VI) ions were eluted from ED 5 by the alkali liquor, far higher than the 56.8 % by distilled water. Then, the ED 5 was washed to neutral with distilled water and reused to adsorb Cr(VI) ions. The adsorption capacity remained high at 108.5 mg g^{-1} after being recycled five times. There was no significant reduction in its adsorption efficiency. The results also revealed that the PEI/PDMAEMA gels were stable under these experimental conditions.

CONCLUSIONS

Using the amino radical polymerization technology, the composite material PEI/PDMAEMA was conveniently fabricated, and the complex grafting process was avoided. The composite material was characterized by FTIR spectroscopy, elemental analysis, thermogravimetric analysis and zeta potential analysis. The equilibrium adsorption amount of Cr(VI) on ED 5 was 122.8 mg g^{-1}. The results of the influence of temperature, pH and XPS analysis showed that the adsorption mechanism was electrostatic interaction, and the forms of Cr(VI) ions adsorbed onto the ED 5 at pH 2 were $HCrO_4^-$ and $Cr_2O_7^{2-}$. The desorption ratio of Cr(VI) ions could be 96.3% using 0.1 mol L^{-1} NaOH solution as the eluent and the composite material PEI/PDMAEMA showed an excellent recyclability efficiency.

SUPPLEMENTARY MATERIAL

Additional Cr(VI) adsorption data are available electronically from http:// //www.shd.org.rs/ JSCS/, or from the corresponding author on request.

Acknowledgments. Preparation of this paper was supported by the National Scientific Foundation of China (No. 81373284) and the 2013 Scientific Research Foundation of Sichuan University for Outstanding Young Scholars.

ИЗВОД

ИСПИТИВАЊЕ МЕХНИЗМА АДСОРПЦИЈЕ ПРИ УКЛАЊАЊУ Cr(VI) ЈОНА ГЕЛОВИМА ПОЛИ(2-(ДИМЕТИЛАМИНО)ЕТИЛ-МЕТАКРИЛАТ)/ПОЛИ(ЕТИЛЕНИМИН)

ZHENGBO HOU, WEIXIA ZHU, HANG SONG, PENGFEI CHEN и SHUN YAO

School of Chemical Engineering, Sichuan University, Chengdu, 610065, China

Композитни хидрогелови базирани на 2-(диметиламино)етил-метакрилату (DMAEMA) и полиетиленимину (PEI) су добијени полимеризацијом амино радикала, што је потврђено инфрацрвеном спектроскопијом са Фуријеовом трансформацијом (FTIR) и елементалном анализом. Механизам адсорпције Cr(VI) на добијеним материјалима је испитиван скенирајућом електронском микроскопијом, одређивањем зета потенцијала и термогравиметријском анализом. Нађено је да процес адсорпције прати кинетику псеудо-другог реда и Лангмиров модел, као и да је максимални адсорпциони капацитет Cr(VI) јона 122,8 mg g^{-1}. Анализом фотоелектронском спектроскопијом X-зрачења (XPS) и pH мерењима је показано да су Cr(VI) адсорбовани на геловима електростатичким интеракцијама, и да SO_4^{2-} у раствору има значајан утицај на процес адсорпције. Уз то, високе вредности pH и јонске јачине погодују редукцији адсорбованих Cr(VI) јона, што се може искористити приликом њихове десорпције са гелова.

(Примљено 14. јула, ревидирано 24. децембра 2014, прихваћено 4. марта 2015)

REFERENCES

1. L. Zhao, J. Sun, Y. H. Zhao, L. Xu, M. L. Zhai, *Chem. Eng. J.* **170** (2011) 162
2. V. Pascal, D. Laetitia, S. Joël, S. Marc, P. Serge, *Appl. Surf. Sci.* **253** (2007) 3263
3. K. J. Cronje, K. Chetty, M. Carsky, J. N. Sahu, B. C. Meikap, *Desalination* **275** (2011) 276
4. V. Janaki, K. Vijayaraghavan, A. K. Ramasamy, B. T. Oh, K. J. Lee, S. Kamala-Kannan, *J. Hazard. Mater.* **241** (2012) 110
5. L. I. Cui, Q. Q. Meng, J. Y. Zheng, X. Wei, Z. F. Ye, *Vacuum* **89** (2013) 1
6. J. H. Shi, B. F. Lin, D. S. Xiao, J. W. Ding, *Appl. Chem. Ind.* **41** (2012) 609
7. T. Chen, T. Wang, D. J. Wang, J. Q. Zhao, X. C. Ding, S. D. Wu, H. R. Xue, J. P. He, *Acta. Phys. Chim. Sin.* **26** (2010) 3249
8. X. Xin, X. He, K. Cui, H. R. Chen, M. N. Sun, L. Yao, *J. Environ. Eng.* **4** (2010) 2273
9. C. H. Xu, D. D. Cheng, B. Y. Gao, Z. L. Yin, Q. Y. Yue, X. Zhao, *Front. Environ. Sci. Eng.* **6** (2012) 455
10. Y. Wu, J. Zhang, J. J. Xiao, J. M. Gao, Q. Zhao, *Wood Sci. Technol.* **48** (2014) 713
11. Y. Wen, Z. Tang, Y. Chen, Y. Gu, *Chem. Eng. J.* **175** (2011) 110
12. Y. Zhu, H. Zhang, H. Zeng, M. Liang, R. Lu, *Int. J. Environ. Sci. Technol.* **9** (2012) 463
13. N. Orakdogen, *Polym. Eng. Sci.* **53** (2013) 734
14. C. C. Li, L. Xu, M. L. Zhai, J. Peng, C. Yang, J. Q. Li, G. S. Wei, *Polymer* **50** (2009) 4888
15. C. C. Li, Y. W. Zhang, J. Peng, H. Wu, J. Q. Li, M. L. Zhai, *Radiat. Phys. Chem.* **81** (2012) 967
16. H. Tokuyama, N. Ishihara, *React. Funct. Polym.* **70** (2010) 610
17. H. M. Abdel-Aziz, T. Siyam, *Water Air Soil Poll.* **218** (2011) 165
18. W. X. Zhu, C. Yang, H. Song, Q. Y. Wang, K. F. Du, *Asian J. Chem.* **25** (2013) 2293
19. W. X. Zhu, H. Song, K. F. Du, H. Zeng, S. Yao, *J. Appl. Polym. Sci.* **128** (2013) 2729
20. X. D. Feng, *Makromol. Chem., Macromol. Symp.* **63** (1992) 1

21. J. Chen, M. Z. Liu, W. Chen, N. Y. Zhang, S. Y. Zhu, S. P. Zhang, Y Xiong, *J. Biomater. Sci. Polym. Ed.* **22** (2011)1568
22. C. C. Li, L. Xu, M. L. Zhai, J. Peng, J. Q. Li, *J. Appl. Polym. Sci.* **120** (2011) 2027
23. Q. Cheng, C. C. Li, L. Xu, J. Q. Li, M. L. Zhai, *Chem. Eng. J.* **173** (2011) 42
24. V. K. Gochev, Z. I. Velkova, M. S. Stoytcheva, *J. Serb. Chem. Soc.* **75** (2010) 551
25. Z. M. O. Rzaev, S. Dincer, E. Piskin, *Prog. Polym. Sci.* **32** (2007)534
26. H. L. Liu, M. Z. Liu, S. P. Jin, S. L. Chen, *Polym. Int.* **57** (2008)1165
27. Y. Chen, W. J. Xu, Y. Q. Xiong, C. Peng, W. Y. Liu, G. Z. Zeng, Y. Peng, *J. Mater. Res.* **28** (2013) 1394
28. G. Bayramoglu, M. Y. Arica, *Chem. Eng. J.* **139** (2008) 20
29. K. Tong, M. J. Kassim, A. Azraa, *Chem. Eng. J.* **170** (2011) 145
30. K. R. Hall, L. C. Eagleton, A. Acrivos, T. Vermeulen, *Ind. Eng. Chem. Fund.* **5** (1966) 212
31. G. Guclu, S. Keles, *J. Appl. Polym. Sci.* **106** (2007) 2422
32. M. Z. Momcilović, M. S. Randelović, A. E. Onjia, A. Zarubica, B. M. Babić, B. Z. Matović, *J. Serb. Chem. Soc.* **79** (2014) 481
33. Y. Liu, Y. Zheng, A. Wang, *J. Environ. Sci.* **22** (2010) 486
34. F. Haghseresht, G. Q. Lu, *Energ. Fuel* **12** (1998) 1100
35. K. Selvi, S. Pattabhi, K. Kadirvelu, *Bioresour. Technol.* **80** (2001) 87.

Journal of the Serbian Chemical Society
JSCS@tmf.bg.ac.rs • www.shd.org.rs/JSCS
J. Serb. Chem. Soc. 80 (7) S248–S249 (2015) *Supplementary material*

SUPPLEMENTARY MATERIAL TO

The adsorption behavior and mechanistic investigation of Cr(VI) ions removal by poly(2-(dimethylamino)ethyl methacrylate)/poly(ethyleneimine) gels

ZHENGBO HOU, WEIXIA ZHU, HANG SONG, PENGFEI CHEN and SHUN YAO*

School of Chemical Engineering, Sichuan University, Chengdu, 610065, China

J. Serb. Chem. Soc. 80 (7) (2015) 889–902

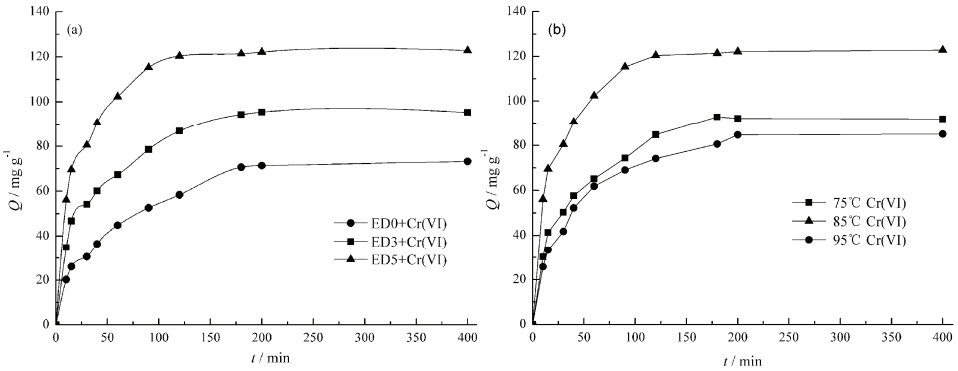

Fig. S-1. Adsorption kinetics of Cr(VI) ions onto gels prepared under the same conditions (temperature: 40 °C; pH 2.0) except for: a) different weight ratios of PEI and b) different reaction temperatures.

* Corresponding author. E-mail: cusack@scu.edu.cn

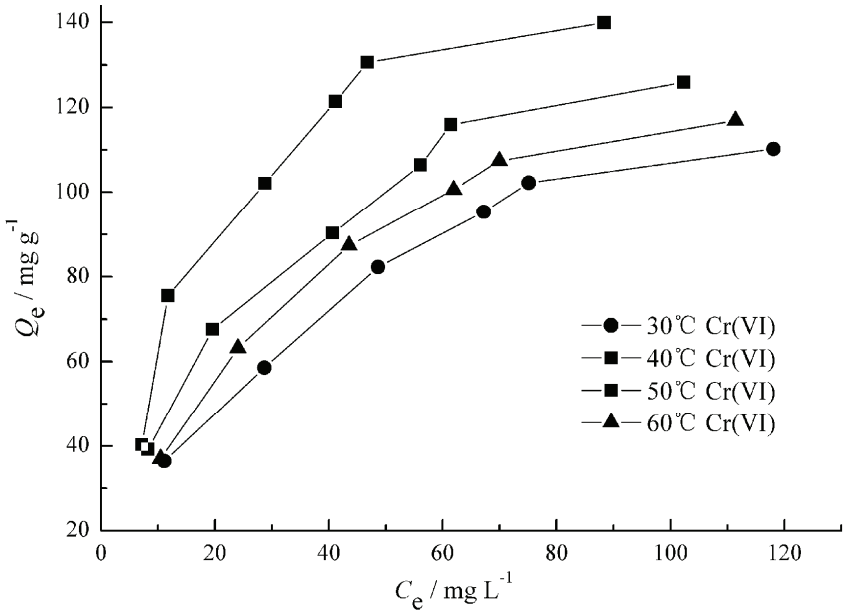

Fig. S-2. Adsorption isotherms of Cr(VI) ions onto ED 5 at pH 2.0 at different temperatures.

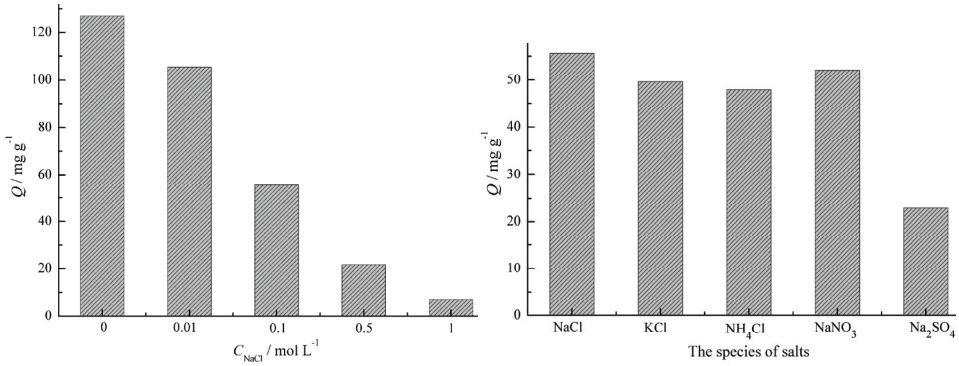

Fig. S-3. The effects of ionic strength and species on the adsorption of Cr(VI) ions. Temperature: 40 °C; pH: 2.0; the concentrations of salts: 0.1 mol L^{-1}.

Journal of the Serbian Chemical Society
JSCS-info@shd.org.rs • www.shd.org.rs/JSCS
J. Serb. Chem. Soc. 80 (7) 903–915 (2015)
JSCS–4768
UDC 543.637–035.67+667.281+546.133.1:66.099.72+541.135
Original scientific paper

Electrochemical decolorization of the Reactive Orange 16 dye using a dimensionally stable Ti/PtO*x* anode

DUŠAN Ž. MIJIN*#, VUK D. TOMIĆ and BRANIMIR N. GRGUR

Faculty of Technology and Metallurgy, University of Belgrade, Karnegijeva 4, 11020 Belgrade, Serbia

(Received 17 September, revised 5 November, accepted 6 November 2014)

Abstract: The electrochemical decolorization of Reactive Orange 16 in a chloride containing solution was studied using a dimensionally stable Ti/PtO*x* anode. Different reaction parameters, agitation speed, applied current, sodium chloride concentration, and dye concentration were varied and the optimum electrolysis conditions were suggested. Hypochlorous acid was suggested to be the active species in the electrochemical decolorization. Moreover, the reaction was studied using UV–Vis spectrophotometry, high-pressure liquid chromatography (HPLC), total organic carbon (*TOC*) and total nitrogen (*TN*) analyses.

Keywords: reactive dye; azo dye; electrolysis, hypochlorite; hypochlorous acid.

INTRODUCTION

The wastewaters from the textile industry contain, among other chemicals, unreacted dyestuffs. Even a small amount of dye in water (≈1 ppm) is highly visible and affects the water transparency, the gas solubility, and possesses potential carcinogenic and mutagenic properties.[1,2] Textile dyes can be classified based on the method of fixation to the textile fiber (*e.g.*, reactive, direct, acid) or chemical structure (*e.g.*, azo, anthraquinone, indigoid).

Azo dyes are synthetic organic colorants with a chromophoric azo group (–N=N–). On the one side, the azo group is attached to an aromatic or heterocyclic nucleus and on the other, to an unsaturated molecule of the carbocyclic, heterocyclic or aliphatic type. Azo colorants are the most widespread and versatile class of organic dyestuffs. As published in the Kirk–Othmer Encyclopedia of Chemical Technology in 2003, there are more than 10,000 Color Index (CI) generic names assigned to commercial colorants. Approximately 4,500 of them are in use, and over 50 % belongs to the azo group of compounds. The broad

* Corresponding author. E-mail: kavur@tmf.bg.ac.rs
# Serbian Chemical Society member.
doi: 10.2298/JSC140917107M

usage range of the azo dyes is due to the number of variations in chemical structure and methods of application, which are not complex in general.[3]

Most dyes are resistant to biodegradation or physico-chemical treatments (e.g., chemical precipitation and separation of pollutants, coagulation, elimination by adsorption, *etc*.).[4–7] These methods are not destructive, leading to the formation of sludge, and thus transferring pollutant from one phase to another, causing a new kind of pollution. An alternative to the mentioned processes are the advanced oxidation processes (AOPs), which are able to decolorize and mineralize dyestuffs and other organic pollutants.[8–13]

Different electrochemical methods, such as direct or indirect anodic oxidation, cathodic reduction or electrocoagulation, could be used for decolorization and/or degradation of dyes.[14–18] In order to achieve better fixation and exhaustion of reactive, direct or substantive dyes, an electrolyte, NaCl or Na_2SO_4, is usually added. The salt also acts as an electrolyte during the further electrochemical treatment.[17] Due to its low price and the formation of strong oxidizing electrolysis products, sodium chloride is considered as one of the best choices.[18] During the electrolysis, depending on the reaction conditions, strong oxidizing species – chlorine, hypochlorous acid and/or hypochlorite are formed on the anode. At pH > 6, hypochlorous acid dissociates to hypochlorite and H^+, and at pH lower than ≈3.5, HOCl reacts with Cl^- to yield Cl_2. A mixture of these species is commonly called "active chlorine".[17–19]

CI Reactive Orange 16 (RO16, M = 617.5 g mol^{-1}), with the structural formula shown in Fig. 1, was the subject of electrochemical degradation studies. The electro-oxidation of RO16 dye was studied using boron-doped diamond (BDD) and dimensionally stable anode (DSA) type electrodes in acidified 0.1 M K_2SO_4.[20] The results showed that the BDD electrode had superior characteristics for color removal and in the mineralization of organic materials present in the dye. Decolorization was achieved within 90 min, following the pseudo-first order reaction kinetics with rate constants ranging from 0.02 to 0.08 min^{-1} for the applied current densities from 75 to 200 mA cm^{-2}. For a commercial DSA electrode, the values of the rate constants were not obtained, because only a 10 % decrease in the initial dye concentration was observed at 200 mA cm^{-2} after 90

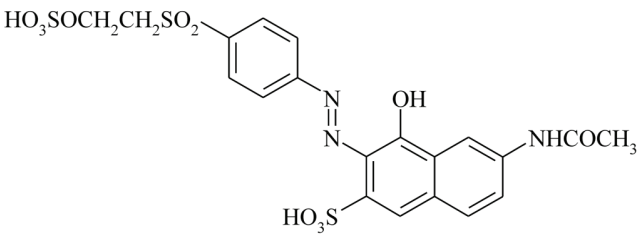

Fig. 1. Structure of CI Reactive Orange 16.

min of electrolysis.[20] The same authors also investigated two different boron-doped diamond films on a Ti substrate for electrochemical degradation of RO16.[21] The highest doped BDD electrode at current densities higher than 75 mA cm^{-2} showed better efficiency for the reduction of aromaticity and azo group fracture. This tendency was confirmed by total organic carbon (*TOC*) and chromatographic measurements.[21]

Electrochemical decolorization of RO16 was also performed in electrochemical flow–cell, using a Pt electrode.[22] The influences of the process variables, *i.e.*, flow–rate, NaCl concentration, applied potential and pH, were studied. Using 1.0 g dm^{-3} NaCl as the supporting electrolyte at 2.2 V *vs*. RHE, the determined first order rate constant was ≈0.025 min^{-1}, and a color removal of 93 % was achieved after 60 min electrolysis. The best *TOC* removal of 57 % was at 1.8 V, without a membrane, indicating that the ideal conditions for color removal are not necessarily the same as those for *TOC*.[22] Dimensionally stable Ru(Ta, Sn)O_2-based anodes were used for the electrochemical oxidation of different reactive dyes, including RO16. The reactions were performed in either the presence or absence of NaCl. At a low chloride concentration (0.01 M), total color removal was obtained after 10 min of electrolysis, and a significant increase in total dye degradation was achieved (reaching *ca*. 80 %, chemical oxygen demand, *COD*, decrease).[23] The oxidation was studied using a combination of electrochemical and photo-electrochemical methods in 0.02 M Na_2SO_4 at a current density of 50 mA cm^{-2} in a photo-electrochemical flow-cell.[24] The photo-electrochemical method was demonstrated to be more efficient considering the specific energy consumption, *TOC* removal and a slightly higher first order rate constant of ≈0.012 min^{-1} compared to the one obtained for the electrochemical method, ≈0.009 min^{-1}. The photo bleaching of RO16 in aqueous solution using TiO_2 thin-film electrodes prepared by the sol–gel method was also studied.[25] The best conditions for maximal photo-electrocatalytic degradation was found to be pH > 10 for a Na_2SO_4 medium and pH < 6 for a NaCl medium, but only for the low dye concentrations. In both cases, 100 % color removal was obtained after 20 min. Oxalic acid was identified by HPLC and UV-Vis spectrophotometric methods as the main degradation product generated after 180 min of photoelectrocatalysis.[25]

In this paper, a study of the electrochemical decolorization of RO16 in sodium chloride-containing solutions using for the first time DSA Ti/PtO*x* is reported. The influences of the basic operational parameters, such as hydrodynamic conditions, applied current, and the initial concentrations of RO16 and NaCl, were studied in order to optimize the process of electrochemical decolorization of RO16.

EXPERIMENTAL

Materials

The textile dye, CI Reactive Orange 16, was obtained from Aldrich (dye content 50 %) and used without purification. Sodium chloride was p.a. grade (Merck). Acetonitrile (HPLC grade) was purchased from J.T. Baker. Deionized water was obtained from a Millipore Waters Milli-Q purification unit.

Electrochemical decolorization

The electrochemical decolorization process was investigated in a cylindrical glass batch reactor, with an electrolyte volume of 500 cm^3. The electrolyte was prepared from distilled water, NaCl and RO16. A 5 cm^2 DSA Ti/PtO*x* anode obtained by thermal decomposition of H_2PtCl_6 in 2-propanol with 1 mg cm^{-2} of platinum loading was used, while the cathode was 10 cm^2 plate made from austenite 18Cr/8Ni stainless steel series 304. The electrodes with a 3-mm gap between them were immersed at the top of the electrolyte. A PAR M273 potentiostat/galvanostat operated in the galvanostatic mode was used for the electrolysis of solution. Mixing of the electrolyte was accomplished by a magnetic stirrer. At certain times during the electrolysis, 3 cm^3 of the solution was taken with a micropipette and its UV-Vis spectrum was instantly recorded. The concentration of dye was followed by measuring the absorption of the solution at 493 nm using a Shimadzu UV-Vis model 1700 spectrophotometer.

HPLC analysis

For HPLC determination, all samples were filtered through 0.45 μm syringe filters and analyzed at 245 nm and at ambient temperature (25 °C) on a SpectraSYSTEM P4000 liquid chromatograph with a SpectraSYSTEM UV1000 detector, equipped with a reversed phase column type Zorbax SB C8 (150 mm×4.6 mm i.d., 5 μm particle size). The mobile phase (flow rate 1.0 cm^3 min^{-1}) was a mixture of acetonitrile and water (30:70, *V*/*V*), 0.1 % formic acid solution. The sample injection volume was 20 μL.

*Total organic carbon (*TOC*) and total nitrogen (*TN*) analyses*

The *TOC* and *TN* analyses during the electrolysis were performed using an Elementar liquiTOC II instrument.

RESULTS AND DISCUSSION

UV–Vis spectral changes

The UV–Vis spectral changes during the electrolysis are shown in Fig. 2. Several peaks were observed in the spectrum of the RO16 at the beginning of the reaction. The peak at 295 nm corresponds to the gamma acetylated acid structure, which is a precursor in the synthesis of RO16. The peak at 254 nm is indicative of benzene ring, and the peak at 386 nm could be associated with the azo group.[24] Finally, the peak at 493 nm corresponds to the hydrazone form of the dye because an azo-hydrazone tautomerism is possible in the RO16 molecule.[17,26] The decreases in the absorption peaks at 386 and 493 nm during electrolysis indicate fast decolorization of RO16 dye over time (Fig. 2). Complete decolorization was observed after ≈10 min of electrochemical treatment, insert in Fig. 2. At the end of the oxidation reaction, the spectrum showed small

peaks at 254 and 295 nm. Considering that the reaction was very fast, the concentrations of hypochlorite and hypochlorous acid are very low and cannot be observed in the spectra (the absorption maximum of hypochlorite is at 292 nm and the absorption maximum for hypochlorous acid is at 236 nm).[27]

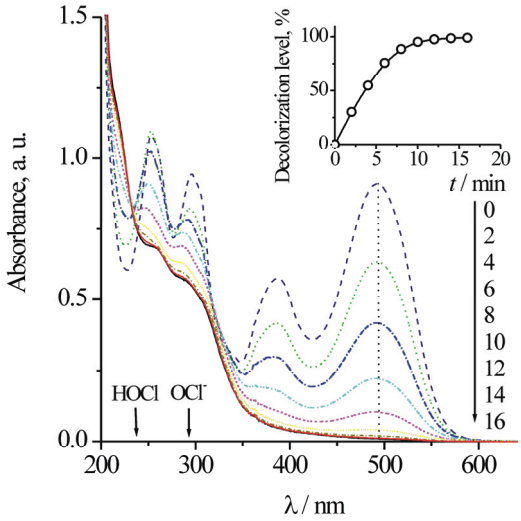

Fig. 2. Typical UV–Vis spectra changes of RO16 (60 mg dm^{-3}) in 10 g dm^{-3} aqueous NaCl water during electrochemical decolorization, I = 100 mA, ω = 250 rpm. Inset: decolorization level over time.

Effect of the applied current

In order to investigate the influence of the current on the electrochemical decolorization of the RO16 dye, currents in the range from 50 to 250 mA were applied. The dependence of the relative dye concentration over time for different values of applied current is shown in Fig, 3a. More than 95 % decolorization was achieved within ten minutes for applied currents greater than 50 mA. Examining different pseudo *n*-orders, the first-order gave the best linearity, and pseudo first-order decolorization rate constants, k_d, min^{-1}, were determined in accordance with the kinetic equation:

$$\ln \frac{c_t}{c_0} = -k_d t \quad (1)$$

From the slopes of the straight lines, Fig. 3, the rate constants were determined and are shown in Fig. 3b. The decolorization rate constant practically linearly increased from 0.14 to 0.33 min^{-1} in the investigated range of applied currents, while electrolysis voltage increased from 3.5 to 5 V. The faster reaction was achieved with current of 250 mA, but considering that the specific energy consumptions with reaction rate increase, some optimum current lies at 100–150 mA. For example, an increase of current from 100 to 250 mA increases the reac-

tion rate 1.5 times, while the specific energy consumption is increased 2.5 times, from 1.1 to 2.8 Wh g^{-1}, calculated using the cell voltage shown in Fig. 3b.

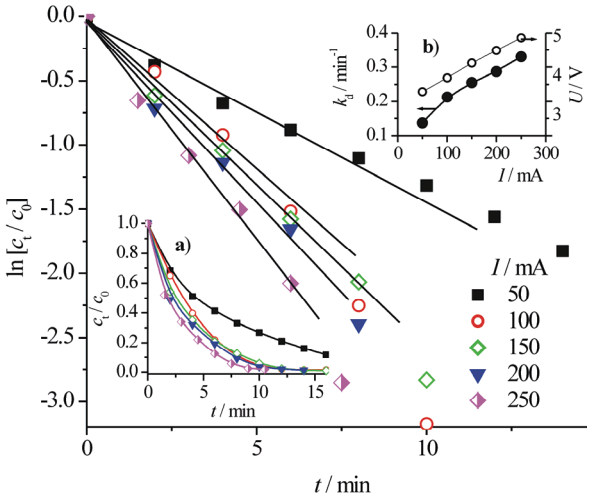

Fig. 3. The logarithmic plot of the relative RO16 concentration *vs*. the electrolysis time for different values of applied current (marked in the figure) under the conditions m(NaCl) = 10 g dm^{-3}, m(RO16) = 60 mg dm^{-3}, ω = 250 rpm. Insets: a) the dependence of the relative RO16 concentration over time for different values of the applied current; b) the dependence of the pseudo first-order reaction rate constants and the electrolysis voltage on the values of the applied current.

The influence of the hydrodynamic conditions

The influence of the solution mixing (rpm of magnetic stirrer) on the RO16 decolorization is shown in Fig. 4. The apparent decolorization rate constant of ≈0.24 min^{-1} are practically independent of the agitation speed, as shown in Fig. 4. During the first five minutes of the electrolysis, the pH increased relatively fast from the initial ≈5.5 to 8, and reached a steady state value of ≈8.5 after 10 min, Fig. 4b. The changes in pH provoked changes in the relative ratio of the different active chlorine species in the solution (see Section: *Possible active chlorine species*).

Considering that diffusion, heterogeneous or homogeneous oxidation rate was highly dependent on the hydrodynamic conditions,[28] the possible explanation is that the rate determining step is an activation controlled (charge transfer) reaction. The only activation-controlled reaction could be the oxidation of the chloride anions to the solvated chlorine, given by Eq. (3).

Effect of the initial sodium chloride concentration

The influence of the initial NaCl concentration on the reaction rate was investigated in the range from 10 to 30 g dm^{-3} and the results are shown in Fig.

5. The determined reaction rate constants increased with increasing salt concentration up to 25 g dm^{-3}, and above that concentration, a small change in the reaction rate is observed, as shown in the insert of Fig. 5.

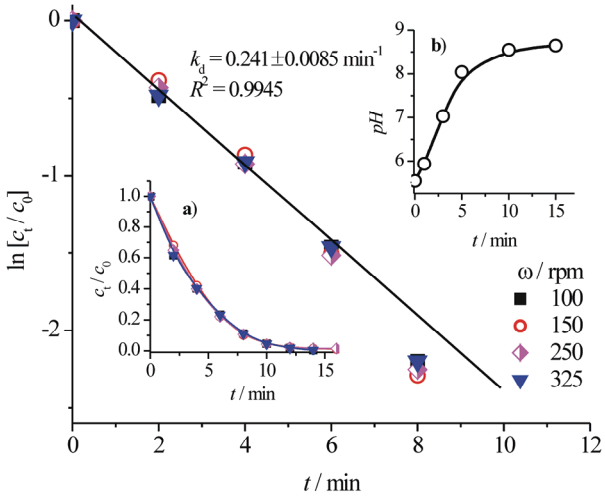

Fig. 4. The logarithmic plot of the relative concentration of the dye *vs*. the electrolysis time for different agitation speeds (marked in the figure), *m*(NaCl) = 10 g dm^{-3}, *I* = 100 mA, *m*(RO16) = 60 mg dm^{-3}. Insets: a) the dependence of the relative RO16 concentration over time for different agitation speeds; b) the change in the pH value during electrolysis.

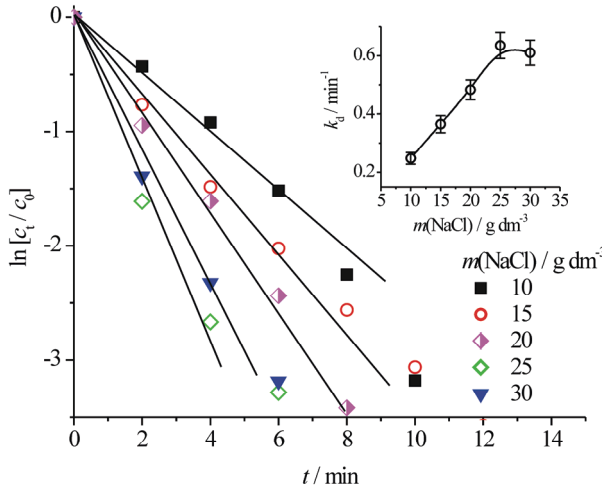

Fig. 5. The logarithmic plot of the relative RO16 concentration *vs*. the electrolysis time for different sodium chloride concentrations (marked in the figure), and in 10 g dm^{-3} Na_2SO_4 during continuous electrolysis. Inset: the dependence of the pseudo first-order reaction rate constants on the sodium chloride concentration, *I* = 100 mA, *m*(RO16) = 60 mg dm^{-3}, ω = 250 rpm.

According to the Faraday law, the amount of the produced active chlorine should be proportional to the passed charge (*It*) and the rate should remain constant independently of the chloride concentration. However, the oxygen evolution:

$$4OH^- = O_2 + 2H_2O + 4e^- \quad (2)$$

and the production of active chlorine (Eqs. (3)–(5)) compete.[19,29] Thus, the current efficiency of active chlorine production is connected with the chloride concentration. Namely, as determined by Kraft *et al.*,[19] in the concentration range of NaCl from 1 to 20 g dm^{-3}, the current efficiency of active chlorine production on a Ti/PtO*x* electrode linearly increases from ≈5 to 75 %. Therefore, in the solution with a NaCl concentration in the range of 10 to 20 g dm^{-3}, the oxygen evolution reaction proceeds at a relatively high rate. In the solution with higher NaCl concentrations, the current efficiency steady state conditions are attained and the amount of the active chlorine production becomes nearly constant.

Possible active chlorine species

In order to resolve which of the active chlorine species are the most active, the following experiment was performed: a solution of 5 g NaCl in 500 cm^3 of water was pre-electrolyzed for 1 and 5 min at 100 mA, and then, 30 mg of RO16 dye was added. The results of these experiments are presented in Fig. 5. It can bee seen that decolorization occurred practically with a similar rate as during the electrolysis with higher currents (Fig. 3a). The rate in the electrolyte pre-electrolyzed during 5 min was ≈20 % faster than in the electrolyte pre-electrolyzed for 1 min.

In Fig. 3, the results obtained during electrolysis with current of 100 mA in a solution containing 10 g dm^{-3} of Na_2SO_4 and 60 mg of RO16 is also shown, because of the possibilities that anodic water oxidation could result in the formation of hydroxyl radicals, which can easily oxidize RO16.[17,30] Under such conditions, no activity was observed. Hence, it could be concluded that hydroxyl radicals were not involved in the reaction mechanism. One more important conclusion from this experiment is that RO16 is not cathodically reduced during electrochemical degradation.

The oxidation of the chloride anions to the hydrated chlorine is given by the complex overall reaction:

$$2Cl^- = Cl_2(aq) + 2e^- \quad (3)$$

which is followed by the fast disproportionation of the hydrated chlorine to HOCl and its dissociation to OCl^-:[13,19]

$$Cl_2(aq) + H_2O = HClO + Cl^- + H^+, K_1 = 5.1\times10^{-4}\ M^2 \quad (4)$$

$$HClO = ClO^- + H^+, K_a = 2.9\times10^{-8}\ M \quad (5)$$

The distribution of different active chlorine species in a solution containing chloride as a function of pH can be calculated starting from the chemical equilibrium equations given above. Assuming that concentration corresponds to activity and that water has unity activity, the following procedure was used starting from the mass balance equation:

$$c(\mathrm{Cl_{2,act}})_T = c(\mathrm{Cl_2}) + c(\mathrm{HOCl}) + c(\mathrm{OCl^-}) \quad (6)$$

The total active chlorine concentration in solution can be calculated using the Faraday law:

$$c\left(\mathrm{Cl_{2,act}}\right)_T = \frac{n(\mathrm{Cl_2})}{0.5\,\mathrm{dm^3}} = \frac{It}{F}\eta_\mathrm{I} \quad (7)$$

where η_I is the current efficiency for chlorine formation. By rearranging Eq. (6), the concentration of hydrated chlorine is obtained:

$$c(\mathrm{Cl_2}) = c(\mathrm{Cl_{2,act}})_T\left[1 + \frac{c(\mathrm{HOCl})}{c(\mathrm{Cl_2})} + \frac{c(\mathrm{OCl^-})}{c(\mathrm{Cl_2})}\right]^{-1} \quad (8)$$

Using a mathematical procedure, it can be evaluated that:

$$\frac{c(\mathrm{HOCl})}{c(\mathrm{Cl_2})} = \frac{K_1}{c(\mathrm{H^+})c(\mathrm{Cl^-})} \quad (9)$$

and:

$$\frac{c(\mathrm{OCl^-})}{c(\mathrm{Cl_2})} = \frac{K_1 K_a}{c^2(\mathrm{H^+})c(\mathrm{Cl^-})} \quad (10)$$

Introducing Eqs. (9) and (10) into Eq. (8), the free solvated chlorine concentration as a function of pH could be calculated. Once the pH dependence of the free chlorine concentration is known, it is possible to calculate, by a similar procedure, the pH dependence of the concentrations of all the other species in the solution. Taking into account that for the NaCl concentration of 10 g $\mathrm{dm^{-3}}$ (0.17 M), current efficiency is 0.45[19] and using Eq. (7), the total active chlorine concentration for 1 and 5 min of electrolysis was calculated to be 0.028 and 0.125 mM. Applying the above-described mathematical treatment, the distribution of different active chlorine species in solution as a function of pH was calculated and shown in Fig. S-1 (Supplementary material to this paper). The pH for 1 and 5 min of electrolysis was ≈6 and 8, respectively, Fig 4b. At these pH values, corresponding concentrations of HOCl are 29 and 37 μM, and for $\mathrm{OCl^-}$ ≈0 and 0.1 mM, respectively. Therefore, the ≈20% higher rate in the electrolyte pre-electrolyzed during 5 min than in the electrolyte pre-electrolyzed for 1 min corresponds to the ratios of HOCl concentration, suggesting that hypochlorous acid is the active species in RO16 decolorization.

Effect of the initial dye concentration

The dependence of logarithm of the relative concentrations over time for different RO16 concentrations, 20–80 mg dm^{-3}, is shown in Fig. 6. As it could be seen in the insert of Fig. 6, increasing the dye concentration decreased the reaction rate. This trend could be connected with the pH distribution of the suggested active HOCl species. Namely, for a low RO16 concentration, *e.g.*, 20 mg dm^{-3}, the decolorization was practically completed within 3 to 4 min and corresponding pH was lower than 7.5. At this pH value, the dominant species is practically pure HOCl. Increasing the dye concentration, the decolorization time and pH increased as well, which is connected with a decrease in HClO concentration and a slower reaction rate. However, the observed behavior could also be explained by taking into consideration that the overall rate of RO16 decolorization was controlled by active chlorine production, as was inferred in the previous section. It could be postulated that the rate of active chlorine production was approximately the same independently of the initial concentration of RO16, because in all the measurements current was the same, I = 100 mA, as well as the chloride concentration, m(NaCl) = 10 g dm^{-3}. Consequently, in the solutions with a lower initial dye concentration, proportionally lower relative concentrations of RO16 were to be expected for the same electrolysis time (Fig. 6). The concentration of generated HOCl active species during the electrolysis is unknown, but from the kinetics point of view, it is reasonable to assume that it was lower in the solutions with a higher initial concentration of RO16. Taking into account that the concentration of active chlorine was included in the pseudo first-order rate constants, the dependence shown in the inset of Fig. 6 was anticipated.

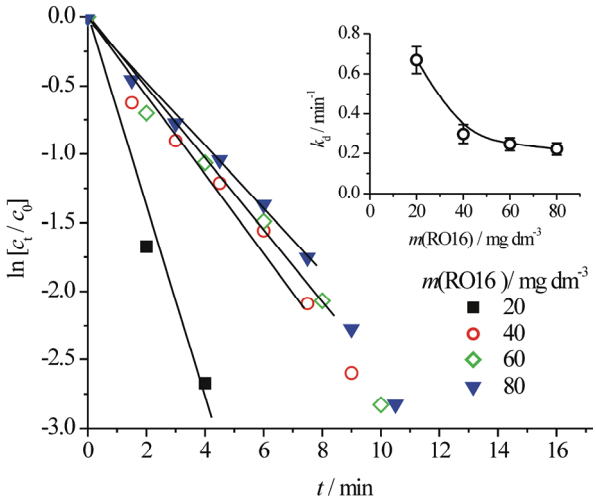

Fig. 6. The logarithmic plot of the relative RO16 concentration against electrolysis time for different initial dye concentrations. Inset: dependence of the pseudo first-order reaction rate constants on RO16 concentration, m(NaCl) = 10 g dm^{-3}, I = 100 mA, ω = 250 rpm.

HPLC and TOC/TN *analyses*

High-performance liquid chromatography (HPLC) was used to obtain a better insight in the decolorization process of the RO16 dye. As suggested by Miglirioni *et al.*,[21] the reaction was followed at 245 nm using HPLC with a UV detector because the appearance of signal at this wavelength is related to the $\pi \rightarrow \pi^*$ transition of conjugated systems, which is characteristic for aromatic compounds. The chromatograms of the RO16 azo dye solution before the electrochemical treatment (0 min) and after 16 min of electrochemical treatment at 100 mA are presented in Fig. S-2 (Supplementary material). The chromatogram for the RO16 azo dye solution before the electrochemical treatment showed four peaks related to aromatic compounds with different polarities and retention times. These aromatic peaks were named in the chromatogram from A to D. The highest intensity peak C is probably related to the RO16 dye while the less intense peaks are probably related to impurities in the 50 % RO16 dye solution. After the electrochemical treatment at 100 mA with DSA Ti/PtO*x* electrode (16 min), peak C had almost disappeared while peaks D and B were reduced. At the same time, new peaks emerged (peaks E–J) due to the reaction indicating the presence of smaller, less polar aromatic molecules.

TOC and *TN* analyses were also performed in order to assess the effectiveness of used electrochemical method in the mineralization of the RO16 dye. The UV-Vis absorption spectrum (Fig. 2) shows that absorption in the visible part of the spectra was almost completely removed. However, the absorption in the UV region was not removed, which indicates the presence of intermediate compounds after color removal. The *TOC* and *TN* changes during the reaction are shown in Fig. S-3 (Supplementary material). As could be seen, ≈10% of the dye was mineralized. The obtained results confirm that the degradation of RO16 was only partial, but the rate of the achieved decolorization is much faster than in photocatalytic processes,[31,32] except when H_2O_2 was added.[33]

CONCLUSIONS

The dimensionally stable Ti/PtO*x* anode was found to be effective in the decolorization process of CI Reactive Orange 16 dye solutions containing chloride. The decolorization proceeded *via* a pseudo-first order reaction with hypochlorous acid as the main active chlorine species. Depending on the electrolysis conditions, the apparent first-order reaction constant was in the range of 0.2 to 0.5 min^{-1}. Complete decolorization within 15 min could be successfully realized with currents in the range of 100 to 200 mA (20–40 mA cm^{-2}), sodium chloride concentrations in the range of 10 to 30 g dm^{-3} and low (few mg dm^{-3}) and medium (~0.1 g dm^{-3}) contents of dye. A negligible effect of the hydrodynamic conditions on the RO16 decolorization was recorded. The specific power consumption was estimated in the range of 1 to 3 kWh kg^{-1}, depending on the

applied current. Some optimum electrolysis conditions can be suggested: 10–15 g dm^{-3} of NaCl, with anodic current density of 20–25 mA cm^{-2} under moderate steering.

HPLC analysis revealed the formation of smaller aromatic molecules, which were less polar than the starting molecule. The obtained results of *TOC*/*TN* analyses confirmed that the degradation of RO16 was only partial.

SUPPLEMENTARY MATERIAL

The distribution of different active chlorine species in solution as a function of pH, HPLC chromatograms and relative *TOC* and *TN* change during electrochemical treatment of the RO 16 dye solution are available electronically from http://www.shd.org.rs/JSCS/, or from the corresponding author on request.

Acknowledgements. The work was supported by the Ministry of Education, Science and Technological Development of the Republic of Serbia under the research projects: ON172013 and ON172046. Authors express their gratitude to the PUC "Belgrade Waterworks and Sewerage" for the *TOC/TN* analyses.

ИЗВОД

ЕЛЕКТРОХЕМИЈСКО ОБЕЗБОЈАВАЊЕ REACTIVE ORANGE 16 БОЈЕ ПОМОЋУ ДИМЕНЗИОНО СТАБИЛНЕ Ti/PtO*x* АНОДЕ

ДУШАН Ж.МИЈИЋ, ВУК Д.ТОМИЋ и БРАНИМИР Н. ГРГУР

Технолошко-металуршки факултет, Универзитет у Београду, Карнегијева 4, 11120 Београд

Електрохемијско обезбојавање CI Reactive Orange 16 је испитивано на димензионо стабилној Ti/PtO*x* аноди у растворима на бази натријум-хлорида. Различити реакциони параметри, као што су брзина мешања, јачина струје, концентрација натријум-хлорида и концентрација боје, су варирани и на основу добијених резултата утврђени су оптимални реакциони услови. Претпостављено је да је активна врста у реакцији обезбојавања хипохлораста киселина. Реакција је праћена помоћу UV–Vis спектроскопије, течне хроматографије високог притиска, као и одређивањем укупног органског угљеника и азота.

Примљено 17 септембра, ревидирано 5 новембра, прихваћено 6 новембра 2014)

REFERENCES

1. P. A. Carneiro, M. E. Osugi, C. S. Fugivara, N. Boralle, M. Furlan, M. V. B. Zanoni, *Chemosphere* **59** (2005) 431
2. S. Meric, D. Kaptan, T. Olmez, *Chemosphere* **54** (2004) 435
3. R. J. Chudgar, J. Oakes, in *Kirk–Othmer Encyclopedia of Chemical Technology*, Vol. 9, 5th ed., John Wiley & Sons, New York, 2007, pp. 349–430
4. E. Foracs, T. Cserhati, G. Oros, *Environ. Int.* **30** (2004) 953
5. I. K. Konstantinou, T. A. Albanis, *Appl. Catal., B* **49** (2004) 1
6. Y. M. Slokar, A. M. Le Marechal, *Dyes Pigm.* **37** (1998) 335
7. B. Ramesh Babu, A. K. Parande, S. Raghu, T. Prem Kumar, *J. Cotton Sci.* **11** (2007) 141
8. A. Di Paola, E. Garcia-Lopez, G. Marci, L. Palmisano, *J. Hazard. Mat.* **211–212** (2012) 3
9. P. Banerjee, S. De, in *Membrane Technologies and Applications*, K. Mohanty, M. K. Purkait, Eds., CRC Press, Boca Raton, FL, 2012, p. 133
10. P.-J. Lu, C.-W. Chien, T.-S. Chen, J.-M. Chern, *Chem. Eng. J.* **163** (2010) 28

11. R. Yuan, S. N. Ramjaun, Z. Wang, J. Liu, *Chem. Eng. J.* **192** (2012) 171
12. W. Baran, E. Adamek, A. Makowski, *Chem. Eng. J.* **145** (2008) 242
13. M. A. Rauf, S. Salman Ashraf, *Chem. Eng. J.* **151** (2009) 10
14. M.-C. Wei, K.-S. Wang, C.-L. Huang, C.-W. Chiang, T.-J. Chang, S.-S. Lee, S.-H. Chang, *Chem. Eng. J.* **192** (2012) 37
15. G. R. de Oliveira, N. S. Fernandes, J. V. de Melo, D. R. da Silva, C. Urgeghe, C. A. Martinez-Huitle, *Chem. Eng. J.* **168** (2011) 208
16. M. Rivera, M. Pazos, M. Ángeles Sanromán, *Desalination* **274** (2011) 39
17. C. A. Martinez-Huitle, E. Brillas, *Appl. Catal., B* **87** (2009) 105
18. D. Ž. Mijin, M. L. Avramov Ivić, A. E. Onjia, B. N. Grgur, *Chem. Eng. J.* **204–206** (2012) 151
19. A. Kraft, M. Stadelmann, M. Blaschke, D. Kreysig, B. Sandt, F. Schroéder, J. Rennau, *J Appl. Electrochem.* **29** (1999) 861
20. F. L. Migliorini, M. D. Alegre, S. A. Alves, M. R. V. Lanza, M. R. Baldan, N. G. Ferreira, *ECS Trans.* **43** (2012) 89
21. F. L. Migliorini, N. A. Braga, S. A. Alves, M. R. V. Lanza, M. R. Baldan, N. G. Ferreira, *J. Hazard. Mat.* **192** (2011) 1683
22. L. Gomes, D. W. Miwa, G. R. P. Malpass, A. J. Motheo, *J. Braz. Chem. Soc.* **22** (2011) 1299
23. R. G. da Silva, S. A. Neto, A. R. de Andrade, *J. Braz. Chem. Soc.* **22** (2011) 126
24. M. Catanho, G. R. Malpass, A. de Jesus Motheo, *Quim. Nova* **29** (2006) 983
25. P. A. Carneiro, M. E. Osugi, J. J. Sene, M. A. Anderson, M. V. B. Zanoni, *Electrochim. Acta* **49** (2004) 3807
26. P. Baldrian, V. Merhautova, J. Gabriel, F. Nerud, P. Stopka, M. Hruby, M. J. Benes, *Appl. Catal., B* **66** (2006) 258
27. L. C. Adam, I. Fábián, K. Suzuki, G. Gordon, *Inorg. Chem.* **31** (1992) 3534
28. B. N. Grgur, D. Ž Mijin, *Appl. Catal., B* **147** (2014) 429
29. J. P. Lorimer, T. J. Mason, M. Plattes, S. S. Phull, D. J. Walton, *Pure Appl. Chem.* **73** (2011) 957
30. C. A. Martínez-Huitle, S. Ferro, *Chem. Soc. Rev.* **35** (2006) 1324
31. D. Mijin, M. Radulović, D. Zlatić, P. Jovančić, *Chem. Ind. Chem. Eng. Q.* **13** (2007) 179
32. O. E. Kartal, G. D. Turhan, *Desalin. Water Treat.* **48** (2012) 199
33. J. Mitrović, M. Radović, D. Bojić, T. Anđelković, M. Purenović, A. Bojić, *J. Serb. Chem. Soc.* **77** (2012) 465.

Journal of the Serbian Chemical Society
JSCS@tmf.bg.ac.rs • www.shd.org.rs/JSCS
J. Serb. Chem. Soc. 80 (7) S250–S251 (2015) *Supplementary material*

SUPPLEMENTARY MATERIAL TO

Electrochemical decolorization of the Reactive Orange 16 dye using a dimensionally stable Ti/PtO*x* anode

DUŠAN Ž. MIJIN*#, VUK D. TOMIĆ and BRANIMIR N. GRGUR

Faculty of Technology and Metallurgy, University of Belgrade, Karnegijeva 4, 11020 Belgrade, Serbia

J. Serb. Chem. Soc. 80 (7) (2015) 903–915

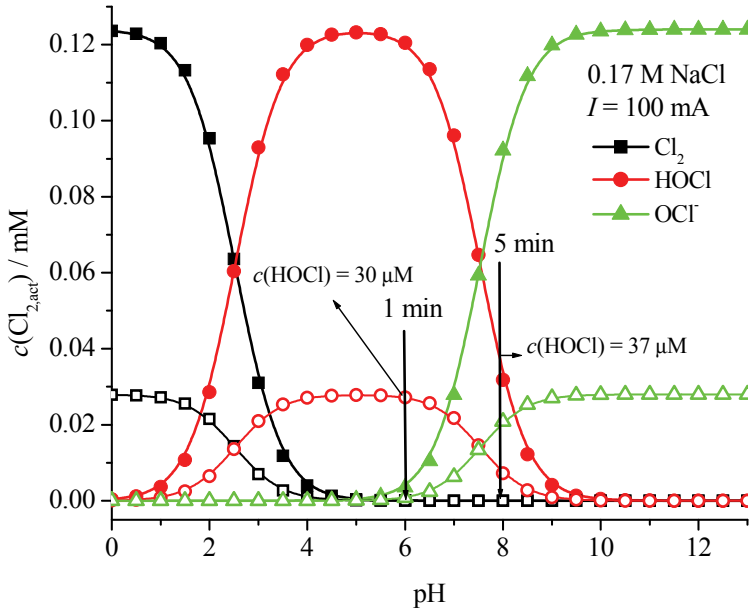

Fig. S-1. The distribution of different active chlorine species in solution as a function of pH after 1 (open symbols) and 5 (closed symbols) min of electrolysis.

* Corresponding author. E-mail: kavur@tmf.bg.ac.rs

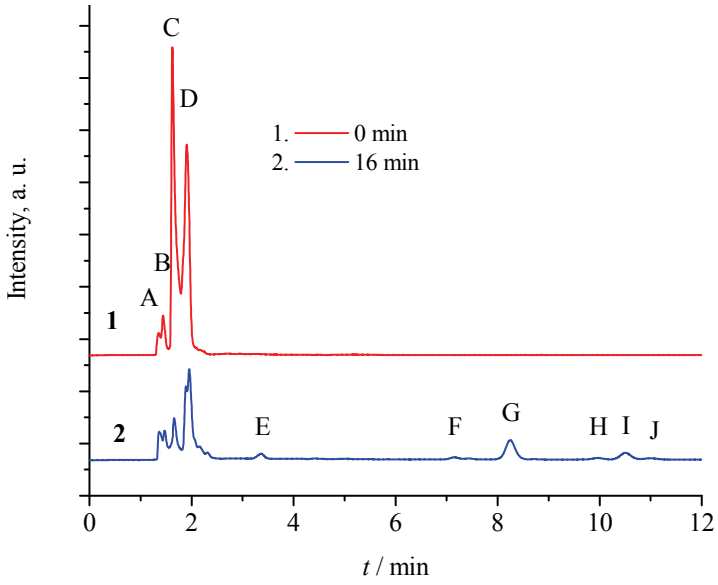

Fig. S-2. HPLC chromatograms of the RO16 dye solution recorded at 245 nm before and after 16 min of electrochemical treatment, m(NaCl) = 10 g dm^{-3}, m(RO16) = 60 mg dm^{-3} I = 100 mA, ω = 250 rpm.

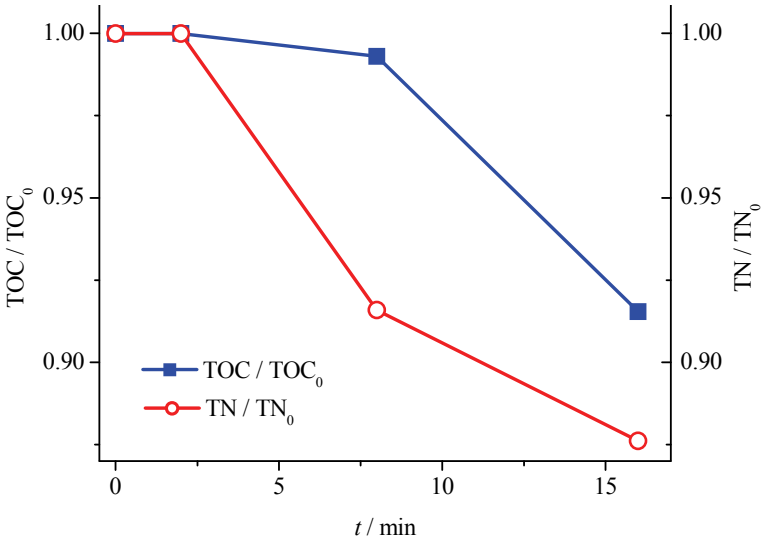

Fig. S-3. The relative *TOC* and *TN* change during electrochemical treatment of the RO 16 dye solution, m(NaCl) = 10 g dm^{-3}, m(RO16) = 60 mg dm^{-3} I = 100 mA, ω = 250 rpm.

Journal of the Serbian Chemical Society
JSCS-info@shd.org.rs • www.shd.org.rs/JSCS
J. Serb. Chem. Soc. 80 (7) 917–931 (2015)
JSCS–4769
UDC 678.652+542.913+547.462.3:
544.351.3:66.095.26
Original scientific paper

Chemical synthesis and characterization of highly soluble conducting polyaniline in mixtures of common solvents

HICHEM ZEGHIOUD[1]*, SAAD LAMOURI[1], ZITOUNI SAFIDINE[1] and MOHAMMED BELBACHIR[2]

[1]*Laboratoire de Chimie Macromoléculaire, Ecole Militaire Polytechnique, BP 17, Bordj El Bahri, Alger, Algeria and* [2]*Laboratoire de Chimie des Polymères, Département de Chimie, Faculté des Sciences, Université d'Oran, BP 1524 El'Menouer Oran 31000, Algeria*

(Received 19 July, revised 29 December 2014, accepted 8 January 2015)

Abstract: This work presents the synthesis and characterization of soluble and conducting polyaniline–poly(itaconic acid) PANI–PIA according to a chemical polymerization route. This polymerization pathway leads to the formation of doped polyaniline salts, which are highly soluble in a number of mixtures between organic common polar solvents and water, the solubility reaches 4 mg mL^{-1}. The effect of synthesis parameters, such as doping level, on the conductivity was investigated and a study of the solubility and other properties of the resulting PANI salts were also undertaken. The maximum of conductivity was found equal to 2.48×10^{-4} S cm^{-1} for fully protonated PANI-EB. In addition, the synthesized materials were characterized by various methods, *i.e.*, viscosity measurements, XRD analysis and FTIR and UV–Vis spectroscopy. Finally, TGA was performed to obtain some information concerning the thermal behaviour of the materials.

Keywords: conducting polymer; PANI; itaconic acid; polymerization; solubility properties.

INTRODUCTION

The synthesis and improvement of new materials with special properties have attracted much attention in the last decade. Polyaniline (PANI) is one of the most promising polymers due to its good flexibility, low cost, oxidative stability and unique conduction mechanism.[1–3] However, there are some major drawbacks, which limit its application, such as low thermal stability and poor solubility in common solvents due to the stiffness of backbone and H-bonding interactions between adjacent chains.[4,5]

* Corresponding author. E-mail: hicheming@yahoo.fr
doi: 10.2298/JSC140719003Z

Recently a number of studies have been devoted to the search for different synthetic methods that allow PANI to be obtained with good solubility in the presence of different polymeric acids with different structures,[6–9] which improve processibility, special electrical conductivity and optical and spectroscopic properties.

Barrios *et al.*[10] reported the electro-synthesis of PANI in the presence of poly(itaconic acid) and they evaluated the effect of the presence of dicarboxylic acids on the electrochemical behaviour of the obtained films. Nevertheless, the electrochemical methods generated polyaniline with very low solubility that was difficult to process and had restricted application.

Travas-Sejdic *et al.*[11] studied the electrochemical properties of self-assembled multilayer films based on polyaniline and two polyanions: poly(styrene sulphonate) (PSSA) and an oligonucleotide (ON), and found by cyclic voltammetry experiments that PANI/PSSA and PANI/ON films had different electrochemical behaviours, with PANI/ON films showing lower electroactivity.

Gizdavic-Nikolaidis *et al.*[12] recently demonstrated that a conductive polymer nanofibrilar network of poly(lactic acid) can be electrospun with PANI, and its copolymers with *m*-aminobenzoic acid (*m*-ABA) from DMSO/THF solutions. Abdul Rahman *et al.*[13] found that the number average molecular weights of the copolymers decreased significantly with increasing *m*-ABA fraction in the copolymers, and the solubility increased with increasing proportion of *m*-ABA. This increase was due not only to the functional COOH groups, but also to the decrease in the average length of the polymer chains.

Gribkova *et al.*[14] reported the chemical polymerization of aniline in the presence of aromatic polyamides containing sulphonic groups. They observed that the presence of the flexible-chain of polyamides with a regular distribution of sulphonic groups along the polymer chain allowed the polyaniline to exhibit a random coil conformation in the presence of strong electrolytes and the formation of water-soluble interpolymer complexes of PANI with polyacids.

Wang *et al.*[15] prepared polyaniline nanorods by chemical oxidative polymerization using itaconic acid as dopant. The polyaniline salt obtained, compared to the undoped form, possessed high productivity, conductivity and excellent solubility in organic solvents such as NMP, THF and DMF, which reached 19 mg mL^{-1}.

The main goal of the present work was the chemical doping of PANI in the presence of poly(itaconic acid) (PIA). PIA is a very exciting material due to its biocompatibility with natural systems. In addition, PIA is very attractive because it has two negatively charged carboxylic groups in each monomer unit. The essential advantage of the resultant PANI was the possibility of producing conductive PANI blends with good solubility. The spectral, thermal and electrical properties of the obtained PANI molecular composites were studied.

EXPERIMENTAL

Materials

Aniline (ANI, 99 % pure) was purchased from Fluka. Other provided materials were hydrochloric acid (35.37 %) from Organics Stinnes Chemicals, methanol (99.5 %) and ammonium peroxodisulphate (APS, 99 %) from Prolabo. Potassium peroxodisulphate (PPS, 99 %) was from Riedel-de Haën, acetone (99 %) from Acros Organics, while ammonia (25 % solution), *N*-methylpyrrolidone (NMP, 99.5 %) and tetrahydrofuran (THF, 99 %) were from Merck. Itaconic acid (99 %) was purchased from Aldrich, dimethyl sulphoxide (DMSO, 100 %) from Analytical Reagent. Deionised water was used throughout the experiments and all chemicals were used without previous purification.

Synthesis of PANI

The synthesis of the PANI-EB was as follows: 4.8 g of aniline (4.75 mL) and 15 ml of HCl were dispersed in 50 mL of deionised water under vigorous stirring at room temperature for 2 h to obtain a uniform solution. Then, an aqueous solution of APS (11.8 g + 50 mL deionised water) was added to the above mixture in one portion (the mole ratio ANI:APS = 1). The resulting solution was stirred for 30 min to ensure complete mixing, and then the reaction was followed by continuous stirring at 2 °C for 4 h. The precipitate that formed was filtered off, washed with deionised water and methanol until the filtrate was colourless to remove excess acid and possible oligomers. Finally, the powder was dried under vacuum for 48 h. Then, the obtained PANI as the emeraldine salt (PANI-ES) was stirred in 1 M solution of ammonium hydroxide at room temperature for 72 h to completely convert it to emeraldine base (PANI-EB) form. Upon filtering and drying under a dynamic vacuum in an oven at 60 °C for 24 h, the base form of PANI was obtained as a blue powder. The yield of the polymerization was 80 %.

Poly(itaconic acid) synthesis

The synthesis was carried out similarly to that described in work of Larez *et al.*[16] Thus deionised water (10 mL) was heated until boiling and left to reach ambient temperature with continuous stirring and under nitrogen bubbling. Itaconic acid (IA, 0.023 mol) and PPS (2.22×10^{-4} mol) were added and the system was sealed and placed in a thermostatic bath at 60 °C with continuous stirring during 48 h. A heterogeneous mixture was initially obtained due to an incomplete dissolving of IA that went transparent after 5 min. After the polymerization reaction time was over, the reactor was left to cool down to room temperature under continuous stirring (about 30 min). Polymer was separated by precipitation in cool acetone. The repeat unit of the resulting polymer (PIA) is shown in Scheme 1.

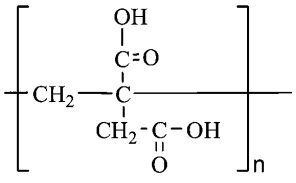

Scheme 1. Chemical structure of the repeat unit of poly(itaconic acid) PIA.

Doping

The polymeric acid-doped PANI was prepared by mixing 0.9 g of PANI-EB (0.0025 mol, based on the approximate tetrametric repeat unit) in a THF dispersion with the appropriate quantity

of poly(itaconic acid) solution of different mole ratios (based on its acidic repeat unit). The suspension was sonicated in a bath-type sonicator for 2 h followed by electromagnetic stirring (12 h) to make the dispersion homogeneous. The dispersion of PANI–PIA was filtered using poly-tetrafluoroethylene membrane filters of pore size 0.45 μm. The resultant powder was washed with large quantities of distilled water until the filtrate became colourless and the powder was dried in an oven at 60 °C for 24 h. The reaction mechanism is shown in Scheme 2.

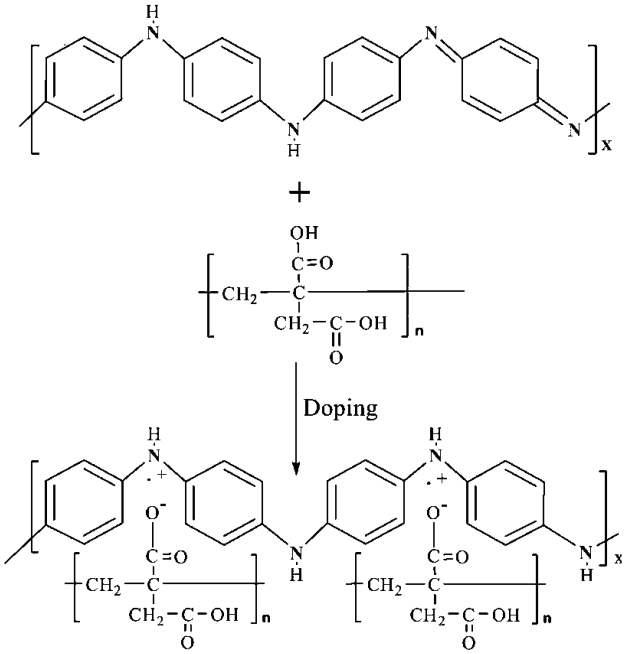

Scheme 2. Mechanism of PANI-EB doping with PIA.

Characterization

The Fourier transform infrared (FTIR) spectra were recorded between 400 and 4000 cm^{-1} from KBr pellets on an infrared Fourier transform spectrometer (Shimadzu type 8400 S). The UV––Vis spectra of all samples dissolved in different solvents were recorded using a UV–Vis spectrometer Shimadzu UV-2401PC, in the wavelength range of 250–900 nm. The intrinsic viscosity measurements of solutions were made using a Micro-Ubbelohde Schott-Gerate viscosimeter. The X-ray powder diffraction patterns were recorded on a PANalytical X'Pert PRO diffractometer fitted with CuK_{α} radiation (λ = 1.5404 nm) at 40 kV and 40 mA in the 2θ range 5––60° region. Thermogravimetric (TG) analysis was performed using a Setaram MTB instrument with "10^{-8}" sensitivity, operating at a heating rate of 10 °C min^{-1}, from room temperature up to 450 °C under an air atmosphere. The sample mass ranged between 3 and 6 mg.

RESULTS AND DISCUSSION

Conductivity measurements

The electrical conductivity measurements of compressed pellets of PIA--doped PANI were made by the conventional four-point probe technique at room

temperature; the data are plotted in Fig. 1. The curve showing the evolution of the electric conductivity (σ) according to the doping level follows an exponential form. Indeed, the values of the electrical conductivity order of 10^{-4} were found for PANI–PIA, whereby a high conductivity value of 2.48×10^{-4} S cm^{-1} for the PANI–PIA was reached when the PANI-EB (conductivity value of 8.14×10^{-10} S cm^{-1}) was fully protonated, showing that the resultant PANI–PIA was less conductive than the PANI–HCl, which has a conductivity of 4.6 S cm^{-1}. This was confirmed by the narrower band gap for PANI–HCl around 3.2 eV compared with the PANI–PIA (Table I). Note that each measured value of conductivity is an average of four measurements for each face of the pellet.

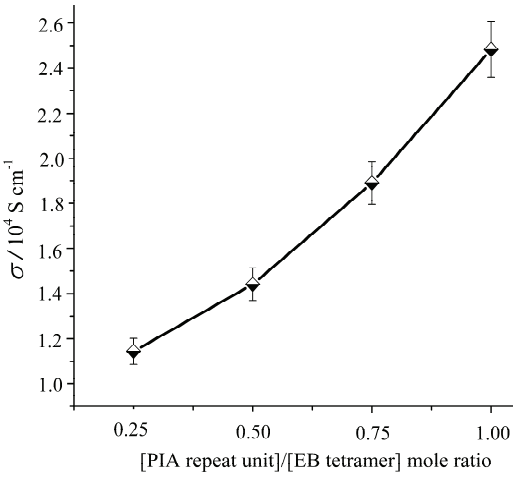

Fig. 1. The conductivity of PANI–PIA at different [PIA repeat unit]/[EB tetramer] mole ratio.

TABLE I. Conductivity and the energy band gap of different forms of PANI

Sample	UV–Vis band, nm		Conductivity, S cm^{-1}	Energy band gap, eV
	1	2		
PANI–HCl	387	467	4.60	3.20
PANI-EB	331	626	8.14×10^{-10}	–
PANI–PIA	304	347	2.48×10^{-4}	4.08

Fourier transform infrared spectroscopy (FTIR)

FTIR spectra of IA and its polymer (PIA) are shown in Fig. 2. The assignments of the FTIR bands of IA, PIA, PANI-EB and PANI–PIA are given in Table II. The spectra of IA and PIA showed a broad band between 2775 and 3480 cm^{-1},[17] which was attributed to O–H stretching vibrations. The spectrum of IA showed peaks at around 1700,[18] 1430[18] and 1220 cm^{-1},[19] indicating the stretching vibrations of C=O (carboxylic acid), C–O–H in plane and C–O, respectively.

The spectrum of the PIA showed the peaks at around 1730,[20] 1400[19] and 1193 cm^{-1},[21] indicating the stretching vibrations of C=O, C–O–H and C–O,

respectively. The peak at 1629 cm^{-1} in the curve (t = 0 h) in Fig. 2,[18] characterizes the presence of C=C bond coming from itaconic acid. However, this peak was absent in PIA spectrum, which confirmed the polymerization of IA.

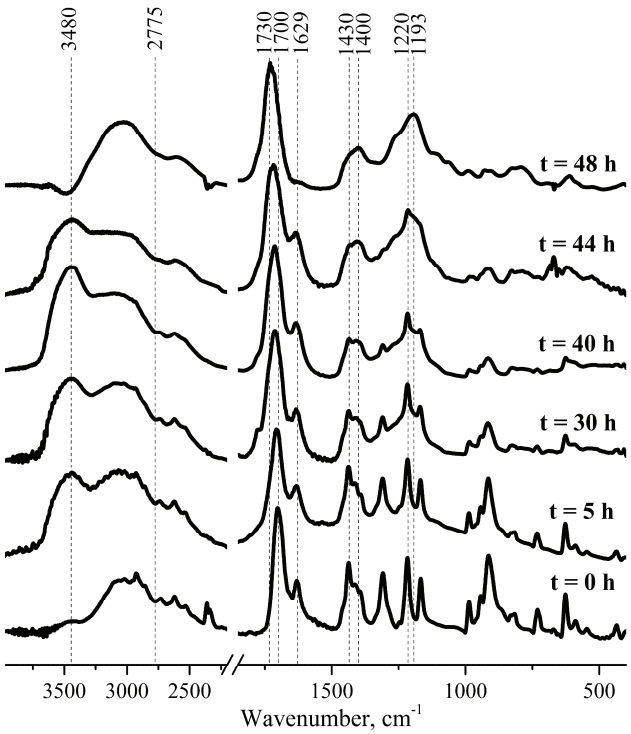

Fig. 2. Kinetics of the polymerization reaction of itaconic acid from IA (t = 0 h) to PIA (t = 48 h) determined by FTIR spectroscopy.

TABLE II. Assignment of FTIR bands (wavenumber, cm^{-1}) of IA, PIA, PANI-EB and PANI–PIA

Sample		Assignment
IA	PIA	
2775–3480[17]	2775–3480[17]	O–H stretching vibration
1700[18]	1730[20]	C=O stretching vibration
1629[18]	–	C=C stretching vibration
1430[18]	1400[19]	C–O–H stretching vibration
1220[19]	1193[21]	C–O in of plane bending vibration
PANI-EB	PANI–PIA	Assignment
3435[22]	3435[22]	N–H stretching vibration
–	1719[27]	C=O stretching vibration
1583[23]	1568[28]	N=Q=N Stretching rings
1494[24]	1485[29]	N–B–N stretching ring
1292[25]	1292[25]	C–N^+ stretching in secondary amines
511[26]	511[26]	C–H out-of-plane bending 1,4 ring

The position of wavenumber of C=O stretching depends on hydrogen bonding and conjugation within the molecule. With polymerisation of IA, the C=O stretching band was shifted to higher wavenumbers, because the possibility of conjugation with a C=C band resulting in delocalization of the C=O group was eliminated on polymerisation.[18] In addition, shifting of the typical bands for the C–O and C–O–H groups were detected. This effect is related to hydrogen bonding between the COOH groups of PIA.

The FTIR spectrum of pure polyaniline (PANI-EB) is shown in Fig. 3. The formation of polyaniline was confirmed from the predominant peaks at the wavenumber of 1583 cm^{-1}, corresponding to C=C stretching of the quinoid ring,[23] 1494 cm^{-1} for C=C stretching of the benzenoid ring,[24] 1292 cm^{-1} for C–N^+ stretching,[25] and 511 cm^{-1} for C–H out-of-plane bending.[26] After PIA doping, the quinoid and benzenoid ring bands were shifted to lower wavenumbers by 15 and 9 cm^{-1}, respectively. This red shift phenomenon, corresponding to the transformation of quinoid rings into benzenoid rings, may result from conjugation effects after doping with the polymeric acid.[28]

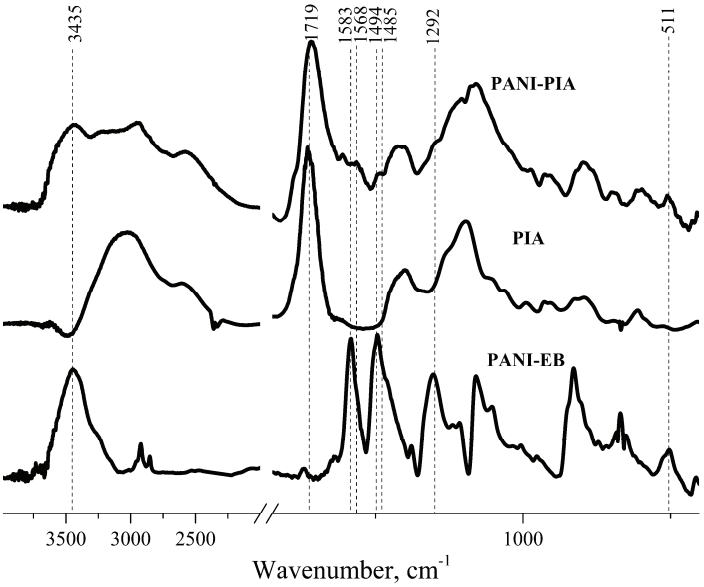

Fig. 3. FTIR spectra of PANI-EB, PIA and PANI–PIA.

UV–Vis spectroscopy

Absorption spectroscopy is a valuable tool for detecting the presence of PANI base and its salts. All the absorption spectra of the PANI–PIA samples and the PIA spectrum, Fig. 4, showed a peak in the range of 249–285 nm, corresponding

to π—π* or n—π* transitions in the carbonyl groups of the poly(itaconic acid),[30] (Table III).

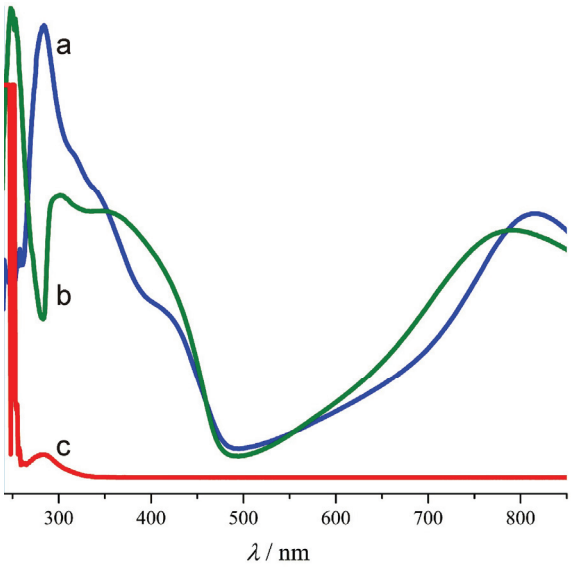

Fig. 4. UV–Vis spectra of: a) water/NMP, b) water/THF and c) PIA and PANI–PIA salts recorded in different solvents.

TABLE III. Absorption bands (λ / nm) of PIA and PANI–PIA samples in different solvents

Sample (solvent)	Attribution of absorption bands			
	π–π* and/or n–π*	π–π*	Polaron–π*	π–Polaron
PIA (water)	282	–	–	–
PANI–PIA (THF/water)	249	304	347	790
PANI–PIA (NMP/water)	285	347	410	816

The electronic absorption spectra of the PANI–PIA samples in different solvents showed bands corresponding to the following transitions: π–π* (304–347 nm), polaron–π* (347–410 nm), and π–polaron (in the region from 790 to 816 nm) of the alternating benzenoid–quinoid structures, respectively.[31,32] The finding of the latter two absorption bands in the electronic spectra of all the PANI–PIA samples indicates that these polymers were well doped.

When the solvent molecules interact with a PANI–PIA, its chain configuration may be changed depending on the structure and polarity of the solvents, which is reflected by peak shifts.[33]

Solubility determination

PANI–PIA dispersion in THF/water mixture (20 mL) was oscillated in a bath-type sonicator for 2 h at room temperature. The suspension was filtrated to remove undissolved polyaniline. The obtained solution was analyzed by UV–Vis spectroscopy to confirm the protonated state of PANI, then it was dried in an oven

at 60 °C for 12 h. The maximum solubility was the quantity of resulting polyaniline powder after drying 20 mL of solvents mixture with an optimal volume ratio, which is measured in mg mL^{-1}. Note that the optimal ratio was determined by the intrinsic viscosity method.

The solutions of PANI–PIA in different solvents are shown in Fig. 5. The picture proves that the PANI synthesized in the present work was highly soluble in tetrahydrofuran/water and NMP/water mixtures with a dark green colour (Fig. 5a and b, respectively).

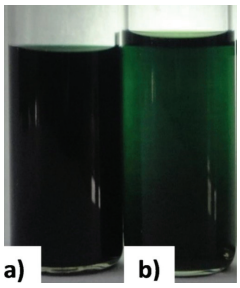

Fig. 5. Photographs of solutions of PANI–PIA in mixtures, a) water/THF = 0.428 and b) water/NMP = 0.428.

The carbonyl groups of extended polyacid chain of the PIA facilitate the solubility of PANI in some polar solvents.[34] PANI–PIA is not soluble in pure THF and NMP. The presence of water with each organic solvent improves the solubility of the PANI–PIA significantly, which could be explained by the number of carboxylic groups that is higher than the number of hydroxyl groups in the dopant which require a solvent with more groups containing hydrogen to create hydrogen bond. These groups (C=O), more negatively charged can create a stronger hydrogen bond with the water hydrogen. This idea is presented schematically in Scheme 3.

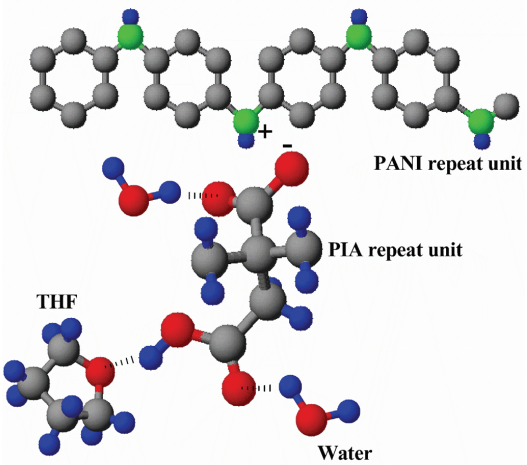

Scheme 3. Effect of the presence of water as co-solvent on PANI–PIA solution in THF.

Intrinsic viscosity

The viscosity of macromolecular substances in solution is one of the most commonly used methods for characterizations. Intrinsic viscosity is defined as the limiting value of the ratio of specific viscosity to concentration of the solute (η_{sp}/c), extrapolated to zero concentration.

Different solutions of PANI–PIA were prepared with different volume ratios of solvents (THF or NMP)/water at room temperature. This method is based on the calculation of the difference between the efflux time of the mixture of solvents (t_0) and polymeric solution (t) between two points in a capillary tube.

Basing on the most recent work performed by Yilmaz *et al.*[35] using the values of constant K and α at room temperature (26 °C) obtained for the leuco-emeraldine form in NMP solution in the presence of LiCl:

$$K = 2.34 \times 10^{-2} \text{ mL g}^{-1} \text{ and } \alpha = 0.73$$

$$[\eta] = K\bar{M}_v^{\alpha} \quad (1)$$

If two values are introduced into the Mark–Houwink equation (Eq. (1)),[36] the obtained value of the intrinsic viscosity $[\eta] = 13.26$ mL g^{-1} of the emeraldine salt form results in an apparent viscosity average molar mass of $\bar{M}_v = 5915$ g mol^{-1}.

The evolutions of the intrinsic viscosity of solutions having various (THF or NMP)/water volume ratios of polyaniline doped with poly(itaconic acid) are shown in Fig. 6. The increase in viscosity with increasing water content indicates an increase in the hydrodynamic volume of the doped polymer chains, consistent with a progressive change in molecular conformation from “compact coil” to “expanded coil”.[37] This type of behaviour indicates that water interacts more strongly with the polymer chains and/or with poly(itaconic acid) (PIA) dopant

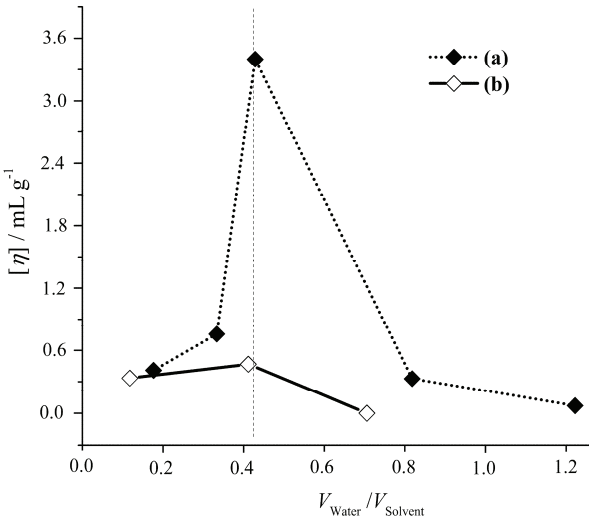

Fig. 6. Relationship between the intrinsic viscosities of polyaniline doped with poly-(itaconic acid) and volume ratio of the mixtures of: a) water/THF and b) water/NMP.

anions than does THF. Conversely, when the value 0.428 for the volume ratio was exceeded, the intrinsic viscosity began to decrease with further water addition, which could be explained as follows: the PANI–PIA chains take an extended coil conformation also because there are H-bonding interactions of the hydrogen of the amine groups with the oxygen present in the molecular structure of THF. When the value of the volume ratio was more than 0.428, the water excess was used to decrease the interaction chain–organic solvent that led thereafter to decreases in the hydrodynamic volume of the chains of the doped polyaniline (compact coil). The change in intrinsic viscosity values is so large that also the quality of solvent/water mixture for PANI-EB and PANI–PIA should be considered. Namely, water in this case can act as a non-solvent. After reaching an optimal proportion between solvent and water (good solvation, intermolecular interaction), its increased share might worsen the solvent quality, which could lead to more compact random coils due to stronger intramolecular chain interaction.[38]

Thermogravimetry (TGA)

The results of the thermogravimetric analysis of the pure PIA and PANI–PIA samples are presented in Fig. 7. Four degradation steps could be observed for PIA (Fig. 7, curve b) in the temperature range from 26–450 °C, with a residue of 30 wt. %. In the temperature region from 50–280 °C, two processes were detected; the first one is assigned to the elimination of free water adsorbed to the hydrophilic polymer and presence of residual solvent in the polymer,[39] and the second to anhydride ring formation in the PIA chain.[40] In the second temperature region, from 280 to 450 °C, two degradation stages were observed, probably related to some decarboxylation and carbonization processes.[16,41]

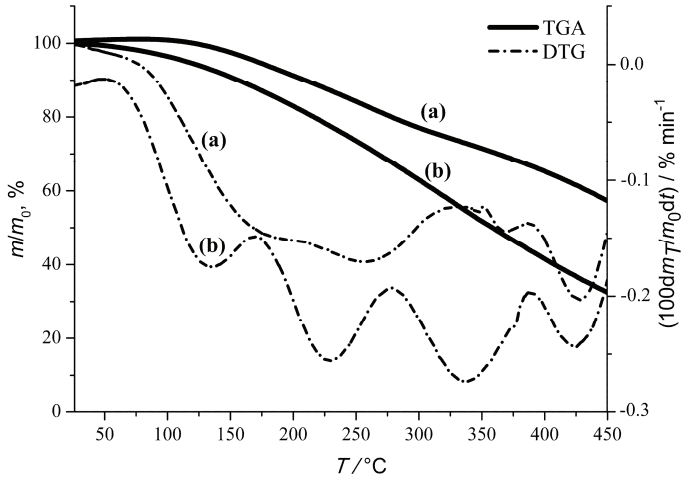

Fig. 7. Thermogravimetric (TG) and differential TG (DTG) curves for: a) PANI–PIA and b) PIA.

In the TGA thermograms of the PANI–PIA shown in Fig. 7, curve a, there are three major stages of weight losses of PANI–PIA powder sample. The first weight loss occurred around 67–198 °C (10 %) resulting from the elimination of water and other volatiles.[42] The second stage in the temperature range 198–337 °C was assigned to the decomposition of excess dopant PIA.[43] The third weight loss at the higher temperature could be attributed to the detachment of doping agent and the chemical decomposition of the short chains of PANI with maximum decomposition rates at 367 and 427 °C, respectively.[44]

It is notable that as much of 50 % of the initial mass was preserved for temperatures up to 500 °C. This residual mass relates to the existence of reticule polymer, which is formed at high temperatures,[45] and the influence of the doping agent on a real thermal stability is not clear in this temperature region.

X-Ray diffraction pattern (XRD)

The X-ray diffraction pattern of PANI-EB, PIA and PANI–PIA are given in Fig. 8. The crystalline (I_c) and amorphous (I_a) peaks were both integrated in 2θ space. From these integrated peaks areas (I_c, I_a), the ratio X_c/X_a can be calculated by $X_c/X_a = 1.8\times(I_c/I_a)$. A Ryland factor of 1.8 is commonly used for semi-crystalline polymers.[45] The percentage of crystallinity X_c (%) was obtained as:[46]

$$X_c\ (\%) = 100 - 100/(1 + X_c/X_a) \quad (2)$$

The XRD pattern of PANI–EB (Fig. 8, curve a) contains some sharps peaks at 2θ 9.57, 15.22, 20.75 and 24.29°, representing the crystal planes of (001), (011), (100) and (110) of dedoped PANI, respectively.[47] The peak intensities are listed in Table IV, indicating the pseudo orthorhombic space.[26] The peak centred at 2θ 24.29° could be ascribed to periodicity perpendicular to the polymer chain

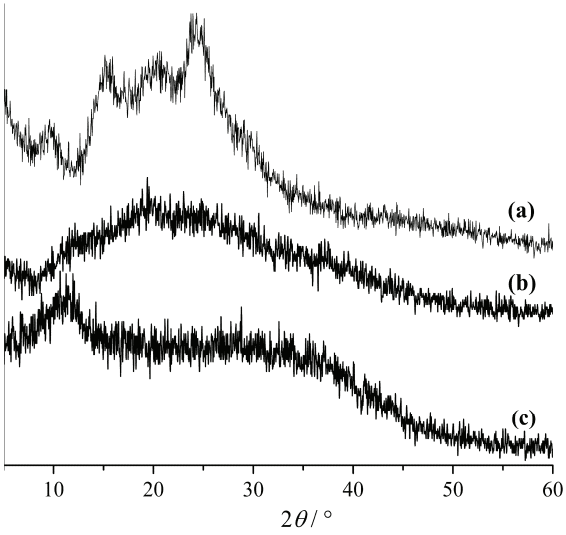

Fig. 8. XRD patterns of: a) PANI-EB, b) PANI–PIA and c) PIA.

(π stacking),[47] and the peak centred at 2θ 20.75° may be ascribed to periodicity parallel to the conjugated chain of PANI (emeraldine base).[48] The sharpness of the peaks represents the degree of orientation of the polymer chains in that particular crystal plane, and the intensity represents the population of crystallites in that plane.[49] This result suggests a low degree of crystallinity of 9.64 %.

TABLE IV. The 2θ values, intensity and indexation (*hkl*) of PANI-EB, PIA and PANI–PIA

Sample	2θ / °	Intensity, a.u.	*d* / Å	(*hkl*)	Crystallinity, X_c / %
	09.57	167.46	09.23	001	9.64
PANI–EB	15.22	176.44	05.82	011	
	20.75	202.06	04.28	100	
	24.29	203.40	03.66	110	
PIA	11.80	016.88	07.50	–	9.50
PANI–PIA	19.99	008.60	04.44	100	
	37.27	005.71	02.41	110	2.03

As shown in Fig. 8, curve c, the poly(itaconic acid) showed a moderate degree of crystallinity (X_c = 9.5 %, broad peaks in the spectrum) and a single sharp peak at 11.8°. On the other hand, the diffractogram of PANI–PIA powder, presented in Fig. 8, curve b showed two peaks; the first at 19.99° and the other at 37.27° with a characteristics distances of 4.44 and 2.41 Å, respectively. It should be noted that the chains of the PANI–PIA were less ordered than those of the PANI-EB, which was confirmed by the value of X_c = 2.03 % for PANI–PIA.

CONCLUSIONS

Soluble conducting polyaniline salts were successfully synthesized *via* chemical polymerization. Undoped and poly(itaconic acid)-doped polyaniline were characterized by a number of methods. The doped polyaniline had good solubility in mixtures of NMP/water and THF/water with a maximum solubility of 4 mg mL^{-1} in the latter mixture at room temperature; on the other hand, this polyaniline salt was not soluble in the pure polar organic solvents (THF and NMP) except when the temperature is above 60 °C. The optimum volume ratio of 0.42 between water and THF was determined by intrinsic viscosity measurements. The electrical conductivity of the doped form of polyaniline presents a proportional relationship with the concentration of the doping agent (PIA). A decrease in crystallinity was detected in the new PANI salt due to the presence of poly(itaconic acid) in the composite.

ИЗВОД

СИНТЕЗА И КАРАКТЕРИЗАЦИЈА ПРОВОДНОГ И У СМЕШИ РАСТВАРАЧА ВЕОМА РАСТВОРНОГ ПОЛИАНИЛИНА

HICHEM ZEGHIOUD[1], SAAD LAMOURI[1], ZITOUNI SAFIDINE[1] и MOHAMMED BELBACHIR[2]

[1]Laboratoire de Chimie Macromoléculaire, Ecole Militaire Polytechnique, BP 17, Bordj El Bahri, Alger, Algeria и [2]Laboratoire de Chimie des Polymères, Département de Chimie, Faculté des Sciences,Université d'Oran, BP 1524 El'Menouer Oran 31000, Algeria

У раду је приказана синтеза и карактеризација растворног и проводног полианилина PANI–PIA добијеног хемијским поступком тј. полимеризацијом. На овај начин је добијена со полианилина допираног поли(итаконском киселином), која је веома растворна у бројним смешама поларних органских растварача и воде, при чему је достигнута растворљивост од 4 mg mL^{-1}. Анализиран је утицај параметара синтезе, као што је степен допирања, на проводљивост, растворљивост и друга својства синтетисаних PANI–PIA соли. Максимална проводљивост у износу од $2{,}48\times10^{-4}$ S cm^{-1} је остварена при потпуном протоновању полианилина у облику емералдинске базе (PANI-EB). Поред тога, синтетисани материјали су додатно карактерисани вискозиметријом разблажених раствора, UV–Vis спектроскопијом, дифракцијом X-зрака (XRD), инфрацрвеном спектроскопијом и термогравиметријском анализом (TGA) за анализу њихових термичких својстава.

(Примљено 19. јула, ревидирано 29. децембра 2014, прихваћено 8. јануара 2015)

REFERENCES

1. Y. G. Han, T. Kusunose, T. Sekino, *J. Polym. Sci., B* **47** (2009) 1024
2. A. Rahy, D. J. Yang, *Mater. Lett*. **62** (2008) 4311
3. F. G. Souza Jr., B. G. Soares, J. C. Pinto, *Eur. Polym. J.* **44** (2008) 3908
4. M. G. Mikhael, A. B. Padias, H. K. Hall Jr., *J. Polym. Sci., A* **35** (1997) 1673
5. J. Q. Dong, Q. Shen, *J. Polym. Sci., B* **47** (2009) 2036
6. K. Shannon, J. Fernandez, *J. Chem. Soc. Chem. Commun*. **5** (1994) 643
7. L. Sun, H. Liu, R. Clark, S. C. Yang, *Synth. Met.* **84** (1997) 67
8. G. L. Yuan, N. Kuramoto, S. J. Su, *Synth. Met.* **129** (2002)173
9. J. Tarver, J. E. Yoo, T. J. Dennes, J. Schwartz, Y. L. Loo, *Chem. Mater*. **21** (2009) 280
10. E. M. Barrios, G. A. Mujica, C. L. Velasquez, Y. Martınez, *J. Electroanal. Chem.* **586** (2006) 128
11. J. Travas-Sejdic, R. Soman, H. Peng, *Thin Solid Films* **497** (2006) 96
12. M. Gizdavic-Nikolaidis, S. Ray, A. J. Easteal, in *Proceedings of Int. Conf. Adv. Mater. Nanotechnol. (AMN-4)*, Dunedin, New Zealand, 2009
13. N. Abdul Rahman, M. Gizdavic-Nikolaidis, S. Ray, A. J. Easteal, J. Travas-Sejdic, *Synth. Met.* **160** (2010) 2015
14. O. L. Gribkova, A. A. Nekrasov, M. Trchova, V. F. Ivanov, V. I. Sazikov, A. B. Razova, V. A. Tverskoy, A. V. Vannikov, *Polymer* **52** (2011) 2474
15. Y. Wang, H. Zheng, L. Jia, H. Li, T. Li, K. Chen, Y. Gu, J. Ding, *J. Macromol. Sci, A* **51** (2014) 577
16. C. Larez, F. Canelon, E. Millan, G. Perdomo, I. Katime, *Polym. Bull.* **49** (2002) 119
17. X. Li, M. Wan, X. Li, G. Zhao, *Polymer* **50** (2009) 4529
18. B. Stuart, *Infrared spectroscopy: fundamentals and applications*, Wiley, Chichester, 2004, p. 71
19. G. Taskın, O. Sanli, G. Asman, *Appl. Surf. Sci.* **257** (2011) 9444

20. S. N. Dobic, J. M. Filipovic, S. L. Tomic, *Chem. Eng. J.* **179** (2012) 372
21. B. D. Mistry, *A Handbook of Spectroscopic Data Chemistry (UV, IR, PMR, ^{13}CNMR and Mass Spectroscopy)*, Oxford Book Co., Jaipur, 2009, p. 26
22. D. S. Patil, J. S. Shaikh, D. S. Dalavi, S. S. Kalagi, P. S. Patil, *Mater. Chem. Phys.* **128** (2011) 449
23. P. Xu, Q. Tang, H. Chen, B. He, *Electrochim. Acta* **125** (2014) 163
24. J. H. Sung, S. J. Kim, K. H. Lee, *J. Power Sources* **126** (2004) 258
25. E. Ozkazanc, S. Zor, H. Ozkazanc, H. Y. Guney, U. Abaci, *Mater. Chem. Phys.* **133** (2012) 356
26. A. Mirmohseni, M. S. Seyed Dorraji, M. G. Hosseini, *Electrochim. Acta* **70** (2012) 182
27. J. M. Filipovic, L. Katsikas, I. G. Popovic, S. J. Velickovic, T. A. Djakov, D. M. Petrovic-Djakov, *J. Therm. Anal.* **49** (1997) 335
28. L. Chen, Y. Zhai, H. Ding, G. Zhou, Y. Zhu, D. Hui, *Composites, B* **45** (2013) 111
29. J. Gong, X. J. Cui, Z. W. Xie, S. G. Wang, L. Y. Qu, *Synth. Met.* **129** (2002) 187
30. Y. Cao, *Synth. Met.* **35** (1990) 319
31. I. Sasaki, J. Janata, M. Josowicz, *Polym. Degrad. Stab.* **92** (2007) 1408
32. J. Chen, B. J. Winther, Y. Pornputtkul, K. West, L. M. Kane, G. G. Wallace, *Electrochem. Solid State Lett*. **9** (2006) 11
33. D. Yang, B. R. Mattes, *J. Polym. Sci., B* **40** (2002) 2702
34. Y. Cao, P. Smith, A. J. Heeger, *Synth. Met.* **48** (1992) 91
35. F. Yilmaz, Z. Kucukyavuz, *Polym. Int*. **59** (2010) 552
36. J. Velickovic, J. Filipovic, D. P. Djakov, *Polym. Bull.* **32** (1994) 169
37. A. G. MacDiarmid, A. J. Epstein, *Synth. Met.* **65** (1994)103
38. E. Zagar, M. Zigon, *Polymer* **41** (2000) 3513
39. S. L. Tomić, J. M. Filipović, *Polym Bull.* **52** (2004) 355
40. S. M. Mokhtar, E. M. Youssef, M. A. Abd El-Ghaffar, *J. Macromol. Sci. – Pure Appl. Chem., A* **38** (2001) 19
41. K. M. Krušić, E. Džunuzović, S. Trifunović, J. Filipović, *Eur. Polym. J.* **40** (2004) 793
42. B. Salma, G. Salma, A. Khurshid, A. S. Anwar-ul-Haq, *Synth. Met.* **162** (2012) 2259
43. H. Farrokhzad, T. V. Gerven, B. V. der Bruggen, *Eur. Polym. J.* **49** (2013) 3234
44. N. Naar, S. Lamouri, B. Belaabed, T. Kouroughli, N. Gabouze, *Polym. J.* **41** (2009) 432
45. D. Tsocheva, T. ZIatkov, L. Terlemezyan, *J. Therm. Anal*. **53** (1998) 895
46. P. J. Rae, D. M. Dattelbaum, *Polymer* **45** (2004) 7615T. Abdiryim, X.-G. Zhang, R. Jamal, *Mater. Chem. Phys.* **90** (2005) 367
47. M. Hasik, A. Drelinkiewicz, E. Wenda, C. Paluszkiewicz, S. Quillard, *J. Mol. Struct.* **596** (2001) 89
48. B. Belaabed, J. L. Wojkiewicz, S. Lamouri, N. El Kamchi, T. Lasri, *J. Alloys Compd.* **527** (2012) 137.

Journal of the Serbian Chemical Society
JSCS-info@shd.org.rs • www.shd.org.rs/JSCS

J. Serb. Chem. Soc. 80 (7) 933–946 (2015)
JSCS–4770

UDC 547.421–036.7+547.42+
544.032.4:532.13+532.14
Original scientific paper

Experimental study of the thermodynamic and transport properties of binary mixtures of poly(ethylene glycol) diacrylate and alcohols at different temperatures

JELENA M. VUKSANOVIĆ[#], IVONA R. RADOVIĆ[#]*, SLOBODAN P. ŠERBANOVIĆ[#] and MIRJANA LJ. KIJEVČANIN[#]

Faculty of Technology and Metallurgy, University of Belgrade, Karnegijeva 4, 11120 Belgrade, Serbia

(Received 9 October 2014, revised 16 January, accepted 19 January 2015)

Abstract: Experimental density ρ, refractive index n_D and viscosity η data of three binary systems of poly(ethylene glycol) diacrylate (PEGDA) + ethanol, + 1-propanol and + 1-butanol were measured at eight temperatures from 288.15 to 323.15 K, with temperature step of 5 K, and at atmospheric pressure. The experimental data were correlated as a function of the PEGDA mole fraction and temperature. The densities and refractive indices of the investigated mixtures could be fitted well with exponential function *vs*. composition, including the temperature dependence of the parameters, while in the case of the viscosities, a polynomial function fits well the composition of the mixtures. In the case of the temperature correlation, all three properties (ρ, ln η and n_D) exhibited linear trends. The viscosity modeling was performed using four models: the UNIFAC–VISCO, ASOG–VISCO, McAllister and the Teja–Rice models. For application of the UNIFAC–VISCO model, interaction parameters of following groups were determined: CH_2=CH/CH_3, CH_2=CH/CH_2, CH_2=CH/OH, CH_2=CH/CH_2O and CH_2=CH/COO. In addition, in the same way, the binary interaction parameters used in the ASOG–VISCO model of the following groups were determined: CH_2=CH/CH_2, CH_2=CH/OH, CH_2=CH/CH_2O and CH_2=CH/COO.

Keywords: density; viscosity; refractive index; new UNIFAC–VISCO parameters; new ASOG–VISCO parameters.

INTRODUCTION

For a complete understanding of the thermodynamic and transport properties of pure organic compounds and multicomponent liquid mixtures, knowledge of their thermodynamic and transport properties over wide composition and tem-

* Corresponding author. E-mail: ivonag@tmf.bg.ac.rs
[#] Serbian Chemical Society member.
doi: 10.2298/JSC141009005V

perature ranges is necessary. Studies of thermodynamic properties contribute to the understanding of the behavior of various organic compounds and their functional groups, and are of great importance for the understanding of the molecular interactions in multicomponent mixtures. This work is a continuation of ongoing research related to determination of thermophysical and transport properties of mixtures containing polymers.[1–5] In this work, a biodegradable and biocompatible polymer, *i.e.*, poly(ethylene glycol) diacrylate (PEGDA), was investigated in binary mixtures with small chain alcohols, *i.e.*, ethanol, 1-propanol, and 1-butanol.

Poly(ethylene) glycol diacrylate (PEGDA) is a low volatility and medium viscosity clear liquid with good flexibility and elongation, good water dispersiblity, low skin irritancy and good reactivity. It is soluble in water and is used as a functional co-monomer for flexible plastics and as a cross linking agent between the molecular chains of polymers.[6] Furthermore, PEGDA is a synthetic, hydrophilic starting material for the production of hydrogels in the presence of a photo-initiator and UV light. This polymer is widely known as a biocompatible and non-immunogenic material suitable for various chemical manipulations, with application in tissue engineering and regenerative medicine.[7] One of the important usages of PEGDA in biological and biomedical applications could be for controlled release of drugs by producing well defined micro- or nano-channels inside the polymer, which would make the release of drugs through the pathways more readily predictable and controlled. A procedure for producing PEGDA particles with specific, internal channels for drug release is described in detail in the literature.[8]

The investigated short-chain alcohols are completely miscible with water and used as solvents in various fields of industry. In this particular case, their application in pharmaceutical industry is of great importance because mixtures of PEGDA and alcohols could be potentially applied in the pharmaceutical industry for the controlled release of drugs. In addition, they find application for the removal of CO_2 from the air or in biochemical applications.[6]

Alcohols are polar compounds with the following dipole moments: 5.67×10^{-30} C·m for ethanol, 5.67×10^{-30} C·m for 1-propanol and 6.00×10^{-30} C·m for 1-butanol.[9] PEGDA, as a hydrophilic polymer, contains polar or charged functional groups (carbonyl groups adjacent to an ether linkage) which make them soluble in polar compounds, such as alcohols. From the chemical structures of PEGDA and alcohols, it is evident that alcohols contain a hydrogen responsible for hydrogen bonding between the molecules of the same alcohol or with an oxygen from the polymer, while in the PEGDA molecule, ester COO groups are present. It could be conclude that these molecules might form intermolecular hydrogen bonds, *i.e.*, hydrogen from the hydroxyl group in alcohols with the oxygen from the COO group in a polymer. There are also van der Waals dispersion

forces and dipole–dipole interactions between alcohols and polymer, and molecules of the same compound. The hydrogen bonding and dipole–dipole interactions will be much the same for all the alcohols, but the dispersion forces will increase as the alcohol becomes larger.

The intention of this work was to investigate how the thermodynamic and transport properties of PEGDA and alcohol mixtures change with respect to the alcohol chain length and with temperature, bearing in mind the possible interactions between the above-mentioned components. Thus, in this work, the densities ρ, refractive indices n_D and viscosities η of three binary systems of poly(ethylene glycol) diacrylate (PEGDA) + ethanol or + 1-propanol or + 1-butanol were measured at eight temperatures (288.15, 293.15, 298.15, 303.15, 308.15, 313.15, 318.15 and 323.15 K) and at atmospheric pressure. Additionally, the viscosity data were modeled using the UNIFAC–VISCO, ASOG–VISCO, McAllister and Teja–Rice models. Generally, if a viscosity calculation is based on already determined parameters given in the literature, the UNIFAC–VISCO and ASOG–VISCO models are actually predictive. However, since in the case of the systems investigated in the present study, some of the parameters were not known, the intention was to determine accurately their values and the UNIFAC––VISCO and ASOG–VISCO models were considered as correlative.

EXPERIMENTAL

Chemicals

Poly(ethylene glycol) diacrylate (PEGDA), with molecular formula $C_{2n+6}H_{4n+6}O_{n+3}$ and with number average molecular weight 700 g mol^{-1}, was purchased from Aldrich (CAS No.: 26570-48-9, Cat. No.: 455008, Lot No.: MKBH4151V). Alcohols of reagent grade: ethanol (≥ 99.9 mass %), 1-propanol (≥ 99.5 mass %), and 1-butanol (≥ 99.5 mass %) were purchased from Merck. The chemicals were kept in dark bottles under an inert atmosphere and ultrasonically degassed before sample preparation.

Apparatus and procedures

The density ρ measurements were performed using an Anton Paar DMA 5000 digital vibrating U-tube densimeter (with automatic viscosity correction). The temperature in the cell was regulated to ±0.001 K with a built in solid-state thermostat. Calibration of the apparatus was performed daily using ambient air and Millipore quality water. A Mettler AG 204 balance, with a precision 1×10^{-7} kg, was used for precise measurement of mass composition for all binary mixtures, using the cell and the procedure described previously.[10] The uncertainty of the mole fraction calculation was less than $\pm1\times10^{-4}$. The experimental uncertainty in density was about $\pm1\times10^{-2}$ kg m^{-3}.

The refractive index n_D measurements were performed using an automatic Anton Paar RXA 156 refractometer, which works with the wavelength of 589 nm. Throughout this procedure, the temperature of the sample was kept constant with a built-in thermostat within an accuracy of ±0.03 K. The estimated experimental uncertainties in the refractive index were about $\pm1\times10^{-4}$.

The viscosity, η, measurements were performed using a digital Stabinger viscometer (model SVM 3000/G2). The instrument contains two measuring cells; one of which is used

for measuring the density of the sample, while the other one measures the dynamic viscosity. The kinematic viscosity was calculated from the measured density and dynamic viscosity. During this procedure, the temperature in the cells was regulated to ±0.01 K with a built in solid-state thermostat. The relative uncertainty in the dynamic viscosity measurements was estimated to be 0.35 %.

The densities, dynamic viscosities and refractive indices of the pure substances at several temperatures and at atmospheric pressure are compared with literature values[7,11-19] in Table I. The agreement with the literature for the density measurements in most cases was within 0.55 kg m^{-3}, while the viscosity measurements were within 0.02 mPa s. The experimental refractive indices of pure components agree with literature values within 8×10^{-4} for alcohols and within 0.002 for PEGDA.

TABLE I. Densities, ρ, viscosities, η, and refractive indices, n_D, of the pure components at temperature T and at atmospheric pressure; the standard uncertainties σ for each variables are $\sigma(T)$ = 0.01 K; $\sigma(p)$ = 5 %; $\sigma(x_1) = \pm1\times10^{-4}$, and the combined uncertainties σc are $\sigma c(\rho) = \pm1\times10^{-2}$ kg m^{-3}; $\sigma c(n_D) = \pm1\times10^{-4}$; $\sigma c(\eta)$ = 0.35 %, at the 0.95 level of confidence ($k \approx 2$)

Substance	T / K	ρ / 10^3 kg m^{-3}		η / mPa s		n_D	
		This work	Lit.	This work	Lit.	This work	Lit.
PEGDA	293.15					1.47012	1.470 [7]
	303.15					1.46618	1.465 [7]
	313.15					1.46228	1.460 [7]
Ethanol	293.15	0.789547	0.7900[11]	1.1885	1.2097[11]		
	298.15	0.785257	0.7857[11]	1.0838	1.0990[11]	1.35999	1.35922[12]
	303.15	0.780942	0.7809[11]	0.98999	0.9971[11]		
	313.15	0.772202	0.7733[11]	0.82807	0.8280[11]		
	323.15	0.763276	0.7636[13]	0.69427	0.7081[13]		
1-Propanol	288.15	0.807931	0.80749[14]				
	293.15	0.803946	0.80375[14]				
	298.15	0.799932	0.79975[14]	1.9222	1.943[15]	1.38334	1.3837 [16]
	303.15			1.7158	1.725[15]		
1-Butanol	293.15	0.810205	0.8097[14]	2.9321	2.941[16]	1.39929	1.39929[16]
	298.15	0.806384	0.8060[14]	2.5656	2.571[16]	1.39725	1.39741[16]
	303.15	0.802538	0.80191[18]	2.2518	2.271[16]	1.39519	1.3959[19]
	308.15	0.798659	0.79807[18]				

RESULTS AND DISCUSSION

The experimental data of density, viscosity, and refractive index for three binary systems (PEGDA + ethanol, PEGDA + 1-propanol, and PEGDA + 1-butanol) at eight temperatures (288.15 to 323.15 K), over the entire composition range and at atmospheric pressure are reported in Table S-I of the Supplementary material to this paper.

Fitting of the experimental values of density and refractive index was performed as a function of PEGDA mole fraction with temperature dependant parameters. The quality of the fitting was estimated by the deviation between experi-

mental value and those calculated by different equations. The best results were obtained using the following equation:

$$\rho, n_D = \exp\left[\left(A_{00} + A_{01}T \right) + \frac{A_{10} + A_{11}T}{x_1 + \left(A_{20} + A_{21}T \right)} \right] \quad (1)$$

where A_{00}, A_{01}, A_{10}, A_{11}, A_{20} and A_{21} are the fitting parameters, x_1 is PEGDA mole fraction and T is temperature.

The viscosity values, unlike density and refractive index values, varied greatly with change in temperature and hence, a single equation that combined the temperature and composition dependencies did not give good results and so fitting the viscosity values as a function of PEGDA mole fraction or temperature was performed separately using the following equations:

$$\eta = B_0 + B_1 x_1 + B_2 x_1^2 + B_3 x_1^3 \quad (2)$$

$$\ln \eta = C_0 + \frac{C_1}{T} \quad (3)$$

where B_0, B_1, B_2, B_3, C_0 and C_1 are the fitting parameters, x_1 is the PEGDA mole fraction and T is the temperature.

For the three binary mixtures at different temperatures and compositions, the parameters of Eq. (1) are presented in Table S-II and the parameters of Eqs. (2) and (3) in Table S-III (Supplementary material). The corresponding root-mean-square deviations (rmsd) σ, defined by Eq. (4) are presented in Tables S-II and S-III of the Supplementary material:

$$\sigma = \left(\frac{\sum_i^n \left(Y_{exp} - Y_{cal} \right)^2}{n} \right)^{1/2} \quad (4)$$

Y_{exp} and Y_{cal} are experimental and calculated values of ρ, η or n_D, respectively, and n is the number of experimental data points.

Comparison of the densities, viscosities and refractive indices of binary systems of PEGDA and alcohols at 288.15 and 323.15 K and at atmospheric pressure are given in Fig. 1a–c, respectively. It is obvious from Fig. 1 that the experimental values of the density, viscosity, and refractive index data of pure PEGDA are significantly higher than those of the analyzed alcohols. In addition, it is evident that the densities and refractive index data of the mixtures increased exponentially with increasing PEGDA mole fraction, while the increase in the viscosities *vs*. PEGDA composition followed a polynomial trend. It can be observed that the density and refractive index increased considerably in the range of

lower PEGDA concentrations (from 0 to 0.3 mole fraction), while approaching higher PEGDA mole fractions, the curves trended to constant values. This means that the influence of PEGDA on the overall densities and refractive indices of the PEGDA + alcohol mixtures was far greater in comparison to the influence of the alcohols. In the case of viscosity, there was a constant increase in the values with increasing PEGDA mole fraction. In addition, it is noticeable that the densities, viscosities and refractive indices of pure compounds and their mixtures decreased as the temperature increased. This temperature influence was the most pronounced for the viscosity data. Namely, the viscosity of pure PEGDA at 288.15 K was almost six times higher than at 323.15 K.

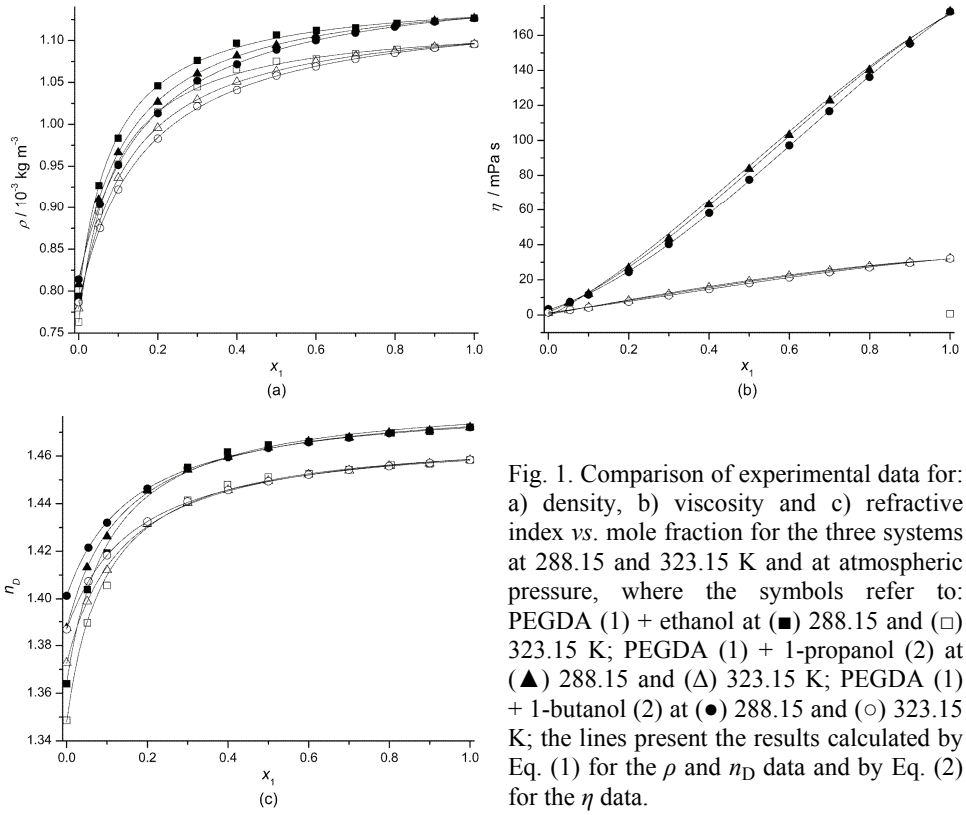

Fig. 1. Comparison of experimental data for: a) density, b) viscosity and c) refractive index *vs*. mole fraction for the three systems at 288.15 and 323.15 K and at atmospheric pressure, where the symbols refer to: PEGDA (1) + ethanol at (■) 288.15 and (□) 323.15 K; PEGDA (1) + 1-propanol (2) at (▲) 288.15 and (Δ) 323.15 K; PEGDA (1) + 1-butanol (2) at (●) 288.15 and (○) 323.15 K; the lines present the results calculated by Eq. (1) for the ρ and n_D data and by Eq. (2) for the η data.

Experimental values of the density and refractive index against temperature at atmospheric pressure are presented in Figs. 2 and 3, respectively, while ln η *vs*. $1/T$ changes at atmospheric pressure are depicted in Fig. 4.

One can conclude that density and refractive index data exhibit linear dependences on temperature, with a decreasing tendency of the property with increasing temperature. Figs. 2 and 3 also prove that the changes of densities and

refractive indices are greater in the range of smaller PEGDA mole fractions (from 0 to 0.3). Function of ln η *vs*. 1/T exhibited a linear trend as well, confirming that with increasing temperature the PEGDA + alcohols mixtures become less viscous (Fig. 4).

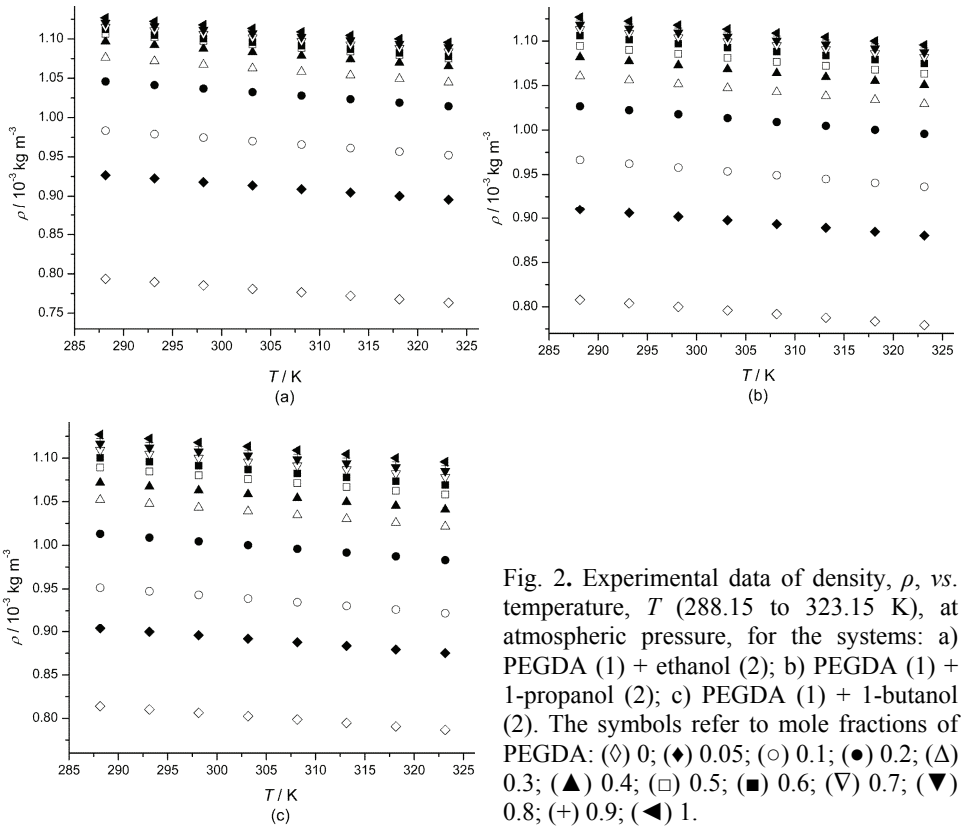

Fig. 2. Experimental data of density, ρ, *vs*. temperature, T (288.15 to 323.15 K), at atmospheric pressure, for the systems: a) PEGDA (1) + ethanol (2); b) PEGDA (1) + 1-propanol (2); c) PEGDA (1) + 1-butanol (2). The symbols refer to mole fractions of PEGDA: (◊) 0; (♦) 0.05; (○) 0.1; (●) 0.2; (Δ) 0.3; (▲) 0.4; (□) 0.5; (■) 0.6; (∇) 0.7; (▼) 0.8; (+) 0.9; (◄) 1.

In addition, modeling of viscosity experimental data was performed using predictive and correlative types of models. In this work UNIFAC–VISCO[20,21] and ASOG–VISCO[22] models were used for the determination of the dynamic viscosity of the three binary mixtures. UNIFAC–VISCO and ASOG–VISCO are group contribution models aimed at activity coefficient determination. In both methods, the activity coefficients in the mixtures are related to interactions between structural groups. Consequently, the parameters characterizing interactions between pairs of structural groups, called group interaction parameters, are necessary (α_{nm} for UNIFAC–VISCO and m_{kl} and n_{kl} for ASOG–VISCO). If the parameters are given in the literature, it is not necessary to determine them again. In this work, new group interaction parameters were determined from the experi-

mentally measured viscosities using the Marquardt[23] optimization technique for the minimization of the objective function:

$$OF = \frac{1}{n}\sum_{i=1}^{n}\left(\frac{\eta_{\mathrm{exp}} - \eta_{\mathrm{cal}}}{\eta_{\mathrm{exp}}}\right)_i^2 \rightarrow \min \qquad (5)$$

where η_{exp} and η_{cal} denote the experimental and calculated values of the dynamic viscosity η and n is the number of experimental data points.

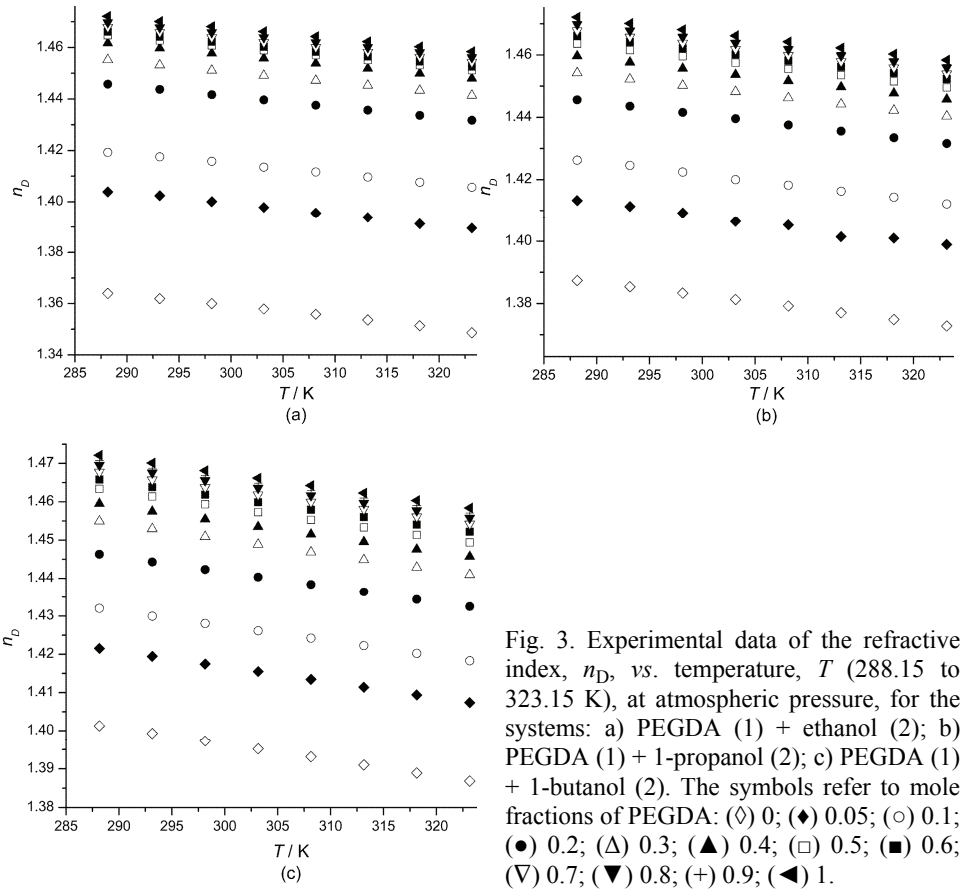

Fig. 3. Experimental data of the refractive index, n_D, *vs*. temperature, T (288.15 to 323.15 K), at atmospheric pressure, for the systems: a) PEGDA (1) + ethanol (2); b) PEGDA (1) + 1-propanol (2); c) PEGDA (1) + 1-butanol (2). The symbols refer to mole fractions of PEGDA: (◊) 0; (♦) 0.05; (○) 0.1; (●) 0.2; (Δ) 0.3; (▲) 0.4; (□) 0.5; (■) 0.6; (∇) 0.7; (▼) 0.8; (+) 0.9; (◄) 1.

The new UNIFAC–VISCO interaction parameters, α_{nm}, between the following groups: CH_2=CH/CH_3, CH_2=CH/CH_2, CH_2=CH/OH, CH_2=CH/CH_2O and CH_2=CH/COO are summarized in Table II. The remaining interaction parameters were taken from the original model[20,21] and previous papers.[5,24]

In the similar way, new ASOG–VISCO group interaction parameters, m_{kl} and n_{kl}, of following groups CH_2=CH/CH_2, CH_2=CH/OH, CH_2=CH/CH_2O,

CH_2=CH/COO were determined using the original interaction parameters[22] and parameters from previous papers.[3,24] The results are summarized in Table III.

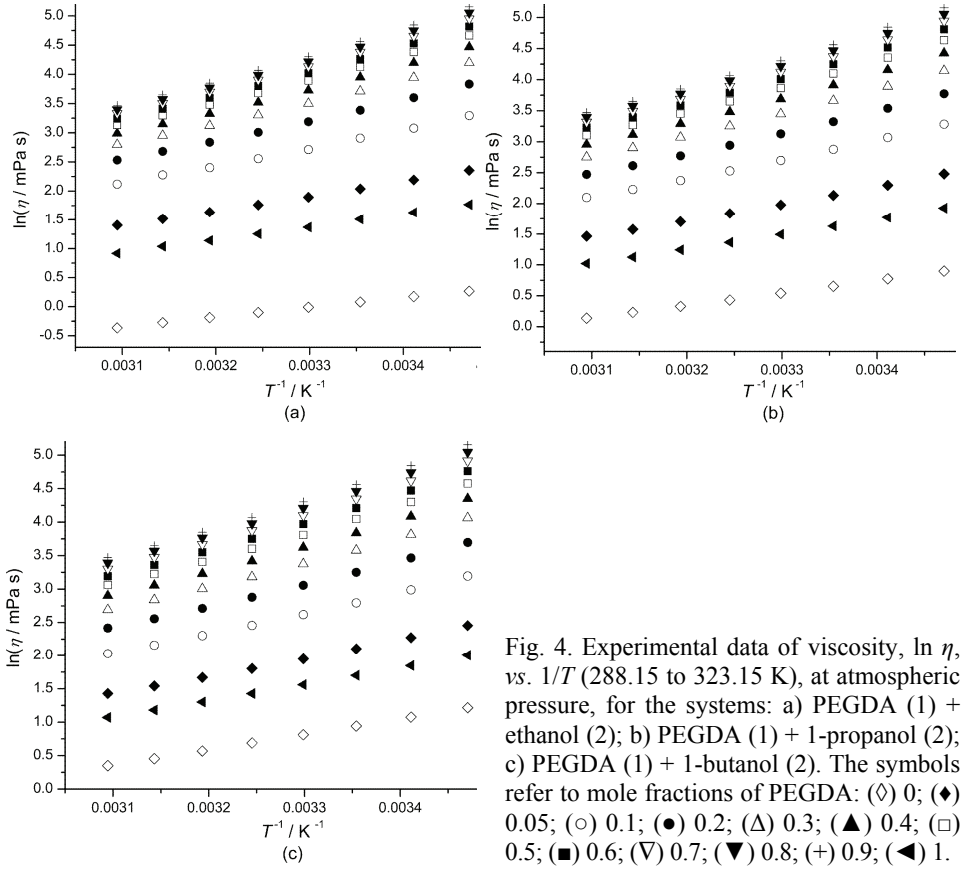

Fig. 4. Experimental data of viscosity, ln η, *vs*. $1/T$ (288.15 to 323.15 K), at atmospheric pressure, for the systems: a) PEGDA (1) + ethanol (2); b) PEGDA (1) + 1-propanol (2); c) PEGDA (1) + 1-butanol (2). The symbols refer to mole fractions of PEGDA: (◊) 0; (♦) 0.05; (○) 0.1; (●) 0.2; (Δ) 0.3; (▲) 0.4; (□) 0.5; (■) 0.6; (∇) 0.7; (▼) 0.8; (+) 0.9; (◄) 1.

TABLE II. The UNIFAC–VISCO interaction parameter, α_{nm}

n/m	CH_3	CH_2	CH_2=CH	OH	CH_2O	COO
CH_3	0	–709.5[a]	–570.861[d]	594.4[a]	–50.17[b]	–172.4[a]
CH_2	66.53[a]	0	1161.742[d]	498.6[a]	–319.930[b]	1172[a]
CH_2=CH	–872.856[d]	1489.036[d]	0	–869.851[d]	–2243.897[d]	–57.440[d]
OH	1209[a]	–634.5[a]	–549.041[d]	0	–619.360[b]	68.35[a]
CH_2O	456.91[b]	–340.250[b]	248.157[d]	25.340[b]	0	–56.95[c]
COO	–44.25[a]	541.6[a]	–445.344[d]	186.8[a]	–137.945[c]	0

[a]Original UNIFAC–VISCO parameters;[20,21] [b]UNIFAC–VISCO parameters from the literature;[5] [c]UNIFAC––VISCO parameters from the literature;[24] [d]new UNIFAC–VISCO parameters

Moreover, the experimental viscosity data were correlated with the one-parameter Teja and Rice,[25,26] and McAllister[27] two-parameter three-body and

three-parameter four-body models. These models are described in detail in a previous papers.[28,29]

TABLE III. The ASOG–VISCO interaction parameters

k/*l*	CH_2	CH_2=CH	OH	CH_2O	COO
			m_{kl}		
CH_2	0	0.2428[d]	–0.3570[a]	–10.9924[b]	0.3682[a]
CH_2=CH	1.7603[d]	0	1.6245[d]	–6.3287[d]	–2.5891[d]
OH	14.1460[a]	–0.3330[d]	0	–2.2661[b]	–40.2000[a]
CH_2O	–33.9591[b]	–173.2012[d]	1.5287[b]	0	–2.9720[c]
COO	0.0952[a]	197.1496[d]	19.1310[a]	–4.7468[c]	0
			n_{kl}		
CH_2	0	356.102[d]	469.650[a]	–1.928[b]	112.590[a]
CH_2=CH	187.229[d]	0	413.379[d]	299.095[d]	298.614[d]
OH	–6137.000[a]	476.584[d]	0	–14.965[b]	11583.000[a]
CH_2O	–8.176[b]	298.966[d]	–127.018[b]	0	–835.188[c]
COO	–383.600[a]	300.577[d]	–5747.000[a]	–433.643[c]	0

[a]Original ASOG–VISCO parameters;[22] [b]ASOG–VISCO parameters from the literature;[3] [c]ASOG–VISCO parameters from the lierature;[24] [d]new ASOG–VISCO parameters

The ability of these models to predict successfully the dynamic viscosities of the investigated binary mixtures and to correlate the experimental viscosity data is presented with percentage deviations, PD_{max}, between the experimental and calculated viscosities, using the following equation:

$$PD_{max} = \frac{100}{n}\sum_{i=1}^{n}\left|\frac{\eta_{exp}-\eta_{cal}}{(\eta_{exp})_{max}}\right|_i \quad (6)$$

where $(\eta_{exp})_{max}$ is the maximum of the experimental η values.

The results obtained by the UNIFAC–VISCO, ASOG–VISCO, Teja–Rice and McAllister models for the mixtures of PEGDA + ethanol or 1-propanol or 1-butanol over the investigated temperature range are given in Table IV. A graphical presentation of the experimental viscosity deviation from the values obtained by the selected models is given in Fig. 5.

TABLE IV. Results of the viscosity prediction and correlation for the investigated binary systems at the temperatures (288.15 to 323.15) K and at atmospheric pressure

T / K	Predictive approach		Correlative approach		
	UNIFAC–VISCO	ASOG–VISCO	Teja–Rice	McAllister-3	McAllister-4
	PD_{max} / %	PD_{max} / %	PD_{max} / %	PD_{max} / %	PD_{max} / %
			PEGDA (1) + ethanol (2)		
288.15	7.62	2.16	11.03	4.46	1.59
293.15	5.79	2.65	10.48	4.66	1.67
298.15	4.08	2.40	10.10	4.88	1.84
303.15	2.82	1.76	9.70	4.97	1.84

TABLE IV. Continued

T / K	Predictive approach		Correlative approach		
	UNIFAC–VISCO	ASOG–VISCO	Teja–Rice	McAllister-3	McAllister-4
	PD_{max} / %	PD_{max} / %	PD_{max} / %	PD_{max} / %	PD_{max} / %
PEGDA (1) + ethanol (2)					
308.15	2.20	1.08	9.38	5.15	1.92
313.15	2.19	0.66	9.04	5.32	2.05
318.15	2.95	1.17	8.88	5.49	2.20
323.15	3.74	1.57	8.51	5.50	2.15
PEGDA (1) + 1-propanol (2)					
288.15	4.66	1.54	5.96	3.01	1.11
293.15	3.14	0.77	5.68	3.13	1.15
298.15	1.76	0.50	5.52	3.30	1.15
303.15	0.87	0.84	5.29	3.40	1.20
308.15	1.39	1.34	5.07	3.49	1.27
313.15	2.78	1.95	4.90	3.59	1.31
318.15	4.17	2.61	4.72	3.66	1.36
323.15	5.32	3.07	4.65	3.73	1.42
PEGDA (1) + 1-butanol (2)					
288.15	4.56	1.56	3.89	2.13	0.65
293.15	3.46	0.78	3.79	2.22	0.68
298.15	2.47	0.66	3.63	2.32	0.78
303.15	1.69	0.51	3.57	2.45	0.72
308.15	1.04	0.47	3.49	2.54	0.78
313.15	0.72	0.44	3.41	2.64	0.82
318.15	1.25	0.44	3.35	2.74	0.86
323.15	1.98	0.45	3.35	2.78	0.92

UNIFAC–VISCO model gave very good results for the prediction of the viscosity of the three investigated binary systems. In almost all cases, the maximum percentage deviation PD_{max} did not exceed 5 %. The largest deviations were obtained at the lowest temperature (systems with ethanol and 1-butanol), or at the highest investigated temperature in the case of the system containing 1-propanol. Inspection of Figs. 5a and 5b confirms this conclusion. The ASOG––VISCO model gave even better results, with maximum percentage deviations PD_{max} of 2.65 % in almost all cases. The best results were obtained for the PEGDA + 1-butanol binary mixture, with PD_{max} of less than 0.78 %, except at 288.15 K, when the deviation was 1.56 %. However, this model fits the experimental data satisfactorily (Fig. 5c). From the results obtained from correlative models, it could be concluded that the best results for all three systems were obtained with the McAllister-4 model. This conclusion is supported by the graphical representation given for the systems PEGDA + ethanol, or + 1-butanol (Fig. 5a and c) where the model correlates the experimental points very well. The Teja–Rice model gave the worst correlations of the experimental data, with the

highest PD_{max} values, up to 11.03 % for the PEGDA + ethanol binary mixtures. This conclusion is obvious from Figs. 5b and 5c, especially at lower temperatures. The best results for all three types of correlative models were obtained for the PEGDA + 1-butanol binary system, for which the lowest PD_{max} deviations were obtained for theMcAllister-4 model (less than 1 %).

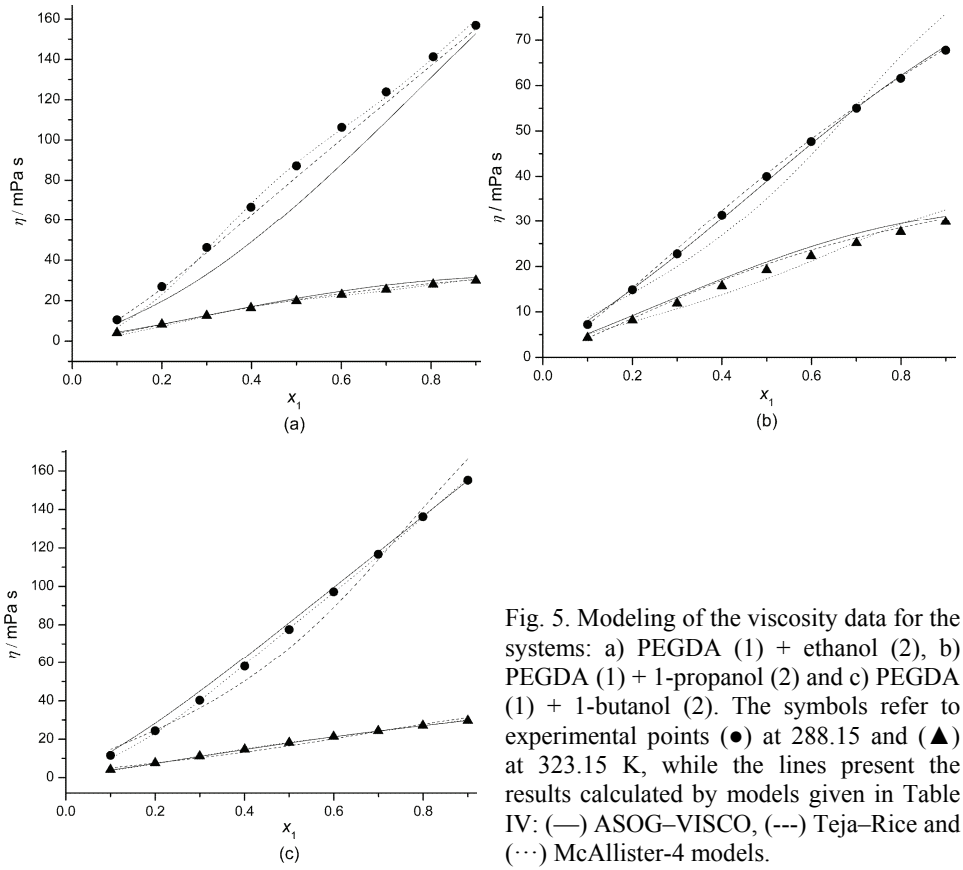

Fig. 5. Modeling of the viscosity data for the systems: a) PEGDA (1) + ethanol (2), b) PEGDA (1) + 1-propanol (2) and c) PEGDA (1) + 1-butanol (2). The symbols refer to experimental points (●) at 288.15 and (▲) at 323.15 K, while the lines present the results calculated by models given in Table IV: (—) ASOG–VISCO, (---) Teja–Rice and (···) McAllister-4 models.

CONCLUSIONS

In this work, the experimental data of the density ρ, viscosity η, and refractive index n_D are reported for PEGDA + ethanol, PEGDA + 1-propanol and PEGDA + 1-butanol binary mixtures at temperatures in the range 288.15 to 323.15 K, with a temperature step of 5 K, over the whole composition range, and at atmospheric pressure. All measured physical properties increased with increasing PEGDA mole fraction and with decreasing temperature. The measured physical properties were correlated as a function of temperature and of PEGDA mole fraction. The densities and refractive indices of the mixtures showed

exponential dependence *vs*. composition, including the temperature dependence of the parameters, while the viscosities exhibited polynomial dependence over the mixture composition. In the case of the temperature correlation, all three properties (ρ, ln η and n_D) exhibited linear trends. The influence of temperature on the viscosity of the mixtures was larger than its influence on the density and refractive index. Moreover, the influence of the PEGDA mole fraction on the overall densities and refractive indices of the PEGDA + alcohol mixtures was far greater in comparison to the influence of the alcohol type. In addition, viscosity modeling was performed using two types of models: the predictive UNIFAC–VISCO and ASOG–VISCO, and the correlative McAllister and Teja–Rice models. The predictive ASOG–VISCO gave better results between the predictive models, while of the correlative models, the best results were obtained using the McAllister-4 equation, for all three investigated binary systems. Furthermore, new UNIFAC–VISCO and ASOG–VISCO binary interaction parameters were determined from the experimental viscosity data.

SUPPLEMENTARY MATERIAL

Experimental data of densities ρ, viscosities η and refractive n_D indices and fitting parameters and root-mean-square deviations for Eqs. (1)–(3) of PEGDA + alcohol binary mixtures are available electronically from http://www.shd.org.rs/JSCS/ or from the corresponding author on request.

Acknowledgement. The authors gratefully acknowledge the financial support received from the Research Fund of the Ministry of Education, Science and Technical Development of the Republic of Serbia and the Faculty of Technology and Metallurgy, University of Belgrade (Project No. 172063).

ИЗВОД

ЕКСПЕРИМЕНТАЛНО ИСПИТИВАЊЕ ТЕРМОДИНАМИЧКИХ И ТРАНСПОРТНИХ СВОЈСТАВА БИНАРНИХ СМЕША ПОЛИ(ЕТИЛЕНГЛИКОЛ)-ДИАКРИЛАТА И АЛКОХОЛА НА РАЗЛИЧИТИМ ТЕМПЕРАТУРАМА

ЈЕЛЕНА М. ВУКСАНОВИЋ, ИВОНА Р. РАДОВИЋ, СЛОБОДАН П. ШЕРБАНОВИЋ и МИРЈАНА Љ. КИЈЕВЧАНИН

Технолошко–металуршки факултет, Универзитет у Београду, Карнегијева 4, 11120 Београд

Експериментални подаци за густину, ρ, индекс рефракције, n_D, и вискозност, η, три бинарна система поли(етиленгликол)-диакрилата (PEGDA) + етанол, + 1-пропанол и + 1-бутанол су мерени на осам температура (288,15 to 323,15 K), са кораком 5 K, и на атмосферском притиску. Експериментални подаци су корелисани у функцији молског удела PEGDA и температуре. Густине и индекси рефракције испитиваних смеша су фитовани експоненцијалном функцијом у зависности од састава, док се у случају вискозности полиномска функција показала као најбоља кроз цео опсег молских удела. У случају температурне зависности, све три величине (ρ, ln η и n_D) показују линеаран тренд. Вискозност је моделована помоћу четири модела: UNIFAC–VISCO, ASOG–VISCO, Mc-Allister и Teja–Rice. Помоћу UNIFAC–VISCO модела одређени су интеракциони параметри следећих група: CH_2=CH/CH_3, CH_2=CH/CH_2, CH_2=CH/OH, CH_2=CH/CH_2O и CH_2=CH/COO. Такође, на исти начин помоћу ASOG–VISCO модела су одређени и бинар-

ни интеракциони параметри следећих група: CH_2=CH/CH_2, CH_2=CH/OH, CH_2=CH/CH_2O and CH_2=CH/COO.

(Примљено 9. октобра 2014, ревидирано 16. јануара, прихваћено 19. јануара 2015)

REFERENCES

1. J. M. Vuksanović, E. M. Živković, I. R. Radović, B. D. Đorđević, S. P. Šerbanović, M. Lj. Kijevčanin, *Fluid Phase Equilib.* **345** (2013) 28
2. M. S. Calado, G. R. Ivaniš, J. M. Vuksanović, M. Lj. Kijevčanin, S. P. Šerbanović, Z. P. Višak, *Fluid Phase Equilib*. **344** (2013) 6
3. D. M. Bajić, J. Jovanović, E. M. Živković, Z. P. Višak, S. P. Šerbanović, M. Lj. Kijevčanin, *Fluid Phase Equilib.* **338** (2013) 282
4. M. Lj. Kijevčanin, E. M. Živković, B. D. Đorđević, I. R. Radović, J. Jovanović, S. P. Šerbanović, *J. Chem. Thermodyn*. **56** (2013) 49
5. D. M. Bajić, G. R. Ivaniš, Z. P. Višak, E. M. Živković, S. P. Šerbanović, M. Lj. Kijevčanin, *J. Chem. Thermodyn*. **57** (2013) 510
6. M. Yasmin, M. Gupta, *Int. J. Thermodyn*. **15** (2012) 111
7. M. Yasmin, M. Gupta, J. P. Shukla, *J. Mol. Liquids* **164** (2011) 212
8. V. Sharma, M. Szymusiak, H. Shen, L. C. Nitsche, Y. Liu, *Langmuir* **28** (2012) 729
9. B. E. Poling, J. M. Prausnitz, J. P. O'Connell, *The Properties of Gases and Liquids*, 5th ed., McGraw-Hill, Singapore, 2007, p. A.20
10. A. Ž. Tasić, D. K. Grozdanić, B. D. Djordjević, S. P. Šerbanović, N. Radojković, *J. Chem. Eng. Data* **40** (1995) 586
11. C. Hou, Z. Jiang, B. Ren, *J. Chem. Eng. Data* **55** (2010) 4943
12. S. Urréjola, A. Sánchez, M. F. Hervello, *J. Chem. Eng. Data* **55** (2010) 482
13. M. A. Mutalib, K. Kurnia, *J. Chem. Eng. Data* **56** (2011) 79
14. J. Riddick, W. B. Bunger, *Techniques of chemistry Vol. II, Organic solvents: Physical Properties and Methods of Purification,* Wiley–Interscience, New York, 1970
15. Selected Values of Properties of Chemical Compounds, Data Project, loose-leaf data sheets, extant, TRC, Texas A&M University, College Station, TX, 1980
16. J. A. Riddick, W. B. Bunger, T. K. Sakano, *Organic Solvents. Physical Properties and Methods of Purification*, 4th ed., Wiley, New York, 1986
17. A. Rodríguez, J. Canosa, A. Domínguez, J. Tojo, *Fluid Phase Equilib*. **216** (2004) 167
18. J. Vijande, M. M. Piñeiro, J. García, J. L. Valencia, J. Legido, *J. Chem. Eng. Data* **51** (2006) 1778
19. L. Sarkar, M. N. Roy, *Phys. Chem. Liq*. **49** (2011) 219
20. J. L. Chevalier, P. Petrino, Y. Gaston-Bonhomme, *Chem. Eng. Sci*. **43** (1988) 1303
21. Y. Gaston-Bonhomme, P. Petrino, J. L. Chevalier, *Chem. Eng. Sci*. **49** (1994) 1799
22. K. Tochigi, K. Yoshino, V. K. Rattan, *Int. J. Thermophys*. **26** (2005) 413
23. D. W. Marquardt, *J. Soc. Ind. Appl. Math*. **11** (1963) 431
24. E. M. Živković, D. M. Bajić, S. P. Šerbanović, I. R. Radović, M. Lj. Kijevčanin, *Fluid Phase Equilib*. **373** (2014) 1
25. A. S. Teja, P. Rice, *Ind. Eng. Chem. Fundam*. **20** (1981) 77
26. A. S. Teja, P. Rice, *Chem. Eng. Sci*. **36** (1981) 7
27. R. A. McAllister, *AIChE J*. **6** (1960) 427
28. M. Lj. Kijevčanin, V. Z. Kostić, I. R. Radović, B. D. Djordjević, S. P. Šerbanović, *Chem. Ind. Chem. Eng. Q*. **14** (2008) 223
29. E. M. Živković, M. Lj. Kijevčanin, I. R. Radović, S. P. Šerbanović, B. D. Djordjević, *Fluid Phase Equilib*. **299** (2010) 191.

Journal of the Serbian Chemical Society
JSCS@tmf.bg.ac.rs • www.shd.org.rs/JSCS
J. Serb. Chem. Soc. 80 (7) S252–S258 (2015) *Supplementary material*

SUPPLEMENTARY MATERIAL TO

Experimental study of the thermodynamic and transport properties of binary mixtures of poly(ethylene glycol) diacrylate and alcohols at different temperatures

JELENA M. VUKSANOVIĆ, IVONA R. RADOVIĆ*, SLOBODAN P. ŠERBANOVIĆ and MIRJANA LJ. KIJEVČANIN

Faculty of Technology and Metallurgy, University of Belgrade, Karnegijeva 4, 11120 Belgrade, Serbia

J. Serb. Chem. Soc. 80 (7) (2015) 933–946

TABLE S-I. Experimental data of densities, ρ, viscosities, η, and refractive indices, n_D, of PEGDA + alcohol binary mixtures in the temperature range 288.15 to 323.15 K and at atmospheric pressure; standard uncertainties, σ, for each variables are $\sigma(T) = 0.01$ K; $\sigma(p) = 5$ %; $\sigma(x_1) = \pm 1\times10^{-4}$, and the combined uncertainties, σ_c, are $\sigma_c(\rho) = \pm 1\times10^{-2}$ kg m^{-3}; $\sigma_c(n_D) = \pm 1\times10^{-4}$; $\sigma_{c(}\eta) = 0.35$ %, at the 0.95 level of confidence ($k \approx 2$)

x_1	ρ / 10^3 kg m^{-3}	η / mPa s	n_D	x_1	ρ / 10^3 kg m^{-3}	η / mPa s	n_D
PEGDA (1) + ethanol (2)							
T=288.15 K							
0.0000	0.793813	1.3056	1.36397	0.5001	1.106579	87.166	1.46472
0.0513	0.926776	5.8557	1.40385	0.6010	1.112252	106.30	1.46611
0.1000	0.983459	10.549	1.41928	0.7000	1.115287	123.85	1.46785
0.2000	1.045931	26.970	1.44576	0.8047	1.120624	141.33	1.46973
0.3000	1.076323	46.252	1.45522	0.9000	1.123135	156.85	1.47038
0.3987	1.096773	66.690	1.46170	1.0000	1.126811	173.59	1.47212
T=293.15 K							
0.0000	0.789547	1.1885	1.36193	0.5001	1.102063	66.525	1.46273
0.0513	0.922428	5.0933	1.40241	0.6010	1.104806	80.078	1.46414
0.1000	0.979024	8.9407	1.41755	0.7000	1.110772	92.609	1.46586
0.2000	1.041435	21.752	1.44371	0.8047	1.116127	104.99	1.46777
0.3000	1.071807	36.608	1.45316	0.9000	1.118635	115.54	1.46841
0.3987	1.092253	51.720	1.45971	1.0000	1.122337	127.08	1.47012
T=298.15 K							
0.0000	0.785257	1.0838	1.35999	0.5001	1.097558	51.880	1.46079
0.0513	0.918001	4.5238	1.40010	0.6010	1.100298	61.948	1.46218
0.1000	0.974586	7.6692	1.41581	0.7000	1.106269	71.074	1.46390
0.2000	1.036939	18.299	1.44168	0.8047	1.111629	79.932	1.46582

* Corresponding author. E-mail: ivonag@tmf.bg.ac.rs

TABLE S-I. Continued

x_1	ρ / 10^3 kg m^{-3}	η / mPa s	n_D	x_1	ρ / 10^3 kg m^{-3}	η / mPa s	n_D
PEGDA (1) + ethanol (2)							
T=298.15 K							
0.3000	1.067296	29.548	1.45114	0.9000	1.114147	87.385	1.46646
0.3987	1.087741	40.997	1.45774	1.0000	1.117853	95.723	1.46814
T=303.15 K							
0.0000	0.780942	0.98999	1.35789	0.5001	1.093060	41.531	1.45886
0.0513	0.913586	3.9406	1.39785	0.6010	1.095805	49.098	1.46024
0.1000	0.970141	6.6501	1.41351	0.7000	1.101780	55.811	1.46198
0.2000	1.032449	15.069	1.43963	0.8047	1.107149	62.283	1.46390
0.3000	1.062797	24.263	1.44913	0.9000	1.109663	67.850	1.46454
0.3987	1.083240	33.127	1.45579	1.0000	1.113381	73.921	1.46618
T=308.15 K							
0.0000	0.776592	0.90491	1.35581	0.5001	1.088575	33.790	1.45697
0.0513	0.909154	3.5103	1.39558	0.6010	1.091325	39.595	1.45834
0.1000	0.965685	5.8188	1.41166	0.7000	1.097304	44.693	1.46007
0.2000	1.027959	12.895	1.43761	0.8047	1.102683	49.630	1.46198
0.3000	1.058302	20.223	1.44719	0.9000	1.105191	53.833	1.46263
0.3987	1.078750	27.218	1.45385	1.0000	1.108930	58.351	1.46424
T=313.15 K							
0.0000	0.772202	0.82807	1.35359	0.5001	1.084103	27.893	1.45506
0.0513	0.904645	3.1239	1.39380	0.6010	1.086860	32.496	1.45645
0.1000	0.961219	5.1336	1.40966	0.7000	1.092842	36.521	1.45818
0.2000	1.023472	11.052	1.43564	0.8047	1.098227	40.430	1.46005
0.3000	1.053814	17.079	1.44527	0.9000	1.100743	43.452	1.46070
0.3987	1.074270	22.701	1.45188	1.0000	1.104486	46.952	1.46228
T=318.15 K							
0.0000	0.767765	0.75816	1.35137	0.5001	1.079643	23.316	1.45311
0.0513	0.900167	2.8255	1.39126	0.6010	1.082406	27.038	1.45452
0.1000	0.956736	4.5616	1.40763	0.7000	1.088392	30.252	1.45625
0.2000	1.018982	9.7554	1.43364	0.8047	1.093790	33.272	1.45810
0.3000	1.049334	14.592	1.44332	0.9000	1.096306	35.627	1.45875
0.3987	1.069794	19.179	1.44992	1.0000	1.100066	38.428	1.46031
T=323.15 K							
0.0000	0.763276	0.69427	1.34857	0.5001	1.075189	19.865	1.45115
0.0513	0.895623	2.5022	1.38954	0.6010	1.077900	22.948	1.45255
0.1000	0.952239	4.0812	1.40565	0.7000	1.083956	25.534	1.45430
0.2000	1.014492	8.3221	1.43175	0.8047	1.089367	28.002	1.45616
0.3000	1.044856	12.573	1.44141	0.9000	1.091885	29.940	1.45679
0.3987	1.065333	16.414	1.44798	1.0000	1.095664	32.136	1.45839
PEGDA (1) + 1-propanol (2)							
T=288.15 K							
0.0000	0.807931	2.4573	1.38736	0.4997	1.094608	83.644	1.46362
0.0508	0.910173	6.8564	1.41324	0.5994	1.106090	103.07	1.46616

TABLE S-I. Continued

x_1	ρ / 10^3 kg m^{-3}	η / mPa s	n_D	x_1	ρ / 10^3 kg m^{-3}	η / mPa s	n_D
PEGDA (1) + 1-propanol (2)							
T=288.15 K							
0.1001	0.966543	11.958	1.42624	0.7004	1.113163	122.69	1.46781
0.1999	1.026686	26.654	1.44562	0.7993	1.118460	140.20	1.46984
0.2999	1.060564	43.501	1.45426	0.8997	1.123611	156.67	1.47074
0.3999	1.081882	63.061	1.45967	1.0000	1.126811	173.59	1.47212
T=293.15 K							
0.0000	0.803946	2.1677	1.38537	0.4997	1.090116	63.947	1.46154
0.0508	0.905986	5.8703	1.41132	0.5994	1.101596	77.818	1.46416
0.1001	0.962254	9.9488	1.42455	0.7004	1.108661	91.694	1.46580
0.1999	1.022280	21.508	1.44358	0.7993	1.113970	103.89	1.46780
0.2999	1.056101	34.414	1.45224	0.8997	1.119120	115.28	1.46872
0.3999	1.077403	48.937	1.45766	1.0000	1.122337	127.08	1.47012
T=298.15 K							
0.0000	0.799932	1.9222	1.38334	0.4997	1.085631	50.051	1.45958
0.0508	0.901723	5.1015	1.40923	0.5994	1.097111	60.253	1.46217
0.1001	0.957954	8.4345	1.42243	0.7004	1.104169	70.063	1.46383
0.1999	1.017874	17.773	1.44158	0.7993	1.109480	78.986	1.46578
0.2999	1.051646	27.756	1.45022	0.8997	1.114632	87.332	1.46674
0.3999	1.072926	38.983	1.45568	1.0000	1.117853	95.723	1.46814
T=303.15 K							
0.0000	0.795891	1.7158	1.38129	0.4997	1.081162	39.980	1.45755
0.0508	0.897515	4.4556	1.40636	0.5994	1.092633	47.665	1.46017
0.1001	0.953651	7.2395	1.41998	0.7004	1.099690	55.018	1.46183
0.1999	1.013476	14.846	1.43958	0.7993	1.105010	61.588	1.46379
0.2999	1.047200	22.769	1.44822	0.8997	1.110155	67.786	1.46478
0.3999	1.068469	31.451	1.45369	1.0000	1.113381	73.921	1.46618
T=308.15 K							
0.0000	0.791813	1.5385	1.37920	0.4997	1.076708	32.517	1.45552
0.0508	0.893236	3.9118	1.40526	0.5994	1.088171	38.441	1.45818
0.1001	0.949333	6.2755	1.41821	0.7004	1.095224	44.168	1.45985
0.1999	1.009075	12.540	1.43754	0.7993	1.100550	49.114	1.46180
0.2999	1.042761	18.960	1.44623	0.8997	1.105693	53.720	1.46280
0.3999	1.064015	25.848	1.45170	1.0000	1.108930	58.351	1.46424
T=313.15 K							
0.0000	0.787692	1.3883	1.37704	0.4997	1.072259	26.872	1.45352
0.0508	0.888949	3.4626	1.40145	0.5994	1.083716	31.531	1.45618
0.1001	0.945001	5.4866	1.41625	0.7004	1.090767	35.991	1.45787
0.1999	1.004673	10.738	1.43557	0.7993	1.096100	39.818	1.45981
0.2999	1.038323	15.999	1.44423	0.8997	1.101241	43.408	1.46083
0.3999	1.059571	21.579	1.44972	1.0000	1.104486	46.952	1.46228
T=318.15 K							
0.0000	0.783522	1.2614	1.37488	0.4997	1.067823	22.516	1.45152
0.0508	0.884636	3.0840	1.40099	0.5994	1.079281	26.251	1.45421
0.1001	0.940651	4.8338	1.41433	0.7004	1.086327	29.806	1.45590

TABLE S-I. Continued

x_1	ρ / 10^3 kg m^{-3}	η / mPa s	n_D	x_1	ρ / 10^3 kg m^{-3}	η / mPa s	n_D
			T=318.15 K				
0.1999	1.000264	9.2867	1.43345	0.7993	1.091670	32.821	1.45787
0.2999	1.033890	13.657	1.44221	0.8997	1.096809	35.637	1.45886
0.3999	1.055137	18.230	1.44773	1.0000	1.100066	38.428	1.46031
			PEGDA (1) + 1-propanol (2)				
			T=323.15 K				
0.0000	0.779300	1.1488	1.37278	0.4997	1.063402	19.229	1.44960
0.0508	0.880283	2.7763	1.39895	0.5994	1.074854	22.290	1.45230
0.1001	0.936280	4.3193	1.41215	0.7004	1.081897	25.165	1.45397
0.1999	0.995856	8.1572	1.43161	0.7993	1.087250	27.604	1.45593
0.2999	1.029459	11.865	1.44037	0.8997	1.092388	29.862	1.45695
0.3999	1.050706	15.672	1.44579	1.0000	1.095664	32.136	1.45839
			PEGDA (1) + 1-butanol (2)				
			T=288.15 K				
0.0000	0.814002	3.3696	1.40128	0.5001	1.089122	77.514	1.46339
0.0539	0.903840	7.4289	1.42152	0.5996	1.100203	97.184	1.46579
0.1001	0.951448	11.632	1.43202	0.6994	1.109189	116.70	1.46774
0.2001	1.013127	24.426	1.44631	0.7993	1.116370	136.23	1.46956
0.2998	1.052143	40.317	1.45495	0.8999	1.122425	155.26	1.47075
0.4004	1.071754	58.088	1.45951	1.0000	1.126811	173.59	1.47212
			T=293.15 K				
0.0000	0.810205	2.9321	1.39929	0.5001	1.084661	59.498	1.46135
0.0539	0.899778	6.3500	1.41946	0.5996	1.095730	73.674	1.46380
0.1001	0.947302	9.6960	1.42996	0.6994	1.104713	87.498	1.46574
0.2001	1.008822	19.843	1.44429	0.7993	1.111886	101.16	1.46756
0.2998	1.047757	31.996	1.45293	0.8999	1.117939	114.38	1.46875
0.4004	1.067325	45.291	1.45747	1.0000	1.122337	127.08	1.47012
			T=298.15 K				
0.0000	0.806384	2.5656	1.39725	0.5001	1.080219	46.442	1.45931
0.0539	0.895739	5.4714	1.41745	0.5996	1.091271	57.220	1.46181
0.1001	0.943150	8.1956	1.42805	0.6994	1.100243	67.356	1.46376
0.2001	1.004523	16.358	1.44230	0.7993	1.107405	77.233	1.46557
0.2998	1.043376	25.815	1.45090	0.8999	1.113458	86.707	1.46679
0.4004	1.062912	35.881	1.45545	1.0000	1.117853	95.723	1.46814
			T=303.15 K				
0.0000	0.802538	2.2518	1.39519	0.5001	1.075785	37.439	1.45727
0.0539	0.891646	4.7591	1.41549	0.5996	1.086830	45.133	1.45986
0.1001	0.938991	7.0189	1.42615	0.6994	1.095781	53.032	1.46183
0.2001	1.000228	13.723	1.44034	0.7993	1.102943	60.318	1.46360
0.2998	1.039005	21.259	1.44887	0.8999	1.108986	67.299	1.46484
0.4004	1.058505	29.260	1.45346	1.0000	1.113381	73.921	1.46618
			T=308.15 K				
0.0000	0.798659	1.9916	1.39313	0.5001	1.071366	30.535	1.45531
0.0539	0.887569	4.1658	1.41344	0.5996	1.082394	36.714	1.45794

TABLE S-I. Continued

x_1	ρ / 10^3 kg m^{-3}	η / mPa s	n_D	x_1	ρ / 10^3 kg m^{-3}	η / mPa s	n_D
PEGDA (1) + 1-butanol (2)							
T=303.15 K							
0.1001	0.934817	6.0799	1.42421	0.6994	1.091340	42.535	1.45994
0.2001	0.995932	11.646	1.43839	0.7993	1.098489	48.162	1.46164
0.2998	1.034639	17.787	1.44686	0.8999	1.104531	53.427	1.46292
0.4004	1.054110	24.131	1.45150	1.0000	1.108930	58.351	1.46424
T=313.15 K							
0.0000	0.794741	1.7672	1.39101	0.5001	1.066960	25.296	1.45332
0.0539	0.883452	3.6706	1.41141	0.5996	1.077973	30.180	1.45600
0.1001	0.930633	5.3106	1.42224	0.6994	1.086915	34.775	1.45805
0.2001	0.991636	9.9944	1.43639	0.7993	1.094056	39.138	1.45967
0.2998	1.030279	15.050	1.44486	0.8999	1.100089	43.191	1.46097
0.4004	1.049725	20.185	1.44956	1.0000	1.104486	46.952	1.46228
T=318.15 K							
0.0000	0.790780	1.5735	1.38890	0.5001	1.062560	21.251	1.45134
0.0539	0.879316	3.2526	1.40939	0.5996	1.073564	25.181	1.45404
0.1001	0.926432	4.6740	1.42023	0.6994	1.082498	28.828	1.45610
0.2001	0.987335	8.6592	1.43438	0.7993	1.089636	32.293	1.45771
0.2998	1.025922	12.883	1.44288	0.8999	1.095662	35.484	1.45900
0.4004	1.045348	17.097	1.44760	1.0000	1.100066	38.428	1.46031
T=323.15 K							
0.0000	0.786774	1.4177	1.38683	0.5001	1.058173	18.188	1.44940
0.0539	0.875197	2.9182	1.40739	0.5996	1.069171	21.403	1.45217
0.1001	0.922213	4.1743	1.41831	0.6994	1.078100	24.385	1.45423
0.2001	0.983035	7.6158	1.43251	0.7993	1.085230	27.144	1.45578
0.2998	1.021567	11.202	1.44095	0.8999	1.091254	29.678	1.45708
0.4004	1.040982	14.756	1.44572	1.0000	1.095664	32.136	1.45839

TABLE S-II. Fitting parameters and root-mean-square deviations (rmsd) σ of Eq. 1 for the PEGDA + alcohol binary mixtures at temperatures (288.15 to 323.15) K and at atmospheric pressure

Property	A_{00}	A_{01} / K^{-1}	A_{10}	A_{11} / K^{-1}	A_{20}	A_{21} / K^{-1}	σ
PEGDA (1) + ethanol (2)							
ρ / 10^3 kg m^{-3}	0.370515	–0.000778	–0.020648	–0.000024	0.073749	–0.000001	0.0023
n_D	0.48360	–0.00031	–0.01491	0.00002	0.18838	–0.00030	0.0016
PEGDA (1) + 1-propanol (2)							
ρ / 10^3 kg m^{-3}	0.375663	–0.000765	–0.028148	–0.000038	0.098665	0.000026	0.0006
n_D	0.47056	–0.00026	–0.00713	–0.00001	0.12950	0.00001	0.0007
PEGDA (1) + 1-butanol (2)							
ρ / 10^3 kg m^{-3}	0.388889	–0.000780	–0.042574	–0.000027	0.135574	0.000002	0.0008
n_D	0.47126	–0.00027	–0.00867	0.00000	0.17556	–0.00005	0.0002

TABLE S-III. Fitting parameters and root-mean-square deviations (rmsd) σ of Eqs. 2 and 3 for the PEGDA + alcohol binary mixtures at temperatures (288.15 to 323.15) K and at atmospheric pressure

Property	T / K	B_0	B_1	B_2	B_3	σ
			PEGDA (1) + ethanol (2)			
η / mPa s	288.15	–0.64267	118.80	158.92	–105.14	1.4619
	293.15	–0.31062	100.60	96.008	–70.420	1.0931
	298.15	–0.07072	86.966	52.898	–44.968	0.8104
	303.15	0.05082	74.390	29.523	–30.759	0.6683
	308.15	0.16603	64.579	12.939	–19.859	0.5122
	313.15	0.25578	55.716	4.4642	–13.902	0.3930
	318.15	0.30445	49.361	–3.8550	–7.7126	0.3054
	323.15	0.32762	42.666	–5.0895	–6.0363	0.2528
			PEGDA (1) + 1-propanol (2)			
η / mPa s	288.15	1.6415	92.930	197.51	–119.60	0.7883
	293.15	1.4509	80.832	125.50	–81.588	0.6454
	298.15	1.2877	71.334	76.395	–53.944	0.5262
	303.15	1.2081	61.561	48.481	–37.827	0.4125
	308.15	1.1356	53.139	31.148	–27.473	0.3246
	313.15	1.0551	46.504	18.475	–19.395	0.2627
	318.15	0.98725	40.787	10.293	–13.894	0.2144
	323.15	0.91941	36.353	4.4007	–9.7536	0.1796
			PEGDA (1) + 1-butanol (2)			
η / mPa s	288.15	2.8354	74.864	197.69	–102.30	0.4282
	293.15	2.4309	65.883	130.57	–72.254	0.3856
	298.15	2.1826	56.316	90.060	–53.174	0.2883
	303.15	1.8880	50.197	58.993	–37.427	0.2595
	308.15	1.6853	43.916	40.558	–28.029	0.2149
	313.15	1.5151	38.557	27.738	–21.034	0.1731
	318.15	1.3601	34.166	18.396	–15.637	0.1455
	323.15	1.2259	30.820	11.304	–11.366	0.1351

Property	x_1	C_0	C_1	σ
		PEGDA (1) + ethanol (2)		
ln (η / mPa s)	0.0000	–5.5483	1677.4	0.0042
	0.0513	–6.0329	2246.8	0.0050
	0.1000	–6.4100	2521.1	0.0097
	0.2000	–7.4548	3089.9	0.0159
	0.3000	–8.1825	3453.8	0.0177
Property	x_1	C_0	C_1	σ
		PEGDA (1) + ethanol (2)		
	0.3987	–8.7488	3720.9	0.0209
	0.5001	–9.1953	3925.5	0.0233
	0.6010	–9.5023	4070.0	0.0257
	0.7000	–9.7806	4193.9	0.0268
	0.8047	–10.022	4301.2	0.0280
	0.9000	–10.269	4402.0	0.0287

TABLE S-III. Continued

Property	x_1	C_0	C_1	σ
		PEGDA (1) + ethanol (2)		
	1.0000	–10.446	4481.6	0.0294
		PEGDA (1) + 1-propanol (2)		
ln (η / mPa s)	0.0000	–6.1308	2023.7	0.0045
	0.0508	–6.4396	2407.0	0.0068
	0.1001	–6.9256	2704.0	0.0130
	0.1999	–7.6696	3148.1	0.0160
	0.2999	–8.2524	3455.9	0.0191
	0.3999	–8.7353	3701.1	0.0210
	0.4997	–9.1750	3907.9	0.0236
	0.5994	–9.5310	4069.8	0.0254
	0.7004	–9.8371	4207.2	0.0275
	0.7993	–10.085	4316.6	0.0282
	0.8997	–10.271	4401.9	0.0285
	1.0000	–10.446	4481.6	0.0294
		PEGDA (1) + 1-butanol (2)		
ln (η / mPa s)	0.0000	–6.8094	2311.3	0.0028
	0.0539	–6.6488	2490.7	0.0068
	0.1001	–7.0270	2725.6	0.0130
	0.2001	–7.5850	3098.9	0.0157
	0.2998	–8.1438	3402.5	0.0193
	0.4004	–8.6100	3640.9	0.0217
	0.5001	–9.0514	3850.2	0.0238
	0.5996	–9.4165	4019.9	0.0255
	0.6994	–9.7206	4159.8	0.0261
	0.7993	–9.9938	4282.4	0.0273
	0.8999	–10.243	4391.6	0.0281
	1.0000	–10.446	4481.6	0.0294

Journal of the Serbian Chemical Society
JSCS-info@shd.org.rs • www.shd.org.rs/JSCS
J. Serb. Chem. Soc. 80 (7) 947–957 (2015)
JSCS–4771
UDC 546.722+66.094.3+544.4:628.112
Original scientific paper

The effect of iron oxidation in the groundwater of the alluvial aquifer of the Velika Morava River, Serbia, on the clogging of water supply wells

BRANKICA MAJKIĆ-DURSUN*, ANĐELKA PETKOVIĆ and MILAN DIMKIĆ

Jaroslav Černi Institute for the Development of Water Resources, Jaroslava Černog 80, Belgrade, Serbia

(Received 4 February, revised 27 June, accepted 3 September 2014)

Abstract: The oxidation of iron(II) dissolved in groundwater and subsequent precipitation of the oxidation products on the screens and discharge pipes of water wells that tap shallow alluvial aquifers leads to the formation of well encrustations. The main goal of the presented research was to determine the reasons for the rapid clogging of water supply wells. In the particular case of the alluvial aquifer of the Velika Morava River, Serbia, the encrustations include mostly iron-(hydr)oxides (62.6 to 76.2 wt. %). Groundwater over-exploitation leads to the mixing of different geochemical zones and the formation of a redox front. During the two-year survey, the concentrations of the dissolved oxygen in the groundwater varied over a wide range from 0.1 to 7.1 mg L^{-1} as the result of unsuitable exploitation regime. The on site measured groundwater temperature, concentrations of dissolved oxygen and pH values, and the laboratory analysis of dissolved iron concentrations showed that iron precipitation was favorable under groundwater over-exploitation conditions.

Keywords: iron encrustations; groundwater over-exploitations; Trnovče; redox front formation.

INTRODUCTION

The rapid formation of encrustations inside the wells of the water supply source Trnovče in Serbia necessitated detailed research of the clogging process. Decreasing groundwater levels and well discharges indicated over-exploitation conditions at this groundwater source. Over-exploitation could be defined as the situation in which the average rate of aquifer abstraction is greater than, or close to, the average recharge rate. Over-exploitation implies intensive use of groundwater, resulting in declining groundwater levels in the wells and over an extended area of the source, changes in the hydraulic gradients and aquifer recharge regime, reduced discharges of natural springs and variations in the oxic

* Corresponding author. E-mail: brankica.majkic@jcerni.co.rs
doi: 10.2298/JSC140204089M

state and groundwater quality, which usually deteriorates due to groundwater inflow from the upland. Case studies of rapid well clogging under over-exploitation conditions were presented in the USA,[1] Germany[2] and France.[3] An unsuitable pumping scheme produces a general decline in the groundwater levels and disturbs the geochemical conditions of the initial system.[3] Under such conditions, anoxic groundwater become oxidized, while the groundwater composition and microbial ecology are changed.[3,4]

Based on the chemical analyses of the groundwater samples, a study of data derived from microbiological analyses and assessments of the data on the static and dynamic groundwater levels inside the wells, the Trnovče source was characterized as an alluvial setting where oxic and anoxic ground waters blend.[5,6] High concentrations of dissolved oxygen in the upper, water unsaturated part, of the aquifer and the inflow of anoxic groundwater featuring elevated iron concentrations from deeper, saturated parts of the aquifer have created a redox front within the well screens (Fig. 1), leading to a thorough precipitation of iron-(hydr)oxides.[6] The conditions that lead to the formation of ferric deposits in water wells were analyzed in this study. Hydrochemical data were collected during a two-year survey (2010–2011), while the discharge data were analyzed for the last ten years.

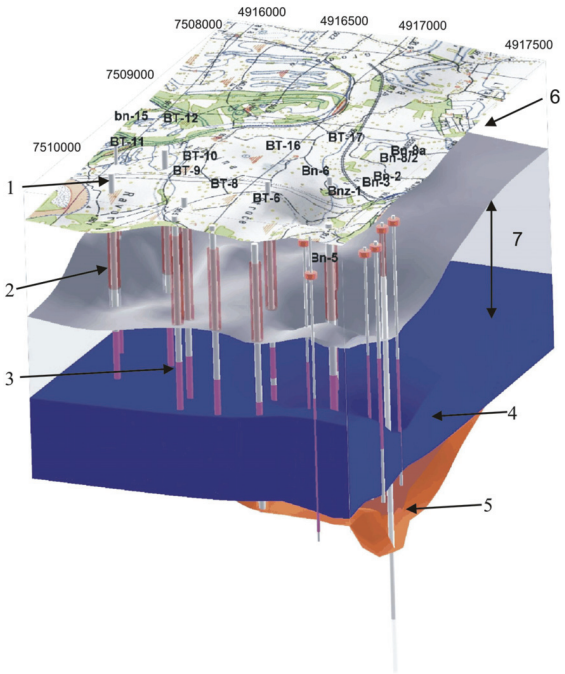

Fig. 1. 3D representation of groundwater levels in the wells and piezometers at the water supply source of Trnovče on 1 September 2011,[5] modified. Legend: 1 – Zero elevation of the well, 2 – well construction, 3 – well screens above the saturation zone, 4 – water saturated part of the aquifer, the thickness of which varies during the year, 5 – aquifer floor consisting of Neogene clays, 6 – semi-pervious overlying stratum, 3–6 m thick, 7 – zone of blending of oxic and anoxic ground waters.

Applin and Zhao[1] were the first to describe chemical clogging of production wells with iron compounds. The chemical oxidation of ferrous to ferric ions by oxygen and subsequent precipitation is a complex process. The oxidation of dissolved Fe(II) from the groundwater to Fe(III) tends to be gradual.[7,8] The overall process involves a variety of partially oxidized low-crystalline Fe(II)–Fe(III) intermediate species in aqueous solution. These Fe-intermediates could recrystallize into a variety of stable iron (hydr)oxide end-products (such as goethite) during time.[9]

The iron oxidation in the presence of dissolved oxygen is expressed as:

$$Fe^{2+} + O_2 + 2H^+ \leftrightarrows Fe^{3+} + 2OH^- \quad (1)$$

The produced Fe^{3+} is immediately hydrolyzed:

$$Fe^{3+} + 3H_2O \leftrightarrows Fe(OH)_3 + 3H^+ \quad (2)$$

The overall reaction that describes formation of insoluble iron encrustations[2,3,8] is given as:

$$4Fe^{2+} + O_2 + 10H_2O \leftrightarrows 4Fe(OH)_{3(s)} + 8H^+ \quad (3)$$

As a result, encrustations appear on the well screen, in the near-well region and, in extreme cases, in the discharge pipes, pumps and equipment installed inside the well (Fig. 2).

Fig. 2. Encrustations in a discharge pipe of Well Bn-6 at the water supply source of Trnovče (picture taken on 1 Sep, 2011).

The rate law of Fe(II) oxidation for mildly acid to neutral waters (pH value 6 to 8) was found to be first-order with respect to the concentrations of both Fe(II) and O_2 and second-order with respect to the OH^-:[7–12]

$$-d[Fe]/dt = k[Fe^{2+}]p(O_2)[OH^-]^2 \quad (4)$$

The reaction is rather fast. At pH less than 4, iron as Fe(II) dominates and the oxidation rate is dependent on the pH value.[9] In addition, studies showed that ferrous oxidation is not dependent on pH if the value exceeds 8.[9,10]

Many researchers[7,8] showed that the formed iron-(hydr)oxides have a catalytic effect on the oxidation of dissolved iron. Tamura *et al.*[7] established an

expanded rate law that includes both Eq. (4) and a heterogeneous reaction at the solid iron-(hydr)oxides surface:

$$r = k_1[Fe^{2+}][O_{2(aq.)}][H^+]^{-2} + k_2[Fe(III)][Fe^{2+}][O_2][H^+]^{-2} \quad (5)$$

In Eq. (5), k_1 is the rate constant for iron oxidation and k_2 represents the product of the equilibrium constant, K_{ads}, for the adsorption of ferrous iron onto ferric oxide and the rate constant, k_s, of the oxidation at the surface of the already formed precipitates.[2,3] Earlier research mentioned that this auto-catalytic effect gains measurable influence only if the initial concentration of Fe(II) is above 3 mg L^{-1}.[7] Houben presented that only newly formed precipitates that coat older precipitates could act as catalyst and states that the catalysis is more a function of the amount of available surface sites than of the total concentration of ferric iron.[8] For understanding the process of well clogging, it is also important to consider that low-crystallinity iron-(hydr)oxides, such as ferryhydrite, are more reactive than thermodynamically more stable iron oxides, such as goethite.

The abiotic oxidation presented by the rate law (5) is insufficient to explain the rapid well clogging, which is often observed. In iron-deposits, large numbers of different bacteria are often found that are able to use iron for their metabolic activity. In the presence of low amounts of dissolved oxygen (0.1–1.0 mg L^{-1}), dissolved iron can cause substantial bacteria growth, particularly iron-oxidizing bacteria such as the stalked *Gallionella* and sheathed *Leptothrix*.[6,13–15] It is believed that these bacteria accelerate iron oxidation.[13,16]

EXPERIMENTAL

The *in situ* groundwater tests included the determination of the physicochemical parameters: redox potential, E_H, groundwater temperature, concentration of dissolved oxygen, mg L^{-1}, the conductance, μS cm^{-1}, and pH value of the groundwater. The measurements were conducted using a multi-parameter probe (SEBA multiparameter Dipper KLL-Q, SEBA Hydrometrie, Germany), with the following electrodes: OPP-polymer for the redox potential and SEBA Oxysens II for oxygen. The multi-parameter probe was equipped with an automated groundwater level sensor that enabled sampling from the same depth in each campaign, and allowed data to be collected from various water column depths, in case of depth profile analyses.

The total iron concentration was determined from an acidic solution[17] using ICP-OES (ICP Spectro Genesis EOP II, Spectro Analytical Instruments, Germany). Fe(II) was analyzed in samples filtered on site (0.45 μm) and preserved with HCl.[17] Well discharge data were collected from individual flow meters, to monitor capacity decline over time. Groundwater levels were measured with a level-meter (SEBA level-meter KLL-T, SEBA Hydrometrie, Germany).

The aggressiveness of iron-related bacteria (IRB) was analyzed using the commercial BART test (IRB BARTs, Draycon Bioconcept Inc.). The IRB aggressiveness in water samples was used to estimate the activity level of the bacteria rather than the number of cells (population commonly presented as colony forming units per ml). The IRB aggressiveness was obtained from the relationship between the time lag (expressed in days) and the first

reaction in the IRB-BART™ tests. The bacteria that may be detected by this test include iron oxidizing and reducing bacteria, the sheathed iron bacteria, *Gallionella*, *Pseudomonas* and enteric bacteria.

Chemical analysis on the encrustations were performed using an INCA energy-dispersion X-ray analysis (EDS) instrument, model JEOL JSM-6610LV, USA. The samples were placed in sterile jars and immediately refrigerated to prevent oxidation after sampling. The samples were dried at a temperature of 60 or 37 °C, if the samples contained manganese.[2,6] For analytical purposes, the samples were ground into powder in an agate mortar. The powdered samples were sputter-coated with 24-carat gold. The detection limits of the applied EDS measurements were 0.2 wt. %.

X-Ray powder diffraction (XRPD) analysis of the sample from well Bn-5 was conducted using a Philips PW-1710 automated diffractometer (equipped with a diffracted beam curved graphite monochromator and an Xe-filled proportional counter), including a Cu-tube operated at 40 kV and 30 mA.

RESULTS AND DISCUSSION

The rate of precipitation of low-crystallinity iron-(hydr)oxides under natural conditions also depends on the groundwater retention time in the well, well pump operation and the groundwater abstraction regime. Apart from the above, the rate of formation of well deposits is affected to a considerable extent by previous well regenerations and the state of "cleanliness" of the near-well region and the well screen. If regeneration was only a short-term, with poor removal of deposited iron-(hydr)oxides, precipitation will be more intensive. The *in situ* measured parameters are given in Table I.

TABLE I. Hydrochemical parameters from the Trnovče water supply source

Well	Sampling date	t °C	pH	$[O_{2(aq.)}]$ mg L^{-1}	$[Fe^{2+}]$ mg L^{-1}	EC µS cm^{-1}	E_H mV
Bnz-1	3/2/2010	13.2	7.1	0.3	1.53	857	163
Bnz-1	24/5/2010	13.1	7.2	1	1.16	814	181
Bnz-1	9/11/2010	13.0	7.1	0.5	1.45	838	156
Bnz-1	13/5/2011	13.2	7.1	0.6	1.13	862	155
Bnz-1	1/9/2011	13.4	7.1	0.4	2.32	863	110
Bn-5	3/2/2010	11.9	7.1	0.8	0.30	532	262
Bn-5	24/5/2010	11.8	7.2	0.1	0.25	620	246
Bn-5	13/5/2011	11.9	7.1	1.2	0.21	619	212
Bn-5	1/9/2011	14.6	7.2	7.1	0.32	672	249
Bn-6	3/2/2010	12.6	7.1	2.3	1.53	623	236
Bn-6	24/5/2010	12.4	7.1	0.8	1.20	635	233
Bn-6	9/11/2010	12.5	7.1	0.5	3.40	644	138
Bn-6	13/5/2011	12.8	7.0	0.8	1.44	645	148
Bn-6	7/11/2011	12.7	7.2	0.1	2.12	541	78
Bn-9G	1/9/2011	12.3	7.1	1.1	0.49	695	280
Bn-9G	7/11/2011	11.9	6.9	7.9	0.82	688	188

The main question is whether the parameter values given in Table I are favorable for the considerable well clogging shown in Fig. 2.

The groundwater at the Trnovče water supply source has pH values between 6.9 and 7.2 (Table I). For roughly neutral groundwater, as in the presented case study, iron oxidation is strongly pH dependent. It also means that small variation in pH values could change the amount of mass converted from ferrous to ferric iron during time. These conditions favor the rapid formation of iron-(hydr)oxide.

On the other hand, the oxidation rate shows a linear dependence on O_2, Eq. (5).[7,10,18] During the two-year survey, the concentrations of dissolved oxygen in the groundwater varied over a wide range (Table I). Generally, as river waters flow into the aquifer, removal of O_2 may occur through oxidation of organic matter or adjacent sediments. There are several reasons for the large variations in O_2 content: the setting of submergible pumps into the screen slot, the declining of static and dynamic groundwater levels into the casing interval, an unsuitable pump work scheme and aquifer recharge mode. Research performed in France[3] showed that the well de-watering process induced important perturbations of the physical and chemical equilibria in the water within the aquifer around the well, which led to deposition of scale materials. An introduction of the piezometric heads into the screen slots (Fig. 1) leads to exposure of the groundwater to atmospheric conditions, resulting in an oxygen uptake (high values presented in Table I). The formation of mixed oxic–anoxic zone, caused by an unsuitable pump work scheme and groundwater abstraction regime, also favors the rapid clogging. Propagation of the clogging process in and around the well and the mixing of different geochemical zones are explained in following separate section.

The concentrations of dissolved oxygen are also important for iron-related bacteria. The results of IRB BART tests indicated that bacterial aggressiveness was high in 16 %, mediate in 36 % and low in 48 % of the samples. Low aggressiveness means that the bacterial population is too small (or that it has very low activity), whereas mediate indicates that there is either a moderately active or modest population of the targeted bacteria. High aggressiveness was shown only by the bacterial consortium sampled on the 1st of September 2011. The most important iron-oxidizing bacteria found in water samples and encrustations, were *Gallionella ferruginea*, *Lepthotrix* sp. and *Siderocapsaceae*. According to Roden *et al.*,[19] Fe(II)-oxidizing bacteria dwell in micro-aerobic environments of low oxygen concentrations (Table I, values less than 1 mg L^{-1}), but Vet *et al.*[16] concluded that *Gallionella* spp. can grow under neutral pH and aerated conditions when chemical iron oxidation is inhibited by low water temperature (about 13 °C) and suppression of auto-catalytic iron oxidation.

The concentration of iron in the groundwater is also important for the formation of encrustations. Usually, drinking water has a relatively small concentration of dissolved iron. In the case of the Trnovče water supply source, the aver-

age concentration of total iron was 1.79 mg L^{-1}, while the maximum value was 18.8 mg L^{-1} (Bnz-1, before the regeneration). The values of the dissolved iron concentrations are given in Table I. The concentrations of iron in the groundwater could vary over the year, depending on the mode of aquifer charging. During the summer or drought periods, the groundwater feeds the Velika Morava River.[20] Charging of the aquifer is slower and the groundwater comes from the upland. Generally, groundwater from deeper part of the aquifer is anoxic and iron is present as dissolved ferrous iron. In contact with dissolved oxygen, the Fe(II) is rapidly oxidized to Fe(III). Pham and White noticed that the rate at which Fe(II) is oxidized to Fe(III) is critical in determining the fate of iron and its bioavailability in many natural waters.[21] In the particular case of Trnovče, this means that bacteria have to compete with rapid chemical oxidation.

The values of the conductance were higher for the Bnz-1 well than for the other wells. Bnz-1 well is located in the hinterland while the other three wells are closer to the riverbed. The values of the redox potential also indicate the mixing of different geochemical zones.

XRPD analysis detected low-crystalline (hydr)oxides and kaolinite in the sample collected from the Bn-5 well (Fig. 3).

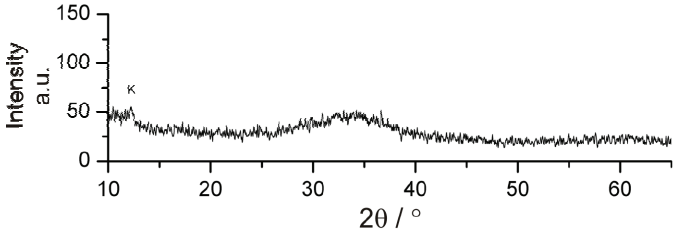

Fig. 3. XRPD pattern of encrustation from Bn-5 well.

Chemical analyses of the encrustations sampled from the water supply wells (Bn-5, Bnz-1, Bn-6 and Bn-9G) performed by EDS revealed the presence of iron and manganese (hydr)oxides. The proportion by weight of manganese (hydr)oxides in the well deposit samples ranged from 0.3 to 21.3 wt. %, while that of iron-(hydr)oxides was from 62.6 to 76.2 wt. %. In addition to these (hydr)oxides, there were also carbonates (5.4 wt. % on average), phosphates (4.3 to 7.2 wt. %) and silicate grains (clay and sand), drawn in from the alluvial matrix through the screen slots. The chemical oxidation of manganese is slower than that of iron. Compared to iron, the rate of manganese oxidation is at least 10^6 times slower in waters with a pH value close to neutral.[22] Chemical oxidation of manganese accelerates with increasing pH value (pH > 8).[22] The joint occurrence of low-crystallinity manganese and iron (hydr)oxides in the deposits of Trnovče wells can be explained by the microorganisms present in the environment.[14] It is well known that the iron-oxidizing bacteria *Leptothrix* sp. are also able to oxidize manganese(II).

Propagation of clogging around the Trnovče wells

Assessments of well clogging rates need to address the groundwater retention time in the near-well region (gravel pack). The Bn-5 well, which exhibited the poorest performance at Trnovče, was selected for detailed analysis. Its drilling diameter is 500 mm, the diameter of the screen 219 mm, and the screen length 7 m. In order to explain the iron hydr(oxide) precipitation process in and around the well screens, leading to screen slot clogging in shallow alluvial aquifers, four phases can be distinguished.[24] These phases illustrate the formation of ferric deposits and a discharge loss for the Bn-5 well.

In the first stage, prior to the development of the water supply source, the underground environment was undisturbed; the aquifer is sub-artesian and the groundwater was anoxic (Fig. 4).[24] In this stage, the concentration of dissolved O_2 was much lower than in stages of exploitation. Following the commissioning of the wells during the second stage, a cone of depression is formed and the front of the potential blending of traces of groundwater with different geochemical zones moved downwards. The initial capacity of the studied well was Q = 15 L s^{-1} (in 1999), lasting over a relatively short time, only until 2001. The third stage of the life cycle of the well began as early as 2002, when its capacity dropped to Q = 7 L s^{-1} (46 % of its initial capacity). In the period 2002–2008, the number of production wells at Trnovče increased to 18; the dynamic groundwater level reached the upper zone of the screen (Figs. 1 and 4), moving the redox front to the water-receiving part of the well. Iron-(hydr)oxides were deposited on the walls of the well screen and casing. As soon as iron-(hydr)oxides were present on the screen slots, the oxidation reaction accelerated and, besides homogeneous oxidation, heterogeneous oxidation also occurred.[3,8,23,24] The first regenerations at this site were conducted in 2004, combining mechanical cleaning with the chem-

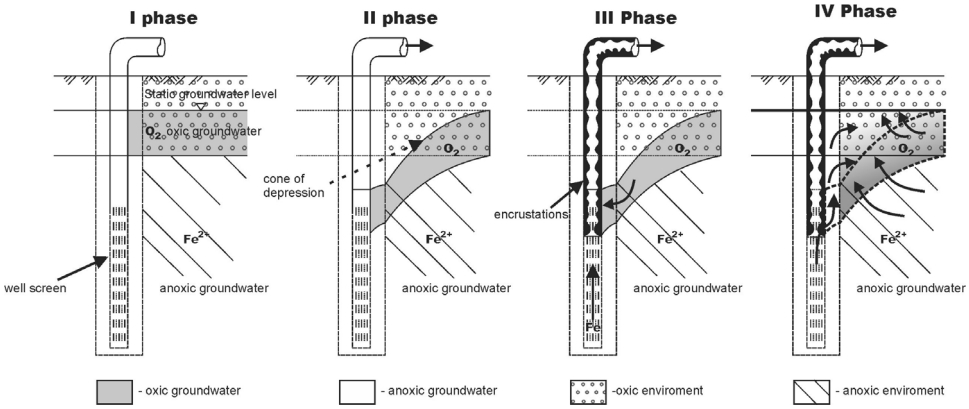

Fig. 4. Stages of well clogging due to blending of oxic and anoxic ground waters[24] with permission from IWA Publishing.

ical action of hydrochloric acid and citric acid as an inhibitor. This procedure increased the capacity of the well to Q = 12 L s^{-1} (Fig. 5). The next regeneration of water supplying Bn-5 well was undertaken in 2008, when the capacity of the well had dropped to 2 L s^{-1}. The same method was applied and the discharge was increased to 8 L s^{-1}.

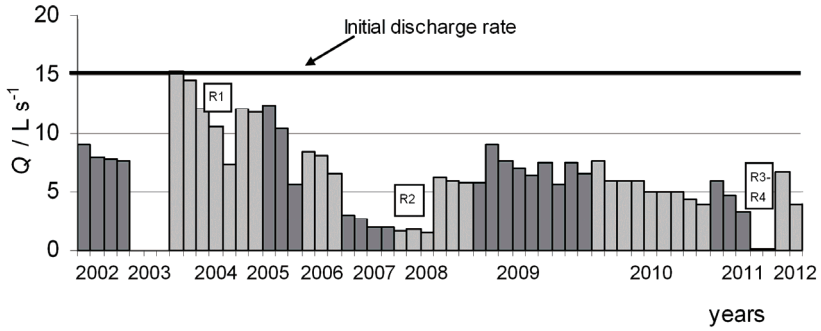

Fig. 5. Declining discharge of Well Bn-5 over 10 years of service.

At stage four, iron was precipitated in the well itself and over an extended area around the well. Insoluble (hydr)oxides were deposited on the grains of the pack in the near-well region, as well as further afield from the well, on alluvial sediment grains. In near-well region, coated grains were found in 2010 during drilling for piezometers near the wells Bnz-1, Bn-5 and Bn-6. Deposition of iron (hydr)oxide on sediment grains reduces porosity and change the entrance velocities in the screen slot. In connection with the problem of a general decline of the groundwater level over the wide area of the Trnovče source, the pumps were occasionally stopped. During the pumping stops (from several hours to more than one month), there was sufficient time for the iron species that remained within the column of water within the well to be oxidize and the screen and casing were encrusted.

This final stage of the life cycle of the well resulted in complete shutdown of the well.

CONCLUSIONS

The exploitation wells at the Trnovče water source are jeopardized by the clogging process. Variations in values of chemical parameters, such as the concentration of Fe(II), dissolved oxygen and redox potential, are the result of an unsuitable pumping scheme and general declining of the groundwater levels. As the groundwater level dropped to the screen zone, the redox front shifted to the water-receiving part of the well. Mixing of water containing oxygen with anoxic groundwater reaching Fe(II) led to mineral encrustations, especially iron (hydr)oxides.

At pH values around 7, as is the case of the Trnovče water source, the chemical oxidation of Fe(II) is strongly pH dependent. Small variations in the measured values could significantly change the oxidation rate. The conditions present in the groundwater are favorable for the rapid oxidation of dissolved iron. Iron-oxidizing bacteria could accelerate this process. The role of bacteria in clogging process depends on the availability of dissolved iron and the concentration of dissolved oxygen.

In alluvial aquifers, variable amounts of ions, catalysts, inhibitors, bacteria and minerals could be present simultaneously. The definition of an exact rate law for such a complex aquatic system is very difficult.

During the precipitation, newly formed precipitates coat older ones. Preliminary results showed high contents of low-crystalline iron and manganese (hydr)oxides inside the water supply wells. With time, if the regeneration methods were not proper, the early formed iron deposits will be re-crystallized into a variety of stable iron oxide end-products. This could be expected in the extended area around the well.

Due to the poor design of the well casings (small diameter and short tail-pipe), the pumps were housed inside the screen and this additionally accelerated precipitation. Iron oxidation did not occur solely inside the well; the process tended to extend into a much wider zone, beyond the well. Especially vulnerable is the well pack, but the process propagates further when there are considerable fluctuations of the groundwater level in the extended zone of the Trnovče water supply source. An adequate exploitation scheme could reduce these phenomena and extend the life of the wells.

Acknowledgment. The authors express their gratitude to the Ministry of Education, Science and Technological Development of the Republic of Serbia for financially supporting this work, Project No. TR37014.

ИЗВОД

ЕФЕКАТ ОКСИДАЦИЈЕ ГВОЖЂА У ПОДЗЕМНИМ ВОДАМА АЛУВИЈАЛНОГ АКВИФЕРА ВЕЛИКЕ МОРАВЕ НА КАПАЦИТЕТ БУНАРА ЗА ВОДОСНАБДЕВАЊЕ

БРАНКИЦА МАЈКИЋ-ДУРСУН, АНЂЕЛКА ПЕТКОВИЋ и МИЛАН ДИМКИЋ

Институт за водопривреду "Јарослав Черни", Јарослава Черног 80, 11226 Београд

Процес оксидације двовалентног гвожђа из подземне воде на филтрима и потисним цевоводима бунара који каптирају плитке алувијалне средине, доводи до формирања бунарских талога. Основни циљ овог истраживања био је утврђивање разлога брзог колмирања бунара за јавно водоснабдевање. У конкретном случају, талоге чине хидроксиди гвожђа (62,6 до 76,2 мас. %). Прекомерна експлоатација бунара доводи до мешања различитих геохемијских зона и формирања редокс фронта. Током две године истраживања, концентрација раствореног кисеоника у подземној води варирала је у широком опсегу од 0,1 до 7,1 mg L^{-1} као последица неодговарајућег експлоатационог режима. Теренска мерења температуре подземне воде, концентрације раствореног кисеоника, pH вредности, као и лабораторијске анализе раствореног гвожђа, показала су да измерене

вредности погодују таложењу гвожђа и формирању наслага, у условима прекомерне експлоатације подземних вода.

(Примљено 4. фебруара, ревидирано 27. јуна, прихваћено 3. септембра 2014)

REFERENCES

1. K. R. Applin, N. Zhao, *Groundwater* **27** (1989) 168
2. G. Houben, C. Treskatis, *Water Well Rehabilitation and Reconstruction*, McGraw-Hill, New York, 2007, p. 67
3. F. Larroque, M. Franceschi, *Environ. Earth Sci.* **64** (2010) 119
4. S. Smith, A. Comeskey, *Sustainable Wells: Maintenance, Problem Prevention and Rehabilitation*, CRC Press, Taylor and Francis Group, Boca Raton, FL, USA, 2010, p. 17
5. B. Majkić-Dursun, Lj. Popović, D. Miolski, O. Anđelković, *Vodoprivreda* **44** (2012) 181 (in Serbian)
6. B. Majkić, *PhD Thesis*, Faculty of Mining and Geology, Belgrade, 2013, p. 223 (in Serbian)
7. H. Tamura, K. Goto, M. Nagayama, *Corros. Sci*. **16** (1976) 197
8. G. Houben, *Groundwater* **42** (2004) 78
9. B. Morgan, O. Lahav, *Chemosphere* **68** (2007) 2080
10. W. Stumm, J. J. Morgan, *Aquatic chemistry: Chemical Equilibria and Rates in Natural Waters*, 3rd ed., Wiley, New York, USA, 1996, p. 686
11. N. El Azher, B. Gourich, C. Vial, M. Belhaj Soulami, M. Ziyad, *Chem. Eng. Process*. **47** (2008) 1877
12. J. N. Geroni, D. J. Sapsford, *App. Geochem*. **26** (2011) 1452
13. E. R. David, J. M. Stevenson, *Water Res.* **29** (1995) 365
14. V. Obradović, B. Majkić-Dursun, A. Petković, M. Dimkić, in *Proceedings of the 41st Annual Conference of the Serbian Water Pollution Control Society*, Divčibare, Serbia, 2012, p. 359 (in Serbian)
15. M. Dimkić, M. Pušić, V. Obradović, S. Kovačević, *Water Sci. Tech.* **65** (2012), 2206
16. W. W. J. M. de Vet, I. J. T. Dinkla, L. C. Rietveld, M. C. M. van Loosdrecht, *Water Res*. **45** (2011) 5389
17. *Standard Methods for the Examination of Water and Wastewater* – SMEWW, 3500-Fe B method, 21st ed., American Public Health Association, American Water Works Association and Water Environment Federation, Washington DC, 2005, pp. 3–77
18. H. Sugimori, Y. Kanzaki, K. Yokota, T. Murakami, *J. Miner. Petro. Sci.* **106** (2011) 142
19. E. E. Roden, D. Sobolev, B. Glazer, G. W. Luther, *Geomicrobiol. J.* **21** (2004) 379
20. M. Komatina, *The Hydrogeology of Šumadija*, Geological and Geophysical Research Institute, Belgrade, Serbia, 1976, p. 38 (in Serbian)
21. A. N. Pham, T. D. Whaite, *Geochim. Cosmochim. Acta* **72** (2008) 3616
22. S. T. Martin, in *Environmental Catalysis*, V. H. Grassian, Ed., Taylor and Francis Group, Boca Raton, FL, 2005, pp. 61–83
23. U. Park, B. A. Dempsey, *Environ. Sci. Technol.* **39** (2005) 6494
24. C. G. E. M. (KEES) van Beek, *Cause and prevention of clogging of wells abstracting groundwater from unconsolidated aquifers*, KWR Water Cycle Research Institute Series, IWA Publishing, London, UK, 2012, p. 115.

Journal of the Serbian Chemical Society
JSCS-info@shd.org.rs • www.shd.org.rs/JSCS
J. Serb. Chem. Soc. 80 (7) 959–969 (2015)
JSCS–4772
UDC Vol. 80::2015::85 Journal of the Serbian Chemical Society
Letter to the Editor

LETTER TO THE EDITOR

A survey on publishing policies of the Journal of the Serbian Chemical Society – On the occasion of the 80th volume

OLGICA NEDIĆ[1]*# and ALEKSANDAR DEKANSKI[2]#

[1]*Institute for the Application of Nuclear Energy (INEP), University of Belgrade, Serbia and* [2]*Institute of Chemistry, Technology and Metallurgy, Department of Electrochemistry, University of Belgrade, Serbia*

(Received 6 March, accepted 6 April 2015)

Abstract: Journal of the Serbian Chemical Society (JSCS) is the scientific journal of the Serbian Chemical Society and this year is celebrating 85 years of its publishing and the 80th volume. After so many years of publishing, the idea of the Editorial Board of the JSCS was to investigate the opinion of the authors, reviewers and Sub-Editors concerning the journal and whether their evaluation and suggestions could aid in its improvement. Questionnaires were sent to the three investigated groups as an e-mail link. The responses were analyzed and only the most general and the most important data are presented in this article. The grades, comments and suggestions showed that most of the contributors are satisfied with the present handling and publishing policy of the JSCS, but certain technical aspects should be improved. After a thorough inspection of the data, the Editorial Board decided to introduce a fully automatic on-line system, to speed-up the peer review process, to improve the Instructions to Authors and Reviewer's Report Form. All these novelties commenced from the beginning of March 2015.

Keywords: peer review; publishing; questionnaire; evaluation

INTRODUCTION

Evaluation of journals, especially the peer review process, has attracted great attention in the last decade. There are number of scientometric methods, mostly of the quantitative type, to express the "value" of the journal.[1–3] The best known is the one that measures journal's impact *via* the citation index. An intensive debate on the positive and negative aspects of the journal evaluation *via* the impact factor (IF) has been in progress for a long time, but officially the IF has been recognized as the measure of impact recognition and a tool for journal

* Corresponding author. E-mail: olgica@inep.co.rs
# Serbian Chemical Society member.
doi: 10.2298/JSC150306036N

ranking.[4] There are other ways to investigate the quality of a periodical and one of which is to determine the opinion of associates of the journal.

After so many years of publishing, the idea of the Editorial Board of the Journal of the Serbian Chemical Society (JSCS) was to investigate the opinion of authors, reviewers and Sub-Editors concerning the journal and to determine whether their evaluation and suggestions could help in the improvement of the quality of the journal and the managing process, and raise the prestige of the JSCS. Prior to this study, an educational article recommending how to write a good scientific paper was published.[5] Both scientific and technical aspect were discussed, as it is equally important to obtain significant research results and to know how to present them.

Journal of the Serbian Chemical Society, as its name says, is an official journal of the Society. The Society was founded in 1897 and its first bulletin appeared in 1899.[6,7] The Journal was first published in 1930 as the Journal of the Chemical Society of the Kingdom of Yugoslavia, the name was changed in 1947 to the Journal of the Chemical Society Belgrade and under the present name, it exists since 1985.[7] In this year, the 80th volume of the JSCS is being published. All papers are published only in English. There are 12 issues per volume, 10–13 articles per issue and 2000–2200 pages a year. The JSCS is an open access publication, without page charges and with on-line submission. It has been indexed in the Science Citation Index Expanded since 1995, in the category Chemistry: Multidisciplinary, and its last impact factor (IF 2014) is 0.871 (rank 114/157); 5-year IF is 1.009 (rank 105/157)*.

The journal is managed as a non-profit making periodical by the members of the Serbian Chemical Society (SCS), who work mostly voluntarily. It is supported by membership fees, various institutions of the University of Belgrade, the Ministry of Education, Science and Technological Development of Serbia and occasionally by sponsors. In the last five years, 2130 articles were submitted of which 872 were accepted. During this period, 7 authors complained about rejection of their papers, 33 withdrew their manuscripts after reviewing and 3 manuscripts were recognized as plagiarism.

A questionnaire is a widely recognized method to obtain relatively reliable data on the posed questions and it is used by many publishers. In contrast to the most publishers who interview the authors of accepted papers, it was decided to interview all contributors to the publishing process. It was felt that by examining the entire partnership network, a more reliable overview could be obtained. Moreover, potential authors, a category of researchers whose manuscripts were not accepted for publication, were also interviewed. In addition, a very important decision was made by the Editor-in-Chief to publish openly the results of the survey.

* Data announced June 2015.

Thus, three questionnaires adapted to suit the three investigated population groups were composed and sent as an e-mail link to all participants in the publishing activity of the journal in the last five years. There were cases when individuals performed two or even all three roles, so they received the appropriate number of questionnaires. The questions were composed to evaluate the publishing process in quantitative and qualitative ways, both at the level of peer review and managing, and the results obtained are presented accordingly.

METHOD AND APPROACH

Study population

There were three groups of persons involved in the study. In total, 2422 invitations were sent: 13 for Sub-Editors, 980 for reviewers and 1429 for authors. Certain number of invitations returned undelivered (80 for reviewers and 170 for authors). The inclusion criterion for the survey was at least one type of activity in relation to the JSCS over a five-year period (November 2009–October 2014).

Questionnaires

The three questionnaires contained some questions that were the same for all participants and others that were more specific, suitable for the role played by the surveyed persons (see Supplementary material to this Letter). The participants were asked for their academic title, research field, professional background, previous experience in the same kind of activity that was being investigated in the survey, before being asked direct questions about the JSCS. The survey contained two types of questions: those to be answered by scaling (from 5, excellent to 1, poor) and those to be answered by choosing offered responses (in some cases more than one response could be chosen). Finally, in the last section of the survey, the participants were given the opportunity to express their personal suggestions and remarks.

The surveys were sent time-shifted: the Sub-Editors first, the reviewers two weeks later and the authors a month later. Two weeks after the first invitation, a reminder was sent to those who had not responded. The reports were collected and analyzed. The results of the survey offered many more correlations and conclusions than presented in this paper, but in order not to overload the article, only the most general and the most important data are shown. Thus, the three surveyed populations were analyzed as entire entities.

Data analysis

Data on questions that were answered by scaling (5–1) are given as an average grade. Data on questions that could be answered by multiple responses were grouped as the frequency of each response and are reported as such (in % of the total number of questionnaires). Suggestions and remarks were grouped according to their similarity and are reported as lists.

RESULTS AND DISCUSSION

Twelve Sub-Editors responded to the survey (92 % of the interviewed), 309 reviewers (43 %) and 511 authors (41 %). Depending on the type of data, the analyzed results are presented graphically (in the case of frequency distributions), in tables (in the case of scaling) or in lists (suggestions and remarks). All surveys were analyzed separately and the results reported by the Sub-Editors are given in Fig. 1, Table I and Frame 1, for the reviewers in Fig. 2, Table II and Frame 2, and for the authors in Fig. 3, Table III and Frame 3.

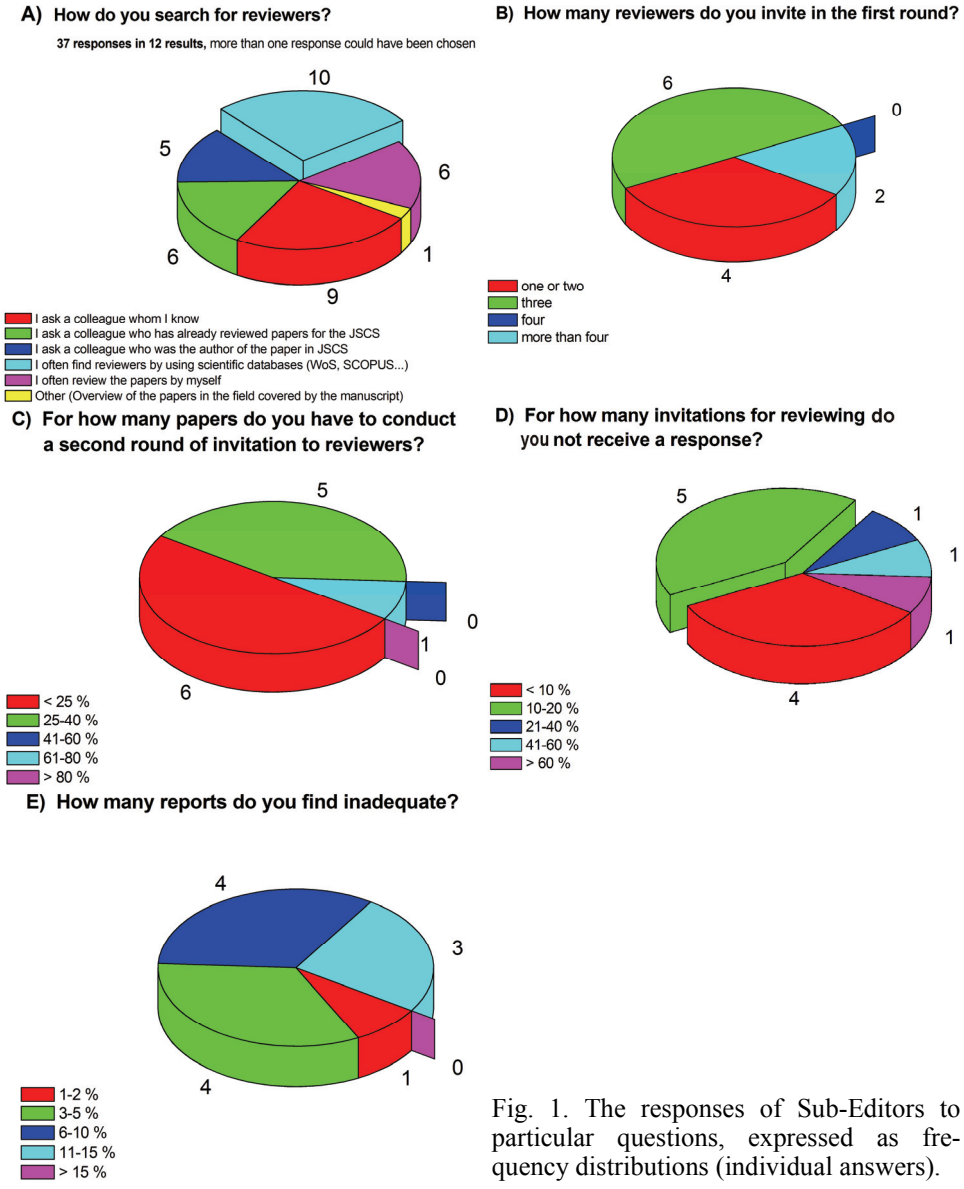

Fig. 1. The responses of Sub-Editors to particular questions, expressed as frequency distributions (individual answers).

TABLE I. Sub-Editors' responses to questions that were recorded by scaling

Question	Grade					Average grade
	5	4	3	2	1	
	Number of responses					
Comprehensiveness of the Instructions to Authors	4	6	2	0	0	4.2
Choice of the questions for reviewers in the form	2	7	3	0	0	3.9
Communication with the Editorial Office	9	2	1	0	0	4.7

FRAME 1. Sub-Editors' major suggestions and remarks grouped by topics

1. Introduction of fully automatic on-line system for submission and management of manuscripts
2. Improvement of the Instructions to Authors (considerable number of inappropriate figures)
3. High tendency of potential reviewers to refuse the invitation to review
4. Examination of manuscripts by use of software to detect plagiarism

Sub-Editors were first asked about the procedure they conduct while searching for reviewers and their general opinion on this process. They responded that they most often find reviewers by using scientific databases (WoS, Scopus,…) or by asking colleagues who they know (Fig. 1A). In the first round, some Sub-Editors invited only one or two reviewers, whereas others invited more, even more than four (Fig. 1B). The responses to this question illustrate the different individual approaches of the Sub-Editors to peer review. Six Sub-Editors conduct a second round of search for reviewers in the case of less than 25 % of the manuscripts, while another six reported a greater number of papers that could not be finalized after the first call (Fig. 1C). The number of unanswered calls for peer review is rather high (expressed as the percentage of the total number of calls in Fig. 1D). Sub-Editors found between 1 and 15 % of reviewers' reports inadequate (Fig. 1E), due to a complete absence of peer review ("publish as is" in contrast to other reports that suggested major revision or even rejection) or due to unprofessional conduct of reviewers (humiliating or malicious attitudes). As for the quality of the reports in terms of their usefulness to authors to improve the manuscripts, ten Sub-Editors evaluated the reports as mostly good, while two Sub-Editors stated that they receive the same number of good and poor reports. Responses to this question probably illustrate the different individual criteria of Sub-Editors. On the grading scale, Sub-Editors valued relatively highly the technical aspects of the publishing process (Table I), giving an overall average grade of 4.3. To improve the work of the JSCS, most Sub-Editors suggested a complete on-line submission and management system (Frame 1).

Reviewers who responded to the survey were from Serbia (43 % of the total number) and from other countries (57 %, Fig. 2A). Slightly more than half reviewers defined themselves as chemists (Fig. 2B) and approximately 70 % were experienced reviewers (Fig. 2C). Reviewers accept to review manuscripts for the JSCS for many reasons, but the predominant one is the professional ethics of an expert who feels that it is part of his scientific activity (Fig. 2D). Reviewers graded technical aspects of the peer review with an average grade of 4.0 (Table II). Most reviewers (58 %) either had no additional remarks or expressed an affirmative opinion in a free form of comments and the greatest number of suggestions were focused on the introduction of a complete on-line system that would enable easier submission and communication (Frame 2).

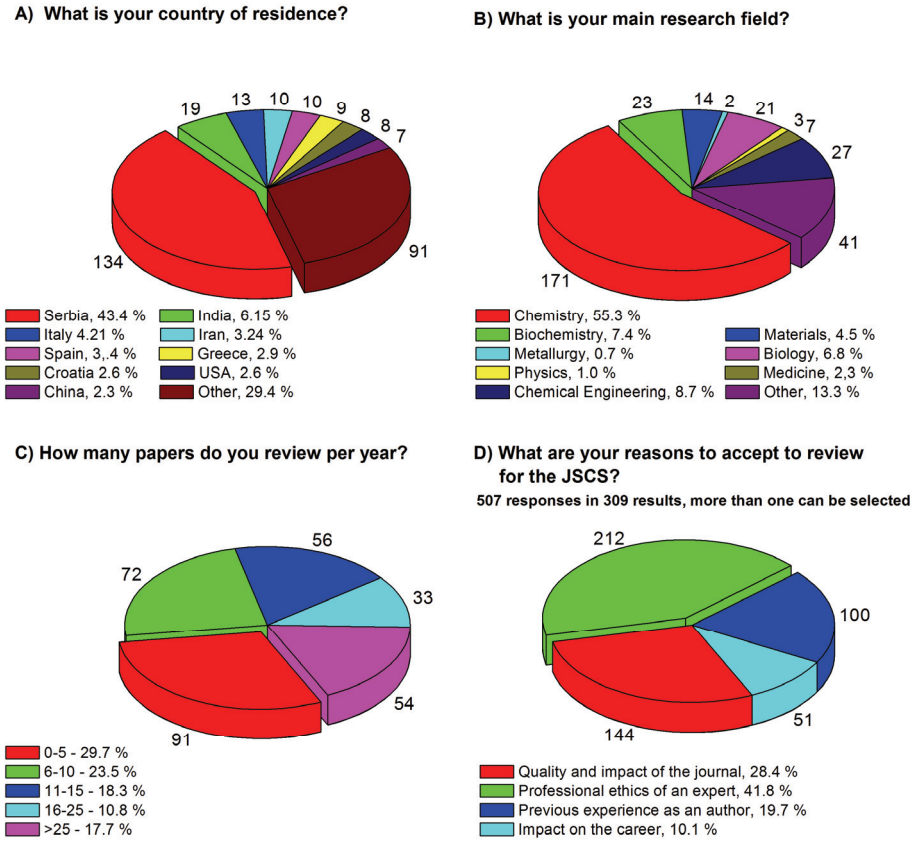

Fig. 2. Reviewers' responses to particular questions expressed as frequency distributions.

TABLE II. Reviewers' responses to questions that were recorded by scaling

Question	Grade					Average grade
	5	4	3	2	1	
	Share of the number of responses,%					
Comprehensiveness of the Reviewer's Report Form	20	57	23	1	0	4.0
Period given for reviewing	20	51	25	4	0	3.9
Communication with Sub-Editors and Editor	40	39	18	3	0	4.2

Authors who responded to the survey were from Serbia (30 % of the total number), as well as from the other countries (70 %, Fig. 3A). The affiliation of the authors illustrates the international character of the JSCS. The main research fields of the authors who submit papers to the JSCS were organic chemistry, analytical chemistry, biochemistry and biotechnology, environmental and inorganic chemistry (Fig. 3B). Early-stage researchers made up 31 % of all authors and the others were more experienced ones (Fig. 3C). The main reasons for sub-

FRAME 2. Reviewers' major suggestions and remarks grouped by topics (number of individual comments)

58 % of all comments were affirmative, +:		
1.	Introduction of fully automatic on-line system for submission and management of manuscripts	26
2.	Free access to Scopus or other databases for the reviewers	11
3.	Prolongation of the period for reviewing	8
4.	Improvement of the Instructions for Reviewers	7
5.	Information to reviewers on the final decision on the manuscript	5
6.	Introduction of scaling in the Reviewer's Report Form	4

mitting their manuscripts to the JSCS, authors report as: quality and the impact of the journal, no publishing fee, previous positive experience and the speed of reviewing (Fig. 3D). Grading of the technical parameters related to JSCS, including periods for reviewing and publishing, resulted in an average grade of 3.7. As for the suggestions and remarks, besides no additional comments or affirmative opinion of 50 % of the interviewed authors, many contributors stated that they would appreciate faster reviewing and publishing after manuscript acceptance (approximately 30 % of suggestions). A significant number of authors suggested improvement of the Instructions to Authors and reduction of the technical requirements for submission (especially for figures). Additionally, a few authors suggested a more careful choice of reviewers and a few recommended elevation of the criteria for article acceptance.

After collection of the surveys, the responses were summarized and analyzed. A meeting of the Editorial Board was organized on this occasion and all points were discussed individually. Certain conclusions were drawn enabling a detailed overview of the entire publishing process of the JSCS, which further led to decisions directed at improvement of the process.

All participants in the survey, in one way or another, strongly supported the idea of a fully automatic on-line system: a) Sub-Editors in order not to have to remind or thank reviewers by themselves and not to have to archive all reports and letters to authors as their own database, b) reviewers in order to have the ability to quickly review the abstract on-line, to have a direct choice to accept or decline to review and to have access to an on-line Report Form and c) authors in order to facilitate the submission step and to speed-up the reviewing process. Members of the Editorial Board agreed that a complete on-line system would improve the management of the JSCS and the decision was made to practice exclusively on-line communication from March 2015.

It was noticed that similar number of reviewers suggested longer (expected) and shorter (unexpected) period for reviewing which initiated deeper data analysis. Reviewers who were also authors could not separate these two roles and the impression of the author dominated the impression of the reviewer.

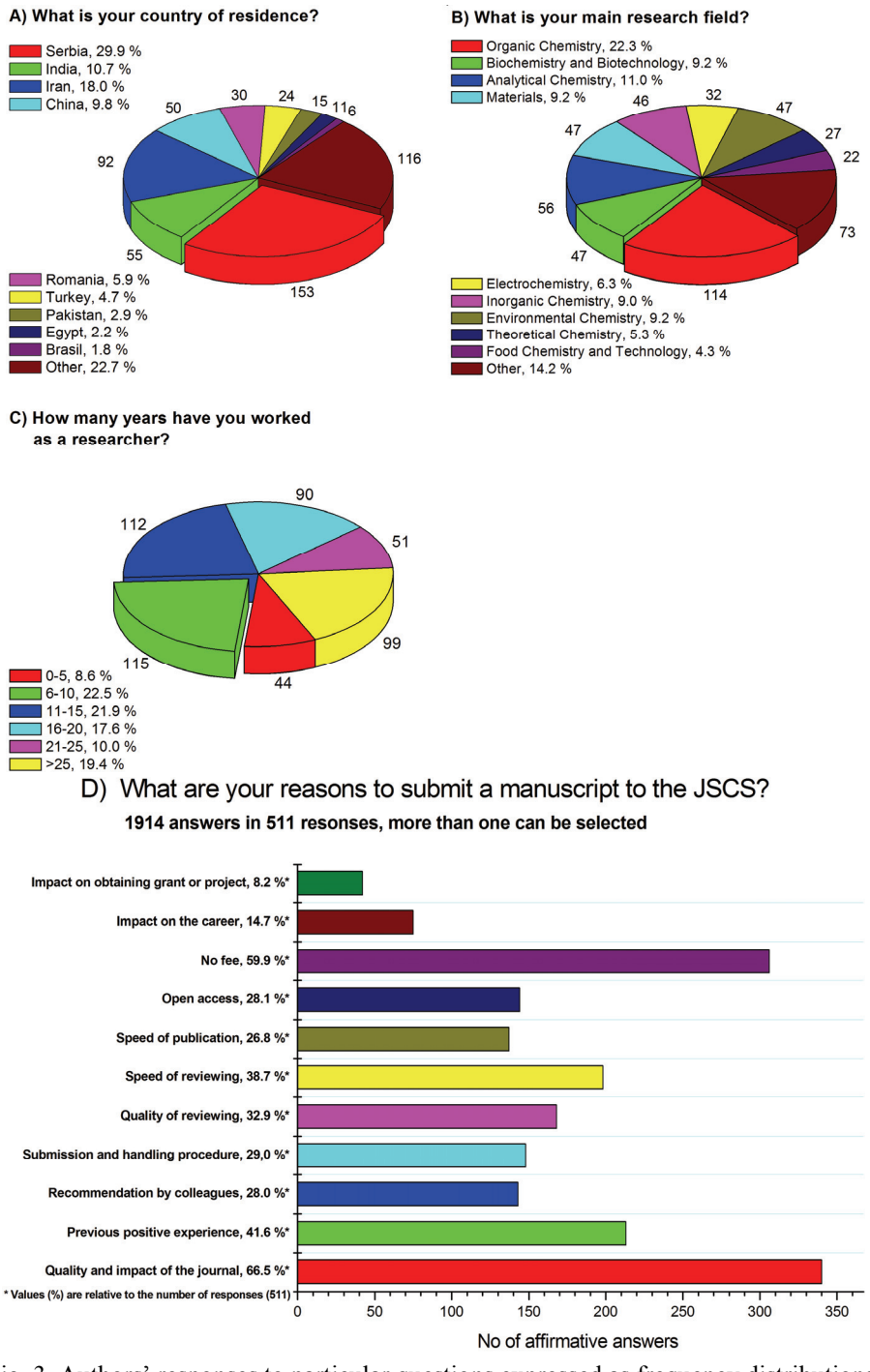

Fig. 3. Authors' responses to particular questions expressed as frequency distributions.

TABLE III. Authors' responses to questions that were recorded by scaling

Question	Grade					Average grade
	5	4	3	2	1	
	Share of the number of responses,%					
Comprehensiveness of the Instructions to Authors	22	41	27	5	5	3.7
Usefulness of the Reviewers' Reports	19	46	27	5	3	3.7
Period for reviewing	22	36	30	9	3	3.6
Period for publishing	19	38	31	7	5	3.6
Communication with Sub-Editors and Editor	35	37	23	3	2	4.0

FRAME 3. Major suggestions and remarks of authors, grouped by topics (number of individual comments)

50 % of all comments were affirmative, +:	
1. Speeding-up reviewing and publishing process	150
2. Improvement of the Instructions to authors and reduction of technical requirements for manuscript submission	88
3. Better choice of reviewers and "blind" review	30
4. Promotion and advertising of the JSCS	15
5. Increasing the number of published articles per year	12
6. Periodical special issues	5
7. Invitation of respectable scientists to write review articles	5
8. Addition of new research fields (chemical education, nano-chemistry, chemistry in agriculture)	5

Authors who suggested faster publishing do not seem to differentiate clearly between peer review and publishing. Members of the Editorial Board agreed to contribute personally to speed-up the reviewing part by faster communication with (potential) reviewers and/or by increasing the number of initially invited reviewers. It is, however, difficult to stimulate researchers to review for the JSCS. Many invited persons do not respond at all, many refuse, some accept but never send the report and a considerable number of reviewers send inappropriate reports. The reasons for such a situation may be seen as a lack of professionalism, not very good opinion on the JSCS based on the journal's ranking and/or prejudices. Potential reviewers from West Europe and North America are among those who most frequently do not respond or decline to review. A similar attitude towards the journal is also valid for the (potential) authors. When nationalities of the JSCS authors were analyzed, it became obvious that contributors from West Europe and North America are rare.

The second part of the publishing process, which includes the actual printing, can hardly be faster, as there are many accepted papers and the JSCS is already publishing more articles per year than similar non-profitable journals run by scientific societies. Since accepted papers receive DOI numbers and are available in an on-line version of the journal few days after their acceptance, the print-

ing step is not crucial from the point of article visibility by the scientific community. Steps will be taken to see how this part of the process could also be improved.

It was interesting to notice that certain number of authors suggested the application of more rigorous criteria for the evaluation of manuscripts. In their opinion, some of the published articles should not have been accepted. Thus, a considerable number of our authors have the potential to produce high quality papers and they will certainly be engaged as reviewers if they agree.

Instructions to Authors and Reviewer's Report form were revised and new versions up-loaded. Moreover, the Editorial board decided to reduce the technical requirements for figures and to make small alterations if necessary without asking authors to do so.

For the moment, the comments and suggestions that raised the greatest concerns were dealt with and some new approaches applied. Other conclusions that could be drawn from the responses in the questionnaires and members of the Editorial board will continue to analyze the data, both at the level of the entire journal and at the level of sections run by particular Sub-Editors.

The Editorial Board thanks all participants of the survey who have helped to evaluate the publishing process in the Journal of the Serbian Chemical Society and to become aware of the imperfections. It is also hoped that the actions undertaken after the survey will be welcomed by past, present and future contributors.

SUPPLEMENTARY MATERIAL

The questionnaires that the Sub-Editors, Reviewers and Authors were requested to fill out on-line are available electronically from http://www.shd.org.rs/JSCS/, or from the corresponding authors on request, as portable document format (pdf) files.

Acknowledgment. This survey and article resulted as part of scientific activity in the COST Action TD1306 "New Frontiers of Peer Review (PEERE)".

ИЗВОД

АНКЕТА О ЧАСОПИСУ „*JOURNAL OF THE SERBIAN CHEMICAL SOCIETY*" – ОБЕЛЕЖАВАЊЕ ШТАМПАЊА 80. ГОДИШТА

ОЛГИЦА НЕДИЋ[1] и АЛЕКСАНДАР ДЕКАНСКИ[2]

[1]*Институт за примену нуклеарне енергије (ИНЕП), Универзитет у Београду и* [2]*Институт за хемију, технологију и металургију, Центар за електрохемију, Универзитет у Београду*

Часопис Journal of the Serbian Chemical Society (JSCS) је научни часопис Српског хемијског друштва и ове године се обележава 85 година његовог излажења и излазак 80. годишта. После толико година објављивања научних радова, жеља Уредништва је била да утврди шта аутори, рецензенти и подручни уредници мисле о часопису и уређивачкој политици, и могу ли њихове процене и предлози помоћи да се делатност часописа побољша. Упитници анкете су послати е-поштом испитаницима. Добијени одговори су анализирани и овде су приказани само најопштији и најзначајнији подаци. Оцене, комен-

тари и предлози су показали да је већина учесника у поступку објављивања задовољна постојећим начином рада и уређивачком политиком, али мисли и да би се одређени технички детаљи поступка могли побољшати. Након сагледавања добијених одговора, Уредништво је донело одлуку да уведе високо-аутоматизовани кориснички сервис за пријаву и обраду радова и тако убрза поступак рецензирања и објављивања, и да поједностави и додатно појасни Упутство за ауторе и Рецензентски формулар. Све наведене новине су уведене 1. марта 2015.

(Примљено 6. марта, прихваћено 6. априла 2015)

REFERENCES

1. K. Iyengar, V. Balijepally, *Scientometrics* **102** (2015) 5
2. J. Garner, A. L. Porter, N. C. Newman, *Scientometrics* **100** (2014) 687
3. C. W. Holsapple, *J. Am. Soc. Inform. Sci. Technol*. **59** (2008) 166
4. P. O. Seglen, *Br. Med. J*. **314** (1997) 498
5. A. Dekanski, *J. Serb. Chem. Soc.* **79** (2014) 1561
6. S. Bojović, *Bull. Soc. Chim.* **49** (1984) 751
7. A. R. Despić, J. A. Jovanović, B. Ž. Nikolić, D. Vitorović, *The Serbian Chemical Society. History, organization, activity*, Serbian Chemical Society, Belgrade, 1996.

Journal of the Serbian Chemical Society
JSCS@tmf.bg.ac.rs • www.shd.org.rs/JSCS
J. Serb. Chem. Soc. 78 (11) S259–S263 (2013) *Supplementary material*

SUPPLEMENTARY MATERIAL TO

A survey on publishing policies of the Journal of the Serbian Chemical Society – On the occasion of the 80th volume

OLGICA NEDIĆ[1]*# and ALEKSANDAR DEKANSKI[2#]

[1]*Institute for the Application of Nuclear Energy (INEP), University of Belgrade, Serbia and* [2]*Institute of Chemistry, Technology and Metallurgy, Department of Electrochemistry, University of Belgrade, Serbia*

J. Serb. Chem. Soc. 80 (7) (2015) 959–969

QUESTIONNAIRE FOR SUB-EDITORS (ORIGINALLY IN SERBIAN)

1. Please indicate the field of chemistry for which you are sub-editing:

Theoretical Chemistry —
Organic Chemistry —
Biochemistry and Biotechnology —
Food Chemistry, Technology and Engineering —
Inorganic Chemistry —,
Polymers —
Analytical Chemistry —
Physical Chemistry —
Spectroscopy —
Electrochemistry —
Thermodynamics —
Chemical Engineering —
Textile Engineering —
Materials —
Ceramics —
Metallurgy —
Geochemistry —
Environmental Chemistry —
History of and Education in Chemistry —

* Corresponding author. E-mail: olgica@inep.co.rs

2. For how long have you been engaged as a JSCS Editor: ____

3. Were you, or are you, a member of the Editorial Board of some other journal?

Yes ___, No ___

4. Please grade:

– The instructions for Authors are:
Excellent ___, Very good ___, Good ___, Weak ___, Bad ___
– The Questionnaire in the Referee's Report is:
Excellent ___, Very good ___, Good ___, Weak ___, Bad ___
– Your communication with the editors (Editor-in-Chief, Sub-Editors, Technical Editors) and the JSCS Office is:
Excellent ___, Very good ___, Good ___, Weak ___, Bad ___
– The Editorial Office practice is:
Excellent ___, Very good ___, Good ___, Weak ___, Bad ___

5. How do you select the reviewers?

I ask colleagues I know to review ___
I preferably choose colleagues who have already reviewed manuscripts for the JSCS in the JSCS ___
I search for potential reviewers using a scientific database (WoS, Scopus, Google Scholar …) ___
I often review the manuscripts myself ___
Others: (please specify) ___

6. How many people do you ask to review in the first round?

1–2 ___, 3 ___, 4 ___, 4< ___

7. Do you ask for an approval for the acceptance to review?

Yes ___, No ___

8. Do you send reminders to the reviewers who are late with reports?

Yes ___, No ___

9. How many manuscripts were subjected annually, in %, to a second round of reviewers' selection?

<25 ___, 25–40 ___, 40–60 ___, 60–80 ___, 80< ___

10. What is the percent of invitations for review to which you received no response at all?

<10 ___, 10–20 ___, 20–40 ___, 40–60 ___, 60< ___

11. What percent of the reviewer's responses did you find inappropriate (lacking expertise or with improper comments)?

<1–2 ___, 3–5 ___, 5–10 ___, 10–15 ___, many more (please specify) ___

12. What was the quality of Reviewers' Reports (competence, clearness, good will for improvement of the manuscript)?

very good ___, good ___, average ___, bad ___

13. Please make additional comments specify the steps of the exiting reviewing procedure to which, in your opinion, special attention should be given (not more than 250 words, please):

14. Do you have any suggestions for improvement of the reviewing procedure (not more than 350 words, please):

QUESTIONNAIRE FOR REVIEWERS

1. Main research field:

_Chemistry
_Chemical Engineering
_Metallurgy
_Physics
_Biochemistry
_Materials
_Biology
_Medicine
_Other: (please specify)

2. Experience as a reviewer (not only for this journal) (Number of reviews during the year):

_0–5 _6–10 _11–15 _16–20 _21–25 _25–30 _>30
_many more: (please specify)

3. Reasons to accept to review for this journal (More than one answer can be selected):

_Quality and impact of the journal
_Professional ethics of an expert
_Previous experience as an author
_Impact on the career

4. How would you rate specific points in article reviewing in JSCS (offered rates: excellent, very good, good, fair, poor):

Comprehensiveness of the Referee's report form:
Appropriateness of questions in the form:

Period given for reviewing:
Communication with corresponding person from the journal:
Acknowledgement of reviewer's effort on behalf of the journal:

5. Rate the importance of the following for a high quality papers (5 – very important…1 – not imortant):

Scientific contribution and originality:
Clarity and conciseness of the written:
Appropriate length of the manuscript:
Conclusions supported by the presented results:
Relation to the recent publications (appropriate references):
Quality of illustrations (including legends and axes labelling):
Nomenclature and units in accordance with SI and IUPAC Recommendations:
English grammar and syntax:

6. Your suggestion to improve reviewing process in JSCS (up to 250 words):

QUESTIONNAIRE FOR AUTHORS

1. Main research field:

_Organic Chemistry
_Biochemistry and Biotechnology
_Analytical Chemistry
_Materials
_Electrochemistry
_Inorganic Chemistry
_Environmental Chemistry
_Theoretical Chemistry
_Food Chemistry and Technology
_Other: (please specify)

2. Years in research:

_0–5 _6–10 _11–15 _16–20 _21–25 _>25

3. Factors to select this journal (More than one answer can be selected):

_Quality and impact of the journal
_Previous positive experience
_Recommendation by colleagues
_Submission and handling procedure
_Quality of reviewing
_Speed of reviewing
_Speed of publication

_Open access
_No fee
_Impact on the career
_Impact on obtaining grant or project

4. How would you rate processing of article in JSCS (offered rates: excellent, very good, good, fair, poor):

Speed of reviewing:
Usefulness of reviewers' comments:
Communication with corresponding person from the journal:
Speed of publishing (Accepted manuscript with assigned doi):
Comprehensiveness of the Guide for authors:

5. My article submitted in JSCS is processed by:

_Inorganic Chemistry Sub-Editor
_Biochemistry & Food technology Sub-Editor
_Materials Science Sub-Editor
_Physical Chemistry Sub-Editor
_Environmental Chemistry Sub-Editor
_Chemical Engineering Sub-Editor
_Polymers Sub-Editor
_Organic Chemistry Sub-Editor
_Analytical Chemistry Sub-Editor
_Electrochemistry Sub-Editor
_Theoretical Chemistry Sub-Editor
_Thermodynamics Sub-Editor
_Editor in Chief
_I do not know

6. How many articles you have published in JSCS in the last 5 years? (please specify):

7. Your suggestion to improve publishing in the Journal of the Serbian Chemical Society (up to 250 words):